Research School of Earth Sciences
Annual Report 2008

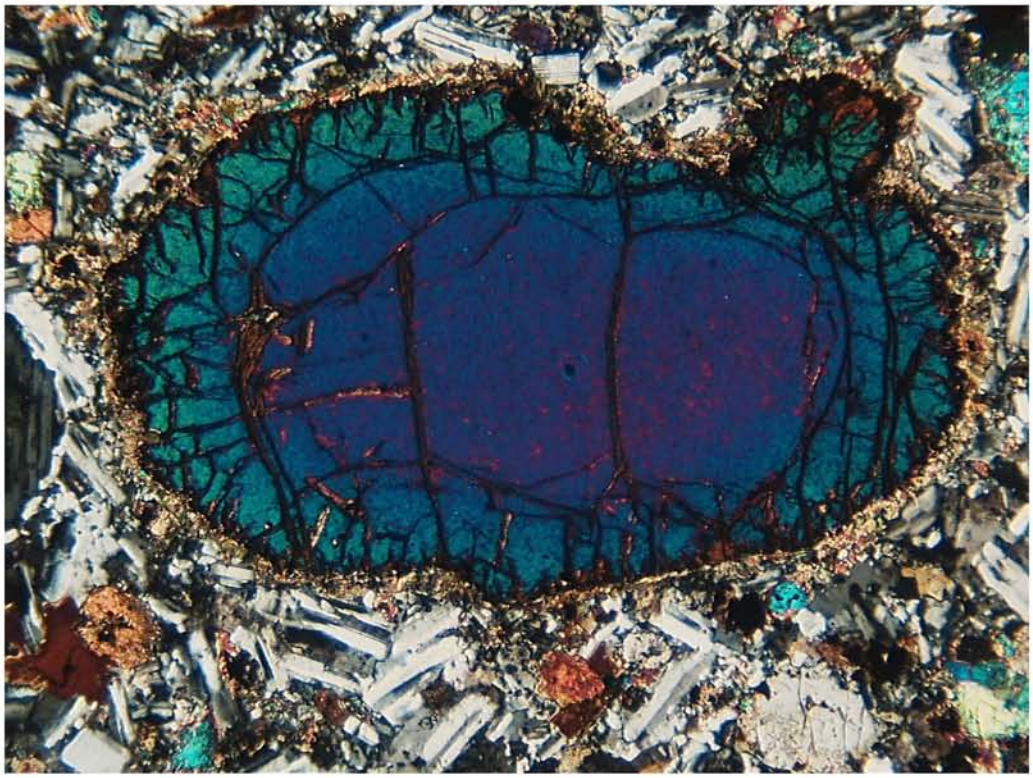

Microphotograph (X Nicols) of an olivine xenocrist embedded in a diorite matrix consisting of plagioclase, clinopyroxene, amphibole, biotite and quartz. The olivine grain is surrounded by a small corona of orthopyroxene. The change in interference colors from core to rim is related with an increase in fayalite component in olivine. Image - Jörg Hermann

THE AUSTRALIAN NATIONAL UNIVERSITY

Director's Introduction 2008

2008 was the first year in which the Research School of Earth Sciences was engaged with the full range of educational activity from undergraduate, honours, Masters by coursework and higher degree research. All education activities are carried out in the *Earth and Marine Science Education Program* and all courses now appear with a single code EMSC irrespective of their origins in the former Research School or Department. I would like to thank the Associate Director – Education, Professor S Cox, for steering the education activities of the School successfully through the year. We have had high numbers in first year in courses shared with the Fenner School and a large Honours class. Most undergraduate teaching is carried at the D.A. Brown Building (#47), but Honours and Masters teaching is concentrated at the Jaeger Building (#61).

The integration of research activities between the D.A. Brown and Jaeger buildings has worked quite well and some rearrangements of facilities are planned to make the best use of technical resources. Movements of staff have been two way and many members of the school keep fit by walking (or cycling) between the two buildings.

The administrative structure in the University continues to evolve. As a result of a University Review of Biological Sciences, the College of Science and the College of Medicine and Health have been reconfigured into the College of Physical Sciences and the College of Medicine, Biology and Environment with a joint college administration for the major functions. The Dean of Science - Prof Byrne is responsible for Education in Science across both colleges. Prof Byrne who is a nuclear physicist also has the role of Director of the College of Physical Sciences within which RSES sits. The full details of the administrative changes are still being worked out, but there has been a subtle but significant shift in the position of the School. Budgetary and Strategic issues are now expected to be worked in a College context.

Members of the School received many honours during the year:

- Prof. B.L.N. Kennett was awarded the Gold Medal in Geophysics from the Royal Astronomical Society and the Peter Baume award for exceptional merit from ANU.
- Prof. R. Grun was elected a Fellow of the Society of Antiquaries of London and the Australian Academy of the Humanities.
- Professor H. O'Neill was elected a Fellow of the Australian Academy of Science
- Prof. M. McCulloch has been made a Fellow of the Geochemical Society
- Prof. G. Lister was elected a Fellow of the Geological Society of America
- The SHRIMP team, comprising Dr John Foster, Dr Peter Holden, Mr Peter Lanc, Mr Ben Jenkins, and Mr Norm Schram, received a Vice Chancellor's Award for Innovation and Excellence in Service Quality

With the election of Prof R. Grun to the Australian Academy of the Humanities for his contributions to archaeology we now have fellows in three Australian Academy (Academy of Science, Academy of Technological Science, Academy of the Humanities) which is unusual for a Science based School.

As a fitting tribute to his very distinguished career in Earth Sciences, Em. Prof S.R. Taylor has been appointed as an Honorary Companion of the Order of Australia. In the internal promotion round for 2008 Drs V. Bennett and M. Norman were promoted to Level D.

The number of grants funded through the Australian Research Council was down once more in 2008, but there was continuing success in the areas of earth physics and climate change.

Two successful LIEF grants will see renewal in mass-spectrometers for environmentally oriented work.

2008 has seen the establishment of the Australian Office for the Integrated Ocean Drilling Program (IODP) at RSES and Prof Neville Exon appointed as Program Scientist. Australian membership of IODP is supported by a multi-year ARC LIEF grant and contributions from a wide-ranging consortium across the country. The IODP membership brings a substantial foreign currency exposure (US$1.4M per year). Fortunately this year's partial subscription (~US$1M) was paid near the top of the A$ rate against the US$ before the recent precipitate decline. The Terrawulf II computer cluster funded through AuScope was formally launched in June, this 384 core system is being used for a wide range of research including atmospheric effects in GPS, through ocean modelling to studies of the Earth core and geodynamo.

The Jaeger 5 extension building with the ground floor SHRIMP stable and second floor offices for the Planetary Sciences Initiative was completed in mid-year. The energy efficient building provides a contrast and complement to the rest of the Jaeger complex. SHRIMP II was successfully moved to the ground floor working area to join SHRIMP RG in the original space. SHIRIMP SI grows in place in the floor and already the general form can be visualised. The offices above are in use and we have gained a valuable area for teaching and small meetings. We have received permission to call this the "D.H. Green Room" in honour of the former Director of the School who has recently 'retired' to Tasmania.

The Campus Planning and Development committee has approved the design for the replacement of the rear section of the Old Hospital Building (OHB-B) that provides an interesting contrast to the Heritage listed OHB-A. This "Jaeger-8" project now awaits release of funding. It will include additional teaching space and a clear front entrance to the School.

Research at RSES mobilises a wide range of geological, geochemical and geophysical techniques and expertise to try to understand the nature of the Earth and its environment. The research is organised through the four main Research Areas: Earth Chemistry, Earth Environment, Earth Materials & Processes and Earth Physics. These research areas link groups with a common style of activity or equipment. Much cross-area cooperation occurs, and many activities transcend area boundaries.

The following pages provide an account of many facets of the research activity of RSES undertaken in 2008.

B.L.N. Kennett
Director, RSES

Earth Chemistry

The chemistry and isotope chemistry of natural materials is highly indicative of provenance and process throughout geological history. Our studies range in time from the earliest solar system through to processes that are actively taking place today, and in scope from planetary systems to individual molecules. Active areas of research centre on planetary studies, metamorphic and igneous geochemistry and geochronology, geochemistry of life processes, and chronology of all processes encompassed.

Most of our analytical work involves detailed analysis on the microscale, or concentrating trace elements from larger samples for high precision analysis. Isotopic systems can reveal both the nature of the processes involved (stable isotopes) as well as the timing of events (radiogenic isotopes), while chemical abundances can reflect protolith contributions and processes affecting various systems including biologic systems. As revealed in this year's research contributions, analytical work can be applied to topics in tectonics, ore genesis, metamorphic petrology, paleoclimate, paleoecology and regolith dating.

Highlights

The J5 building extension was completed in 2008. The project involved doubling the length of the extant building and adding a second floor to house offices, a seminar room (The D. H. Green Room), and geochemistry laboratories. Starting in July, SHRIMP II was moved from J3 to its new position in the J5 SHRIMP building and is now operational again. Construction of SHRIMP SI has now recommenced and is proceeding well with expectations of testing in mid 2009. The fit out of the J5 chemistry laboratories is underway with installation of extraction hoods nearly complete. These laboratories will be established under the direction of Dr Yuri Amelin. The completion of the office space upstairs sees a focal point for the Planetary Science Institute at RSES.

Personnel

Dr Stewart Fallon joined Earth Chemistry in 2008. In January 2009, Dr Vickie Bennett will be taking leave of absence from RSES to take up a position at Johnson Space Center, Houston.

The SHRIMP team, comprising Dr John Foster, Dr Peter Holden, Mr Peter Lanc, Mr Ben Jenkins, and Mr Norm Schram, received a Vice Chancellor's Award for Innovation and Excellence in Service Quality for 2008.

PhD studies were completed by Diane Valente, Courtney Gregory, and Joe Hiess. Congratulations Doctors.

Postgraduate studies were commenced by Ms Heejin Jeon [supervised by Dr Ian Williams], Mr Alexandr Stepanov [Dr Daniela Rubatto], Mr Jung Woo Park [Professor Ian Campbell].

U-Pb ages of angrites

Yuri Amelin[1] and Tony Irving[2]

[1]*Research School of Earth Sciences, Australian National University, Canberra, ACT 0200, Australia*

[2]*Deptartment of Earth and Space Sciences, University of Washington, Seattle, WA 98195, USA*

Angrites form a small but remarkable group of meteorites. These very old differentiated achondrites experienced much less secondary processing than most meteorites, and their peculiar mineralogy and geochemistry facilitates precise dating with several isotopic methods. The group includes a variety of the specimens, ranging from "basaltic" rocks with prominent vesicles that formed rapidly quenched melts, to plutonic igneous rocks with cumulate textures and annealed plutonic rocks. Recent findings of new angrites, mainly in the deserts of northwest Africa and in Antarctica, increased their number from one in 1970's (Angra dos Reis, or AdoR, originally the prototypical meteorite of this group, which is now considered an anomalous angrite) to 16 in 2008.

Angrites are singularly well suited to serve as benchmarks of the early Solar System chronology. The ages of some of these meteorites were determined in 1970's to early 90's, and AdoR has been long known as one of the oldest rocks in our Solar System, but precision and accuracy of these dates are insufficient for constructing a detailed timescale of the early Solar System events. The ages of recently found angrites were not known at all. Recent developments in Pb isotopic analysis of meteorites: using ^{202}Pb-^{205}Pb double spike optimized for isotopic dating, and a new procedure for efficient removal of common Pb, provides a background for revisiting and refining chondrite chronology.

Precise U-Pb ages for seven angrites are determined with double spike (^{202}Pb-^{205}Pb) thermal ionization mass spectrometry. The data for three angrites with well preserved U-Pb isotopic systems are shown in Fig. 1. The implications of these ages are threefold. First, they demonstrate that AdoR and LEW are not coeval, and the group of "slowly cooled" plutonic angrites is genetically diverse. Second, the new age of LEW suggests an upward revision of ^{53}Mn-^{53}Cr "absolute" ages by 0.7 Ma. Third, a precise age of D'Orbigny allows consistent linking of the ^{53}Mn-^{53}Cr and ^{26}Al-^{26}Mg extinct nuclide chronometers to the absolute lime scale.

Furthermore, these data show that the angrite parent body underwent prolonged high temperature igneous (both volcanic and plutonic) activity and metamorphism for at least 7 Ma during a period very early in solar system history. It is difficult to conceive of a thermal mechanism by which this could be accomplished unless the parent body was a relatively large, differentiated planet.

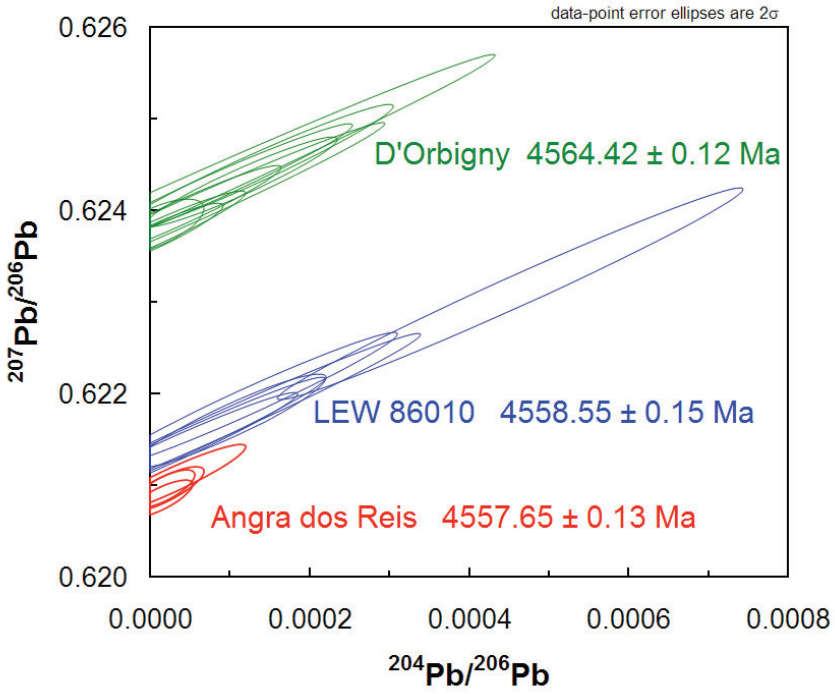

Figure 1. *Pb isotopic data for pyroxenes from Angrites AdoR and LEW 86010, and pyroxenes and whole rock fractions from D'Orbigny, plotted in a $^{207}Pb/^{206}Pb$ vs. $^{204}Pb/^{206}Pb$ isochron diagram, and the weighted average $^{207}Pb^*/^{206}Pb^*$ ages.*

Tungsten isotopic compositions of presolar silicon carbide grains: implications for ^{182}hf-^{182}w and ^{187}re-^{187}os chronometers

J. N. Avila[1], T. R. Ireland[1], F. Gyngard[2], S. Amari[2], E. Zinner[2]

[1]Research School of Earth Sciences and Planetary Science Institute, The Australian National University, Canberra ACT 0200, Australia. [2]Laboratory for Space Sciences and Physics Department, Washington University, St. Louis, MO 63130, USA.

The *s*-process nucleosynthesis in the Hf-Ta-W-Re-Os path has received considerable attention lately (Fig. 01). New neutron capture cross-sections for ^{174,176,177,178,179,180,182}Hf, ^{185}W and ^{186,187,188}Os have been reported (Sonnabend et al., 2003; Mosconi et al., 2006; Wisshak et al., 2006; Vockenhuber et al., 2007), and small anomalies in W and Os isotopes have been observed in primitive meteorites (Brandon et al., 2005; Yokoyama et al., 2007; Qin et al., 2008). However, as suggested by Vockenhuber et al. (2007) and Sonnabend et al. (2003), model calculations for *s*-processes nucleosynthesis appear to underestimate ^{182}W and overestimate ^{186}Os, and this may have implications for the ^{182}Hf-^{182}W and ^{187}Re-^{187}Os chronometers. Tungsten isotopes are particularly important because they are affected by several branching points (^{182}Ta, ^{181,182}Hf, and ^{185}W), which also affect Re and Os isotopes. Here we report W isotopic measurements in presolar SiC grains in order to provide additional constraints on *s*-process nucleosynthesis.

^{182,183,184,186}W and ^{180}Hf were measured with SHRIMP RG at ANU in an aggregate of presolar SiC grains (KJB fraction) extracted from the Murchison meteorite (Amari et al., 1994). Tungsten isotopes were measured as WO^+ ions, which have a higher yield than the atomic species ($WO^+/W^+ \sim 3$). An O^- primary ion beam of 5 nA was focused to sputter an area of 20 mm in diameter. SHRIMP RG was operated at a mass resolving power of m/_m= 5000 (at 1% peak). At this level, isobaric interferences were well resolved from the WO^+ species. NIST silicate glasses and synthetic SiC were used to monitor instrumental mass fractionation and isobaric interferences.

The W isotopic compositions are anomalous in comparison to those observed in normal solar system materials. The SiC grains appear to be enriched in ^{182}W and ^{184}W relative to ^{183}W, as expected for *s*-process nucleosynthesis in AGB stars (e.g. Qin et al., 2008). However, an unexpected enrichment in ^{186}W is observed. The low ^{180}Hf/^{183}W ratios determined here imply a low contribution from radiogenic ^{182}W after SiC condensation, otherwise the ^{182}W excesses would be even higher. The enrichment in ^{182}W appears to be plausible, given the observation that the calculated *r*-process residue of ^{182}W ($N_r = N_\odot - N_s$) has a significant positive deviation from the smooth *r*-abundance distribution (Wisshak et al., 2006; Vockenhuber et al., 2007). A lower *r*-process component of solar ^{182}W would imply a shorter time interval between the last *r*-process contribution to solar ^{182}Hf and the formation of solid parent bodies (Vockenhuber et al., 2007).

As discussed by Sonnabend et al. (2003), the stellar *s*-process model shows a 20% overproduction of ^{186}Os, and consequently it underestimates the *s*-process contribution to ^{187}Re. The enrichment observed in ^{186}W requires the activation of the ^{185}W branching point during AGB thermal pulses, when marginal activation of the ^{22}Ne(α,n)^{25}Mg source produces neutron densities as high as $N_n = 5 \times 10^9$ neutrons cm^{-3} (Lugaro et al., 2003), bypassing ^{186}Os. This result is in disagreement with ^{96}Zr depletions in SiC grains, which indicate that the ^{22}Ne(α,n)^{25}Mg source was weak in their parent stars (Nicolussi et al., 2003). However, the overabundance of ^{186}Os could also be the result of uncertainties in the nuclear physics data.

Amari S. et al. 1994. Interstellar grains in meteorites. I. Isolation of SiC, graphite, and diamond; size distributions of SiC and graphite. *Geochimica et Cosmochimica Acta* 58: 459-470.

Brandon A. et al. 2005. Osmium Isotope Evidence for an s-Process Carrier in Primitive Chondrites. *Science* 309: 1233-1236.

Lugaro M. et al. 2003. Isotopic Compositions of Strontium, Zirconium, Molybdenum, and Barium in Single Presolar SiC Grains and Asymptotic Giant Branch Stars. *Astrophysical Journal* 593: 486-508.

Mosconi M. et al. 2006. Experimental challenges for the Re/Os clock. *Nuclei in the Cosmos IX*: 381-387.

Nicolussi G. et al. 1997. s-Process Zirconium in Presolar Silicon Carbide Grains. *Science* 277: 1281-1283.

Qin L. et al. 2008. Tungsten Nuclear Anomalies in Planetesimal Cores. *Astrophysical Journal* 674: 1234-1241.

Sonnabend K. et al. 2003. The s-Process Branching at ^{185}W. *Astrophysical Journal* 583: 506-513.

Vockenhuber C. et al. 2007. Stellar (*n*, _) cross sections of ^{174}Hf and radioactive ^{182}Hf. *Physical Review C* 75: 15804.

Wisshak K. et al. 2006. Fast neutron capture on the Hf isotopes: Cross sections, isomer production, and stellar aspects. *Physical Review C* 73: 45807.

Yokoyama T. et al. 2007. Osmium isotope evidence for uniform distribution of *s*- and *r*-process components in the early solar system. *Earth and Planetary Science Letters* 259: 567-580.

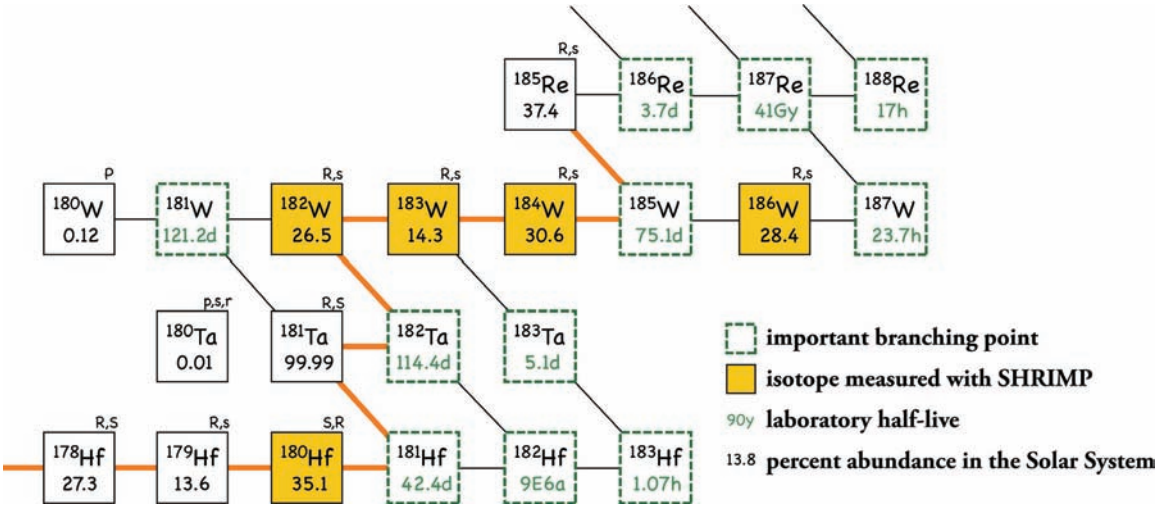

Figure 1.

Small continents on the Hadean Earth: New Isotopic Evidence from combined Hf and ^{142}Nd Isotopic Signatures

Vickie C. Bennett[1], Joe M. Hiess[1], Alan D. Brandon[2] and Allen P. Nutman[3]

[1] *Research School of Earth Sciences, Australian National University, Canberra, ACT 0200*

[2] *NASA Johnson Space Center, Houston, TX 77058, USA*

[3] *Chinese Academy of Geological Sciences, Beijing 100037, P.R. China*

Questions of the antiquity and volumes of Earth's ancient continental crust have been actively debated for more than 100 years and remain controversial. One view is that massive amounts of continental crust formed very early in Earth's history and persisted to the present, with new crustal growth balanced by recycling into the mantle. In direct contrast are models calling for progressive growth of the continental mass over geologic time, with small volume early continents. These debates take on added significance when considered in conjunction with potential early life habitats and the timing and mechanisms of formation of Earth's major chemical domains after the initial stages of planetary accretion.

We have taken a new perspective on Earth's early history by combining information from two isotopic systems (^{176}Hf/^{176}Hf formed from decay of ^{176}Lu; half-life=37.1 Gy) and ^{142}Nd/^{144}Nd (formed by decay of now extinct ^{146}Sm; half life =103 My), whose signatures are preserved in the oldest rocks. The analysed samples include 3.63 -3.87 Ga (billion years old) rare, early crustal relicts from southwest Greenland, Western Australia, and China. Hafnium isotopic data from well-characterised and U-Pb dated zircons extracted from these rocks show that the oldest rocks have initial Hf isotopic compositions that are the same as bulk Earth and primitive meteorite compositions (Hiess et al, in review), indicating that the source of these rocks did not experience early Lu/Hf modification. In contrast the ^{142}Nd isotopic compositions measured from the same rocks as yielded the zircons, are distinct from both modern rocks and from primitive meteorites (Bennett et al., 2007) requiring Hadean Sm/Nd fractionation.

Modelling of the trace element pattern of the Hadean (>4.0 Ga) mantle, as defined from the combined isotopic data, shows that it could not have been generated by extraction of average low Sm/Nd, low Lu/Hf continental crust (Figure 1). This is in contrast to the modern Earth, where the continental crust and the upper mantle have complementary isotopic and trace element characteristics. Thus, continent formation could not have been the primary mechanism of differentiation on the Hadean Earth. Furthermore, owing to the effectiveness of crust formation at changing Lu/Hf ratios, the near-chondritic Hf isotopic data require that the preserved earliest continents were of very limited extent, likely less than 5% of the present day continental mass. The chemistry of the Hadean mantle as recorded by the short and long half-life isotopic systematics of the oldest rocks points towards models of early silicate differentiation in a global terrestrial magma ocean.

Bennett, VC, Brandon AD and Nutman AP (2007) Coupled ^{142}Nd-^{143}Nd Isotopic Evidence for Hadean Mantle Dynamics. *Science* **318**: 1907-1910.

Hiess J, Bennett VC, Nutman AP. and Williams IS (In revision) In situ U-Pb, O and Hf isotopic compositions of zircon from Eoarchaean rocks, southern West Greenland: New Views of old Crust. *Geochimica et Cosmochimica Acta.*

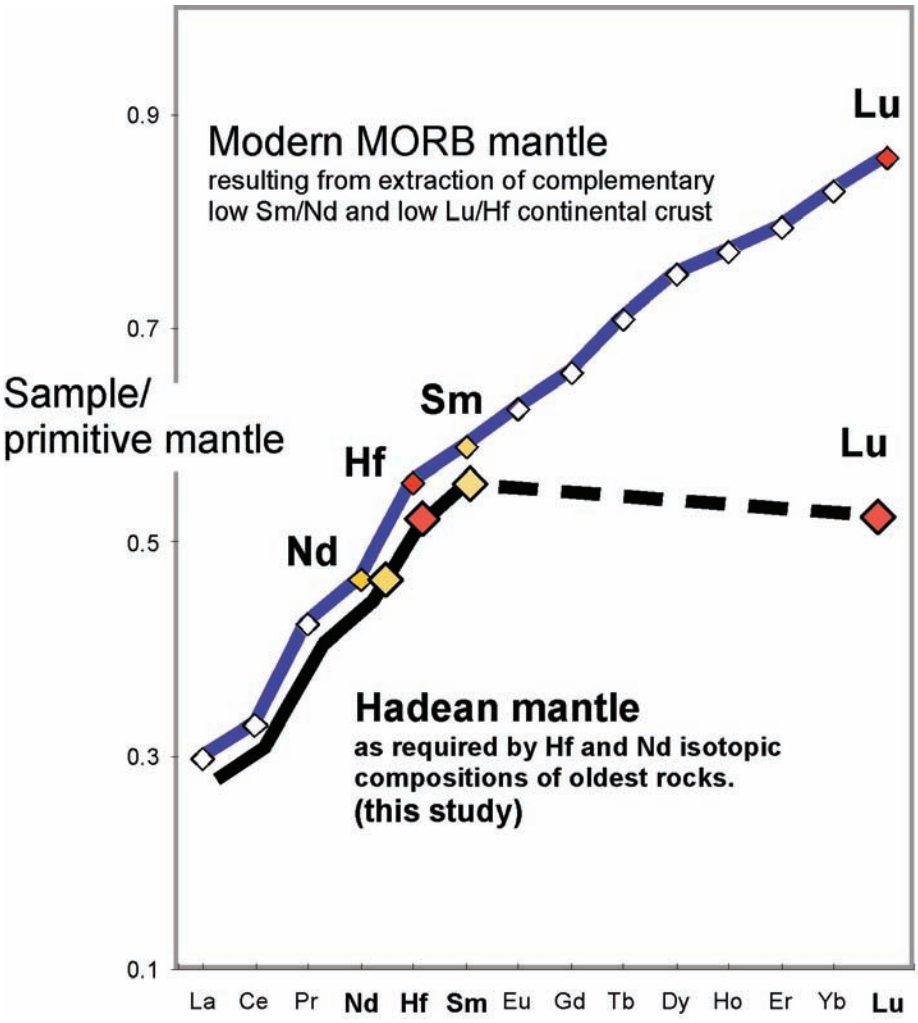
Modern MORB mantle
resulting from extraction of complementary
low Sm/Nd and low Lu/Hf continental crust
Lu
Sm
Hf
Nd
Lu
Hadean mantle
as required by Hf and Nd isotopic
compositions of oldest rocks.
(this study)
Sample/
primitive mantle
0.9
0.7
0.5
0.3
0.1
La Ce Pr Nd Hf Sm Eu Gd Tb Dy Ho Er Yb Lu

Figure 1.

Integrating community proteogenomics and lipid biogeochemistry to unravel ancient evolutionary history

Jochen J. Brocks[1] and Jillian Banfield

[1]*Research School of Earth Sciences, Australian National University, Canberra, ACT 0200, Australia*

[2] *Dept. of Earth and Planetary Science, University of California, Berkeley, CA 94720-4767, USA*

The first appearance of a metabolic pathway that allowed microorganisms to exploit a new and previously untapped energy source, such as methanogenesis, sulfate reduction and photosynthesis, must have had profound effects on the chemical composition of the atmosphere and oceans. It is a captivating goal of geobiology to determine when such physiologies first appeared in Earth history and to correlate these events with the associated chemical and isotopic changes in the rock record. One of the best methodologies to track the first appearances of microorganisms in the geological record is the search for biomarker molecules. Biomarkers can be preserved in billion years old sedimentary rocks and are often the only direct methodology to study ancient microbial ecosystems. If we want to match biomarkers from ancient rocks with the organisms that produced them we rely on information about lipids detected in extant organisms grown in cultivation. However, currently the vast majority of all microorganisms defies isolation, and their lipid biosynthetic capacities, as well as their roles in ecosystems, remain largely obscure. Consequently, our knowledge about the distribution of biomarkers in nature remains highly fragmentary.

Figure 1 shows how environmental genomics and proteomics on natural microbial consortia may help to solve the problem. It summarizes how these methodologies could be combined with lipid biogeochemistry to assemble a phylogenetic tree of the three domains of life where all nodes are (roughly) dated, all branches are annotated with a complete set of lipids that are produced by each lineage, and each lineage is linked to the sequences of the genes required for their biosynthesis. Development and use of phylogenetic trees for lipid genes and their products should provide quantitative data about the frequency of lateral gene transfer and convergent evolution in lipid biosynthetic pathways, and should allow us to determine a level of confidence with which a biomarker from a well-dated ancient rock can be assigned to a particular biological origin.

Ram R. J. et al. and Banfield J. F. (2005) Community proteomics of a natural microbial biofilm. *Science* **308**, 1915-1920.

Tyson G. W. et al. and Banfield J. F. (2004) Community structure and metabolism through reconstruction of microbial genomes from the environment. *Nature* **428**, 37-43.

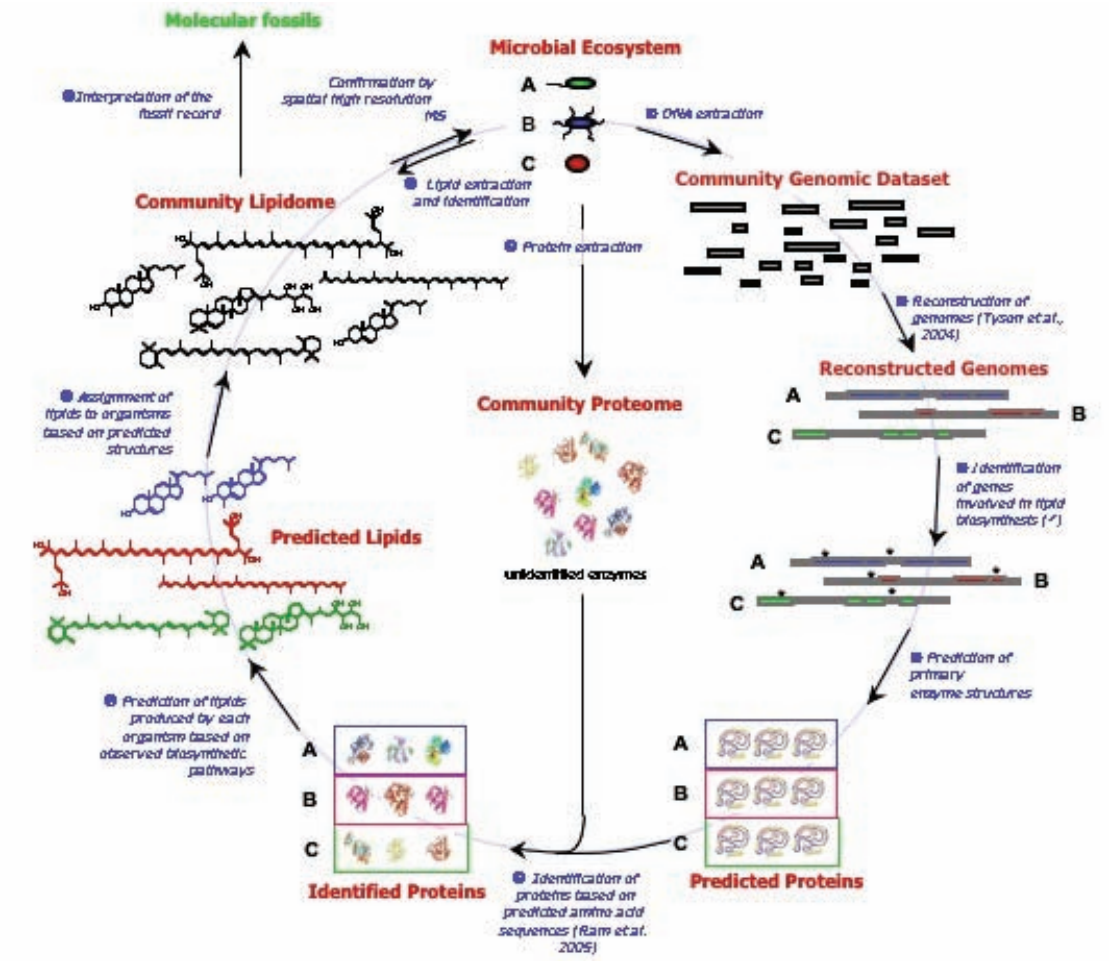

Figure 1. *With nearly completely reconstructed genomes and the knowledge which genes were expressed at the time when the sample was taken, it should, in principle, be possible to assign each lipid detected in a 'community lipidome' to an organism or group of organisms in the consortium, even if these organisms can not be isolated and grown in culture: DNA is extracted from a natural sample, fragments are sequenced (♂) and sequences assembled to reconstruct (near) complete genomes of all dominant (>5% relative abundance) bacteria and archaea (♂). Genes involved in lipid biosynthesis are identified (③) and primary protein structures predicted based on base sequences (④). Proteins involved in lipid biosynthesis that were extracted from the same environmental sample (⑤) can then be identified based on predicted primary protein structures and assigned to individual organisms (⑥). Based on enzymes that are part of well-studied lipid biosynthetic pathways and that were detected in the environmental sample, it should be possible to predict major lipid end-products (⑦) and, thus, to assign actual lipids in the environment to individual organisms or group of organisms (⑧, ⑨). The identification of lipids of organisms that defy isolation may significantly improve our understanding of the sources and environmental significance of fossils lipids in the geological record (⑩).*

Supercontinents, supermountains and the rise of atmospheric oxygen

[1]Ian Campbell and Charlotte Allen

[1] *Research School of Earth Sciences, Australian National University, Canberra, ACT 0200, Australia*

Atmospheric oxygen concentrations in the Earth's atmosphere rose from negligible levels in the Archaean Era to about 21% at present day. This increase is thought to have occurred in six steps, 2.65, 2.45, 1.8, 0.6, 0.3 and 0.04 billion years ago, with a possible seventh event identified at 1.2 billion years ago. The timing of these steps correlates with the amalgamation of Earth's landmasses into supercontinents. We suggest that the continent-continent collisions required to form supercontinents produced chains of supermountains. These supermountains eroded quickly and released large amounts of nutrients such as iron and phosphorous into the oceans, leading to an explosion of algae and cyanobacteria, and thus a marked increase in photosynthesis, and the photosynthetic production of O_2.

Enhanced sedimentation during these periods promoted the burial of a high fraction of organic carbon and pyrite, thus preventing their reaction with free oxygen, and leading to sustained increases in atmospheric oxygen.

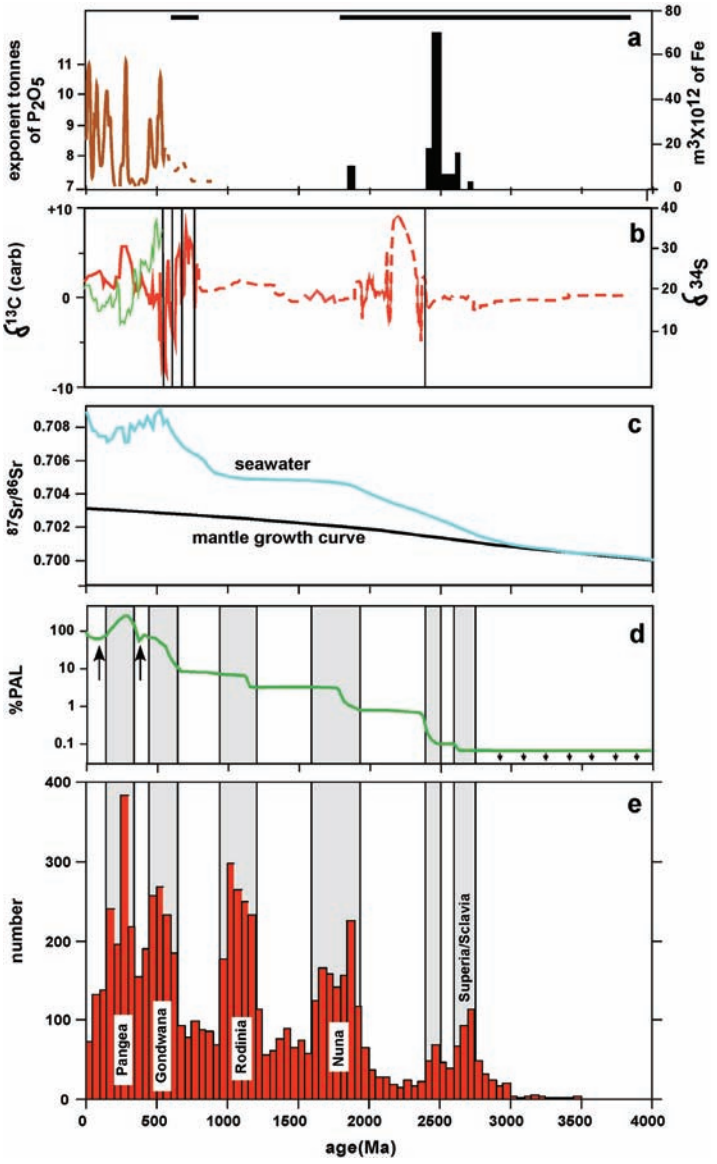

Figure 1. *Supercontinent ages compared with variations in atmospheric O_2 and related variables. a, Tonnes of P_2O_5 in phosphate deposits and Fe in iron formations. b, $^{13}\delta C$ in marine carbonates (red) and $^{34}\delta S$ in sulfate (green). Black lines correspond to ice ages. c, $^{87}Sr/^{86}Sr$ in seawater. d, Atmospheric O_2 showing the steps described in the text. Arrows point to periods of low atmospheric O_2. e, U/Pb ages of 5246 concordant detrital zircons from 40 major rivers supplemented by 1136 Australian dune zircons and 583 from Antarctic Palaeozoic sediments.*

Hf isotopes in rutile measured in-situ by LA-MC-ICPMS

Tanya Ewing[1], Daniela Rubatto[1], Jörg Hermann[1] and Steve Eggins[1]

[1] *Research School of Earth Sciences, Australian National University, Canberra, ACT 0200, Australia*

Hf isotopes are commonly measured in zircon and used to trace input from different mantle reservoirs and crustal components. In contrast, the Hf isotope systematics of rutile (TiO_2), a common accessory mineral in a variety of geological settings, are relatively unexplored.

The recent studies of Choukroun et al. (2005) and Aulbach et al. (2008) have revealed that rutile records a much greater range of $^{176}Hf/^{177}Hf$ ratios than is seen for zircon. These studies have also highlighted the potential for the in-situ measurement of Hf isotopes in rutile using Laser Ablation Multi-Collector Inductively Coupled Mass Spectrometers (MC-LA-ICPMS). However, as yet no detailed study of the accuracy of these in-situ measurements for rutile has been made. As rutile contains very low levels of Hf compared to zircon, proving the reliability of in-situ Hf isotope measurements is a critical first step in exploring the potential of this method to contribute to petrological studies.

We have used a number of approaches to assess the accuracy, precision and limitations of in-situ analysis for Hf isotopes in rutile, as well as refining analytical and data reduction methods for analysis of low levels of Hf. Some novel adaptations have been made, such as the use of synthetic rutiles doped with Hf to monitor change in mass bias over the course of a session and provide an external correction factor where required.

The accuracy of Hf isotope measurements for rutile on our Neptune MC-ICPMS in laser ablation mode is demonstrated by comparison with solution MC-ICPMS values for a rutile containing c.30ppm Hf. The $^{176}Hf/^{177}Hf$ values obtained from the two methods were in excellent agreement. Accuracy is confirmed by the agreement of $^{176}Hf/^{177}Hf$ values for plutonic rutile and zircon – which should record the same Hf isotope signature in an igneous system – from a single trondjhemite sample.

The precision of individual rutile analyses is lower for laser ablation than for solution analyses, but combining populations of 10 to 15 analyses to give a weighted mean significantly improves the precision. This level of precision has proved ample to distinguish between different rutile samples, or between rutile and other minerals that record a different Hf isotope signature.

It is already clear that in-situ Hf isotope measurements for rutile may have exciting applications to petrological problems. An early case study on rutile and zircon from the Duria garnet peridotite has demonstrated that Hf isotope analysis of metamorphic rutile can provide complementary information to isotopic information obtained from zircon. LA-MC-ICPMS analyses of zircon and rutile from the Duria peridotite revealed clearly distinct Hf isotopic ratios for the two minerals: the rutile records a mantle signature, whereas zircon isotopic ratios provide evidence for crustal input. This is in keeping with the metamorphic history of the peridotite as determined by Hermann et al. (2006) based on petrographic analysis and trace element geochemistry. The ability to analyse Hf isotopes in rutile therefore allows us to access isotopic information about parts of the metamorphic history that are not recorded by zircon.

Aulbach S, O'Reilly SY, Griffin WL, Pearson NJ (2008) The eclogite mantle reservoir: $^{176}Hf/^{177}Hf$, Nb/Ta and Zr/Hf of rutile. *Nature Geoscience* **1**:468-472

Choukroun M, O'Reilly SY, Griffin WL, Pearson NJ, Dawson JB (2005) Hf isotopes of MARID (mica-amphibole-rutile-ilmenite-diopside) rutile trace metasomatic processes in the lithospheric mantle. *Geology* **33**(1):45-48

Hermann J, Rubatto D, Trommsdorff V (2006) Sub-solidus Oligocene zircon formation in garnet peridotite during fast decompression and fluid infiltration (Duria, Central Alps). *Mineralogy and Petrology* **88**(1-2):181-206

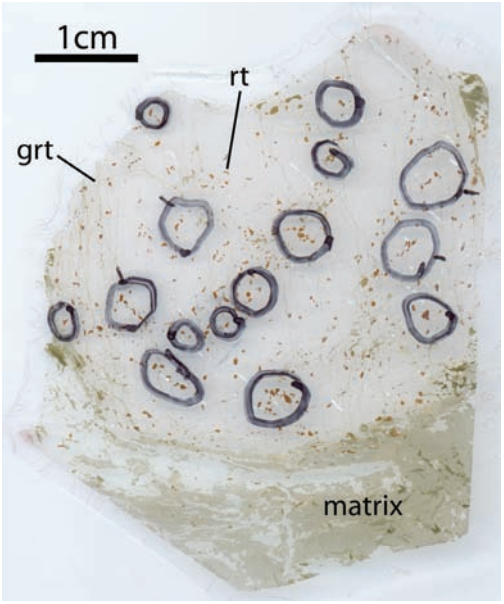

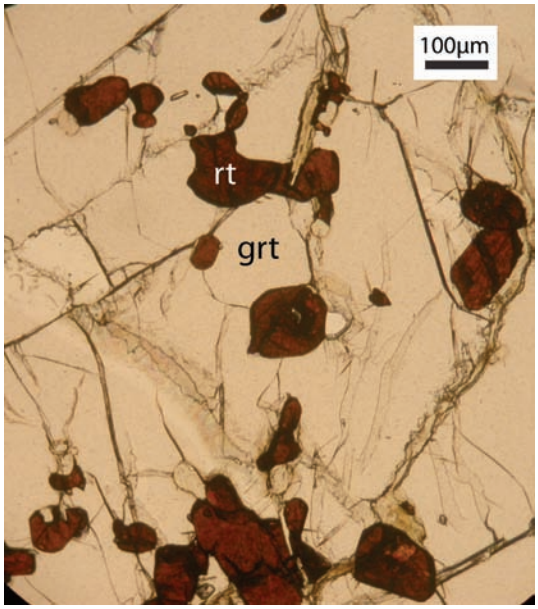

Figure 1. (left) Large thin section of garnet (grt) megacryst including numerous large rutiles (rt). Using LA-MC-ICPMS, Hf isotopes can be measured in-situ for rutiles in this thin section. Areas of interest for analysis have been circled in black pen.

Figure 2. (Right) Close-up photo of rutiles (rt) included in garnet (grt) in the thin section shown in Fig. 1.

A simple radiocarbon dating method for determining the age and growth rate of deep-sea sponges

Stewart Fallon[1], Kelly James[1], Rebecca Norman[1], Michelle Kelly[2] and Michael Ellwood[1]

[1] *Research School of Earth Sciences, Australian National University, Canberra, ACT 0200, Australia*

[2] *National Centre for Aquatic Biodiversity & Biosecurity, National Institute of Water & Atmospheric Research (NIWA) Ltd, Auckland, New Zealand*

While radiocarbon-dating is a well established technique in aging marine carbonates, the ability to reliably age siliceous organisms remains largely unexplored. Attempts have been made to carbon date the proteinaceous material bound within fossil diatoms frustrules isolated from sediment cores [1,2] and siliceous sponges [3]. The proteinaceous material bound within siliceous spicules is potentially a new and exciting way to age sponges and to date sediments devoid of carbonate material. Indeed the carbon dating of siliceous spicules in the Southern Ocean where carbonates are absent, or not well preserved, could help to validate paleoceanographic and paleoclimatic proxies and further elucidate physical and chemical changes within the oceans interior.

As filter-feeding organisms ubiquitous to the world's oceans, marine sponges obtain carbon from the food they consume, incorporating low levels (0.05%) into the spicules they produce. The carbon intrinsically incorporated into the spicule matrix from the surrounding water, is protected from contamination and can potentially provide dates in opal rich sediment cores as well as providing information on extension rates in living siliceous organisms. The following is an interpretation of ^{14}C analysis by accelerator mass spectrometry to constrain currently unknown growth rates of deep-sea sponges.

The Ross Sea sponge (TAN0402/67) was sub-sampled and cleaned using either sequential acid digestion alone, or acid digestion followed by roasting. Samples cleaned using sequential acid digestion alone needed to be placed inside a second quartz tubes to confer sufficient strength for combustion. In certain cases, these samples contained significantly more carbon than anticipated (Figure 1a). Elevated percentage carbon is attributed to insufficient removal of contaminant carbon (sponge tissue) by omitting the pre-roasting step.

The results for the percentage of carbon extracted and $\Delta^{14}C$ for samples where pretreatment included incremental increases in roasting temperatures is presented in Figure 2b. These results indicate that the optimal roasting is >400 °C. Above this temperature all the external carbon is removed yielding low but consistent results for both percentage carbon recovered and the radiocarbon $\Delta^{14}C$ results for proteinaceous material bound within the siliceous matrix (Figure 1b). The age results for sponge TAN0402/67 collected from the Ross Sea are presented in Figure 1c. A linear increase in age versus length was obtained for this sponge, although there is a significant water reservoir affect on the radiocarbon results.

The estimate $\Delta^{14}C$ value for organic carbon consumed by the sponge is about –150‰ based on modern organic carbon sedimentation in the Ross Sea. Our $\Delta^{14}C$ results for the outer part of the sponge, at about –140‰, are close to the modern organic carbon sedimentation value thereby confirming that the sponge faithfully records the $\Delta^{14}C$ signature of the organic carbon it consumes. After correcting for the reservoir age of the water, the extension rate for this sponge is around 2.9 mm yr^{-1}. Using this extension rate and a length 15 cm along the axis of growth, we estimate that sponge TAN0402/67 is around 440 years old. This novel technique for elucidating extension

rates in sponges and more broadly for dating siliceous organisms is testament to the broad applications of $^{14}C/^{12}C$ ratios by accelerator mass spectrometry as both a paleo- and modern oceanographic tool.

Hatté, C., Hodgins, G., Jull, A.J.T., Bishop, B. and Tesson, B., 2008. Marine chronology based on 14C dating on diatoms proteins. Marine Chemistry, 109(1-2): 143-151.

Zheng, Y., Anderson, R.F., Froelich, P.N., Beck, W., McNichol, A.P. and Guilderson, T., 2002. Challenges in radiocarbon dating organic carbon in opal-rich marine sediments. Radiocarbon, 44(1): 123-136.

Ellwood, M.J., Kelly, M. and Richer de Forges, B., 2007. Silica banding in the deep-sea lithistid sponge Corallistes undulatus: Investigating the potential influence of diet and environment on growth. Limnology and Oceanography, 52(5): 1865–1873.

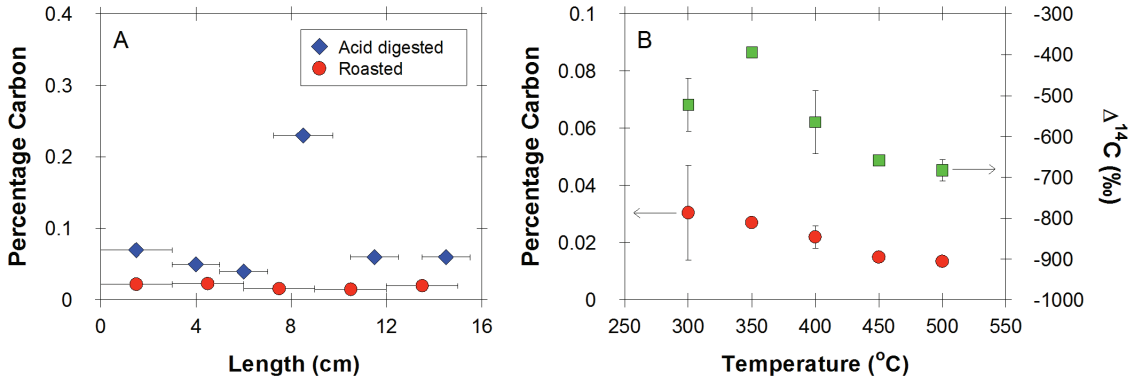

Figure 1. *A) Percentage carbon versus length for samples oxidised with sequential acid digestion (acid digested) and acid digested followed by combustion at 450 °C for 12 hours (Roasted). B) Percentage carbon and $\Delta^{14}C$ versus roasting temperature. Sample points are the mean of two replicates while the error bars indicate the range.*

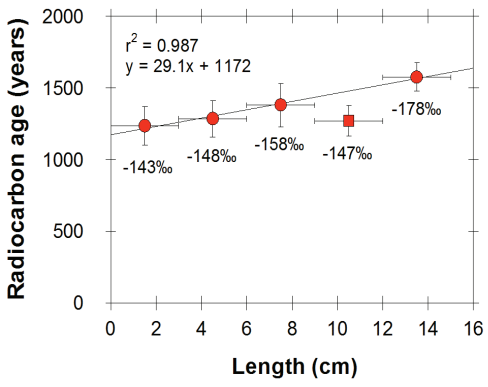

Figure 2. *Radiocarbon age versus length along the axis of growth for samples removed from sponge TAN0402/67. The red square indicates a sample that was not included in the calculation of sponge extension rate.*

Argon enters the retentive zone: Reassessment of diffusion parameters for K-feldspar

Marnie Forster[1] and Gordon Lister[1]

[1] *Research School of Earth Sciences, Australian National University, Canberra, ACT 0200, Australia*

$^{40}Ar/^{39}Ar$ apparent age spectra have been measured for unusually retentive potassium feldspars from the South Cyclades Shear Zone, Ios, Greece. The data obtained helped constrain the age and duration of the operation of this crustal-scale shear zone. We investigated traditional methods used to analyse Arrhenius plots by simulating the effect of step-heating experiments on argon loss. Fractals were used to define theoretical distributions of diffusion domain size and volume, allowing recognition of a Fundamental Asymmetry Principle (FAP) which is required if line fitting is to be consistent with the multi-domain diffusion hypothesis. The FAP means that a fitted line must divide the population by rank order. Points from data obtained earlier in the sequence of step heating experiments must lie on the fitted line, or to the right of it. Points from data obtained later in the sequence must lie on the fitted line, or to the left of it. Applying the FAP has lead to the estimation of higher activation energies.

To understand whether these results are limited, for example, to the K-feldspars from this study, data from previously published papers was examined (Fig. 1a), including data from the UCLA archive. The results obtained, using multi-domain diffusion modelling (Lovera *et al.* 1997) led us to an in depth look at the method and the fundamentals behind these methods. Analysis of Arrhenius data should take account of the Fundamental Asymmetry Principle since this is an inherent part of any multi-domain diffusion model. Results showed that if the Fundamental Asymmetry Principle is not applied (Fig. 1a b), numerical analysis will invariably underestimate the value of activation energy used in simulating the effect of step-heating experiments on fractal volume-size distributions (Fig. 1c d).

It was found that the application of the Fundamental Asymmetry Principle, determined from modeling using *eAr software* makes a considerable difference in respect to the magnitude of the activation energies estimated. The average of activation energy for K-feldspar is significantly higher than previously reported. These results imply that the Argon Partial Retention Zone for the most retentive domains in K-feldspar can expand into the ductile regime (i.e. with temperatures ~400-450°C), as recorded for the South Cyclades Shear Zone (Fig 1e). This means that K-feldspar can routinely be used as a geochronometer to estimate the timing and duration of events in complexly deformed terranes.

Baldwin SL, Lister GS, (1998) Thermochronology of the South Cyclades shear zone, Ios, Greece: effects of ductile shear in the argon partial retention zone. *JGR*, **103,** 7315–7336.

Lovera OM, Grove M, et al (1997) Systematic analysis of K-feldspar $^{40}Ar/^{39}Ar$ step heating results: I. Significance of activation energy determinations. *Geo Cosmochimica Acta,* **61**: 3171-3192.

Forster MA, Lister GS (2008) Argon enters the retentive zone: reassessment of diffusion parameters for K-feldspar in the South Cyclades Shear Zone, Ios, Greece. *Lithos, in press.*

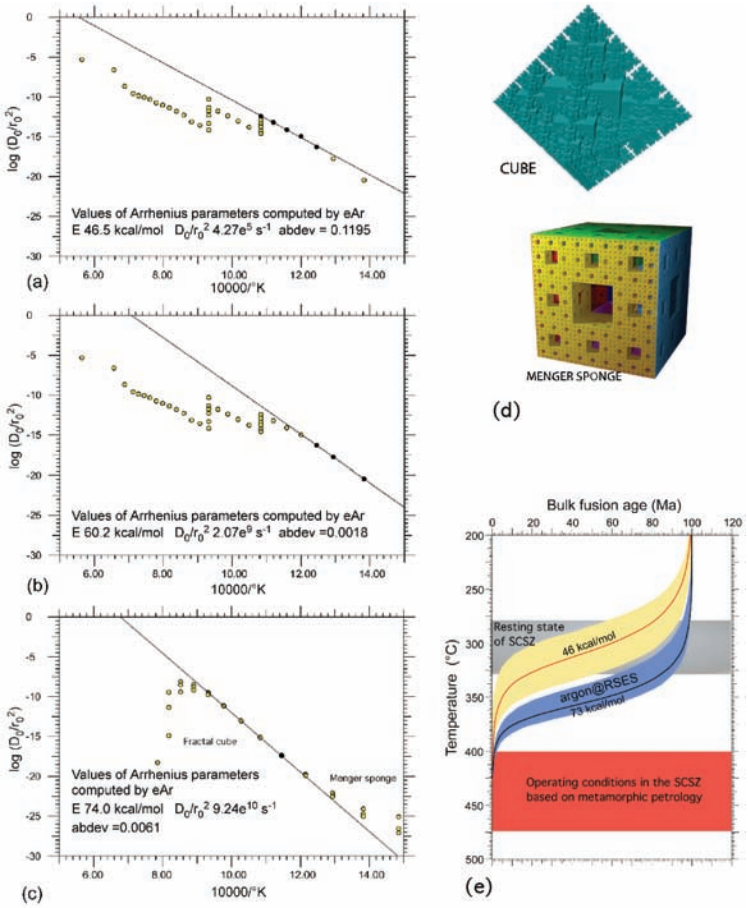

Figure 1. *Arrhenius plots where (a) activation is calculated at 46.5 kcal/mol (Baldwin & Lister 1998). The fundamental asymmetry principle (FAP) has not been followed in this calculation and the activation energy incorrect; (b) when the FAP is applied to this same plot the calculated activation energy is much higher, 60.2 kcal/mol; (c) mathemical calculation using the fractual cube and Menger sponge (d) (http://members.cox.net/fathauerrecent/FractalCrystal.html) (http://en.wikipedia.org/wiki/Menger_sponge) used in the mathematical representation of the Arrhenius plot; (e) A Temperature / Time plot show the region where the shear zone is at rest and where the shear zone operated, temperature calculated from mineral paragenesis.*

Behaviour of allanite during incipient partial melting in the Southern Central Alps

Courtney Gregory[1], Daniela Rubatto[1], Jöerg Hermann[1] and Alfons Berger[2]

[1] *Research School of Earth Sciences, Australian National University, Canberra, ACT 0200, Australia*

[2] *Institute of Geological Sciences, University of Bern, CH-3012 Bern, Switzerland*

The chemical and U-Th-Pb isotopic behaviour of accessory allanite during incipient partial melting was investigated in a field-based study of upper-amphibolite facies migmatites in the southern Central Alps (Switzerland). Orthogneiss and leucosome sampled from the core of the migmatite zone (peak T of ~680-720°C) to its limit (T ~650°C), contained both zircon and allanite, which permitted a comparison of U-Th-Pb systematics in these phases.

Allanite found in orthogneiss showed complex internal zoning (see backscatter electron or BSE image in Fig. 1), suggestive of multi-stage growth. Bright BSE cores with high La/Lu and Th/U and low Eu/Eu* chemical signatures yielded Permian ages and thus were inherited from the pre-Alpine magmatic protolith. In contrast, chemically distinct overgrowths and single grains gave age populations between 30 ± 1 Ma and 23 ± 1 Ma in line with an Alpine metamorphic origin. Textural and inclusion relationships with major melt-formed minerals and their LREE-depletion supports the interpretation that allanite was an anatectic phase. Further evidence is provided by comparing magmatic and metamorphic mineral Eu compositions (Fig. 1).

Plagioclase did not impose a negative Eu anomaly on co-existing metamorphic phases because 80-90 % of the bulk-rock Eu was actually hosted in metamorphic allanite and titanite. To account for this, it is suggested that metamorphic allanite and titanite formed during feldspar breakdown, which would have occurred above the wet solidus for this system (i.e. at T > 650°C).

The inheritance of Permian cores provides first hand evidence for minimal Pb diffusion in allanite during Alpine partial melting (i.e. ~7 million years above 650°C). Importantly, in samples where co-existing zircon had rare or limited metamorphic overgrowths (i.e. at T < 700°C), allanite was the only accessory mineral chronometer that recorded the Alpine event. The U-Th-Pb system in allanite therefore presents a solid, complementary approach for the geochronology of low-temperature (~650-700°C) partial melt processes in the crust.

Accepting allanite as a melt-product, the youngest U-Th-Pb age obtained from a discordant leucosome indicates that the Alpine melting regime lasted over several million years (until 23 Ma) and later than previously accepted. Combined with previous constraints, the prolonged high temperature evolution down to 23 Ma requires a subsequent period of fast cooling (~100 ± 20°C/Ma) for the studied samples.

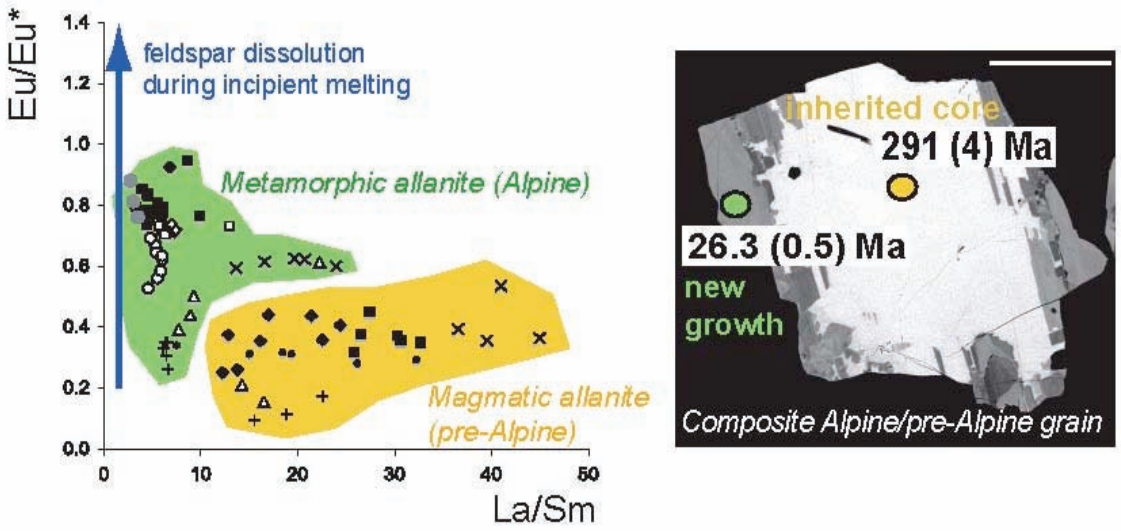
Eu/Eu*
1.4
1.2
1.0
0.8
0.6
0.4
0.2
0.0
feldspar dissolution
during incipient melting
Metamorphic allanite (Alpine)
Magmatic allanite
(pre-Alpine)
0
10
20
30
40
50
La/Sm
Inherited core
291 (4) Ma
26.3 (0.5) Ma
new
growth
Composite Alpine/pre-Alpine grain

Figure 1

An inclusion suite of "granitic" phases within 3.81 Ga tonalite zircons: Restrictions for studying Hadean crustal evolution with detrital zircons

Joe Hiess[1] and Allen P. Nutman[2]

[1] *Research School of Earth Sciences, Australian National University, Canberra, ACT 0200, Australia*

[2] *Institute of Geology, Chinese Academy of Geological Sciences, 26 Baiwanzhuang Road, Beijing 100037, PR China*

Petrogenetic interpretation of Hadean detrital zircons is problematic, because their source rocks are no longer preserved. Tonalites represent the dominant component of Eoarchaean (3500–4000 Ma) crustal rocks and therefore form an important reference point for the interpretation of Hadean detrital zircons, and Earth's earliest crustal evolution.

We conducted an electron microprobe survey of inclusions contained within igneous zircons from the best-preserved ca. 3810 Ma meta-tonalite sample G97-18 from West Greenland. Crystalline inclusions were K-feldspar, plagioclase, quartz, hornblende, biotite, ilmenite and apatite. Additionally, one globular polymineralic inclusion interpreted as crystallised melt occurs at the surface of a polished grain mount (Fig. 1). This consists of plagioclase + quartz + K-feldspar around a biotite lath. Other similar, but rare globular inclusions were seen buried within other zircons below the polished surface. These phases, particularly the presence of K-feldspar and plagioclase in broadly equal amounts, suggest the zircons crystallised from a residual granitic (sensu-stricto) melt, as opposed to a tonalitic melt. SHRIMP U-Pb dating of zircons with inclusions indicates that they grew at ca. 3810 Ma, the accepted igneous age of the rock.

This inclusion suite is compatible with the low Ti-in-zircon temperatures for G97-18 igneous zircon (Hiess et al., 2008). Therefore, low Ti-in-zircon temperatures and "granitic" inclusions reported for Hadean detrital zircons do not necessitate crystallisation from low temperature granites. Such features could also be found within Hadean zircons that crystallised late from a higher temperature zircon-undersaturated melt of tonalitic composition.

Hiess J, Nutman AP, Bennett VC, Holden P (2008) Ti-in-zircon thermometry applied to contrasting Archean igneous and metamorphic systems. *Chemical Geology* **247**: 323-338.

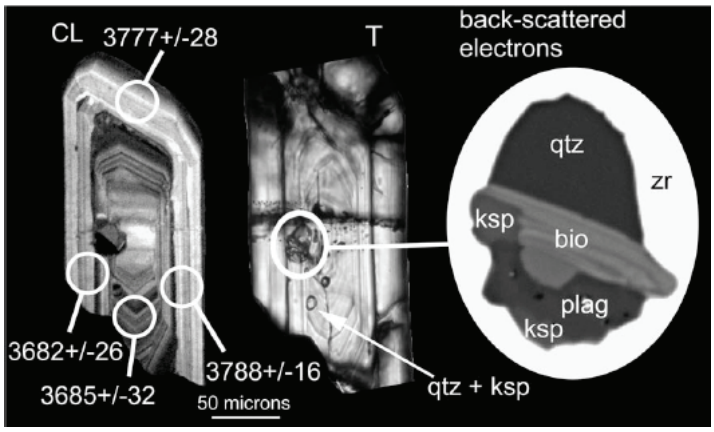

Figure 1. Cathodoluminescence (CL) and transmitted light (T) images for a single globular polymineralic inclusion exposed at the mount surface (at least one more appears to be present at depth in other grains), interpreted as a crystallised melt inclusion. Shown to the right is an enlarged back-scattered electron image of the globular inclusion. Note that the lower edge of the biotite is altered to chlorite. Errors on SHRIMP $^{207}Pb/^{207}Pb$ ages (Ma) are 2_.

Links between abiogenic-methane and gold, indicated by Ar, Ne and Cl in fluid inclusions

M.A. Kendrick1[1], M Honda[2], J.L. Walshe[3] and K.J. Petersen[4]

[1] *The School of Earth Sciences, The University of Melbourne, VIC 3010, Australia*

[2] *Research School of Earth Sciences, Australian National University, Canberra, ACT 0200, Australia*

[3] *CSIRO, ARRC, 35 Stirling Highway, Kensington, WA 6151, Australia*

[4] *School of Earth and Geographical Sciences, The University of Western Australia, WA 6009, Australia*

The processes that mobilise gold through the Earth's crust and concentrate it in ore deposits have been widely debated. Most workers emphasise the importance of CO_2-H_2O fluids and phase separation or wall-rock reaction as depositional mechanisms. However, the possible importance of mantle components and the significance of CH_4-dominated fluid inclusions have been subject to speculation. The Yilgarn Terrane of Western Australia is richly endowed with gold-only ore deposits that have a low concentration of base metals, and are associated with quartz ±carbonate veins in regionally-significant, mid-crustal (3-15 km), shear zones that formed in an arc or back arc setting. Recent mapping of mineral alteration assemblages in the world class St Ives Gold Camp, in Western Australia, has shown high grade gold occurs preferentially at the intersection of 'oxidised' pyrite-magnetite-hematite-anhydrite bearing veins that are dominated by H_2O-CO_2 fluid inclusions; and 'reduced' pyrrhotite-pyrite bearing quartz veins that are dominated by CH_4 fluid inclusions

H_2O- and CO_2-dominated fluid inclusion assemblages have maximum $^{40}Ar/^{36}Ar$ values of ~21,000 (Fig. x-a) and ppb 36Ar concentrations, consistent with the involvement of magmatic fluids. Based on the fluid inclusion abundances, this suggests Cl must be present as HCl in CH_4 as well as NaCl in rare H_2O fluid inclusions. Provided Cl has a lower abundance in CH_4 than in the H_2O-CO_2 fluid inclusions, this measurement also suggests CH_4 has the lowest ^{36}Ar concentration. As wall-rock reaction increases the ^{36}Ar concentration of the volatile phase, this inference precludes a CH_4 source by localised reduction of CO_2. Instead, the high $^{40}Ar/^{36}Ar$ value favours an abiogenic CH_4 origin in the deep-crust or mantle. The Ne isotope data reveal a mantle component in pre- to early-gold pyrites, but the quartz-hosted H_2O and CO_2 fluid inclusions are dominated by atmospheric and crustal Ne (Fig. x-b). If all these fluids had a magmatic origin, this pattern is consistent with the changing style of regional magmatism from bimodal (mafic-flesic) prior to mineralisation to dominantly Ca-poor granite during the main-stage of gold deposition. The maximum $^{21}Ne/^{22}Ne$ value of 0.55 determined for CH_4-dominated fluid inclusions corresponds to the maximum $^{40}Ar/^{36}Ar$ value of ~50,000. The highest $^{21}Ne/^{22}Ne$ values require a source in which U is hosted by a mineral with an O/F value of greater than the upper-crustal average for U minerals. If CH_4 was generated by serpentinisation of deep-crustal mafic intrusions, the Ne data would be consistent with precursor H_2O-CO_2 fluids derived from lower-crustal rocks in which zircon or pitchblende were important U hosts.

These Ar and Ne data suggest CO_2-H_2O was derived from a lower crustal magmatic source and conclusively demonstrate that CH_4 had an independent 'abiogenic' origin. As CH_4 fluid inclusions or graphite are found in many gold-only ore deposits, we suggest that oxidation of abiogenic CH_4, possibly sourced from as deep as the Earth's mantle, has been a critical and overlooked control on the formation of many of the planets largest gold deposits.

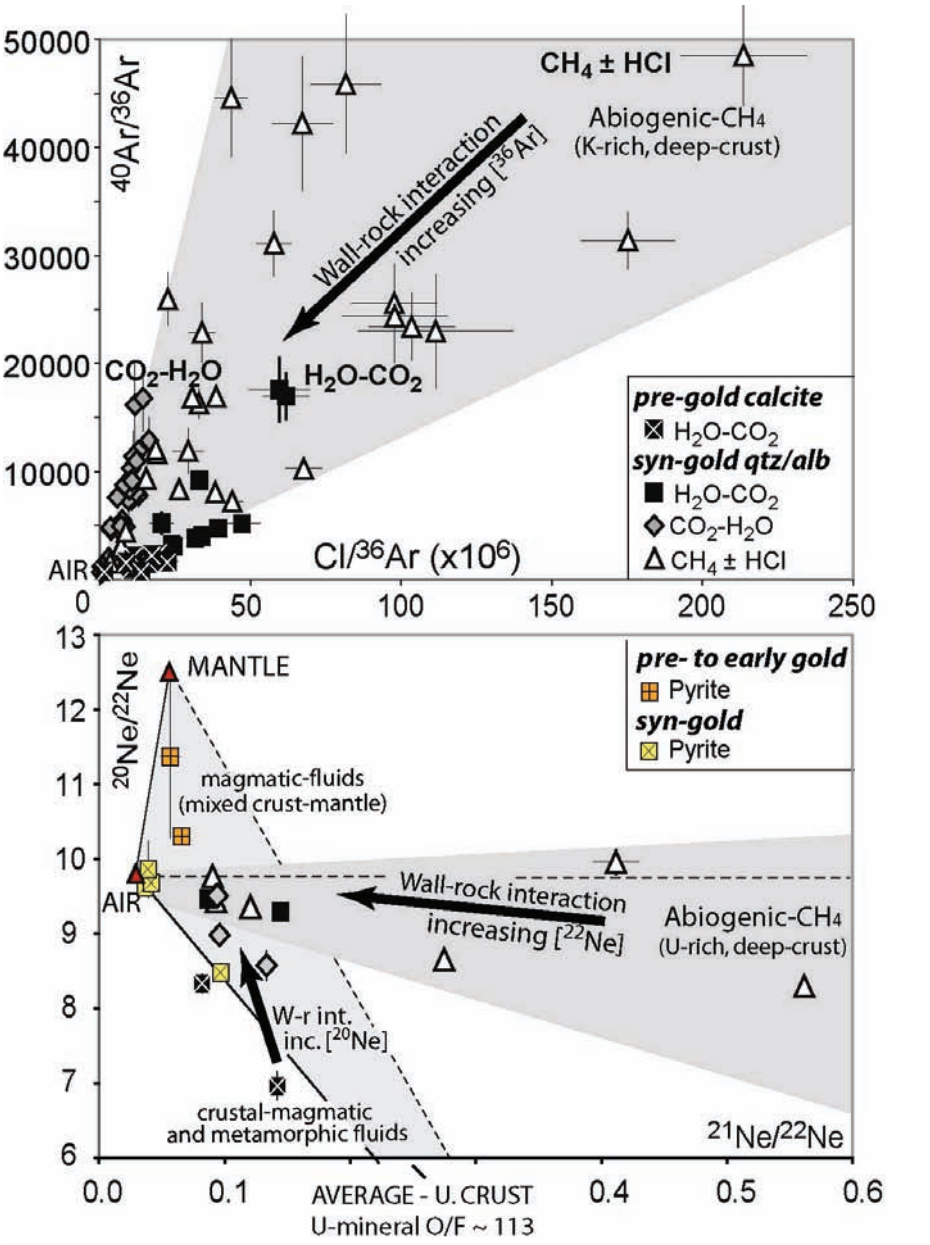

Figure 1. *Fluid inclusion noble gas data for pre- to syn-gold minerals of the St Ives Gold Camp, Western Australia: a) Cl/^{36}Ar versus ^{40}Ar/^{36}Ar; b) ^{21}Ne/^{22}Ne versus ^{20}Ne/^{22}Ne. The high Cl/^{36}Ar values determined for CH_4 fluid inclusions suggest Cl is present as HCl and imply a parts per trillion ^{36}Ar concentration. CO_2-H_2O fluid inclusions have higher ^{36}Ar concentrations. The convergence of mixing trends and increase in ^{36}Ar concentration is interpreted to result from fluid interaction with mafic host-rocks rich in seawater-derived noble gases. Note that few of the deeply-derived fluids have Ne isotope compositions within the light grey envelope that could be explained by mixing atmospheric or mantle Ne with 'average-crustal' Ne. This suggests Ne-isotope heterogeneity in the lower crust; assuming an atmospheric intercept, the best fit slope for CH_4 indicates a source region in which U-minerals have an O/F value of close to the average crustal O/F value of 752.*

Contamination-free biomarker analysis of shales using oxidative microwave digestion

Janet Hope and Jochen J. Brocks

Research School of Earth Sciences, Australian National University, Canberra, ACT 0200, Australia

Surficial contamination of drill core and outcrop samples with anthropogenic hydrocarbons is a common phenomenon and can compromise the analyses of molecular fossils, particularly of lean and very ancient samples. A survey studying the molecular content of the exterior and interior portions of 26 rock samples from a wide range of drill cores and outcrops, found that all samples were surficially contaminated with petroleum products [1]. For compact and impermeable rock samples, surficial contaminants can be removed by trimming of surfaces [1]. However, we demonstrated that this is not possible for fissile and fractured samples where contaminants may have entered fissures and cracks. We tested whether contaminant hydrocarbons can be removed with solvents by extracting intact pieces of diesel stained shale with dichloromethane using an Automated Solvent Extractor (ASE). After 3 extraction cycles only ~40% of the diesel was removed, demonstrating that solvent rinsing does not efficiently eliminate surficial petroleum products. In a second experiment, we subjected diesel stained shale with hot concentrated nitric acid in a microwave digestion oven. This treatment successfully removed 98.5 to 100% of the contaminant hydrocarbons from the shale.

We further tested the microwave digestion technique on a Precambrian shale. Figure 1 shows the hydrocarbons of this sample after heating of the rock in concentrated nitric acid at 180°C for 30 minutes. The treatment successfully removed nearly 100% of all contaminants while the indigenous diamondoid and polyaromatic hydrocarbons were retained. The experiments demonstrate that our oxidative microwave digestion technique is highly efficient for the removal of surficial hydrocarbons and other contaminants.

Brocks J. J., Grosjean E., and Logan G. A. (2008) Assessing biomarker syngeneity using branched alkanes with quaternary carbon (BAQCs) and other plastic contaminants. Geochim. Cosmochim. Acta **72**, 871-888.

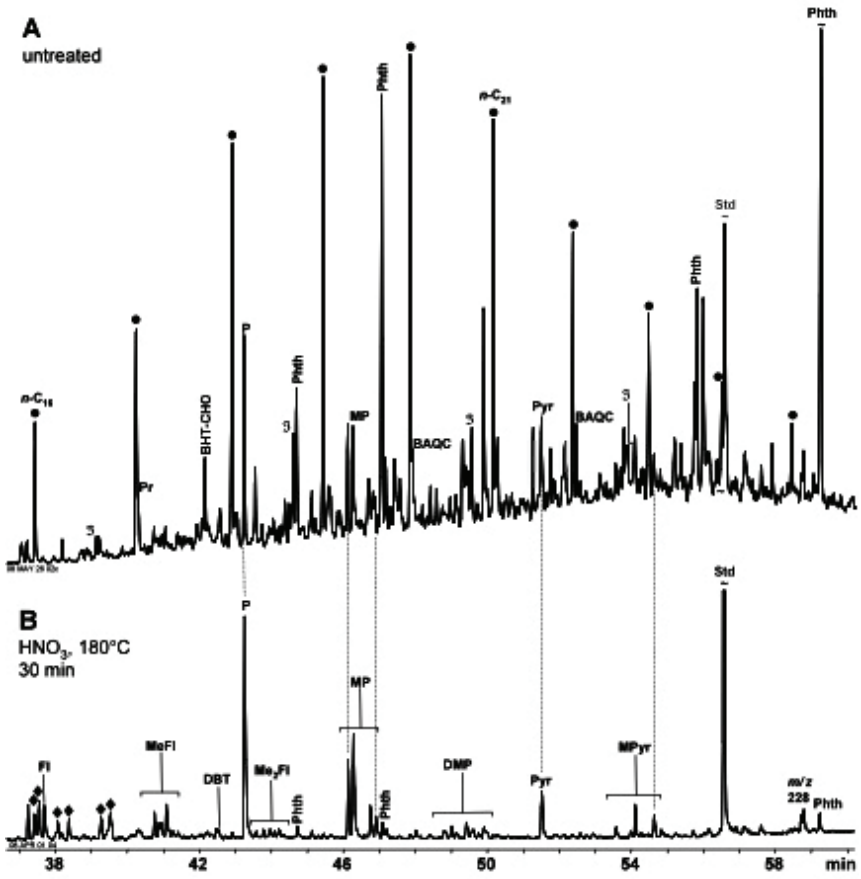

Figure 1. Mass chromatograms of the hydrocarbons of a 1.6 billion year old sample from the McArthur Basin in northern Australia. **(A)** Untreated sample showing a mixture of contaminants and indigenous biomarkers. **(B)** Predominantly indigenous hydrocarbons after treatment of the rock sample with hot nitric acid. BAQC = 5,5-diethylalkanes (branched alkanes with quaternary carbon); BHT-CHO = 3,5-di-tert-butyl-4-hydroxybenzaldehyde; Fl = fluorene; DBT = dibenzothiophene; DMP = dimethylphenanthrenes; MeFl = methylfluorenes; Me2Fl = dimethylfluorenes; MP = methylphenanthrenes; MPyr = methylpyrenes; P = phenanthrene; Phth = phthalates; Pyr = pyrene; Std = standard; ♦ = alkyl diadamantanes; ⬟ = alkylcyclopentanes; • = n-alkanes.

The Mystery of the Missing Solar Wind Oxygen in Lunar Soil

Trevor Ireland[1], Michelle Bannister[2], and Masahiko Honda[1]

[1]*Research School of Earth Sciences, Australian National University, Canberra, ACT 0200, Australia*

[2]*Research School of Astronomy and Astrophysics, Australian National University, Canberra, ACT 0200, Australia*

We have previously reported an isotopically heavy component (5% enriched in ^{17}O and ^{18}O) in the lunar soil that is preserved in the top few hundred nanometers of lunar metal grains. The location of this component appears consistent with the site expected for solar wind oxygen. However, McKeegan and colleagues reported at the Lunar and Planetary Science Conference this year that solar wind appears enriched in ^{16}O. We have carried out measurements on a larger number of grains from a variety of soils in an attempt to elucidate this discrepancy. Many more grains have been discovered with ^{17}O, ^{18}O enrichments with surprisingly few having ^{16}O-rich compositions, and none around the 6% enriched composition reported by McKeegan et al. (2008). Further analyses by Hashizume and Chaussidon (2008) also reveal ^{17}O, ^{18}O-rich compositions in modern lunar soils, while ^{16}O rich compositions in ancient soils are typically mass-dependently fractionated. The question then arises, what happened to the solar wind oxygen on the surface of the Moon.

We have measured Ne isotopic compositions in olivine grains from the lunar soils and these are consistent with solar wind implantation. It should therefore be expected that solar wind oxygen should be present in the surfaces of these grains. We cannot measure olivine grains for implanted solar-wind oxygen because of the high intrinsic concentration of oxygen in olivine. The issue is either the high density of the lunar metals biasing metal grains from exposure to the solar wind, or an issue of preservation. To address this, we will attempt to measure Ne in these metal grains to ascertain their exposure history. The solar wind exposure takes place at lunar surface temperatures of around 100°C. At such temperatures, oxygen diffusion is probably a major issue in retention in the lunar grains, particularly with the high flux of hydrogen carried by the solar wind. These issues will be examined with experiments on oxygen diffusion in metals under appropriate physical conditions.

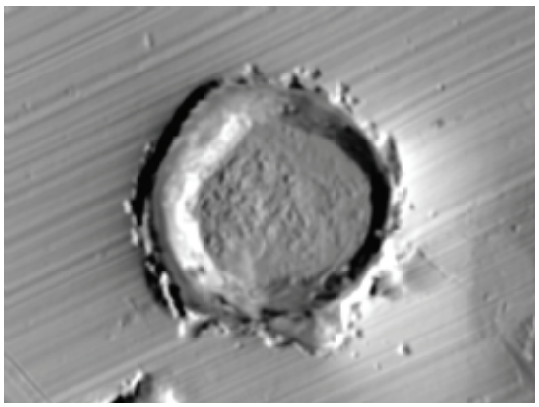

While solar wind appears poorly represented in the metal grains, the component enriched in ^{17}O and ^{18}O is quite widespread. This component may be carried in cometary water, which is expected to have an isotopically heavy composition. The preservation of this component may be related to subsurface reaction of water with Fe metal.

Preliminary zircon U-Pb dating of late Paleozoic granites across the boundary between the Lachlan and New England fold belts

Heejin Jeon[1], Ian Williams[1] and Vickie Bennett[1]

[1] *Research School of Earth Sciences, Australian National University, Canberra, ACT 0200, Australia*

Lachlan and New England fold belts are major tectonic components of eastern Australia. Because the boundary between them is totally covered by the huge Sydney basin, their tectonic relationship is unclear. However, the Carboniferous granites in the north-eastern Lachlan Fold Belt show similarities in age and composition with granites (Chappell et al., 1988) and volcanics (Shaw and Flood, 1993) in the New England Fold Belt. Based on these data, we could infer that the two fold belts might share the same basement and lower crustal structure. Therefore, our purpose is to trace the geologic history and decipher their relationship under the crust through the signature recorded in similar aged granites (Carboniferous to Permian) across the boundary between the Lachlan and New England fold belts. The combination of *in situ* U/Pb - O - Hf isotopic data for zircon will be a key for this study (e.g., Kemp et al., 2007).

Although a large amount of isotopic work on the granites of the Lachlan Fold Belt has been done over 30 years, there is little published work for the Carboniferous granites. Zircon from the Oberon, Bathurst and Gulgong batholiths has been dated. The ages of the granites dated so far range from ~340 to ~330 Ma. There is no simple age trend north to south, but the granites immediately west of Lithgow do appear to become younger from west to east.

Zircon has also been studied from the Banalasta (~290 Ma) and Inlet (~250 Ma) granites of the Bundarra and Moonbi supersuites, respectively, in the New England Fold Belt. Zircons of Banalasta show Carboniferous cores around 330 Ma old, while those of Inlet have no old cores at all. These preliminary results are not enough to conclude, but a beautiful story would be envisaged soon because O and Hf isotopic analyses for dated zircon grains are in progress now.

Shaw, S.E. and Flood, R.H., 1993. Carboniferous magmatic activity in the Lachlan and New England Fold Belts. In: Flood P.G. & Aitchison J.C. eds. New England Orogen eastern Australia NEO'93 Conference, pp. 113–121. University of New England, Armidale.

Kemp, A.I.S., Hawkesworth, C.J., Foster, G.L., Paterson, B.A., Woodhead, J.D., Hergt, J.M., Gray, C.M. and Whitehouse, M.J., 2007, Magmatic and Crustal Differentiation History of Granitic Rocks from Hf-O Isotopes in Zircon, *Science*, **315**: 980-983.

Chappell, B.W., White, A.J.R., and Hine, R., 1988, Granite provinces and basement terranes in the Lachlan Fold Belt, southeastern Australia, *Australian Journal of Earth Sciences*, **35**, 505-521.

Figure 1. *Typical feature of Bathurst and Gulgong batholiths that contain big pink feldspar crystals.*

Evolution of the Angrite Parent Body and Concordancy of Isotope Chronometers in Angrite Meteorites

Seann J. McKibbin[1], Trevor R. Ireland[1], Yuri Amelin[1], Hugh St. C. O'Neill[1]

[1] *Research School of Earth Sciences, Australian National University, Canberra, ACT 0200, Australia*

The small achondrite meteorite clan classified as angrites have unique mineralogy, chemistry and oxygen isotopic compositions that strongly suggest they share a single parent body. They come in two broad petrologic groups: quenched 'volcanics' such as D'Orbigny and Sahara 99555, and 'plutonics/metamorphics' like LEW 86010. They are particularly suited to isotopic dating using the Pb-Pb chronometer and the short-lived (extinct) Mn-Cr system ($^{53}Mn \rightarrow {}^{53}Cr$, $t_{1/2}$ = 3.74 My) from which age differences between meteorites can be obtained. The angrites have yielded ages in these systems spanning a period of Solar System history critical to understanding of protoplanet formation (~4564.5 to ~4557.5 Ma from Pb-Pb).

However, concordancy between the two decay systems has been poor, with Pb-Pb isotopes recording up to 7 My of evolution between early volcanic and later plutonic varieties, while the Mn-Cr ages preserve a difference in ages of only ~5.5 My for the same meteorites [1]. To investigate this discrepancy, the Mn-Cr systematics of D'Orbigny and Sahara 99555 have been reinvestigated using the SHRIMP-RG ion-probe. Results support an early Mn-Cr age for both meteorites, and reinforce the discordancy between D'Orbigny and LEW 86010 in the Mn-Cr/Pb-Pb systems. However, the new result for Sahara 99555, along with improved agreement in the community over its Pb-Pb crystallisation age, suggests that this meteorite is concordant when compared with the younger LEW 86010 (Figure 1). This means that the two meteorites sample a common isotopic reservoir evolving in time, with no complications from diffusive closure occurring in different minerals at different times, and no later disturbance.

The emerging consensus is that angrite basalts crystallised from lava flows or a magma ocean around 4564.5 Ma, and magmatism and thermal activity continued until at least 4557.5 Ma as the protoplanet cooled. Further work will centre on angrites NWA 4590 and NWA 4801, which have not yet been dated using the Mn-Cr system.

Wadhwa M, Amelin Y, Bizzarro M, Kita N, Kleine T, Lugmair G, Yin Q (2007) Comparison of short-lived and long-lived chronometers: Towards a consistent chronology of the early Solar System. *Workshop on the Chronology of Meteorites and the Early Solar System* pp. 173. LPI Contribution No. 1374, Lunar and Planetary Institute, Houston.

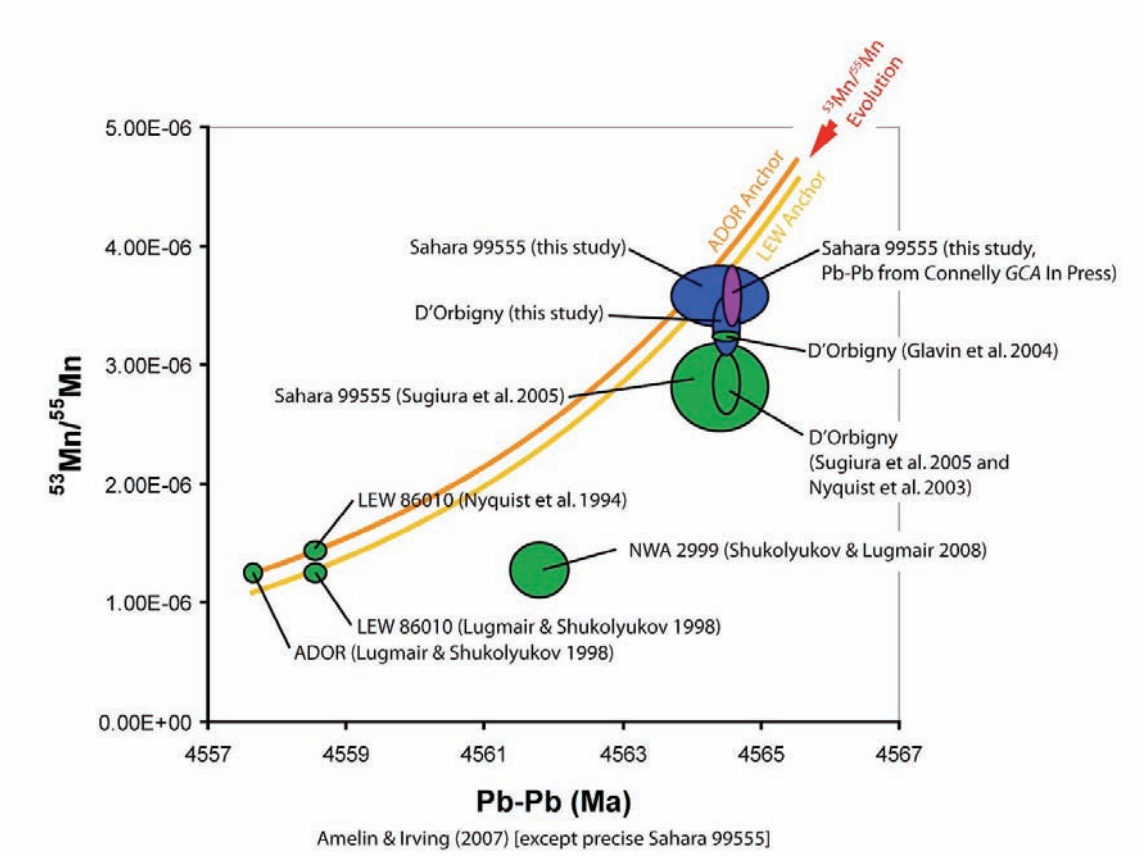
$^{53}Mn/^{55}Mn$ Evolution
ADOR Anchor
LEW Anchor
Sahara 99555 (this study)
Sahara 99555 (this study, Pb-Pb from Connelly GCA In Press)
D'Orbigny (this study)
D'Orbigny (Glavin et al. 2004)
Sahara 99555 (Sugiura et al. 2005)
D'Orbigny (Sugiura et al. 2005 and Nyquist et al. 2003)
LEW 86010 (Nyquist et al. 1994)
NWA 2999 (Shukolyukov & Lugmair 2008)
LEW 86010 (Lugmair & Shukolyukov 1998)
ADOR (Lugmair & Shukolyukov 1998)
5.00E-06
4.00E-06
3.00E-06
2.00E-06
1.00E-06
0.00E+00
$^{53}Mn/^{55}Mn$
4557
4559
4561
4563
4565
4567
Pb-Pb (Ma)
Amelin & Irving (2007) [except precise Sahara 99555]

Figure 1.

Copper concentrations in silicate mineral phases of the Boggy plain zoned intrusion

Jung Woo Park[1] and Ian H. Campbell[1]

[1] *Research School of Earth Sciences, Australian National University, Canberra, ACT 0200, Australia*

Understanding copper geochemistry in an evolving magmatic system is important because it may give the information about the relationship between copper mineralization and the magma and the variation of physical and geochemical condition, e.g. oxidation state and sulfur and water contents, of the magma.

Copper is a distinctively chalcophile element and therefore it strongly partitions into sulfide melts if the magma is S-saturated. However, depending on the physical and chemical condition of magma, dissolved copper in the magma as Cu^{+1} or Cu^{+2} can be trapped in a silicate mineral as an intrinsic element. Cu^{+2} is likely to be substituted for Fe^{+2} or Mn^{+2} in Fe-Mg silicates and Cu^{+1} for Na^{+1} in feldspar or hornblende because of their similar charge and radius (Stanton, 1994). Ewart et al. (1973) obtained 11-53 ppm copper in pyroxenes and 0-27 ppm in plagioclases of the Tonga-Kermadec volcanic island chain and found the copper levels in the plagioclases have positive correlation with whole-rock copper concentration. Wedepohl (1974) lists mean copper contents of 9.4-18, 9-17 and 2-45 ppm in amphibole, biotite and plagioclase of granitic rocks respectively.

Copper concentrations in silicate minerals were analyzed by LA-ICPMS in order to document variations in copper contents in the selected minerals during differentiation of the Boggy Plain magma, and their relationship with whole rock copper concentration.

Copper concentration in plagioclase are slightly higher in the mafic rocks of $FeO^t+MgO>14.5$ per cent, and copper contents of the northern gabbro which contains the highest whole rock copper concentration is distinctively enriched in copper compared with the felsic rocks of Boggy Plain zoned pluton (Figure 1). Except for several anomalously high copper values, the majority of them of plagioclases from outer/inner granodiorite and adamellite ($FeO^t+MgO<14.5$ %) are lower in order of 2-5 than them of mafic rocks. The mean copper contents of intermediate-felsic rocks range from 0.2 to 1 ppm showing a flat trend along with further magma differentiation. The Average values of copper concentration in plagioclase of Boggy Plain zoned pluton (0.18-2.2 ppm) is significantly less than that of the El Abra-Pajonal suite intrusion (0.4-69.1 ppm; Dianne 2008). This difference between the two suites can be partly explained by higher whole rock copper contents (12.5-5493 ppm) of the El Abra-Pajonal suite intrusion.

In order to estimate the amount of copper hosted by silicates phase, copper concentrations in other major silicate minerals are measured and mass balanced. This analysis yields silicate selective copper abundances ranging from 0.5 to 7.3 percent of whole-rock copper abundance. It indicates that the subtraction of copper by silicate crystallization is insufficient for the observed decrease of whole-rock copper in Boggy Plain rocks of $FeO^t+MgO<14.5$ per cent and the additional mechanism is required, e.g. the formation of Cu-bearing sulfide or Cu loss in vapor phase.

Ewart F, Bryan W, Gill, J. (1973) Mineralogy and geochemistry of the younger volcanic islands of Tonga, SW Pacific. *Journal of Petrology* **14**: 429-465

Dianne LV (2008) The geology, geochemistry and geochronology of the El Abra mine, Chile, and the adjacent Pajonal-El Abra suite of intrusions, Unpublished Ph.D. thesis, The Australian National University, 777 p.

Stanton RL (1994) Copper. In *Ore elements in arc lavas*: New York, Oxford University Press, p. 53-74.

Wedepohl, K.H. (1974). Copper. In *Handbook of geochemistry* (ed. K. H. Wedepohl). Springer-Verlag, Berlin.

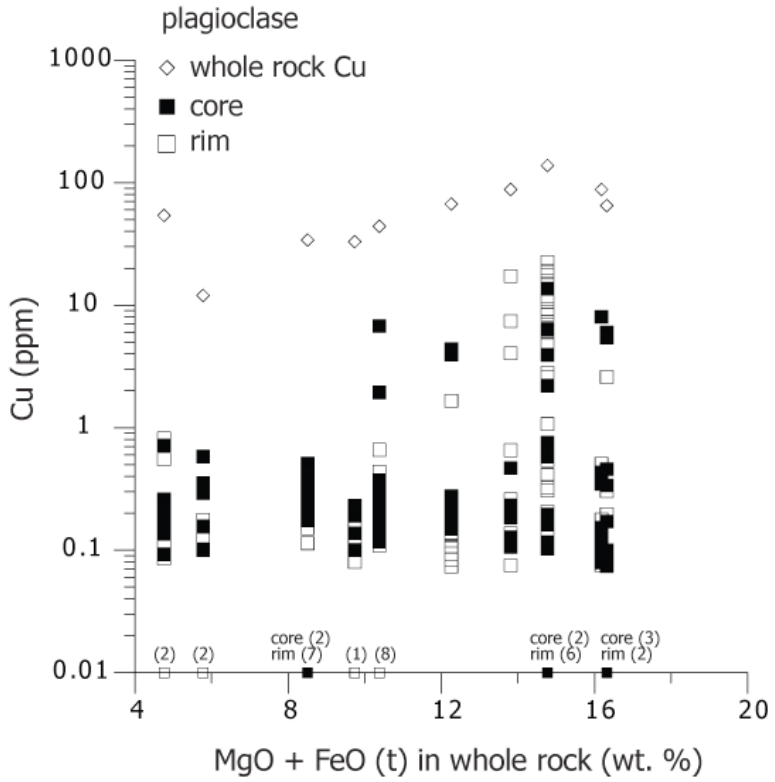

Figure 1. *Copper concentration in plagioclase of the Boggy Plain zoned pluton. Values below detection limits are on the x-axis and numbers in the brackets are number of analysis points of them.*

Dating the allanite-monazite metamorphic reaction

Daniela Rubatto[1], Courtney Gregory, Emilie Janots and Ioan Gabudianu- Radulescu

[1] *Research School of Earth Sciences, Australian National University, Canberra, ACT 0200, Australia*

[2] *Institute of Geological Sciences, University of Bern, Bern, Switzerland*

[3] *Institute for Geography and Geology, Copenhagen, Denmark*

U-Pb geochronology is one of the most widely used methods for the investigation of the timing of crustal processes. One main limitation of the application of U-Pb geochronology to metamorphism is the lack of direct links between the age measured and the conditions at which the dated minerals formed. In this respect, dating metamorphic reactions that can be placed in pressure-temperature space is particularly appealing.

One metamorphic reaction between U-Pb minerals that has been widely reported is the mutual replacement of allanite and monazite (figure 1 and 2). With the recent set-up of a protocol for accurate dating of allanite by SHRIMP ion microprobe (Gregory et al. 2007) it has become possible to date this reaction in-situ. We applied this method to the two geological settings where allanite-monazite reactions are most commonly documented.

1) Monazite replacing allanite is observed in prograde greenschist to amphibolite facies metamorphism of metapelites in the Central Alps (Fig. 1). Petrographic observations and thermobarometric calculations allow placing the reaction at T = 560-580°C, whereas initial allanite formation occurred at T = 430-450°C. In-situ SHRIMP U-Th-Pb dating of allanite (31.5 ± 1.3 and 29.2 ± 1.0 Ma) and monazite (18.0 ± 0.3 and 19.1 ± 0.3 Ma) constraints the time elapsed between 430-450°C and 560-580°C, which implies an average heating rate of 15-8 °C/My (Janots et al., in press).

2) During subduction-related metamorphism, the replacement of monazite by allanite is associated to increasing pressure. This is observed in the silvery micaschists of the Gran Paradiso Massif, Western Alps where microstructural relationships among major and accessory minerals indicate the following prograde sequence of U-Th bearing accessory minerals: florencite -> monazite -> allanite (Fig. 2). Thermobarometric calculations indicate that the allanite-bearing peak assemblage was stable at P = 2.3 ± 0.4 GPa and T = 570 ±30 °C, while monazite formed earlier at pressures over 2.0 GPa. SHRIMP dating of allanite yielded 34.5 ± 0.8 Ma, interpreted as the age of the high-pressure metamorphic peak. Prograde monazite yielded an age of 37.5 ± 0.9 Ma, implying a minimum duration of ~3 Ma for the Alpine subduction event (Gabudianu Radulescu et al., in press).

Gregory C, Rubatto D, Allen C, Williams IS, Hermann J, Ireland T (2007) Allanite micro-geochronology: a LA-ICP-MS and SHRIMP U-Th-Pb study. *Chemical Geology* **245**:162-182

Janots E, Engi M, Rubatto D, Berger A, Gregory C, Rahn M (in press) Metamorphic rates in collisional orogeny from in situ allanite and monazite dating. *Geology*

Gabudianu Radulescu I, Rubatto D, Gregory C, Compagnoni R (in press) The age of HP metamorphism in the Gran Paradiso Massif, Western Alps: a petrological and geochronological study of "silvery micaschists". *Lithos*

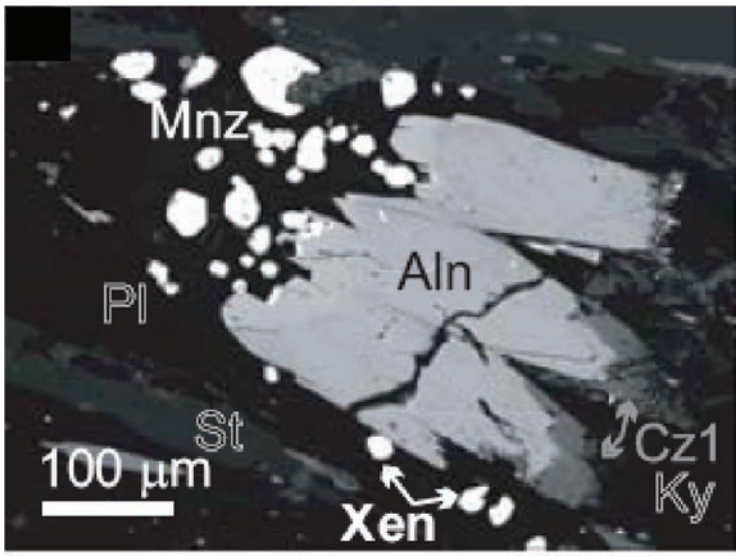

Figure 1.

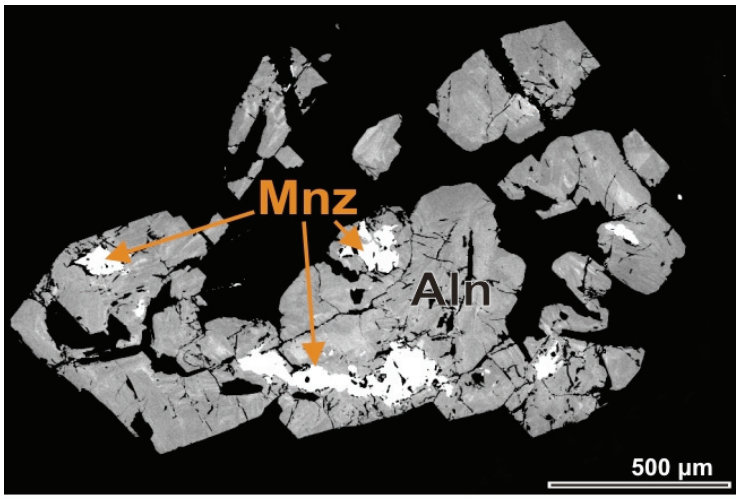

Figure 2:

Molecular Fossils of the Neoproterozoic-Cambrian Interval: Lipid Biomarker Geochemistry and Ancient Microbial Ecosystems

Richard Schinteie[1], Jochen J. Brocks[1]

[1] *Research School of Earth Sciences, Australian National University, Canberra, ACT 0200, Australia*

Numerous microorganisms survive and flourish in environments that are often considered "extreme" from an anthropogenic view point. Such environments include hydrothermal vents, hydrocarbon seeps, and acid hot springs. Hypersaline environments are another type of setting where microorganisms live under salinity regimes exceeding those of seawater. In order to understand the evolution of ecosystems from such settings, Neoproterozoic and Cambrian halite-bearing evaporites were investigated for their lipid biomarker content. This time frame encompasses tremendous environmental and biotic changes (e.g., major glaciations, oxygenation of the deep ocean, evolution and radiation of microorganisms, and the first appearance of animals). While previous work identified potential halophiles in the Cambrian and Precambrian, we aim to present a more detailed investigation of biotic evolution over a significant period of geologic time.

In order to assess changes in microbial ecosystems over geologic time, it is important to focus on a variety of different environmental settings. Dissimilar environments offer different ecological niches which organisms can exploit. Such niches may respond differently to environmental changes over time.

Thus far, the results look very promising and has let to the discovery of lipid biomarkers that are over 1 billion years old. I am also trying to investigate rock samples from that period that originated in shallow water, particularly hypersaline facies. So far, most investigations concentrated on deep water facies. I have collected rock samples from drill cores (Figure 1) held at Australian drill core repositories. These rocks are from shallow water facies and contain numerous evaporate (salt-bearing) sequences.

A major theme in any chemical work dealing with ancient life is the interpretation of molecules as original contemporaneous components of a rock sample or as more recent additions in the form of contamination. Therefore, I investigated techniques aimed at removing potential contaminants from rock samples. Thus far, the techniques have worked very well and helped me determine which biomarkers were likely derived from the Precambrian-Cambrian interval and which samples are contaminants (e.g. from the use of drilling fluids, fingerprints etc).

Figure 1.

In situ oxygen isotopic analyses of zircon from granites of the Bega Batholith, south-eastern Australia

Ian S. Williams[1] and Bruce W. Chappell[2]

[1] *Research School of Earth Sciences, Australian National University, Canberra, ACT 0200*

[2] *School of Earth and Environmental Sciences, University of Wollongong, Wollongong, NSW 2522*

The oxygen isotopic composition of granites is a sensitive indicator of both their source materials and the low-temperature processes that occurred as or after the magma cooled. Oxygen isotopes have been used extensively, particularly in the USA, for studies of granite genesis. Granite O isotopic compositions are normally measured on whole rocks or major minerals, but these are susceptible to late alteration. A major recent advance in the study of granite O isotopes has been the recognition that the O isotopic composition of zircon accurately reflects the O composition of the melt from which it precipitated (e.g. Monani & Valley, 2001). Because zircon grains are commonly strongly zoned and in many cases contain older cores, the ideal method of measuring the isotopic composition of the melt-precipitated components is *in situ* analysis by secondary ion mass spectrometry.

Over the past few years, the SHRIMP II ion microprobe has been progressively upgraded for the high precision isotopic analysis of light elements, including O. In addition, sample mounting procedures have been modified and analytical protocols developed to minimise variations in instrumental mass fractionation (Ickert et al., 2008). The resulting ability to measure the O isotopic composition of single 25 µm spots on a crystal with a precision and accuracy of better than 0.4‰ has opened up a range of new opportunities for the study of granite petrogenesis in Australia.

The Bega Batholith, SE of Canberra, consists of ~130 plutons of I-type granite covering ~8900 km^2. These have been grouped into a series of suites that show remarkably systematic regional changes in chemical and isotopic composition. East to west, across the elongation of the suites and the batholith as a whole, in granites of any given general bulk composition there is, for example, a systematic decrease in Na, Sr, (Al, P) and increase in Ca, Sc, (Rb, V). East to west, the granites become more isotopically evolved, initial $^{87}Sr/^{86}Sr$ rising from 0.704 to 0.709 and ϵNd falling from +4.3 to -8.7 (Chappell et al., 1990). It is generally agreed that these changes are due to a westerly increasing sediment component in the magmas, but whether that originates in the lower or upper crust or mantle, and whether the magmas also contain a juvenile mantle component, are matters of vigorous debate.

The early O isotopic work done on eastern Australian granites by O'Neil and Chappell (1977) and O'Neil et al. (1977) showed a clear distinction between the whole-rock O isotopic compositions of the I- and S-type granites, consistent with the proposed contrasts in their source materials. Later Chappell et al. (1990) reported mean whole rock $d^{18}O$ values for seven supersuites from the Bega Batholith ranging from 8.2 to 10.0‰. The range in individual granite compositions exceeded 6‰, some values reflecting the effects of late magmatic and/or post emplacement interaction with meteoric water.

A major study of the age and O isotopic composition of selected granites from the Bega Batholith is now nearing completion. Analyses of over 600 zircons from 30 plutons representing a range of bulk chemical compositions, mainly from the eastern and western sides of the batholith, has shown that there is a broad trend for the granites to be younger in the east than in the west. Contrary to expectations, however, with a few notable exceptions, the mean isotopic composition of the O in the granite zircons shows no clear regional trend. The range of mean O isotopic

compositions of the zircons is much smaller than the range of whole rock compositions, consistent with the expectation that the zircon isotopes are much more resistant to alteration than those in the whole rock, thereby more closely reflecting the original O isotopic compositions of the magmas. The radiogenic and stable isotopic systems in the granites appear to be for the most part decoupled.

The next stage of this project will be to measure the Hf isotopic compositions of the same spots on the same grains as have been analysed for O. In combination with the O isotopes, this is expected to give a clearer indication of the relative contribution of bulk juvenile and crustal components to the magmas.

Chappell, B.W., Williams, I.S., White, A.J.R. & McCulloch, M.T. (1990) Excursion Guide A-2, Granites of the Lachlan Fold Belt. *BMR Record* **1990/48**: 93 pp.

Ickert, R.B., Hiess, J., Williams, I.S., Holden, P., Ireland, T.R., Lanc, P., Schram, N., Foster, J.J. & Clement, S.W. (2008) Determining high precision, in situ, oxygen isotope ratios with a SHRIMP *II*: Analyses of MPI-DING silicate-glass reference materials and zircon from contrasting granites. *Chemical Geology* **257**: 114–128.

Monani, S. & Valley, J.W. (2001) Oxygen isotope ratios of zircon: magma genesis of low d18O granites from the British Tertiary Igneous Province, western Scotland. *Earth and Planetary Science Letters* **184**: 377–392.

O'Neil, J.R. & Chappell, B.W. (1977) Oxygen and hydrogen isotope relations in the Berridale batholith. *Journal of the Geological Society, London* **133**: 559-571.

O'Neil, J.R., Shaw, S.E. & Flood, R.H. (1977) Oxygen and hydrogen isotopic compositions as indicators of granite genesis in the New England Batholith, Australia. *Contributions to Mineralogy and Petrology* **62**: 313-328.

Earth Environment

As for other parts of the School, the size of the Group increased substantially due to the amalgamation of RSES with the former Department of Earth and Marine Sciences. Several members of staff joined the Group [De Deckker, Ellis [partim], Opdyke and Young] together with their students and technical staff.

Members of the Earth Environment group undertake research on environmental and climate change with particular emphasis on the interactions between humans and the environment. The group specialises in the development of diagnostic environmental proxies within an absolute chronologic framework that spans a few decades to several hundred thousand years of Earth history. The purpose is to document and understand past changes that have particular relevance to help predicting future ones. With the considerable current awareness and concern about environmental changes, the relevance of the group's research is paramount and of direct relevance to society. The future of the Great Barrier Reef is one of these concerns with biogenic carbonate build ups and ocean acidification.

Our researchers and their students and collaborators [Eggins, McCulloch, Opdyke, Trotter and Walther] are involved in growing organisms such as the marine microscopic, calcitic foraminifera under controlled conditions and also determining changes in calcification and temperature in shallow and deep-sea corals. Several of those people are also conducting research to determine proxies for pH changes in the oceans. Experimental research, monitoring and data gathering dealing with silica budgets in the Southern Ocean are the concern of other research teams [Ellwood and Wille]. Gagan, Treble and Ayliffe are involved in investigations on speleothem spanning different ages with the aim of determining past climatic signals. Some of that work concerns links between human evolution and climate in Indonesia. Gagan, Sosdian and students are also involved in isotopic analyses on shallow water corals from a variety of localities.

De Deckker continues his work on Holocene sequences, both from marine and lacustrine origins using biogenic carbonates, and is also involved in fingerprinting the geochemistry and microbiology of aeolian dust.

Another aspect of the Group's research deals with human impacts on environment, across very different time scales. Of principal concern is the impact of terrigenous sediments and nutrients on reefal systems [McCulloch and Trotter] and in estuaries [Ellis] over short time scales. Grün and colleagues [Aubert and Eggins] deal with much longer time scales and on sites that are important to cultural and environmental history such as the Willandra Lakes World Heritage area, in particular, developing new techniques for dating human teeth and bones.

Landscape evolution is also an important focus of several members of the Group. Pillans, Fitzsimmons and Barrows are further developing dating techniques, such as palaeomagnetism, optically stimulated luminescence and cosmogenic nuclides to characterise geomorphic changes, denudation and weathering changes.

In situ oxygen isotope analysis of faunal material using a secondary ion micro-probe: a new tool for palaeoecology and archaeology.

Maxime Aubert[1], Ian Williams[1], Rainer Grün[1], Tegan[1] Kelly, Ian Moffat[1] and Marie-Hélène Moncel[2]

[1]*Research School of Earth Sciences, Australian National University, Canberra, ACT 0200, Australia*
[2]*Département de Préhistoire Muséum National d'Histoire Naturelle 1 Rue René Panhard, 75013 Paris, France*

We have applied *in situ* oxygen isotope analysis on Neanderthal and herbivore teeth from the archaeological site of Payre as well as fossil fish otoliths from Australia. The high resolution of the oxygen isotope analysis allows weekly to bi-weekly resolution of human teeth. We observed large variations in the oxygen isotopic composition in the enamel of herbivore teeth, which were on a scale expected from seasonal variations. The range of isotopic variations in Neanderthal tooth enamel was much smaller, perhaps reflecting a more restricted range of diet and/or more uniform sources of drinking water when the teeth were growing. The application of fish otoliths from the Australian Willandra Lakes World Heritage area showed significant isotopic variations indicating seasonal variations but also a general trend towards heavier oxygen isotopes, which may be due to an enrichment in heavy isotopes as a result of increased evaporation (Fig 1). We will pursue with the oxygen isotope research on fish otoliths as these seem ideal archives of past environmental conditions.

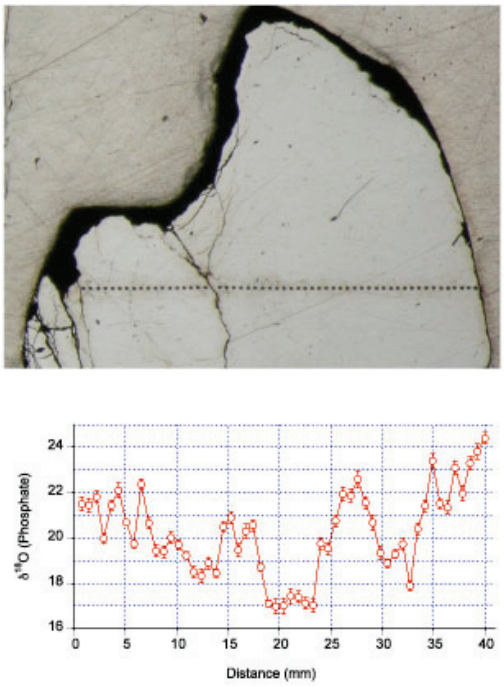

Figure 1. *Oxygen isotopic compositions of a fossil otolith from the Australian Willandra Lakes World Heritage area showing a general trend to heavier oxygen isotopes, indicating an enrichment in heavy isotopes due to increased evaporation*

Past glacial cycle monsoon variation recorded in speleothems from Flores, Indonesia.

L. K. Ayliffe[1], M. K. Gagan[1], M. T. McCulloch[1], G. E. Mortimer[1], J-x. Zhao[2], J. Hellstrom[4], R. N. Drysdale[3], S. Lewis[1], W. S. Hantoro[5], B. W. Suwargadi[5]

[1] *Research School of Earth Sciences, The Australian National University, Canberra, ACT 0200, Australia.*
[2] *Radiogenic Isotope Laboratory, Centre for Microscopy and Microanalysis, University of Queensland, St. Lucia, Queensland 4072, Australia.*
[3] *Environmental and Climate Change Research Group, University of Newcastle, Callaghan, NSW 2308, Australia.*
[4] *School of Earth Sciences, The University of Melbourne, Victoria 3010, Australia.*
[5] *Research and Development Center for Geotechnology, Indonesian Institute of Sciences, Jalan Cisitsu No. 21/154 D, Bandung 40135, Indonesia.*

Tropical speleothems are ideal archives of changes in past rainfall as they can be dated precisely with the U-Th technique and their $d^{18}O$ values can be interpreted in terms of rainfall intensity as tropical rainfall $d^{18}O$ values are inversely proportional to rainfall amount (Dansgaard, 1964). Here we present some preliminary $d^{18}O$ results over the past ~90ka from speleothems from the island of Flores, Indonesia. Located at the southern-most extent of the Intertropical Convergence Zone (ITCZ) in the Austral summer and just within the current southern boundary of the Western Pacfic Warm Pool (WPWP) Flores is ideally situated to record changes in each of these major climate systems.

Several stalagmites and flowstones were collected from deep within Liang Luar Cave (8°32'S, 120°27'E) in 2006 and 2007. Oxygen isotope results of two stalagmites and two flowstone cores are shown in Figure 1. As can be seen good agreement is observed between the oxygen isotopes of the faster growing stalagmites and the much slower growing flowstones where they overlap in age. This suggests that speleothem calcite is being deposited under conditions of near isotopic equilibrium in this cave environment.

Although much work still remains to firmly establish the chronology of the >50ka flowstone record, some interesting trends are emerging from the younger portion of our speleothem record. In contrary to what might be expected, monsoon intensity appears not markedly reduced during past cool phases such as the LGM and stage 3 compared to the Holocene. Rather at times of lowered sea level, monsoon intensity appears more directly coupled to southern hemisphere insolation changes compared to times of high sea level, Fig. 1. This effect could be the result of increases in the degree of continentality experienced at times of low sea level, and consequent greater impact of insolation changes on monsoon strength.

Dansgaard W. (1964) Stable isotopes in precipitation. *Tellus* **16**:436-468
Sturman A, Tapper N. (1996) *The Weather and Climate of Australia and New Zealand*. Oxford University Press: Oxford

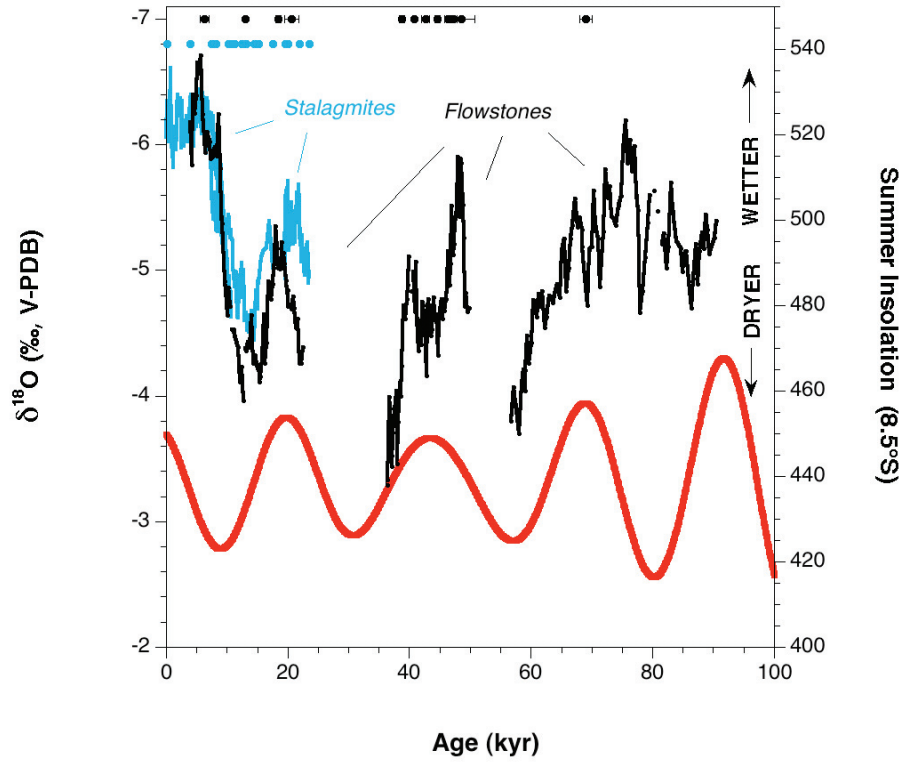

Figure 1. *Speleothem d^{18}O records from Flores (8°32'S, 120°27'E) (stalagmites (blue) & flowstones (black)) compared with summer insolation at 8.5°S (red). d^{18}O values are not corrected for the effects of changes in global ice volume or regional temperatures. Ice volume changes would amount to corrections of ~+1‰ (at 20ka) and ~+0.6‰ (at 50k) to speleothem calcite d^{18}O values. Temperature reductions of ~2-3.5°C (such as was likely experienced during the LGM at the site) would also result in further corrections of +0.4‰ to +0.7‰ calcite d^{18}O values.*

Geochemical and microbiological fingerprinting of airborne dust that fell in Canberra, Australia in October 2002

Patrick De Deckker[1], Raeid M. M. Abed[2], Dirk de Beer[2], Kai-Uwe Hinrichs[3], Tadhg O'Loingsig[4], Enno Schefuß[3], Jan Berend Stuut[3], Nigel J. Tapper[4] and Sander van der Kaars[5]

[1] *Research School of Earth Sciences, The Australian National University, Canberra ACT 0200, Australia*
[2] *Max Planck Institute for Marine Microbiology, Celsiusstraße 1, 28359 Bremen, Germany*
[3] *Department of Geosciences & MARUM - Center for Marine Environmental Sciences, University of Bremen, D-28334 Bremen, Germany*
[4] *School of Geography and Environmental Science, Monash University Vic 3800, Australia*
[5] *Department of Palynology and Climate Dynamics, Albrecht-von-Haller-Institute for Plant Sciences, University of Göttingen, Untere Karspüle 2, 37073 Göttingen, Germany*

During the night of October 22-23, 2002, a large amount of airborne dust fell with rain over Canberra, located some 200 km from Australia's east coast, and at an average altitude of 650m. It is estimated that during that night about 6 $g.m^{-2}$ of aeolian dust fell. We have conducted a vast number of analyses to "fingerprint" some of the dust and used the following techniques: grain size analysis, SEM imagery, major, trace and rare earth elemental, plus Sr and Nd isotopic analyses, organic compound analyses with respective compound-specific isotope analyses, pollen extraction to identify the vegetation sources, molecular cloning of 16S rRNA genes in order to identify dust bacterial composition. DNA analyses show that most obtained 16S rRNA sequences belong mainly to three groups: *Proteobacteria* (25%), *Bacteriodetes* (23%), and *gram-positive bacteria* (23%). In addition, we investigated the meteorological conditions that led to the dust mobilisation and transport using model and satellite data.

Grain sizes of the mineral dust show a bimodal distribution typical of proximal dust, rather than what is found over oceans, and the bimodal aspect of size distribution confirms wet deposition by rain droplets. The inorganic geochemistry points to a source along/near the Darling River in NW New South Wales, a region that is characteristically semi-arid, and both the organic chemistry and palynoflora of the dust confirm the location of this source area. Meteorological reconstructions of the event again clearly identify the area near Bourke-Cobar as being the source of the dust. This study paves the way for determining the export of Australian airborne dust both in the oceans and other continents.

De Deckker, P., R. M. M. Abed, D. de Beer, K. Hinrichs, T. O'Loingsigh, E. Schefuß, J. W. Stuut, N. J. Tapper, and S. van der Kaars, 2008, Geochemical and microbiological fingerprinting of airborne dust that fell in Canberra, Australia, in October 2002, Geochem Geophys. Geosyst., **9**, Q12Q10, doi:10.1029/2008GC002091.

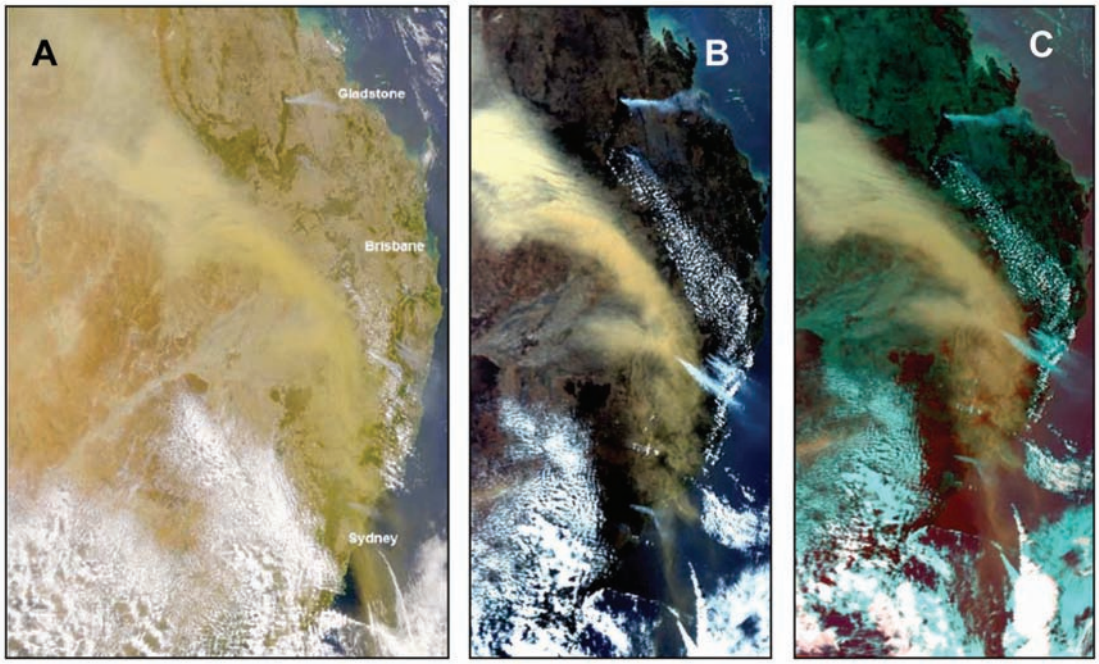

Figure 1. *(A) SeaWiFS satellite image 09:00 hours local eastern standard time (EST) on 23 October 2002 (taken from McTainsh et al., 2005), showing the main dust plume passing over eastern Australia (note the smoke plumes from bushfires in south east Queensland and central east NSW, which indicate wind directions at the time of the event), (B): 13:25 hours EST – MODIS colour-optimised Red-Green-Blue image and (C) processed with the Miller Dust Enhancement Algorithm.*

Phasing and amplitude of sea level and climate change during the penultimate interglacial

Andrea Dutton[1], Edouard Bard[2], Fabrizio Antonioli[3], Tezer Esat[1], Kurt Lambeck[1] and Malcolm T. McCulloch[1]

[1] Research School of Earth Sciences, Australian National University, Canberra, ACT 0200, Australia
[2]CEREGE, CNRS and Universite Aix-Marseille III, Europole de l'Arbois, 13545 Aix-en-Provence Cedex 4, France
[3]ENEA - Special Project Global Change, Rome 00060, Italy

Direct markers of sea level position during the Quaternary are often limited to archives near or above present sea level, such as corals which grew near the sea surface during interglacial highstands. Submerged speleothems provide a means to access the history of sea level oscillations across a range of depths below present sea level. Because the dense calcite comprising speleothems is less susceptible to alteration than corals, this archive also has the potential to extend reconstructions of sea level position farther back in time. A collection of unique speleothems from Argentarola Cave, Italy have been recovered which contain alternating layers of spelean calcite (formed during subaerial exposure) and *Serpulid* calcite (formed during cave submergence by seawater). We have extended the sea level reconstruction from Argentarola farther back in time and have examined additional specimens from different depths to complement the existing dataset [1,2]. This work has resolved the timing and magnitude of multiple sea level highstands during marine isotope stage (MIS) 7.

We have generated 36 U-Th ages of the speleothem calcite to constrain the timing of cave submergence by seawater, represented in these specimens by the marine serpulid overgrowths. Our data show that sea level highstands above -18 m were attained ~5,000-8,000 years prior to northern hemisphere (NH) insolation maxima during MIS 7.5 and 7.1. In contrast, MIS 7.3 commences within 1,000 years of the NH insolation maximum and peaks near -18 m, despite having the strongest insolation forcing of the triplet. This delayed phasing and dampened amplitude of the MIS 7.3 highstand is attributed to extensive glaciation during MIS 7.4 and highlights the significance of cryosphere response time to the climate system.

[1] E. Bard, F. Antonioli and S. Silenzi, (2002) Sea-level during the penultimate interglacial period based on a submerged stalagmite from Argentarola Cave (Italy). *Earth and Planetary Science Letters* **196**: 135-146.

[2] F. Antonioli, E. Bard, E.-K. Potter, S. Silenzi and S. Improta (2004) 215-ka History of sea-level oscillations from marine and continental layers in Argentarola cave speleothems (Italy). *Global Planetary Change* **43**: 57-78.

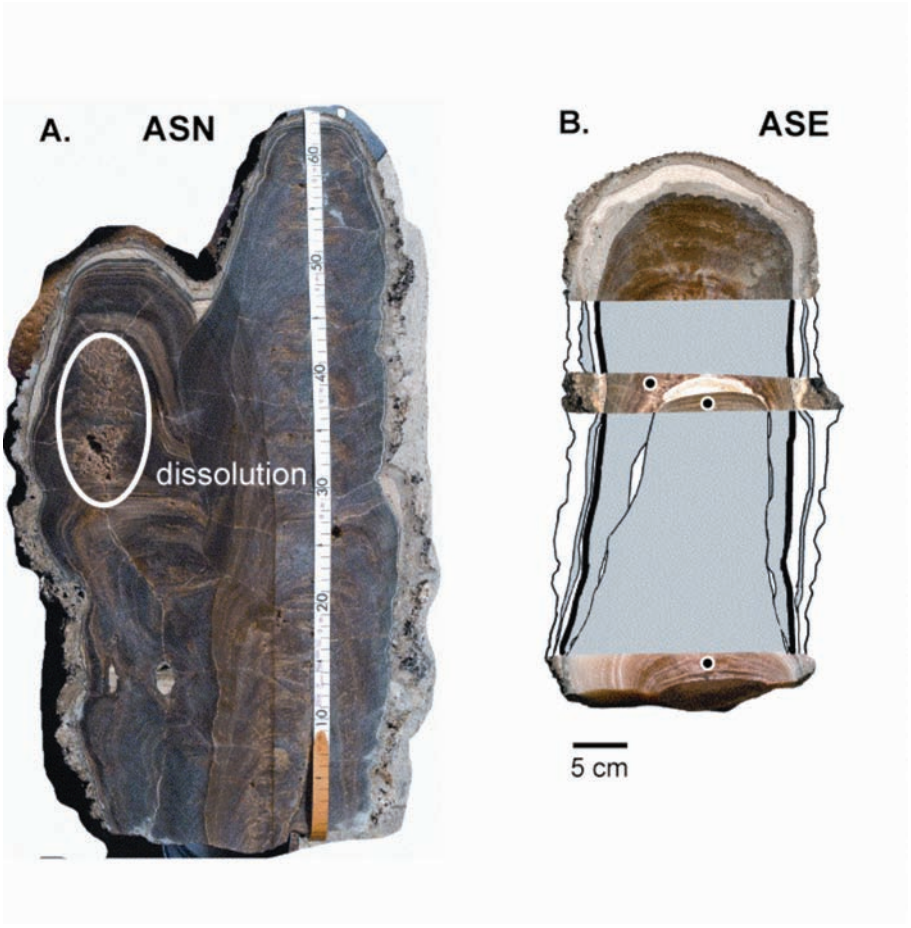

Figure 1. *Marine serpulid overgrowths present in two stalagmites were dated by bracketing U-Th ages of speleothem calcite above and below the marine layers. A. Argentarola stalagmite N (ASN). Large scale dissolution is visible in part of the speleothem (below the areas we sampled). B. Argentarola stalagmite E (ASE) drawing spliced together with photographs. Sample positions denoted by black circles in ASE.*

Winter-time dissolved iron and nutrient distributions in the Subantarctic Zone from 40-52S; 155-160E

Michael Ellwood[1], Philip W Boyd[2] and Philip Sutton[3]

[1] *Research School of Earth Sciences, Australian National University, Canberra, ACT 0200, Australia*
[2] *National Institute for Water and Atmospheric Research (NIWA), Centre for Chemical and Physical Oceanography, Department of Chemistry, University of Otago, Dunedin, New Zealand.*
[3] *National Institute for Water and Atmospheric Research (NIWA), Wellington, New Zealand*

In the Southern Ocean, mesoscale iron fertilization experiments have clearly demonstrated that iron plays a pivotal role in controlling primary production in polar and subpolar High Nitrate Low Chlorophyll (HNLC) waters. There has been considerable debate about the relative magnitude of different iron sources to surface waters in these regions, such as upwelling, dust or entrainment from island and continental self sediments. However, despite the rapidly emerging field of iron biogeochemistry, there are few vertical profiles of dissolved iron concentration, and almost no winter iron data.

During 2006 we generated the first comprehensive winter dataset for dissolved iron and nitrate distributions (0-1000 m depth) between 40 °S - 52 °S, which transects the Subantarctic zone (SAZ), west of New Zealand (Figure 1).Surface iron concentrations (<0.2 nmol Fe kg^{-1}) were conspicuously low, i.e., probably biologically limiting even at winter-reserve levels, at frontal zones between 43 °S (Subtropical Front) and ~51 °S (Subantarctic Front) (Figure 2). A fivefold range in iron:nitrate molar ratios was observed along the transect, with Subtropical waters, where blooms occur, having the highest ratios in subsurface waters. The major wintertime supply of dissolved iron in the SAZ is from Ekman advection of waters from the south (but calculated source water dissolved iron is ~0.2 nmol Fe kg^{-1}), suggesting that mixed-layer dissolved iron concentration is controlled by how long these southern waters remain at the surface (~3 years).

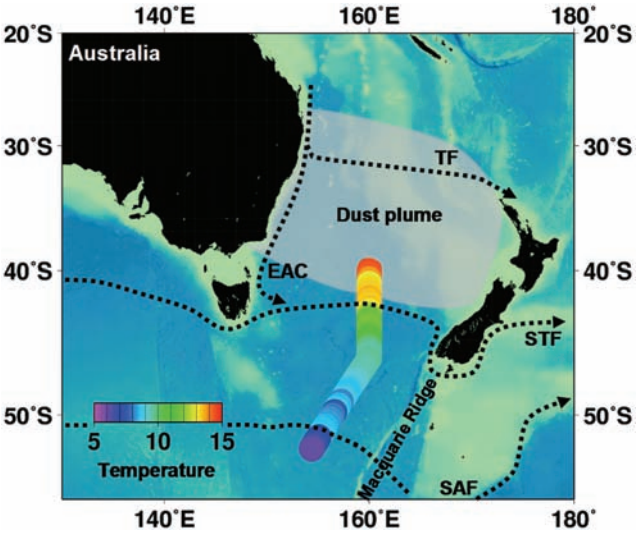

Figure 1

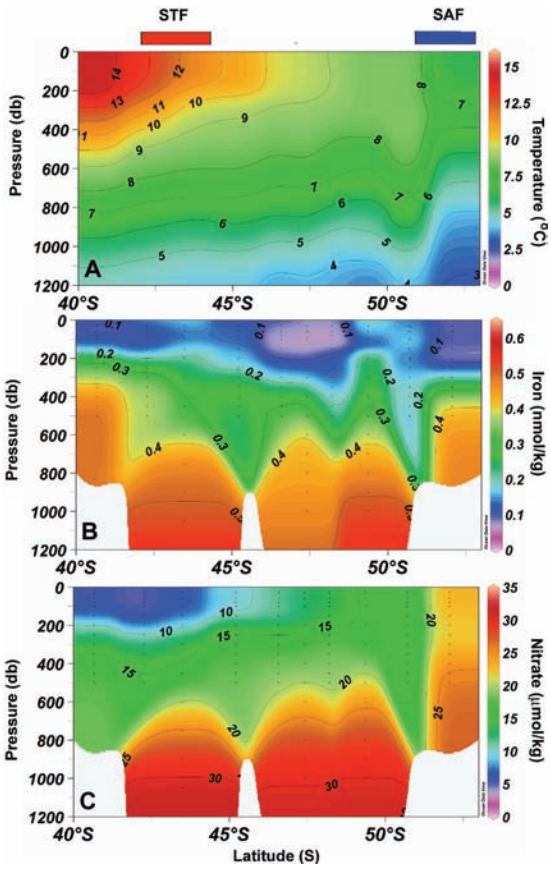

Figure 2

Reconstructing the history of drought and aridity in Australia: Evidence from Lake George

Kathryn E. Fitzsimmons[1], Timothy T. Barrows[1], Geoff A.T. Duller[2] and Helen M. Roberts[2]

[1] *Research School of Earth Sciences, Australian National University*
[2] *Institute of Geography and Earth Sciences, Aberystwyth University, Aberystwyth, UK*

Australia is the driest inhabited continent on Earth. However, evidence preserved in the landscape suggests that arid and drought conditions have varied in intensity through time and space. Aridity during the late Quaternary presided over considerable expansion of desert dunefields across Australia (e.g. Fitzsimmons et al. 2007a, b), the drying of lake basins, and increased dust transport.

It is unclear how the present relatively arid, warm conditions relate to the cold, dry climate responsible for desert expansion during the late Quaternary, or to the current severe droughts. This knowledge gap is primarily due to the fact that there are few systematic records of regional aridity and drought in Australia. The key to understanding the development of aridity is to produce a chronological framework for terrestrial aridification. Recent and continuing work at the luminescence dating laboratory in the Research School of Earth Sciences aims to produce such a chronological framework, focusing on key sites which preserve landscape features responsive to aridity, such as dunes and lake shorelines.

Lake George is the largest freshwater lake in mainland Australia when full, and provides one of the most complete records of Quaternary sedimentation in the southeastern part of the continent. The lake is presently ephemeral in response to drought conditions, but sediments within the basin preserve evidence of multiple permanent and dry lake conditions in the past. Cross bedded gravels exposed in the southern part of the lake basin indicate the existence in the past of a substantial water body with water depth in excess of 20 m. Stratigraphic sequences and lake shorelines at the northern end of the lake record multiple periods of lake filling. Lacustrine sediments within the northern part of the lake basin are overlain by a thin veneer of alluvial material and aeolian dust representing shoreline retreat late in the Holocene.

Optically stimulated luminescence (OSL) dating has been applied to the various geomorphic features associated with the lake, with an examination of aeolian, fluvial and lacustrine sediments. The single aliquot regenerative dose (SAR) OSL dating protocol has been applied using both single aliquots and single grains for samples from the different geomorphic settings. We are presently seeking to extend the chronology beyond the limits of conventional SAR OSL dating through the use of thermally-transferred OSL (Tsukamoto et al. 2008), and are contributing to the development of this new technique.

We are working to reconstruct past lake levels based on the sedimentology of the dated units, and to relate these to environmental change in the region during the Late Quaternary. The preliminary OSL chronology shows a striking correlation between lake filling events at Lake George and permanent lake conditions/ high water tables across humid, semi-arid and arid Australia (Figure 1). The Holocene and oxygen-isotope stage 5 filling events at Lake George correspond to warm sea-surface temperatures (Barrows et al. 2007). Lake filling events also appear to correspond to relatively humid periods between major arid episodes in the desert dunefields of central Australia, also identified by OSL dating in the luminescence laboratory at the Research School of Earth Sciences (Fitzsimmons et al. 2007a).

Barrows, T.T., Juggins, S., De Deckker, P., Calvo, E., Pelejero, C. (2007) Long-term sea-surface temperature and climate change in the Australian-New Zealand region. *Paleoceanography* **22**: PA2215.

Fitzsimmons, K.E., Rhodes, E.J., Magee, J.W., Barrows, T.T. (2007a) The timing of linear dune activity in the Strzelecki and Tirari Deserts, Australia. *Quaternary Science Reviews* **26**: 2598-2616.

Fitzsimmons, K.E., Bowler, J.M., Rhodes, E.J., Magee, J.W. (2007b) Relationships between desert dunes during the late Quaternary in the Lake Frome region, Strzelecki Desert, Australia. *Journal of Quaternary Science* **22**: 549-558.

Tsukamoto, S., Duller, G.A.T., Wintle, A.G. (2008) Characteristics of thermally transferred optically stimulated luminescence (TT-OSL) in quartz and its potential for dating sediments. *Radiation Measurements* **43**: 1204-1218.

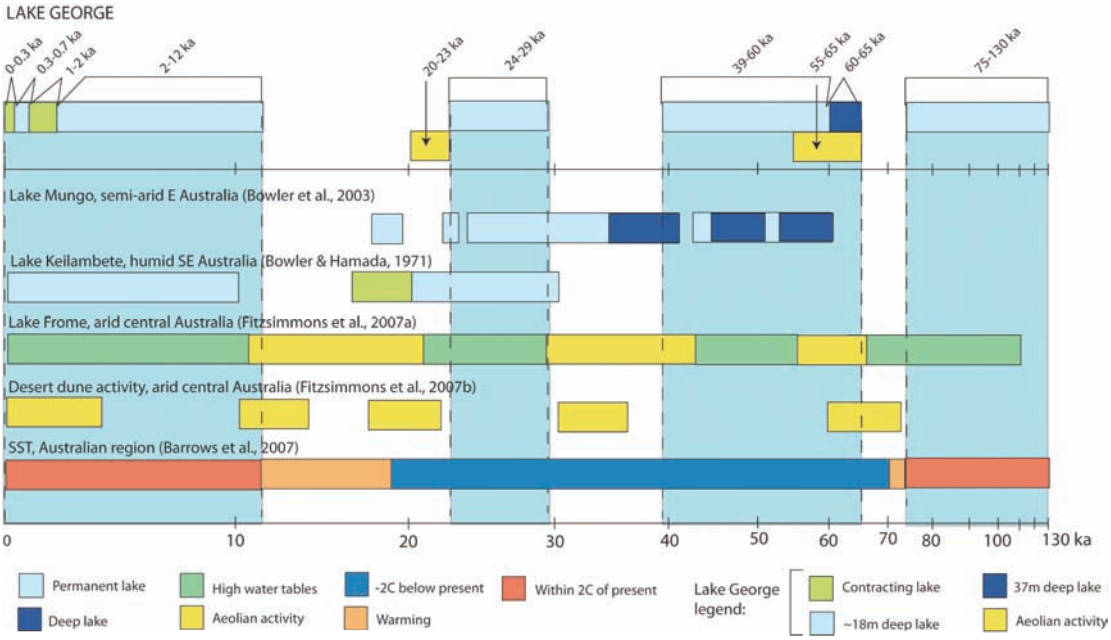

Figure 1. *Summary of late Quaternary lake level change at Lake George, southeastern Australia, and comparisons with palaeoenvironmental records from Lakes Mungo (semi-arid) and Keilambete (humid), groundwater levels and dune activity at Lake Frome (arid), desert dune activity (arid zone) and sea-surface temperatures in the Australian-New Zealand region.*

Speleothem carbon-isotope response to an explosive volcanic eruption ~12 ka ago near Liang Bua, Flores, Indonesia

Michael K. Gagan[1], Heather Scott-Gagan[1], Joan A. Cowley[1], Jian-xin Zhao[2], Linda K. Ayliffe[1], Wahyoe S. Hantoro[3] and Bambang W. Suwargadi[3]

[1] *Research School of Earth Sciences, The Australian National University, Canberra, ACT 0200, Australia*
[2] *Centre for Microscopy and Microanalysis, The University of Queensland, Brisbane, Qld. 4072, Australia*
[3] *Research and Development Center for Geotechnology, Indonesian Institute of Sciences, Jalan Cisitsu No. 21/154 D, Bandung 40135, Indonesia*

Knowing what caused the surprisingly recent extinction of the dwarf hominin *Homo floresiensis* ("the Hobbit") ~18-12 ka (thousand years ago) on the island of Flores in eastern Indonesia is an intriguing question of great international interest. At present, we do not know if predation by modern humans or severe climate change pushed the Hobbit beyond its adaptive capability. However, a prominent volcanic ash layer overlies remains of the Hobbit recovered from Late Pleistocene sediments in Liang Bua cave, suggesting that an explosive volcanic eruption could have altered the local ecosystem at ~12 ka, and played a role in the Hobbit's demise (Morwood et al., 2004).

Interestingly, out of the ~850 volcanic sulfate signals recorded by the GISP2 (Greenland) ice core over the past 100 kyr, including the Toba super-eruption ~73 ka (Zielinski et al., 1997), the largest and most abundant volcanic signals occur between 17 ka and 6 ka, when the Hobbit became extinct (Fig. 1a). It is thought that crustal stresses associated with post-glacial sea-level rise may have significantly increased explosive volcanic activity in island arc systems, such as Indonesia, during this period.

In 2006, our ARC *Discovery* grant team (Gagan et al., 2006) collected several speleothems (cave calcite deposits) from Liang Luar cave (located ~1 km from Liang Bua) that show clear dark laminae at ~12 ka, which may be indicative of volcanic ash. High-resolution analysis of carbon-isotope ratios ($^{13}C/^{12}C$) in the speleothem calcite shows a sharp increase in ^{13}C at ~12 ka, suggesting that vegetation cover may have been substantially reduced for ~300 years (Fig. 1b).

On tropical islands, like Flores, isotopically light carbon derived from oxidation of abundant soil organic matter dominates speleothem $^{13}C/^{12}C$ because forested tropical soils have CO_2 partial pressures 1-2 orders of magnitude greater than that of the overlying atmosphere (Kessler and Harvey, 1999). Therefore, an abrupt reduction in vegetation cover, soil productivity, and soil CO_2 production following local deposition of volcanic ash would reduce the supply of isotopically light carbon to the cave drip-water, thus raising speleothem $^{13}C/^{12}C$.

Explosive island arc volcanic eruptions are rich in sulphur, so our follow-up approach will be to measure S concentrations in speleothem calcite (using SHRIMPII at RSES) as an indicator of sulfate rain-out. It is also possible that fresh volcanic ash above caves could be detected by LA-ICP-MS measurements of leachable metals (e.g. Ni, Cu, Zn, Mo, Ti, Co, Rb) and rare earth elements in speleothem calcite. Precise U-series dating of these multi-proxy records will shed light on the timing of large volcanic eruptions and the innate ability of humans to adapt to natural catastrophes and environmental change.

Gagan MK, Zhao J-x, Drysdale RN, Hantoro WS, Schmidt GA, ARC *Discovery* Grant DP0663274 (2006-2008): Monsoon extremes, environmental shifts, and catastrophic volcanic eruptions: Quantifying impacts on the human history of southern Australasia.

Kessler TJ, Harvey CF (1999) The global flux of carbon dioxide into groundwater. *Geophysical Research Letters* **28**: 279-282.

Morwood MJ, Soejono RJ, Roberts RG, Sutikna T, Turney CSM, Westaway KE, Rink WJ, Zhao J-x, van den Bergh GD, Awe Due R, Hobbs DR, Moore MW, Bird MI, Fifield LK (2004) Archaeology and age of a new hominin species from Flores in eastern Indonesia. *Nature* **431**: 1087–1091.

Zielinski GA, Mayewski PA, Meeker LD, Whitlow S, Twickler MS (1996) A 110,000-yr record of explosive volcanism from the GISP2 (Greenland) ice core. *Quaternary Research* **45**: 109-118.

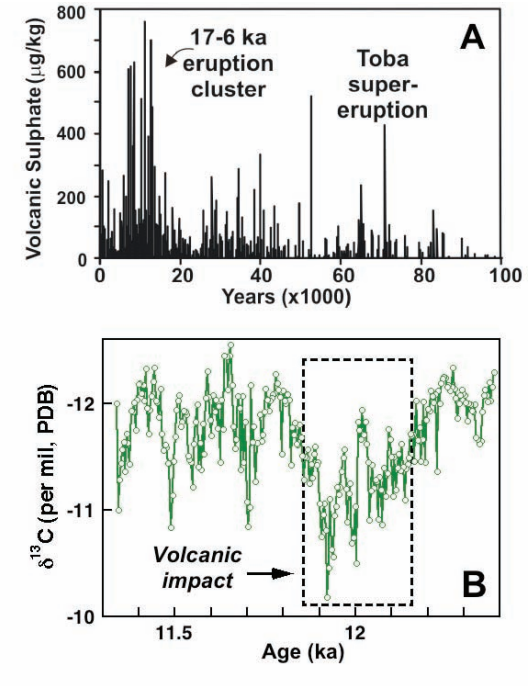

Figure 1. Volcanic impacts. *(**A**) 100-kyr volcanic sulphate record from the GISP2 (Greenland) ice core (after Zielinski et al., 1997). The Toba super-eruption (~73 ka) and abundant volcanic signals between 17 ka and 6 ka coincide with key turning points in human history. **(B)** 4-year resolution speleothem $^{13}C/^{12}C$ record from Liang Luar cave, Flores, showing potential decrease in vegetation cover lasting ~300 years (dashed box) at the time of ~12 ka volcanic eruption, and disappearance of the Hobbit.*

The relevance of parametric U-uptake models in ESR age calculations

Rainer Grün

Research School of Earth Sciences, Australian National University, Canberra, ACT 0200, Australia

Ever since the inception of ESR dating of tooth enamel, it was clear that the unknown uranium uptake history has to be addressed in dose rate calculations. Various parametric models have been proposed for the reconstruction of U-uptake in dental tissues, notably early (EU), linear (LU) and very recent (RU) uptake. The EU model has some physical meaning, it presents the closed system and provides the minimum age. The RU model is physically less meaningful, but provides the maximum age. The main virtue of these parametric models lies mainly in their reasonable simple computability. Nevertheless, many publications have either favoured a particular U-uptake model, for the convenience of being able to explain a dating result, or claimed that the correct age of the sample lied somewhere between the EU and LU results. However, without any knowledge of the U-uptake history, it is only safe to assume that the correct age of a sample lies somewhere between the EU and RU calculations. Depending on the contribution of the U in the dental tissues to the total dose rate, this difference ranges between negligible and utterly enormous.

U uptake can be modelled by combining ESR and U-series data. Although the explicit U-uptake in nature may occur in multiple phases, two models can bracket virtually all possible scenarios, as long as no U-leaching occurs. Grün et al. (1988) used a smooth diffusion function: $U(t) = U_m (t/T)^{p+1}$, where U(t) is the uranium concentration at the time t, U_m the measured, present day U-concentration, T the age of the sample and p the uptake parameter. This system provides minimum age estimates for given ESR/U-series data sets. A delta function, where U_m is accumulated instantly at the apparent closed system U-series age of the dental tissue, provides the maximum age. For younger samples, the differences between these two models are relatively small, which means that the explicit U-uptake history has little effect on the age calculation. For older samples (> 700 ka), with larger differences between the closed system U-series and ESR age estimates, the differences may be large (by more than a factor of 2).

To get more general insights into the general behaviour of U-uptake, published p-values were compiled and separated into two groups, from cave sites (and rock shelters) and open air sites. For the cave sites, most of the p-values of the dentine fall between about -1 and 1, but still a significant number give higher values (Figure 1A). All enamel values fall within -1 and 0.5 (Figure 1B). Note, however, that many of the teeth with high p-values in the dentine had not their enamel analysed (partly because of low U-concentrations). Most of the measured p-values in cement, p(CE), indicate a more rapid accumulation in cement than dentine (Figure 1C). This is expected, as the cement is located on the outside of the tooth. The relationship between p(EN) and p(DE) is random, most values lying in a band of 0.5 around the 1:1 line. The results on the open air sites are markedly different (Figure 2). Most p(DE) and p(EN) lie outside the -1 to 0 range (Figures 2A and B). A large number of results show p-values of > 2. There is no trend whether enamel or dentine experienced a faster uptake (Figure 2C).

The p(CE) values are reasonably close to p(DE). For open air sites it is impossible to define a range of p-values that could be used for general approximations. It is even not possible to claim that the correct uptake is somewhere between EU and RU, because there is a significant number of sites where model violations have been observed (the closed system U-series age is older than the corresponding ESR age) or U-leaching (with $^{230}Th/^{234}U$ ratios lying outside the isotope evolution diagram). In the former case it is not unequivocally clear whether U-leaching has occurred of whether the ESR results underestimate the correct age because of problems with the distributions of the orientated and non-orientated CO_2^- radicals (Grün et al. 2008a), thermal transfer processes (Joannes-Boyau and Grün, submitted), reworking of

samples, or the usual vagrancies in dose rate estimation. Leaching has been observed in a range of sites (Grün et al. 2008b, Grün, unpublished data).

The differences between cave and open air sites can probably be explained through the different sedimentological histories of the sites. Caves are systematically excavated because archaeologists know that ancient humans preferred to live in rock shelters and caves. Until excavated, the sedimentary stack is usually undisturbed. In contrast, many open air sites are discovered because erosion, starting at some time in the past, had provided an indication that a site was present. Erosion causes changes in the hydrological environment, e.g., by re-activation of drainage and changing the ground water table. This is accompanied with renewed U-mobilisation. Not surprisingly, many U-series age estimates of open air sites seem to reflect this change in the hydrology rather than the age of the sample.

To conclude, the statement that the correct ESR age of a sample probably lies somewhere between the EU and LU uptake age calculations is incorrect. It is not even true that the correct age lies always somewhere between the EU and RU model calculations, because there have been occasions of model violations and U-leaching. Any ESR dating study on teeth with substantial U concentrations in the tissues requires U-series age estimates. Anything else is simply a tenesmic approach to dating.

Grün, R., Aubert, M., Joannes-Boyau, R., Moncel, M.H. (2008a) High resolution analysis of uranium and thorium concentrations as well as U-series isotope distributions in a Neanderthal tooth from Payre using laser ablation ICP-MS. *Geochimica Cosmochimica Acta* 72: 5278-5290.

Grün, R., Joannes-Boyau, R., Stringer, C. (2008b) Two types of CO_2^- radicals threaten the fundamentals of ESR dating of tooth enamel. *Quaternary Geochronology* 3: 150-172.

Grün, R., Schwarcz, H.P. and Chadam, J.M. (1988) ESR dating of tooth enamel: Coupled correction for U-uptake and U-series disequilibrium. *Nuclear Tracks and Radiation Measurements* 14: 237-241.

Joannes-Boyau, R., Grün, R. (submitted). Thermal behaviour of orientated and non-orientated CO_2^- radicals in tooth enamel. *Radiation Measurements.*

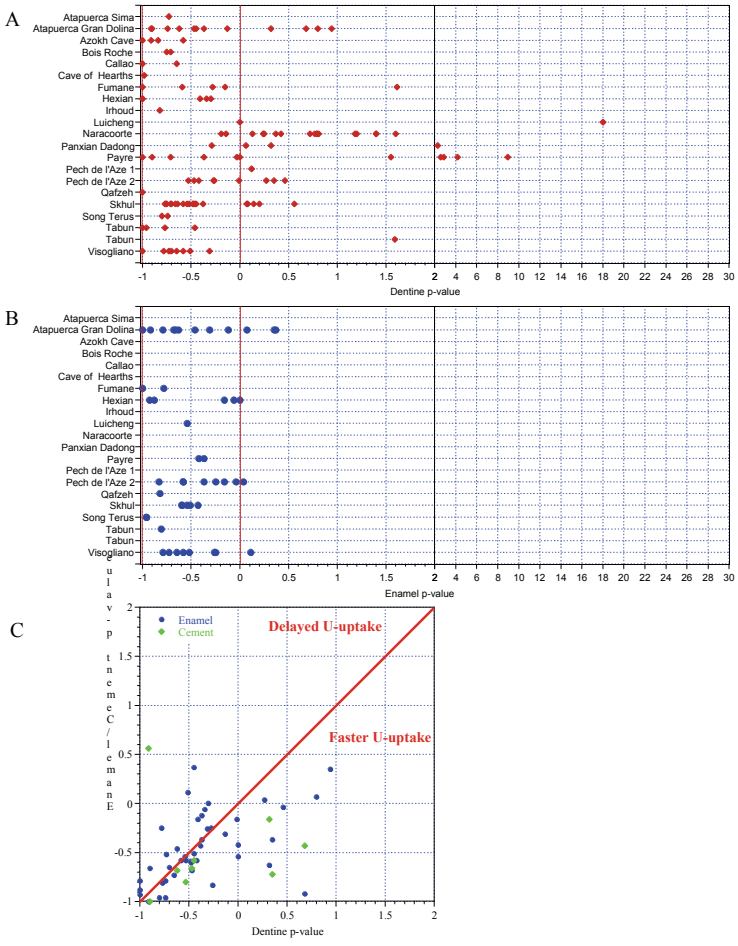

Figure 1.
Compilation of p-values from cave sites
A: p-values from dentine
B: p-values from enamel
C: Relationship between p(EN), p(CE) and p(DE).

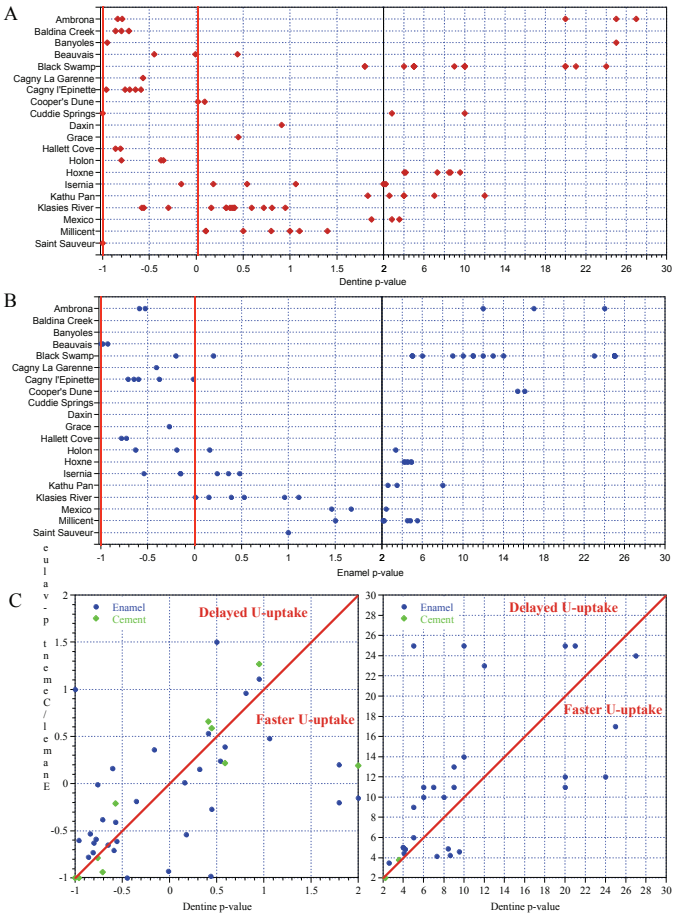

Figure 2.
Compilation of p-values from open air sites
A: p-values from dentine
B: p-values from enamel
C: Relationship between p(EN), p(CE) and p(DE).

Warming and Acidifying Ocean and Coral growth

Jung Ok Kang[1] and Malcolm T. McCulloch[1]

[1] *Research School of Earth Sciences, Australian National University, Canberra, ACT 0200, Australia*

Coral reefs generally are developed within relatively narrow area when environmental controls on the growth of corals including seawater temperature, light, and aragonite saturation states, water motion, and water quality are satisfied. Increasing atmospheric carbon dioxide concentration has been affected on coral reefs mainly through two kinds of mechanisms. Firstly, global warming or climate change has caused rising seawater temperature and extraordinally warm temperature cause corals to bleach. This process has already had a serious impact on the world's coral reefs, with almost 30% of corals having disappeared since the beginning of the 1980s by bleaching events (Hoegh-Guldberg, 2005). Besides, the rise in the concentration of carbon dioxide in the atmosphere has an influence on coral reefs since a decrease of ocean acidity by increasing atmospheric carbon dioxide lower the aragonite saturation states of seawater, declining available carbonate ions of seawater to calcification.

Several experimental and modelling studies were performed under conditions expected in the 21st century and the results show that acidifying ocean will compromise coral calcification. Thermodynamic calculation shows that a doubling of carbon dioxide in seawater will be a decline in carbonate ion concentration of 25-35% to the preindustrial concentration (Landon et al., 2000). Moreover, the worst cast of modelling study argues that total preindustrial to 2100 calcification decrease could be as high as 17% to 35% depending on the regions (Kleypas et al., 1999). The shapes of the calcification versus aragonite saturation curve which are from laboratory studies and crucial in predicting future changes in coral reef, however, still have many uncertainties because the data is scare and is constrained with a first approximation of the general response of coral reefs. In addition, time of exposure to manipulating conditions is too short to apply to the real world and the synergistic interaction of elevated temperature and lowering aragonite saturation state is unknown.

Therefore, my project aims to understand how anthropogenic climate change and increasing ocean acidity affect coral reefs in real and various paleo-evironmental proxies will be used to provide the evidences of the changes in coral-reef pH representing ocean acidity and sea surface temperature indicating global warming and the responses on coral calcification rate. For the first place, the massive corals of genus *Porites* were collected from Southern Great Barrier Reef in October of this yesr (Figure 1). Since they are long lived, distributed widely throughout the Indo-Pacific Ocean, from inshore to offshore waters, their skeletal records are useful as a tool for detecting long-term changes in environmental conditions in ocean surface waters. At the same time, the determination of calcification rate for *Porites* corals collected in 2006 from Pompey complex is in progress.

Hoegh-Guldberg O (2005) Low coral cover in a high-CO_2 world. *Journal of Geophysical Research* **110**: C09S06

Kleypas JA, Buddemeier RW, Archer D, Gattuso J-P, Opdyke BN (1999) Geochemical consequence of increased atmospheric carbon dioxide on coral reefs. *Science* **284**: 118-120

Langdon C, Takahasi T, Sweene C, Chipma D, Goddard J, Marubini F, Arceve H, Barnett H, Atkinson MJ (2000) Effect of calcium carbonate saturation state on calcification rate of an experimental coral reef. *Global Biogeochemical Cycles* **14**: 639-654

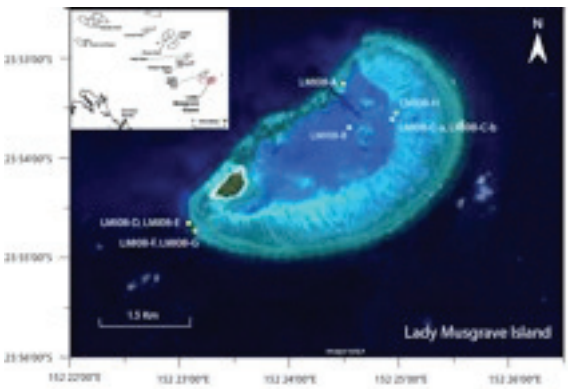

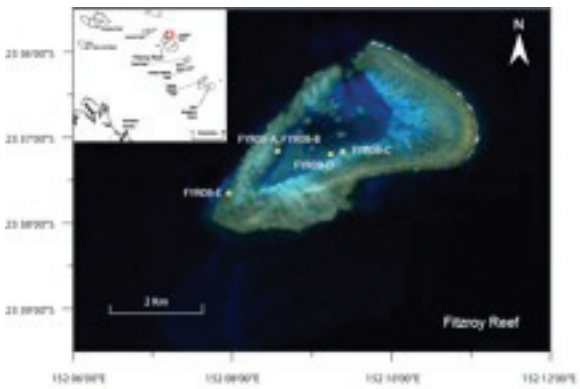

Landscape evolution and palaeoenvironment reconstruction of the Lake Mulurulu Lunette, Willandra Lakes World Heritage Area, NSW

Tegan E Kelly, Rainer Grün, Ian Moffat, Maxime Aubert, Tim Barrows.

Research School of Earth Sciences, Australian National University, Canberra, ACT 0200, Australia

The Willandra Lakes are a dry lake system consisting of a number of ancient lakes in the western region of the Murray basin. The area has significant scientific value, providing detailed palaeoenvironmental and palaeoclimatic records of arid, ice-age Australia as well as a rich and unique archaeological record. Lake Mungo, resting place of Australia's oldest dated aboriginal remains, has been a popular lake for study, while Lake Mulurulu, the northern-most lake in the system, is relatively understudied, despite its abounding potential. The aim of the current study is to combine isotope palaeoecology, geochronology, stratigraphy and sedimentological techniques to study the Mulurulu Lake lunette, thus creating a detailed geomorphological and palaeoenvironmental history of the lake, putting the aboriginal occupation of the area into an environmental context.

Techniques being utilised in the study include stable isotope analyses of wombat teeth, mollusk shells, emu egg shells and fish otoliths to provide palaeoenvironmental records of the area (e.g. Fig 1). This information is put into a geochronological context through ESR dating of wombat teeth, radiocarbon dating of mollusk shells and otoliths and AAR dating of egg shells. Detailed stratigraphic and sedimentological analyses (e.g Fig 2) further provide information about the history of the lake, and are also put into a geochronological context, through OSL dating of sediments.

Research questions being addressed include the history of the current deflation regime at the site, past seasonality and wetting-drying cycles in the region, climate change, timing and reasons for local species extinctions and how these factors relate to the human occupation of the area. Additionally, by utilising independent methods of palaeoenvironment reconstruction (i.e. stratigraphy and geochemistry) and geochronology (i.e. ESR and OSL), the competency and reliability of the techniques are tested.

The study is backed by an ARC-Linkage grant and is being conducted in collaboration with a number of other researchers from ANU, Latrobe, Bond and UQ universities as well as the local aboriginal groups (3TTG inc.) from the area. Associated work is being conducted on other lake lunettes in the region and the overall project integrates geological, geochronological, archaeological, palaeontological and palaeoenvironmental research at the Willandra Lakes World Heritage Area, providing a thorough analysis and understanding of one of Australia's most significant and unique areas of cultural and environmental history.

Figure 1. a) An otolith (fish ear bone) in cross-section, showing growth lines. b) ^{18}O isotope ratios along a transect of an otolith, measured using the SHRIMP II. The increasing values indicate increasing evaporation and hence aridity, while the fish was growing. c) The transect that these data represent. (Courtesy of Maxime Aubert)

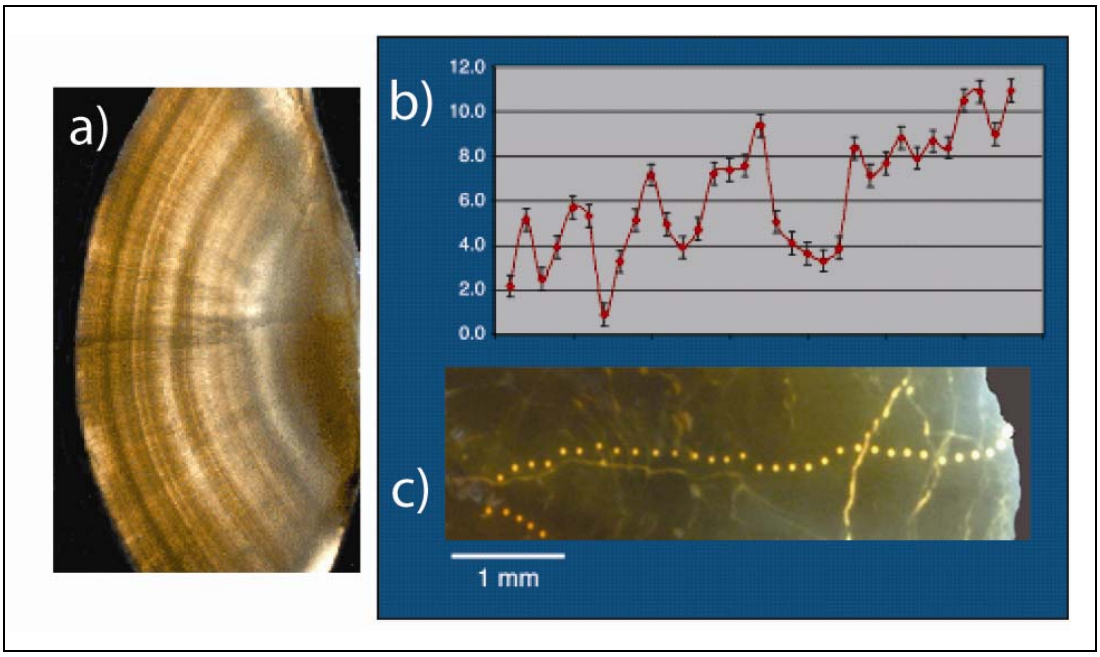

Figure 2. An example profile of the Mulurulu lunette. Approx. 5x vertical exaggeration.

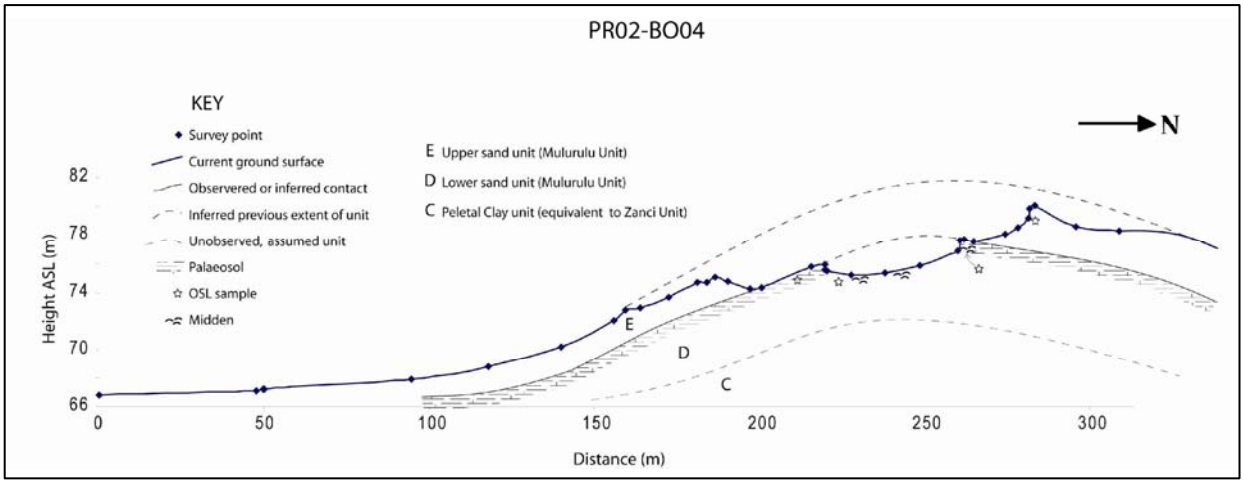

Modelling climate and water isotope variability in southern Indonesia with GISS ModelE-R

Sophie C. Lewis[1], Allegra N. LeGrande[2], Maxwell C. Kelley[2], Gavin A. Schmidt[2], Linda K. Ayliffe[1]

[1] *Research School of Earth Sciences, The Australian National University, Canberra, ACT 0200, Australia*
[2] *NASA Goddard Institute for Space Studies and Center for Climate Systems Research, Columbia University, 2880 Broadway, New York, NY 10034*

Water isotope records collectively provide some of the most extensive proxy evidence for past climate. However, a known or assumed relationship between water isotopes and climate is required for the interpretation of these records. Climate variability on annual to orbital timescales impacts the hydrologic cycle and influences water isotope distribution, with varying impacts on individual climate variables and water isotopes. As such, the relationship between water isotopes and climate may not remain constant through time. The goal of this study is to examine the relationship between climate and water isotope variability in southern Indonesia to facilitate understanding of late Quaternary changes in monsoon rainfall recorded by oxygen isotopes in speleothems.

We assess the relationship between water isotopes and climate and infer the primary mechanisms controlling water isotope variability on various time scales using multiple simulations of current and past climate (Holocene through glacial). The GISS ModelE-R, a fully coupled atmosphere-ocean GCM equipped with water isotope as well as other tracers, is ideal for tracing the source of water isotope variability. We investigate the mechanisms controlling water isotope variability through the addition of isotopic tracers that allow us to explicitly track water vapour and precipitation sources to a region.

We find that the relationship between water isotopes and climatic variables is different at various timescales and that this relationship can change during abrupt climate excursions. Model results support the interpretation of isotopic variability in tropical speleothem records and allow a greater understanding of late Quaternary changes in precipitation. For example, model simulations of precipitation variability in southern Indonesia show a significant northward shift in precipitation source region during the middle Holocene (Figure 1). This change in source area of precipitation likely results from a southward shift in the position of the Intertropical Convergence Zone through the Holocene (Wanner et al., 2008), which would have altered the isotopic composition of rainfall recorded in speleothems in southern Indonesia.

Ultimately, model outputs indicate that the isotopic composition of rainfall delivered to a speleothem site is dependent on numerous dynamic variables, including rainfall amount, precipitation source region and transport trajectory from source to rainout. Model simulations of water isotope variability greatly assist in interpreting oxygen isotopes variability within speleothem records of the palaeomonsoon.

Wanner, H., Beer, J., Bütikofer, J., Crowley, T. J., Cubasch, U., Flückiger, J., Goosse, H., Grosjean, M., Joos, F., Kaplan, J. O., Küttel, M., Müller, S. A., Prentice, I. C., Solomina, O., Stocker, T. F., Tarasov, P., Wagner, M. & Widmann, M. (2008) Mid- to Late Holocene climate change: an overview. *Quaternary Science Reviews,* 27, 1791-1828.

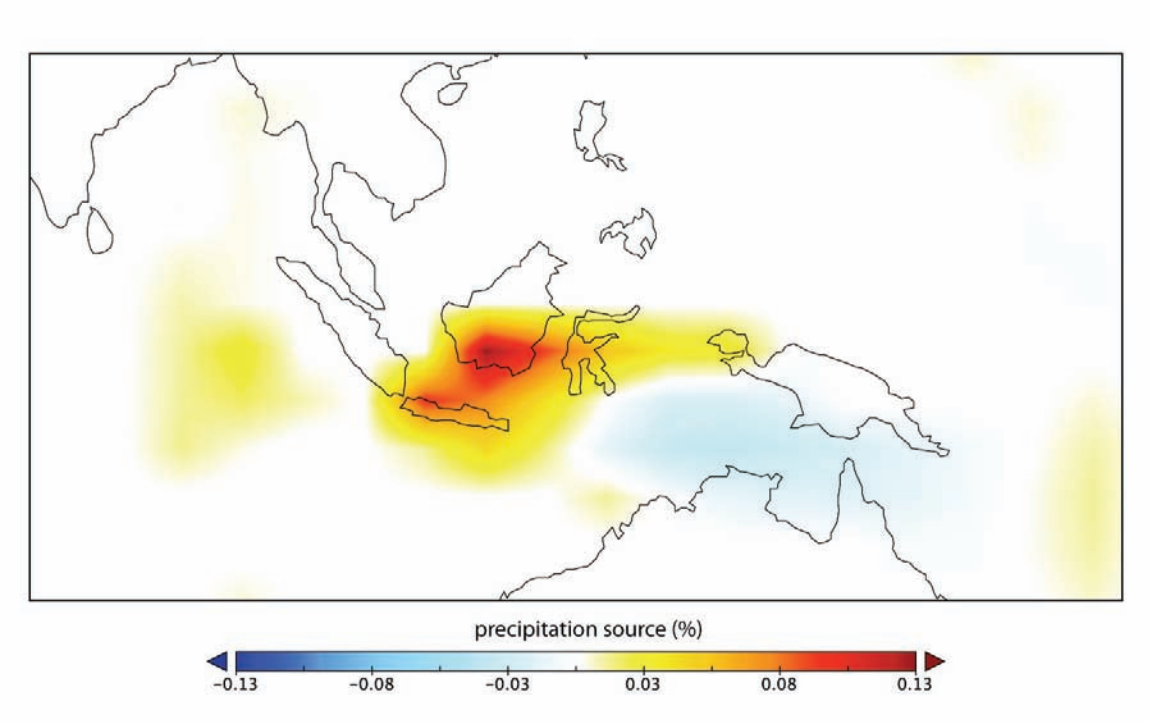

Figure 1. *Difference in precipitation source region to southern Indonesia between 6 kyr and modern GISS ModelE-R simulations.*

Ocean Acidification in the Great Barrier Reef

Malcolm McCulloch[1], Gangjian Wei[2] and Graham Mortimer[1]

[1] *Research School of Earth Sciences, Australian National University, Canberra, ACT 0200, Australia*
[2] *Key Laboratory of Isotope Geochronology and Geochemistry, Guangzhou Institute of Geochemistry, Chinese Academy of Sciences, Guangzhou 510640, China*

Over the past century atmospheric CO_2 has risen by over 30%, from pre-industrial values of ~280 ppm to present-day levels of over 380 ppm, and is continuing to rise at an unprecedented rate of ~2 ppm per year. If unabated, this rate of increase will result in a doubling of CO_2 by sometime later this century. Unlike the atmosphere where CO_2 causes warming through its strong physical interaction with infrared radiation, in the oceans it is a highly reactive species causing a major perturbation to the chemistry of surface waters. This perturbation arises from dissolution of CO_2 in surface waters resulting in an increase in the concentration of carbonic acid, and a reduction in seawater *p*H or what has become known as 'ocean acidification'. This in turn is leading to an overall decrease in the carbonate ion concentration, the key component controlling calcification in marine organisms.

Ocean acidification is thus of major concern not only because it will ultimately lead to dissolution of calcium carbonate organisms as aragonite undersaturation is approached, but also because the rate of coral calcification appears to be directly proportional to the degree of carbonate ion concentration, even in oversaturated conditions. Thus coral reefs will be at risk as calcification decreases while bio-erosion and chemical dissolution increases. Unfortunately, very little is known about the regional variability of ocean acidification on decadal to centennial time scales, especially since the industrial era. Our current knowledge of ocean acidification is mainly dependent on model calculations and unlike other key climatic indices, such as temperature and salinity, seawater pH has seldom been recorded in marine observations due to the non-routine nature of the measurements. Accordingly, long-term continuous seawater pH records are scarce, with records of several decades now only becoming available from the off-shore sites of Hawaii and Bermuda. This lack of knowledge hinders attempts to properly evaluate not only the current status of ocean acidification, but importantly future trends and likely impacts on calcification of marine biota.

Boron isotope systematics in marine carbonate provide an alternative solution acting as a potential long-term proxy for seawater pH, due to an isotopic fractionation between the boric acid and borate ion species, with their relative proportions being controlled by seawater pH. However in order to utilize this system, high precision measurements of B isotopic compositions are needed to determine the relatively small shifts in seawater pH that are predicted since the commencement of the industrial era. We have pioneered this approach using B measurements in the carbonate skeleton of long-lived (~200 year) *Porites* corals from the Great Barrier Reef.

Our initial results indicate that the long-term pre-industrial variation of seawater pH in this region is partially related to the decadal-interdecadal variability of atmospheric and oceanic anomalies in the Pacific. The 1998 oscillation is co-incident with a major coral bleaching event indicating the sensitivity of skeletal $\delta^{11}B$ compositions to loss of zooxanthellate symbionts. Importantly, from the 1940's to the present-day, there is a general overall trend of ocean acidification with pH decreasing by about 0.2 to 0.3 units. Correlations of $\delta^{11}B$ with $\delta^{13}C$ during this interval indicate that the increasing trend towards ocean acidification over the past 60 years in this region is the result of enhanced dissolution of CO_2 in surface waters from fossil fuel burning at a significantly larger than anticipated from model calculations.

This suggests that the increased levels of anthropogenic CO_2 in atmosphere has already caused a marked trend towards acidification in the coral reefs during the past decades. Observations of surprisingly large decreases in pH across important carbonate producing regions, such as the Great Barrier Reef of Australia, raise serious concerns about the impact that Greenhouse gas emissions may already be having on coral calcification in the Great Barrier Reef.

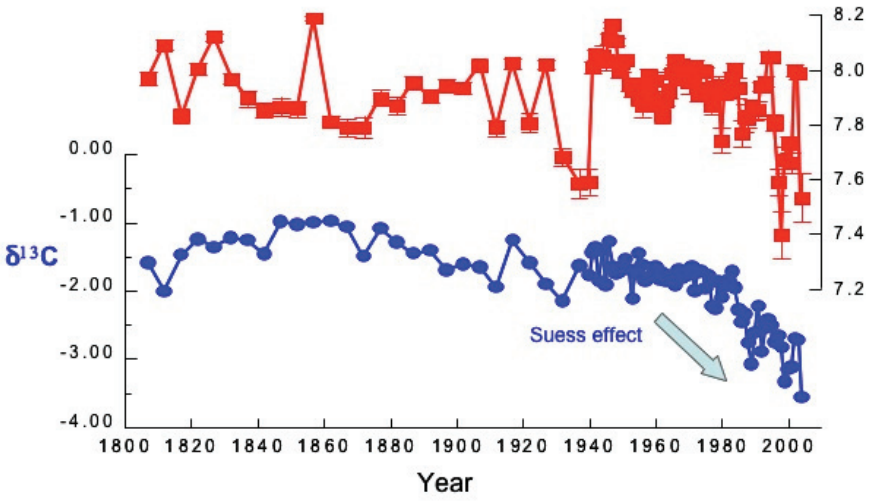

Figure 1.

Weathering history of rock art on Burrup Peninsula, Western Australia

Brad Pillans[1], Stephen Eggins[1], Tony Eggleton[1], Keith Fifield[2] and Richard Roberts[3]

[1] Research School of Earth Sciences, Australian National University, Canberra, ACT 0200, Australia
[2] Research School of Physical Sciences & Engineering, Australian National University, Canberra, ACT 0200, Australia
[3] School of Earth & Environmental Sciences, University of Wollongong, NSW 2522, Australia

In July 2007 the renowned Aboriginal rock art of the Dampier Archipelago (including Burrup Peninsula) in Western Australia was included in the National Heritage List. Some hundreds of thousands of rock engravings (petroglyphs) were made on weathered rock surfaces by pounding, pecking, abrading and scoring using rock tools. It is claimed that the Dampier Archipelago contains the largest known rock art gallery in the world. Industrial development at the nearby port of Dampier has stimulated research to underpin conservation strategies for the rock art.

The weathered, outer layers of rocks (dominantly granophyre) on the Burrup Peninsula consist of a thin, discontinuous surface varnish (up to ~200 microns thick) and underlying weathered zone or rind (up to ~1 cm thick), mainly composed of hematite, kaolinite, quartz, K-feldspar and phosphates. These are the typical insoluble residues from rock weathering and they are at the surface simply because they are very slow to dissolve in rain water. The dark reddish- to blackish-brown colour of the rock varnish contrasts with the pale brown colour of the underlying weathering rind. The pale weathering rind is exposed in the majority of petroglyphs, providing a distinctive colour contrast with surrounding dark coloured varnish.

Laser ablation-ICPMS depth profiling of the rock varnish indicates geochemical microlamination that may be related to changing long-term environments as described by Liu & Broecker (2008) in their study of rock varnish microlamination in the western USA. Together with our field observations, the geochemistry of the varnish is consistent with an origin from direct chemical precipitation of dissolved elements in rain water, rather than from leaching of the underlying rock or from slow diagenesis of dust particles deposited on the rock surfaces – see discussion by Thiagarajan & Lee (2004).

From our field observations, we identify three modes of physical rock breakdown each of which impinges on the long term stability of rock surfaces and associated petroglyphs:

1. Flaking of thin (mm-scale) surface layers associated with the development of a weathering rind and/or rock varnish.
2. Fracturing along major rock joints (cm- to m-scale), resulting in block fall from steep slopes and cliffs. Note, however, that in between the very infrequent block fall events, erosion will likely be dominated by mm-scale flaking.
3. Fire-induced fracturing around the margins of rock outcrops caused during burning of adjacent vegetation (Dragovitch 1994).

Overall, our results indicate that the weathered granophyre rock surfaces containing petroglyphs, on Burrup Peninsula, are extremely resistant to erosion over thousands of years. Major contributing factors include low rainfall, resistant rock and the presence of stable secondary minerals on rock surfaces. We are currently undertaking a program of cosmogenic nuclide measurements to quantify rates of erosion on rock surfaces associated with petroglyphs.

Dragovich D (1994) Fire, climate, and the persistence of desert varnish near Dampier, Western Australia. *Palaeogeography, Palaeoclimatology, Palaeoecology* **111**: 279-288.

Liu T, Broecker WS (2008) Rock varnish evidence for latest Pleistocene millenial-scale wet events in the drylands of western United States. *Geology* **36**: 403-406.

Thiagarajan N, Lee C-TA (2004) Trace-element evidence for the origin of desert varnish by direct aqueous atmospheric deposition. *Earth and Planetary Science Letters* **224**: 131-141.

Figure 1.

Silicon isotopic composition of marine sponges: Understanding isotopic variations using a mass balance approach

Jill Sutton[1], Martin Wille[1], Michael Ellwood[1], William Maher[2], Michelle Kelly[3], Stephen Eggins[1]

[1] *Research School of Earth Sciences, Australian National University, Canberra, ACT 0200, Australia*
[2] *Ecochemistry Laboratory, University of Canberra, ACT, 2601, Australia*
[3]*National Centre for Aquatic Biodiversity and Biosecurity, National Institute of Water & Atmospheric Research (NIWA) Ltd, Auckland, New Zealand*

In this study, relationships were investigated between coupled sponge and seawater samples for Si isotope fractionation compared with equivalent Si concentrations from the water column. The Southern Ocean was chosen for field work as it is the only oceanic area where diatom productivity is dominant and it is a useful natural laboratory for oceanic Si research with concentration gradients stratified by latitude and depth (higher concentrations at lower latitudes and depths). Accordingly, siliceous sponges from both the Hexactinellid and Demosponge classes were sampled at a variety of latitudes and depths. Results were compared to a new model that assumes variable Si isotope fractionation dependent on the Si concentration of seawater. The new model offers a new perspective on what controls biological fractionation in biogenic opal and in turn, will yield a novel interpretation of the paleo-oceanic distribution of Si.

Figure 1. *Iceberg near Antarctica in the Southern Ocean.*

Calibrating the speleothem O isotope signal to rainfall

Pauline C. Treble[1,2] and Matthew J. Fischer[1]

[1] *Australian Nuclear Science and Technology Organisation, Lucas Heights, NSW 2234, Australia*
[2] *Research School of Earth Sciences, Australian National University, Canberra, ACT 0200, Australia*

Oxygen isotopes ($\delta^{18}O$) are the most commonly used paleoclimate proxies in speleothems (see McDermott, 2004) and are being used in current research by Dr Treble to reconstruct records of natural rainfall variability for southwest Western Australia. This region has suffered a significant decrease in rainfall since the 1970s and longer records are needed to understand why. The relationship between speleothem $\delta^{18}O$ and rainfall was reported in a previous publication (Treble et al., 2005) and was further examined in detail by Fischer and Treble (2008). The findings of this latter study challenge the common expectation with climate proxies is that we can apply short-interval calibrations to interpret trends in proxy data back in time. These findings have wide application to the interpretation of speleothem $\delta^{18}O$ records in general, and are summarised here.

Two datasets were originally used to examine the relationship between speleothem $\delta^{18}O$ and rainfall. The first are measurements of $\delta^{18}O$ in daily rainfall events for 2001 which show that larger rainfall events contain less of the heavier isotope, ^{18}O. The second are measurements of speleothem $\delta^{18}O$ between 1911-1992 which can be closely compared with changes in the instrumental period (Figure 1, upper panel; Treble et al., 2005). The speleothem record showed that $\delta^{18}O$ rose after 1970, consistent with the decrease in the frequency of large rainfall events. But importantly, the speleothem record showed that this simple inverse relationship between rainfall amount and $\delta^{18}O$ did not hold, evidenced by the higher $\delta^{18}O$ values between 1930-55 when there was no decrease in rainfall.

This key finding led to the publication, Fischer and Treble (2008), where the simple rainfall amount-$\delta^{18}O$ regression model was improved to include inter-annual climate variance. The new model was modulated by dominant modes of inter-annual climate variability or climate indices (calculated as the principal components of sea level pressure over the study period). The new model produced a positive shift in $\delta^{18}O$, similar to that in the speleothem record between 1930-55. This suggests that the dominant modes of interannual variability can cause shifts in vapour source regions (or other effects), which can affect $\delta^{18}O$ independent of amount-type effects. In southwest Australia, it appears that the interannual mode most responsible for isotopic changes related to vapour source, is Zonal Wave 1 (ZW1). An EOF-based reconstruction of ZW1 over the last century suggests that a negative ZW1 state from 1930-55 favoured the advection of ^{18}O-enriched moisture from low latitudes, while a positive ZW1 state post-1970 resulted in more ^{18}O-depleted moisture advected from the sub-polar region (Figure 1, lower panel).

As a result of the study summarised here, we now have an improved regression model for $\delta^{18}O$ rainfall in southwest Australia that replicates key patterns at daily to interdecadal timescales. This is a statistical forward model and thus it can be used to compare paleoclimate simulations to proxy data. The inversion of the model will require a multi-proxy approach (e.g., isotopes and rainfall amount-sensitive trace elements), because the new model relies on two predictors ($d^{18}O$ depends on both precipitation amount and vapour source). In general terms, this study illustrates the importance of understanding the multiple factors which influence speleothem $\delta^{18}O$ and demonstrate for the first time, the effect of interannual climate modes on rainfall $\delta^{18}O$.

Fischer, M.J., Treble, P.C. (2008) Calibrating climate-delta O-18 regression models for the interpretation of high-resolution speleothem delta O-18 time series. *Journal Of Geophysical Research-Atmospheres* **113(D17)**: D17103.

McDermott, F. (2004) Palaeo-climate reconstruction from stable isotope variations in speleothems: a review. *Quaternary Science Reviews* **23(7-8)**: 901-918.

Treble, P.C., Chappell, J., Gagan, M.K., McKeegan, K.D., Harrison, T.M. (2005) In situ measurement of seasonal delta O-18 variations and analysis of isotopic trends in a modem speleothem from southwest Australia. *Earth And Planetary Science Letters* **233(1-2)**: 17-32.

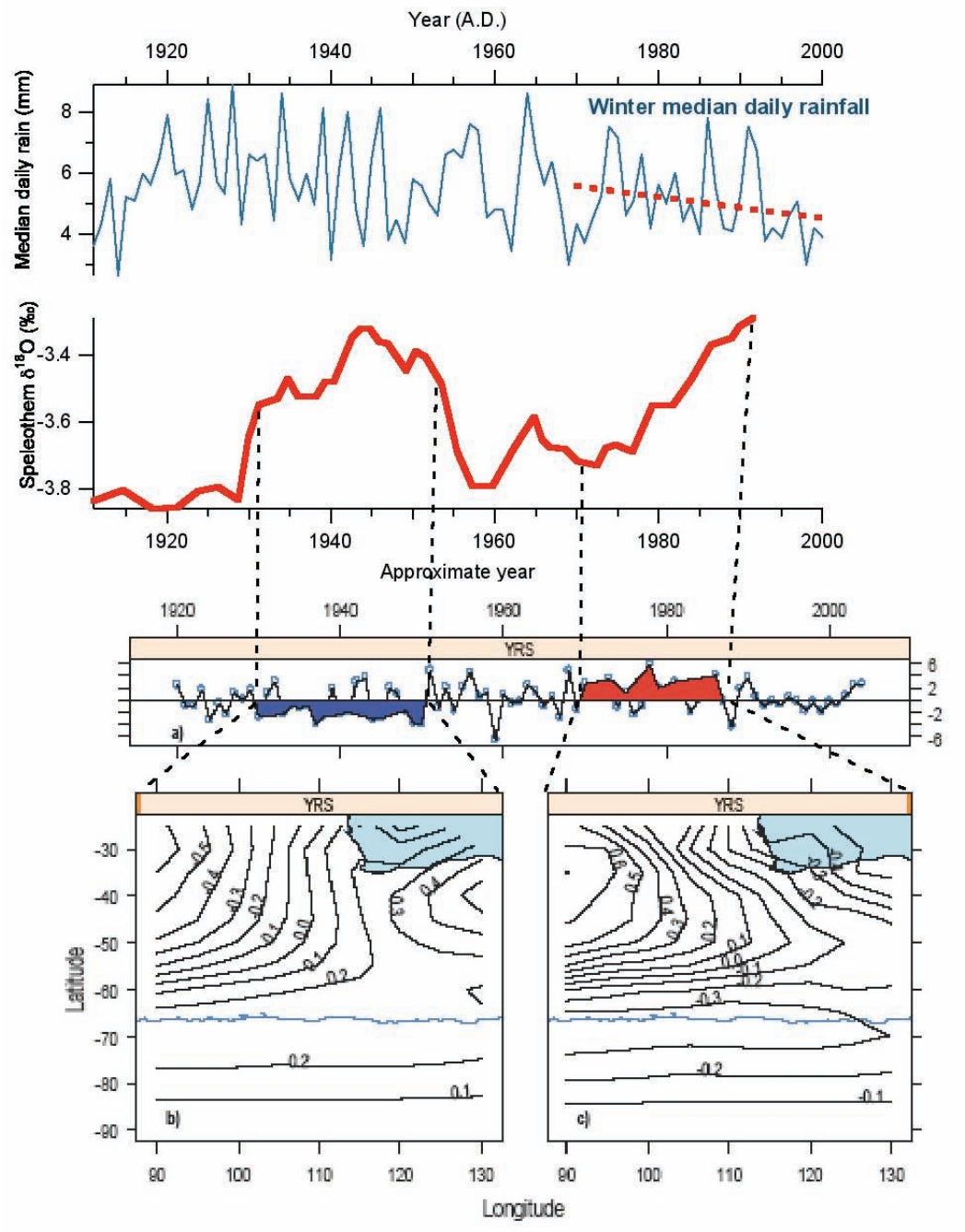

Figure 1.

Did Cooling Oceans Trigger Ordovician Biodiversification? Evidence from Conodont Thermometry

Julie Trotter[1], Ian Williams[1], Chris Barnes[2], Christophe Lécuyer[3] and Robert Nicoll[1]

[1] *Research School of Earth Sciences, Australian National University, Canberra, ACT 0200, Australia*
[2] *School of Earth and Ocean Sciences, University of Victoria, BC, Canada*
[3] *Laboratoire CNRS UMR 5125 Paléoenvironnements and Paléobiosphere, Université Claude Bernard Lyon 1, Villeurbanne, France*

The Ordovician Period, long considered a Supergreenhouse state, saw one of the greatest radiations of life in Earth's history. Previous temperature estimates of up to ~70°C have spawned controversial speculation that the oxygen isotopic composition of seawater must have evolved over geological time. We present a very different global climate record determined by *in situ* ion microprobe (SHRIMP) oxygen isotope analyses of Early Ordovician–Silurian conodonts. This record shows a steady cooling trend through the Early Ordovician reaching modern equatorial temperatures that were sustained throughout the Middle and Late Ordovician. This favourable climate regime not only implies that the oxygen isotopic composition of Ordovician seawater was similar to today, but that climate played an overarching role in promoting the unprecedented increases in biodiversity that characterized this period.

Published in Science, July 2008:

Trotter, J., Williams, I., Barnes, C., Lecuyer, C., Nicoll, R. (2008) Did cooling oceans trigger Ordovician Biodiversification? Evidence from conodont thermometry, Science, Vol 321, 25 July, 550-554.

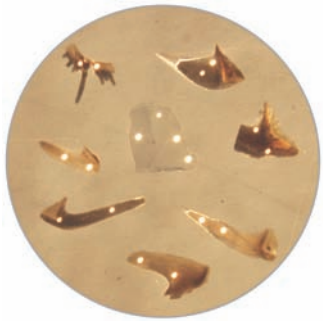

Figure 1. *Portion of a polished epoxy mount showing ion microprobe pits, excavated during in situ oxygen analysis using the SHRIMP II, in conodonts and a Durango apatite grain (centre).*

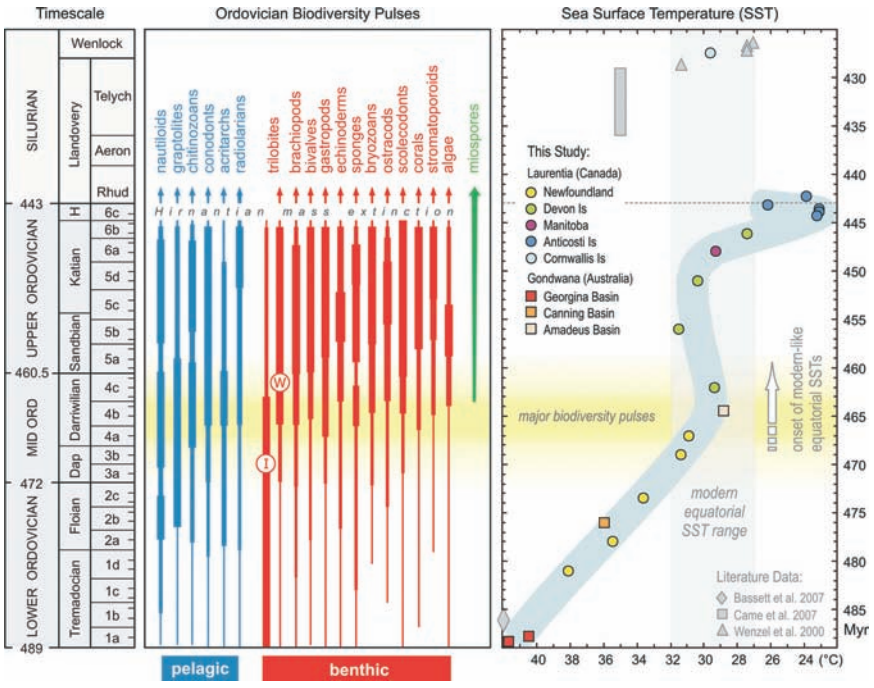

Figure 2. *Generalized global biodiversity pulses and tropical seawater temperature trend through the Ordovician.*

Silicon and Boron isotopic signatures in marine sponges

Martin Wille[1], Jill Sutton[1], Andrea DeLeon[1], Michael Ellwood[1], Steve Eggins[1] and William Maher[2]

[1] Research School of Earth Sciences, Building 47, Daley Road, Australian National University, ACT 0200, Australia
[2] Ecochemistry Laboratory, Institute for Applied Ecology, Faculty of Applied Science, University of Canberra, Canberra, ACT 2601, Australia

The Southern Ocean is widely regarded as playing a key role in influencing atmospheric pCO_2 over glacial-interglacial timescales; the mechanism by which this influence is exerted is, however, poorly constrained. Diatom production constitutes about 40% of the total oceanic primary production, making them key players in the modulation of atmospheric CO_2 concentrations and global climate. Additionally better understanding of changes in the surface and deep water carbonate system (eg pH, alkalinity) would provide invaluable insight into the driver(s) of millennial scale climate change. Here, the boron and silicon isotope composition of biogenic silica (siliceous sponges), is being investigated as a potential seawater pH and paleo-productivity proxy.

Relationships were investigated between coupled sponge and seawater samples for Si isotope fractionation compared with equivalent Si concentrations from the water column. Our new results and the subsequent new model offers a new perspective on what controls biological fractionation in biogenic opal and in turn, will yield a novel interpretation of the paleo-oceanic distribution of silicon.

Boron analysis of siliceous sponges aims to examine the nexus between seawater pH, biogenic silica and boron, and thus the utility of boron in siliceous organisms (namely sponges and diatoms) as a pH proxy. First order Comparison between boron and silicon signatures obtained from the same sponge material suggest a coupling between Silicon and Boron system in marine sponges.

Oldest complete vertebrate eye preservation from the fossil record

Gavin C. Young[1]

[1] *Research School of Earth Sciences, The Australian National University, Canberra, ACT 0200, Australia*

The XCT scanning facility in the ANU Research School of Physical Sciences & Engineering has been used on a unique fossil specimen from the 400 million-year-old limestones at Burrinjuck near Canberra (Early Devonian in age). The image below shows the complete eye capsule of an extinct placoderm (armoured) fish, reconstructed from the XCT scanning data using the ANU-developed *Drishti* program. The specimen was originally removed, perfectly preserved, from limestone using acetic acid. Burrinjuck is one of only a few vertebrate fossil localities in the world where extremely thin layers of 'perichondral' bone investing the surface of a cartilage can be preserved and extracted intact. The cartilage at the back of the eyeball was fused to the sclerotic bones forming a ring around the eye opening. The soft part of the eye was completely encapsulated, and all the nerves and blood vessels passing between the eye and the brain are preserved as openings or canals through the cartilage. The new CT scans permit the internal structure of the eye capsule to be studied in great detail.

One of the issues concerning structure of the vertebrate eye is the homology of the six extraocular muscles controlling eye movement. In every vertebrate species these are always innervated by the same three cranial nerves (III, IV, VI). However there are consistent differences of pattern between all living jawless and jawed vertebrates, which are assumed to have evolved at the branching point between these two major groups.

Previously there was no direct evidence of this from the fossil record, but analysis of the nerve canals and muscle attachment points in the placoderm eye capsule, compared to preserved braincase specimens from Burrinjuck, suggested that this extinct group had an extraocular muscle arrangement unknown in any other vertebrate species, living or extinct. This research was published in the Royal Society journal *Biology Letters*, the image below being used on the cover of the journal.

The structure of the vertebrate eye has been used for centuries as an example of biological complexity that proved an 'intelligent designer' created life on the planet. Modern proponents of 'Intelligent Design' present the vertebrate eye as an example of 'irreducible complexity'. Charles Darwin argued in *The Origin of Species by Means of Natural Selection* (1859) that the evolution of complex organs could be explained by natural selection, but the absence of known intermediate stages was due to incompleteness of the fossil record. In an invited contribution to a special issue on eye evolution for the American journal *Evolution: Education and Outreach* I elaborated on the eye capsule evidence, and illustrated a number of other specimens from the famous Burrinjuck fossil locality that demonstrate the structure of the brain in early vertebrates.

This research is supported by ARC Discovery Grant DP0772138.

References

Young, G.C. 2008a. Number and arrangement of extraocular muscles in primitive gnathostomes - evidence from extinct placoderm fishes. *Biology Letters*, **4**: 110-114. [doi:10.1098/rsbl.2007.0545]

Young, G.C. 2008b. Early evolution of the vertebrate eye - fossil evidence. *Evolution: Education and Outreach* (2008) **1**(4): 427-438 [doi:10.1007/s12052-008-0087-y]

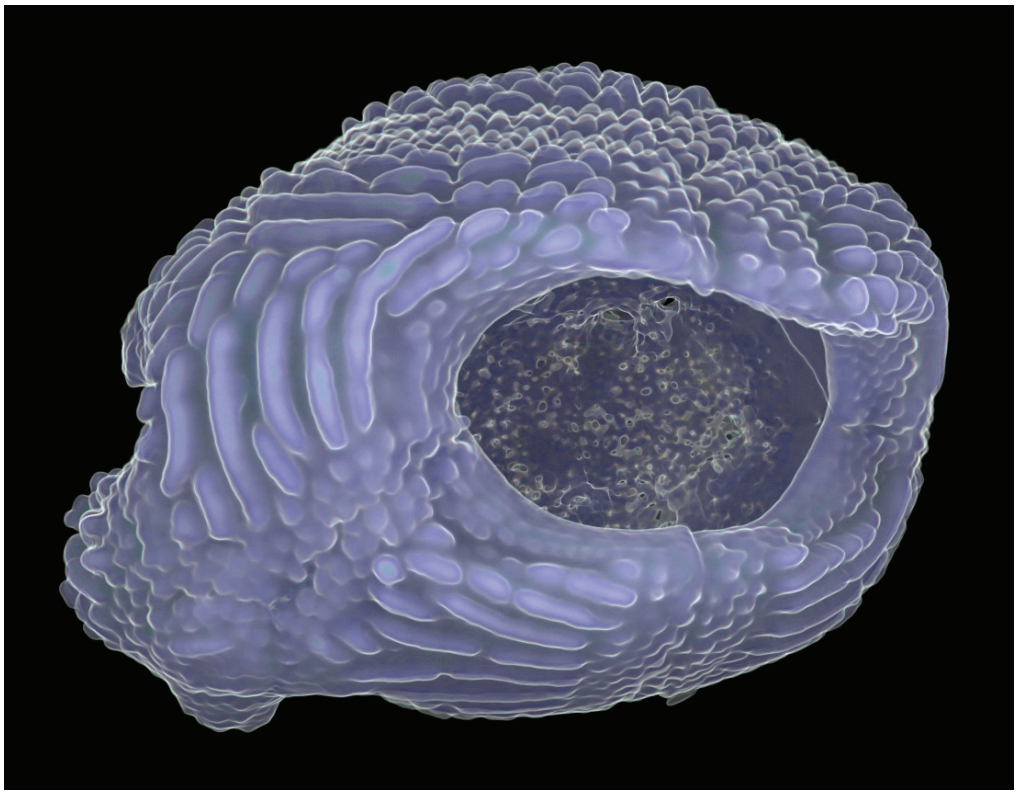

Figure 1. *A 3-D image created by the Drishti program from XCT scanning data of the acid-extracted eye capsule of the placoderm Murrindalaspis from Burrinjuck, NSW (micro X-ray tomography by Dr T. Senden; 3-D rendering using Drishti software by Dr A. Limaye)*

Earth Materials and Processes

The Earth Materials and Processes area comprises groups in Experimental Petrology, Rock Physics, Thermochronology, and Structure & Tectonics. Our research centres around laboratory based measurements under controlled conditions, simulating those occurring in nature, but these activities are complimented by a rich array of analytical equipment and are supported by extensive field-based observations, often in collaboration with scientists from other institutions, nationally and internationally. Through such investigations we are developing understanding of the structure and chemical composition of planetary interiors, and the processes by which they evolve. Our interests start at the very beginning of solar system history with how the Earth and other rocky planets accrete, but also covers the ongoing processes of mantle convection, volcanism, metamorphism, global tectonics and the formation of ore deposits.

Areas of current research activity include:

- The making of terrestrial planets. Chemical constraints on the accretion of the Earth and similar planets from the solar nebula, and the processes of core formation; mineralogical and chemical properties of the deep mantle and their influence on global tectonics.

- The nature of the Earth's upper mantle. Experimental studies and thermodynamic modelling of the phase equilibria relevant to upper mantle melting and ultra-high-pressure metamorphism associated with crustal thickening and subduction; experimental and microstructural studies of phenomena associated with lattice defects and grain boundaries including incorporation of water into nominally anhydrous minerals and microscopic mechanisms of seismic wave attenuation; experimental studies and modelling of grain-scale melt distribution and its implications for melt transport, rheology and seismic properties.

- Coupling between fluid flow and fault mechanics in the continental crust Experimental studies of the role of fault healing and sealing processes in controlling the time dependence of fault strength and permeability at high temperatures and pressures; complementary field-based and modelling studies exploring fluid-driven growth of shear networks with applications to understanding the development of lode gold systems, especially in the Western Australian goldfields.

- Oxidation state and coordination of metal ions at high temperatures. Studies of crystals, melts and hydrothermal solutions by X-ray absorption spectroscopy, using synchrotron radiation. Studies of silicate glasses and melts to very high temperatures under controlled redox conditions. Analysis of hydrothermal solutions trapped in synthetic fluid inclusions is providing important basic information on metal complexes at high temperatures.

Experimental Petrology Introduction

The Experimental Petrology Group uses a laboratory-based experimental approach combined with field observations to study the Earth, its origin, evolution and mineral wealth. The group operates a wide range of experimental apparatuses for generating the high temperatures and pressures that are needed to reproduce the natural conditions within the Earth. The equipment includes: high temperature furnaces capable of reaching 1800°C, several of which are equipped for precise control of oxygen and sulfur fugacities by gas mixing; eleven solid-media piston-cylinder devices for generating pressures to 6 GPa and temperatures in excess of 2000°C, a multi-anvil apparatus, which can presently achieve pressures of 27 GPa; and a well-equipped hydrothermal laboratory.

These high-temperature, high-pressure apparatuses are complimented by an array of microbeam analytical techniques, including a Cameca SX100 electron microprobe; laser-ablation ICP-MS, which is now being used regularly to analyse trace-elements in experimental run products; a STOE STADIP powder X-ray diffractometer; and FTIR spectroscopy for the determination of H2O, CO2 and other volatile species in minerals and glasses. To complement this latter facility, the group acquired a Agilent 6850 Gas Chromatograph, which has been combined with a capsule-piercing device to enable the extraction and analysis of small quantities of C-O-H fluids from high-pressure experimental run products.

As well as the conventional 1/2 inch and 5/8 inch apparatus for use to 4 GPa, the group's piston-cylinder laboratory also runs a high-pressure device that is now operating regularly at 6.5 GPa; the laboratory also has two large-capacity piston-cylinder devices that take 30 mm and 50 to 65 mm diameter pressure assemblies respectively, enabling pressure to be controlled extremely accurately, and which are capable of synthesising relatively large volumes of high pressure phases for detailed mineralogical studies. A novel diamond composite hard material, developed in these apparatuses and now under commercial production, offers promise as an anvil material to extend the pressure range of the multi-anvil apparatus above 26 GPa, thereby allowing detailed experimental exploration of the pressure-temperature regime of the Earth's lower mantle. To further this research the multi-anvil apparatus has now been refurbished and provided with full computer control of pressure and temperature.

In recent years the group has become increasingly involved in developing methods to characterise geologic materials by X-ray absorption spectroscopy (XANES) and related techniques that use synchrotron radiation. Research in this area is presently concentrating on oxidation states in silicate melts, including in-situ measurements at temperatures to 1500°C, and speciation in ore-forming hydrothermal solutions. Members of the group continue to investigate conditions and processes in the Earth's upper mantle (Professors David Green and Hugh O'Neill, Dr Robert Rapp), and metamorphism in the continental crust (Dr Joerg Hermann), as well as the physical chemistry of ore-forming solutions (Drs John Mavrogenes, Katy Evans).

On twinning and microstructures in calcite and dolomite

Andrew G. Christy[1], Ann-Kristin Larsson[2]

[1] *Research School of Earth Sciences, Australian National University, Canberra, ACT 0200, Australia*
[2] *Research School of Chemistry, Australian National University, Canberra, ACT 0200, Australia*

Electron diffraction of the rhombohedral carbonate minerals can show additional diffraction spots which have been ascribed to various metastable Ca-Mg ordering schemes that remain unknown as macroscopic minerals. We have found that such reflexions can be produced by nanoscale twin domains which appear to be widespread in both biogenic and abiogenic carbonates. Because of the many metrical pseudosymmetries in the calcite structure, such twins can produce diffraction resembling that of commensurate modulated structures. Twin nanodomains on {104}, in particular, can produce the diffraction patterns of any of the supposed "g", "m" and "n" superstructures, provided only that the usual carbonate orientational order is lost in the twin. Thus, these superstructures may not actually exist, and controversies surrounding their occurrence may not be irrelevant. {018} twins are also common, and diffract similarly to a fivefold superstructure.

Larsson A-K, Christy AG (2008) On twinning and microstructures in calcite and dolomite. *Amer. Mineral.* **93**: 103-113.

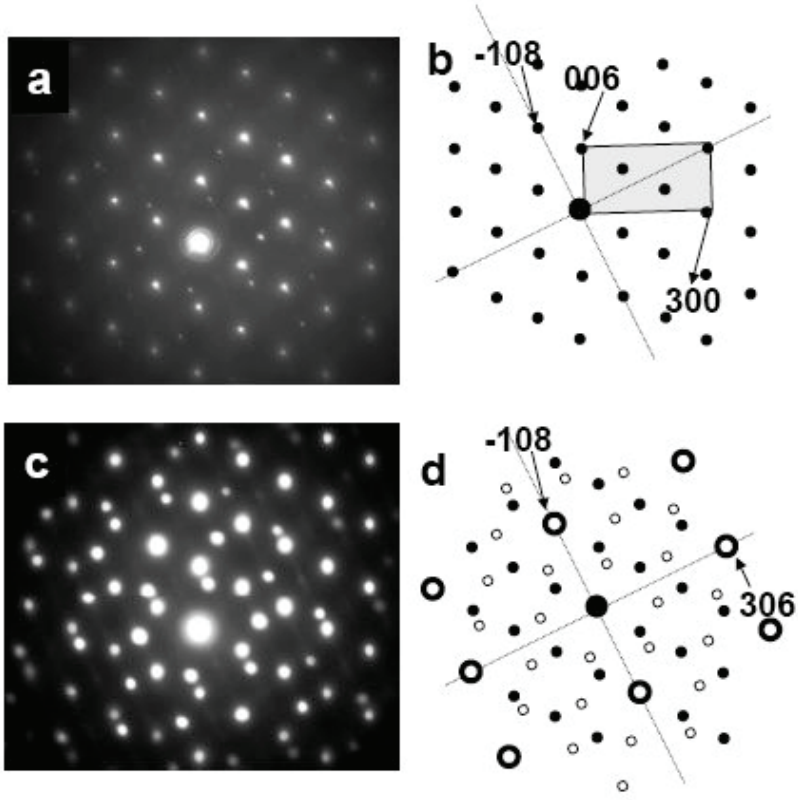

Figure 1. Electron diffraction patterns of a calcite crystal from a sea urchin shell. (a) Selected area is about 1 mm diameter, weak diffraction can be seen that is additional to that of the host crystal. (b) Indexed, consistent with viewing direction [010]. (c) Smaller selected area of 100 nm diameter, enhancing reflexions from a small {018} twin domain which gives trhe appearance of a fivefold superstructure.

Multiple element diffusivities in natural olivine xenocryst from high-Mg diorite

Jörg Hermann[1], Qian Qing[1], Hugh St.C. O'Neill[1]

[1] *Research School of Earth Sciences, The Australian National University, Canberra, ACT 0200, Australia*

Despite solid-state diffusion being central to many geological processes, little is known about the factors controlling the rates of diffusion of different species in silicate minerals. Theoretical modeling of diffusivities in silicates suffers from a general lack of empirical data against which the modeling can be tested.

Olivine xenocrysts (0.5-3 mm in diameter, up to 20% in volume) were found in the chilled margin of one of the plutons of high-Mg diorite from Handan-Xingtai, central North China block, which was formed at an intracontinental setting. These hybridized high-Mg dioritic rocks formed during cooling from ~ 1000°C. One crystal with favorable dimensions and orientation, and despite some dissolution still retaining a crystal face, indicating minimal dissolution (Fig. 1), was selected for detailed study. Concentration profiles of Mg, Fe, Mn and Ni were determined by electron microprobe. The olivine was normally zoned in Mg/Fe, with Fo# [100*Mg/(Mg + Fe^T)] decreasing from core (89.1-93.2) to rim (73.2-81.4). Element mapping with the electron microprobe showed a gradual change of Fe, Mg, and Mn contents (Fig. 2). Concentration profiles of trace elements (Li, Na, Al, P, Ca, Sc, Ti, V, Cr, Mn, Co, Ni and Y) were then determined along the same or similar profiles by laser-ablation inductively-coupled plasma mass spectrometry (LA-ICP-MS). The profiles were acquired using different spot sizes as well as continuing scans using a 7 x 70 µm slit (Fig. 2).

The obtained data (Fig. 3) allow trace diffusion coefficients to be evaluated relative to Mg-Fe interdiffusion under conditions that cannot be accessed in the laboratory. The effective diffusion coefficients of many trace elements (Li, Ca, Sc, Mn, Co, Ni and Y) fall within a factor of three of each other and of the mean Mg-Fe interdiffusion coefficient, in agreement with results from laboratory experiments at higher temperatures (Spandler et al. 2007). By contrast, the profiles for Na, Ti and V imply much faster diffusion rates, while P shows no discernible diffusion. The Al and Cr profiles, which are well correlated with each other, are highly complex and variable on a small length scale. These data show that the diffusion coefficients of cations in olivine are not simple functions of either ionic charge or ionic radius. Using published Mg-Fe interdiffusion coefficients (Dohmen and Chakraborty, 2007), the characteristic residence time of the olivine xenocryst is modeled to be about 10^2 to 10^3 years.

Dohmen R, Chakraborty S (2007) Fe-Mg diffusion in olivine _: point defect chemistry, change of diffusion mechanisms and a model for calculation of diffusion coefficients in natural olivine. *Physics and Chemistry of Minerals* **34**, 409-430, doi: 10.1007/s00269-007-0158-6

Spandler C, O'Neill, HStC. Kamenetsky V.S. (2007) Survival times of anomalous melt inclusions from element diffusion in olivine and chromite. *Nature* **447**, 303-306. doi: 10.1038/nature05759.

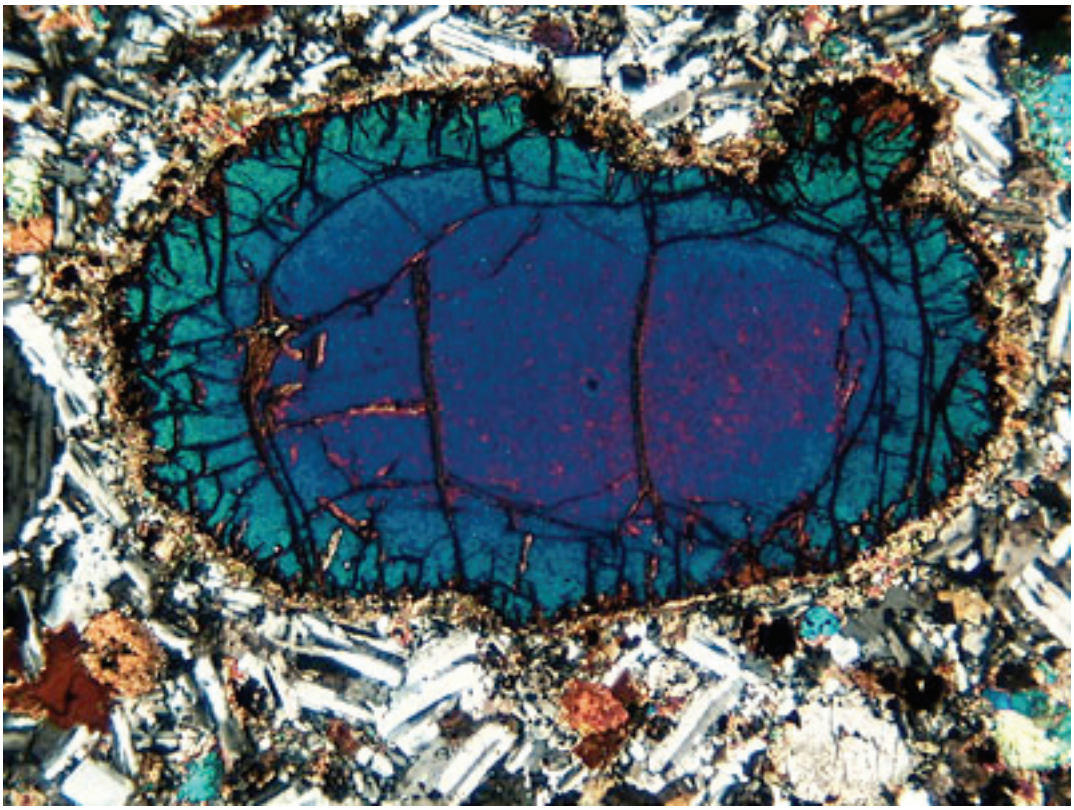

Figure 1. Microphotograph (X Nicols) of an olivine xenocrist embedded in a diorite matrix consisting of plagioclase, clinopyroxene, amphibole, biotite and quartz. The olivine grain is surrounded by a small corona of orthopyroxene. The change in interference colors from core to rim is related with an increase in fayalite component in olivine.

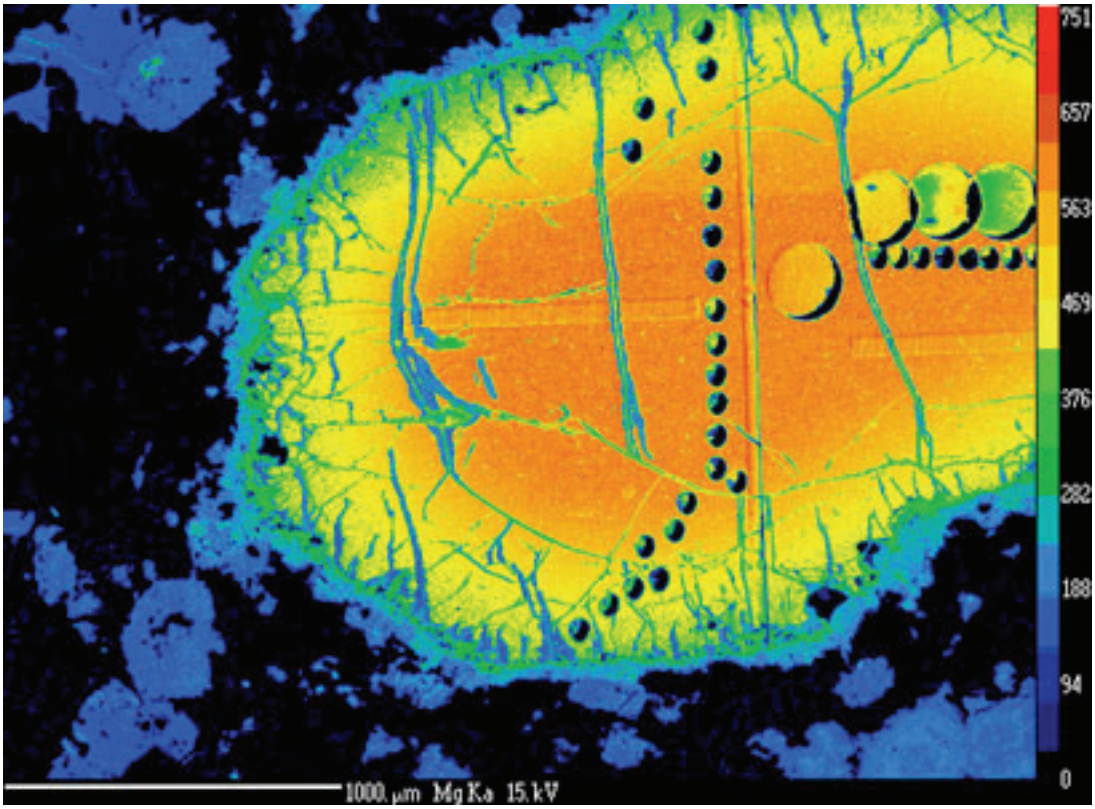

Figure 2. Mg distribution X-ray map of the investigated olivine. Mg continuously decreases from core to rim. Also shown are the different ablation pits (180 µm, 70 µm spot size) and the tracks from the LA-ICP-MS analyses.

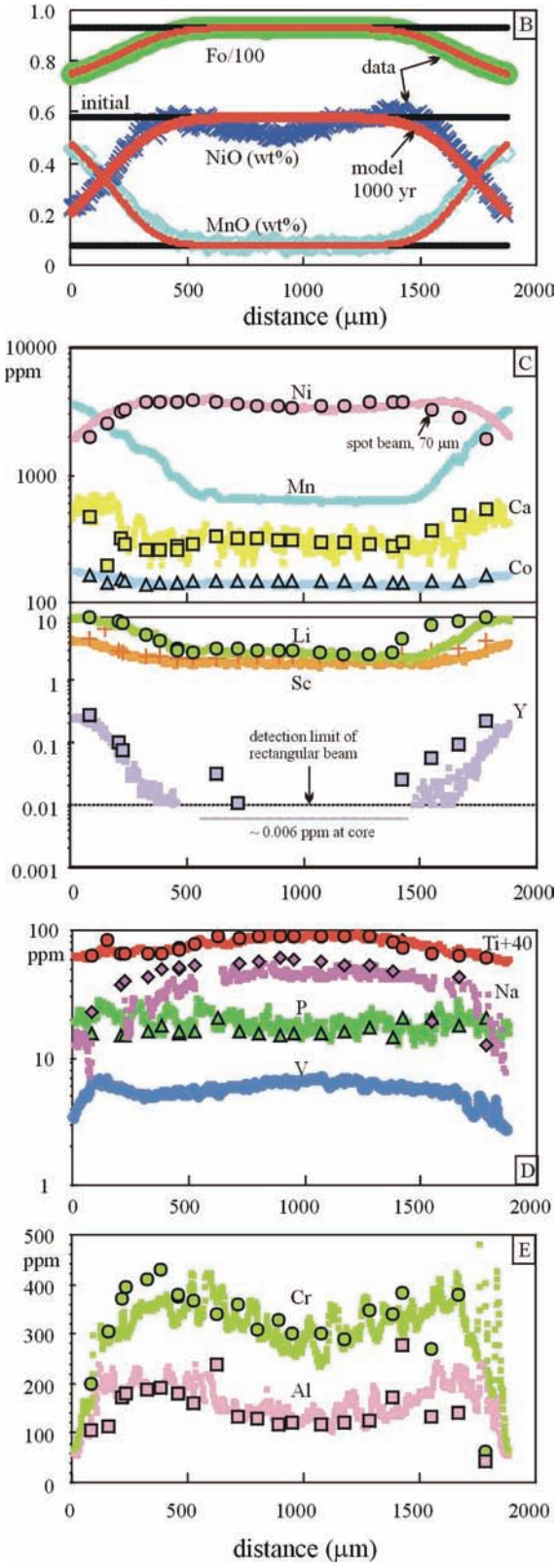

Figure 3. Profiles through the olivine grain. B) Major element data for the forsterite content and NiO and MnO in wt.% from electron microprobe analysis. The red line refers to modeled diffusion profiles indicating that the olivine had a ~1000 year residence time at 950-1000°C. C), D) and E) Trace element profiles in olivine determined with LA-ICP-MS analyses (all values in ppm). Continuous lines were measured in scan mode whereas symbols refer to single spot analyses. Note the similar diffusion behavior of ions with different charges such as Li (1+), Mn (2+) and Y (3+).

Determination of Selenium Concentrations in NIST SRM 610, 612, 614 and Reference Materials using the Electron Probe, LA-ICP-MS and SHRIMP II

Frances E Jenner[1], Peter Holden[1], John A. Mavrogenes[1],
Hugh St.C. O'Neill and Charlotte M. Allen

[1] *Research School of Earth Sciences, Australian National University, Canberra, ACT 0200, Australia*

Selenium (Se) is a trace element with distinctive geochemical properties, which have yet to be exploited in petrology because of the analytical difficulties associated with its low concentrations in geological materials. Selenium (Se) has 6 naturally occurring stable isotopes; ^{74}Se, ^{76}Se, ^{77}Se, ^{78}Se, ^{80}Se and ^{82}Se and is both volatile and strongly siderophile. Constraining the range of Se concentrations in mantle-derived rocks is important to studies of planetary differentiation, partial melting models and recycling of lithospheric components into the mantle.

The abundance of Se in the mantle is not well known, but has been estimated to be 79 ppb by assuming chondritic Se/S (Palme and O'Neill 2003). Due to the time-consuming and often complicated sample preparation techniques used by previous studies (see Johnson and Bullen 2004 for a comprehensive review) and the high levels of analytical sensitivity required, little is known about the behaviour of Se in igneous systems.

In situ analysis of geological materials such as natural volcanic glasses and minerals, using LA-ICP-MS, allows the rapid measurement of major and trace element data for a wide range of elements that are below the detection limits of the electron microprobe (EMP). The quantification of LA-ICP-MS data of unknown samples is dependent on the analysis of calibration materials, such as NIST SRM 610 and 612. Currently, no published value is available for the concentration of Se in NIST SRM 612. We have used a combination of EMP, Sensitive High Resolution Ion Microprobe II (SHRIMP) and/or LA-ICP-MS techniques to measure the concentration of Selenium (Se) in NIST SRM 610, 612, 614 and a range of reference materials. The new reference value for Se in NIST 612 was then to measure the concentrations of Se in natural volcanic glasses.

Johnson, T. M., Bullen, T. D. (2004). Mass-Dependant Fractionation of Selenium and Chromium Isotopes in Low-Temperature Environments. In: Johnson, C. M., Beard, B. L., Albaréde, F. (Editors), Geochemistry of non-traditional stable isotopes. Reviews in Mineralogy and Geochemistry. Mineralogical Society of America, pp 289-317.

Palme, H, O'Neill, H. St.C. (2003). Cosmochemical Estimates of Mantle Composition, Treatise on Geochemistry. Elsevier Ltd., pp. 1-38.

XANES Analysis of Ni & Co in silicate glass: A Preliminary Investigation of Pressure Induced Changes in Their Coordination Environment

Jesse Jones[1], Hugh St.C. O'Neill[1] and Andrew Berry[2]

1 Research School of Earth Sciences, Australian National University, Canberra, ACT 0200, Australia
2 Department of Earth Science and Engineering Imperial College London, South Kensington London SW7 2AZ United Kingdom

The XANES region of the x-ray absorption spectrum (typically within 30-50 eV of the absorption edge) is strongly sensitive to both formal oxidation state and local coordination chemistry of the element under analysis. Pre-edge features in many transition-metal k-edge spectra provide a qualitative means to determine their coordination environment. Whilst s-p (orbital) is the primary transition for Ni and Co (1s core electron) K-edge spectra, elements of their pre-edge features reflect the degree to which local geometry around the absorbing atom allows hybridization of p-d orbitals, increasing the availability of transition states for the 1s core photo-electron and hence the pre-edge absorption intensity. The extent (if any) to which the intensity and shape of these pre-edge peaks are seen to vary with pressure, indicates a change in allowable hybridization associated with shifts between octahedral, distorted octahedral and tetrahedral symmetry.

To examine the possibility of pressure induced changes in the coordination chemistry of Ni and Co in silicate melt (taking silicate glass as the closest available analogue to a liquid melt structure) a series of high pressure experiments was conducted using a piston-cylinder apparatus (at 1500^{o}) to produce uniform high pressure glasses at 10, 20, 30 & 40 kb for each element. XANES analysis of the experimental glasses was carried out at the KEK PF synchrotron, Tsukuba, Japan. After the appropriate data reduction, our results indicate that whilst Co shows no apparent shift in its coordination environment over the applied pressure range, a systematic change in the coordination symmetry of Ni can be seen to occur toward the upper 40 kb limit of the study. This shift to a lower pre-edge peak intensity at higher pressures suggests a transition from tetrahedral coordination, where increased p-d hybridization occurs at lower pressures, toward a more centro-symmetric octahedral symmetry reflected by the lower intensity 40 kb peak. Further experiments are planned to examine this shift over an expanded pressure range.

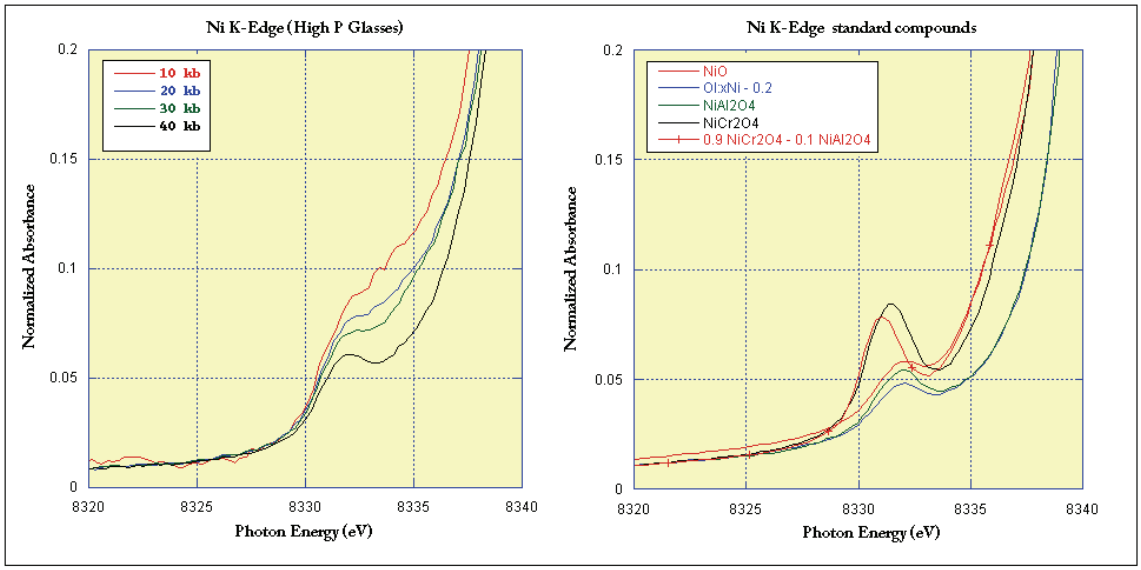
Ni K-Edge (High P Glasses)
10 kb
20 kb
30 kb
40 kb
Normalized Absorbance
Photon Energy (eV)
Ni K-Edge standard compounds
NiO
OlxNi - 0.2
NiAl2O4
NiCr2O4
0.9 NiCr2O4 - 0.1 NiAl2O4
Normalized Absorbance
Photon Energy (eV)

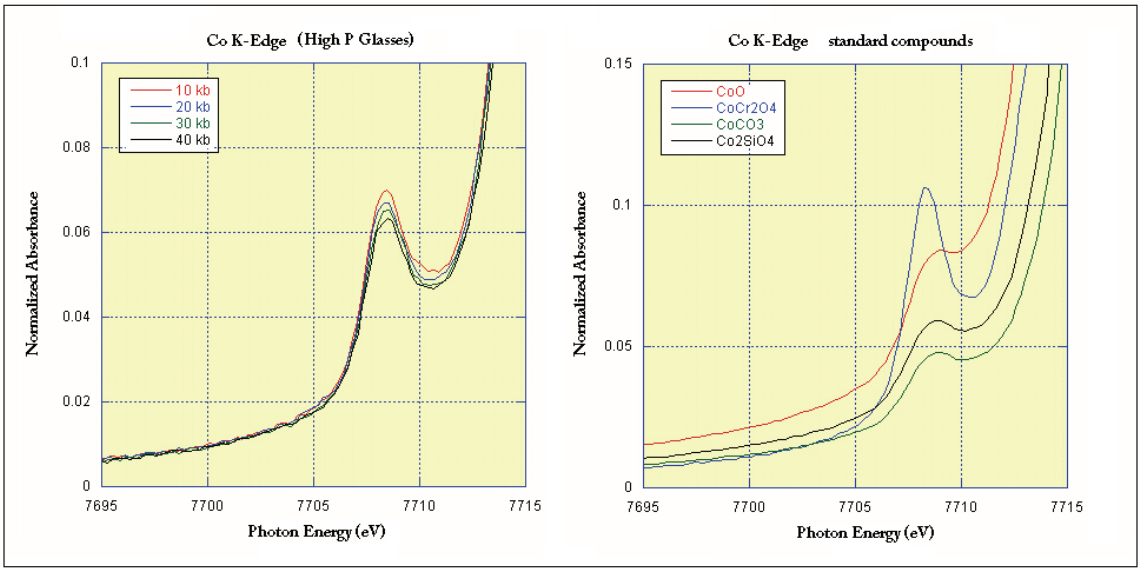
Co K-Edge (High P Glasses)
10 kb
20 kb
30 kb
40 kb
Normalized Absorbance
Photon Energy (eV)
Co K-Edge standard compounds
CoO
CoCr2O4
CoCO3
Co2SiO4
Normalized Absorbance
Photon Energy (eV)

Trial to establish muscovite-paragonite solvus by synthesis experiments

Huijuan Li [1], Hugh O'Neill[1], Jörg Hermann[1] and Ulli Troitzsch[1]

[1] *Research School of Earth Sciences, Australian National University, Canberra, ACT 0200, Australia*

Since the pioneering work of Eugster and Yoder (1955), numerous efforts have been made to study the nature of Ms-Pa solvus and its application as geothermometry by experimental work (Flux & Chatterjee, 1986 and references therein). Guidotti (1994) stated: "Unfortunately, field, experimental and thermodynamic investigations of Pg-Ms equilibria have yielded conflicting results".

In this study, we planned to obtain Ms-Pa solvus brackets at various T and 20 kbar by hydrothermal treatment of a variety of gel starting materials using Piston-Cylinder apparatus. Paragonite can be stable at a wider temperature interval at 20 kbar and high pressure will contribute to a faster and closer approach to the equilibrium.

The XRD spectra of all the runs accord with the spectra of 2M1 polytype mica. Through a calibration curve expressing cell volume *V* (Å) as a function of X_{ms}, we can obtain the compositions of predominant K-rich mica which are plotted in Fig 1. For run C3170 at 700°C, 20kbar, single phase mica was formed (blue circle in Fig 1), of which similar compositions were got from probe (X_{ms}=0.645) and XRD (X_{ms}=0.622). For runs at 650°C, 20kbar with 50%Ms+50%Pa as starting material, two phases of micas coexist, and the composition for K-rich mica is around X_{ms}=0.58. K-rich mica with X_{ms}=0.6587 was formed and Na-rich mica decomposed to Jadeite and Kyanite in run D1004 at 600°C, 20kbar. We obtain a graphical Ms limb of the solvus which locates at lower temperature than it should be according to the models in Chatterjee & Flux (1986) and Roux & Hovis (1996).

Eugster HP, Yoder HS (1995) Micas: The join muscovite-paragonite. *Carnegie Inst. Washington Yearbook* 54, 124-126

Guidotti CV, Sassi FP, Blencoe JG, Selverstone J (1994) The paragonite-muscovite solvus: I P-T-X limits derived from the Na-K compositions of natural, quasibinary paragonite-muscovite pairs. *Geochimica et Cosmochimica Acta* 58, 2269-2275

Chatterjee ND, Flux S (1986) Thermodynamic mixing properties of muscovite-paragonite solid solutions at high temperatures and pressures, and their geologic applications. *Journal of petrology* 27, 677-693

Roux J, Hovis GL (1996) Thermodynamic mixing models for muscovite-paragonite solutions based on solution calorimetric and phase equilibrium data. *Journal of petrology* 37, 1241-1254

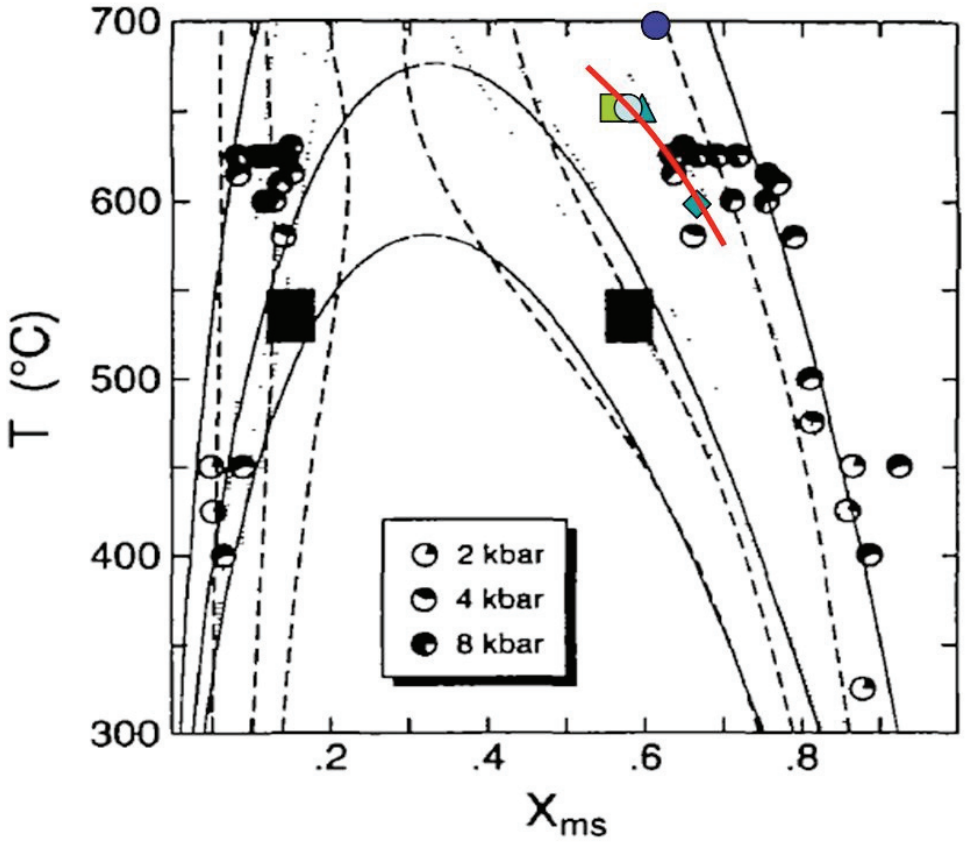

Figure 1. Comparison of results in this study with the solvi calculated at 2, 6 and 15 kbar using Model D (continuous lines), Model A (dashed lines) and chatterjee & Flux (1986) (dotted lines). The rectangular boxes and circles are compositions for natural micas from Grambling (1984) and Guidotti et al. (1994). (from Roux & Hovis, 1996)

The redox state of terrestrial basalts determined by V/Sc olivine-melt partitioning data

Guil Mallmann[1], Hugh O'Neill[1], Frances Jenner[1], Marc Norman[1], Steve Eggins[1], Richard Arculus[1] and Chris Ballhaus[2]

[1] Research School of Earth Sciences, Australian National University, Canberra, ACT 0200, Australia
[2] Mineralogisch-Petrologisches Institut, Universität Bonn, Poppelsdorfer Schloss, Bonn 53115, Germany

The dependence of the partitioning of V between olivine and silicate melt ($D_V^{ol/m}$) on oxygen fugacity was used to estimate directly the redox state of primitive terrestrial basaltic and picritic magmas at that stage in their evolution when they begin to crystallize olivine. The effect of other variables was accounted for by rationing $D_V^{ol/m}$ to $D_{Sc}^{ol/m}$, because the partitioning of Sc, a redox insensitive element having approximately the same incompatibility at terrestrial oxygen fugacities, is shown to depend rather similarly on melt composition. The method was calibrated on basaltic compositions equilibrated in the laboratory (one atmosphere) at QFM and QFM-2.7 between 1300 and 1400°C. We demonstrated that this method can be effective over the entire range of redox conditions observed in geological and cosmochemical materials, and therefore may serve as a universal redox indicator in olivine-phyric mafic volcanic rocks. Our preliminary assessment indicates accuracy in relative oxygen fugacity between 0.2 to 0.5 log units, but precision typically better than ±0.2 log units. The method was applied to 41 mid-ocean ridge (MORB), 25 ocean island (OIB), and 13 island arc (IAB) recent primitive basalts and picrites. The data indicate that MORBs and OIBs record a very restrict range of redox conditions, between QFM and QFM+1, with no clear distinction between them. However, IABs record consistently more oxidizing conditions, ranging from QFM+0.5 to QFM+3 (average at QFM+1.7). Except for MORBs, for which the data cluster exactly on the maximum redox condition ever reported, the results presented here are in good agreement with previous estimations using various methods in minerals and melts.

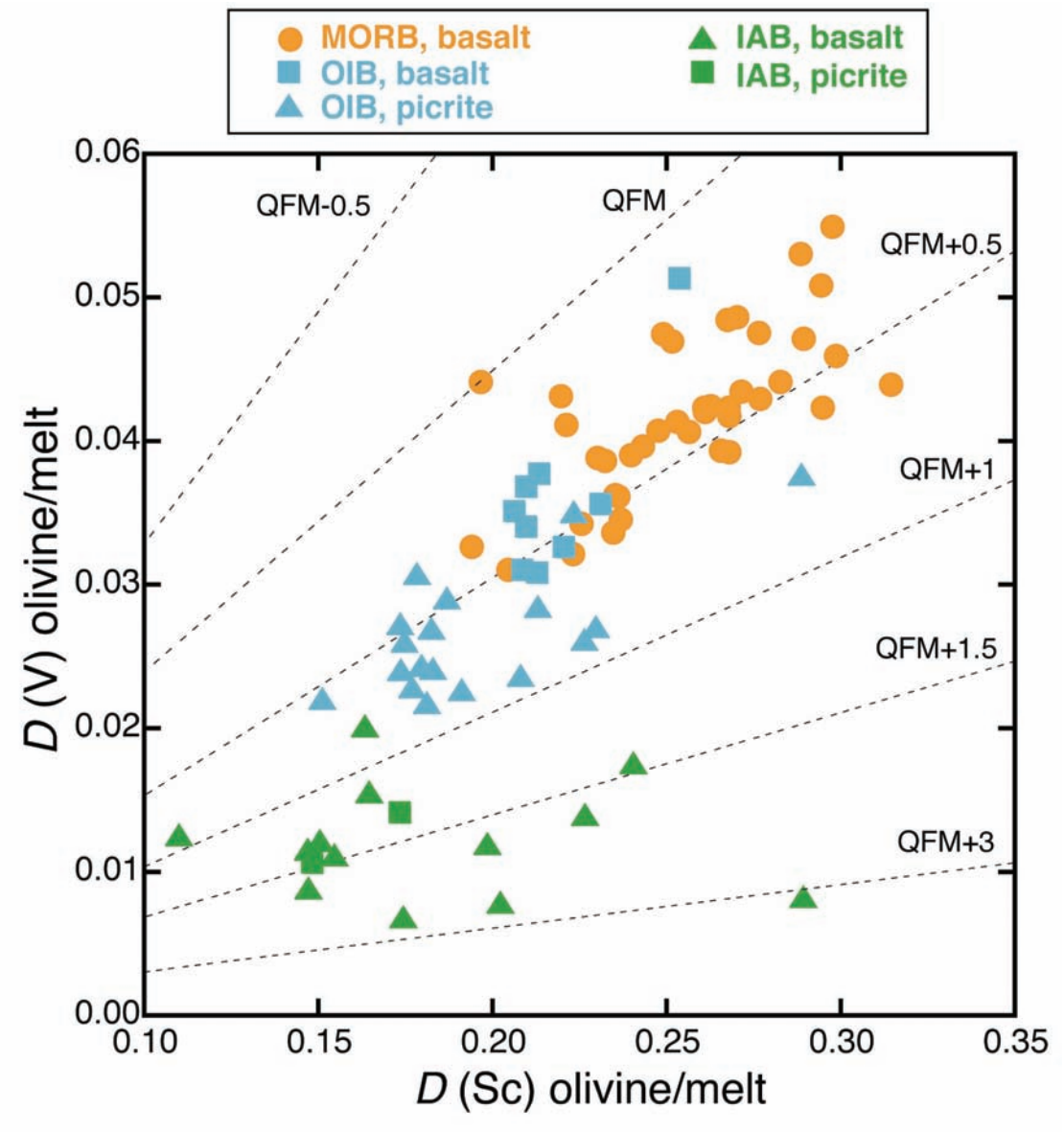

Figure 1. Partition coefficients obtained empirically for V and Sc between olivine phenocryst and silicate melt (glass or matrix). The positive correlation between is indicative of effects (possibly melt composition) other than oxygen fugacity. The dashed lines, illustrating values of oxygen fugacity relative to the QFM buffer, were calculated based on the experimental partitioning data.

Experimental investigation of fluid transfer in sub-arc mantle conditions

Cassian Pirard[1] and Jörg Hermann[1]

[1] *Research School of Earth Sciences, Australian National University, Canberra, ACT 0200, Australia*

Fluid transport from the subducted slab to the locus of partial melting in the mantle wedge in volcanic arcs is a process which is still strongly debated. Two end member mechanisms are considered: 1) porous fluid transfer through the mantle or 2) focused fluid flow in dykes/channels. These two processes are very different and the composition of reacted fluids arriving at the locus of partial melting in the mantle wedge must have different trace element signatures depending on which process is involved.

The main goal of this experimental study is to constrain the change in composition of the fluid as a result of these two ways of fluid transport. Experiments were performed on natural San Carlos olivine representing a simplified mantle and various pre-synthesized, trace element doped, hydrous felsic glass identified as slab-extracted melts (Fig.1)(Hermann & Spandler, 2008). Synthesis piston cylinder experiments were carried out in gold capsules for a week in the range 700°-1100°C and 35kbar which represent average values for the extraction of slab-fluids into the mantle (Fig.2).

Porous fluid transport was simulated by mixing a 1 to 4 ratio of fine grained hydrous felsic glass with fine grained olivine. One end of the capsule was filled with carbon spheres in order to collect the reacted quenched fluid at the end of the run. These mixed charges show an olivine-orthopyroxene-biotite±garnet± amphibole assemblage in equilibrium with a fluid (Fig. 1a). Fluid traps collected in K_2O-rich experiments (amphibole barren) were analyzed with laser ablation ICP-MS. Fluid composition was calculated using Ce as internal standard and normalized on the initial felsic glass. It appears that the crystallization of phlogopite has a strong impact on the composition of the fluid. The K_2O/H_2O ratio is considerably diminished (Fig. 2) and the LILE have a strong affinity to follow potassium in phlogopite whereas LREE, MREE and HFSE tend to be enriched into the fluids. In the case of the H_2O-rich experiments, the presence of amphibole and biotite modify the system. Fluids are less abundant and most of the initial starting material is retained in a hydrous peridotitic mix.

Focused fluid was simulated by a layered experiment of hydrous felsic glass overlying coarse olivine grains. A carbon spheres fluid trap was placed over the olivine layer. Significant differences are observed in this type of experiment compared to the mixed experiments. A reaction zone consisting of an orthopyroxenite layer ±garnet only occurs at the interface between olivine and the felsic glass and neither phlogopite nor amphibole has been observed (Fig.1b). In consequence, the glass composition is very similar to the starting composition and the shielding provided by the garnet-orthopyroxenite reduced strongly interactions with olivine, keeping the K_2O/H_2O high. LILE remain high in the quenched glass and REE and HFSE are less affected with respect to the initial starting glass.

These two types of experiments show that there are strong differences in transport behaviour of LILE in the mantle wedge dependent on the fluid flow mechanism. The high K_2O/H_2O and LILE contents observed in arc lavas suggest that fluid transfer in sub-arc conditions can occurs by channelled flow. In case of porous flow, fluids are strongly affected by the crystallization of biotite and LILE are retained in the residue (Fig. 2). However, the melting of such hydrous peridotite residues containing both micas and amphiboles could potentially lead to the formation of arc lavas as well.

Hermann J, Spandler C (2008) Sediment melts at sub-arc depths: an experimental study. *Journal of Petrology* **49**:717-740

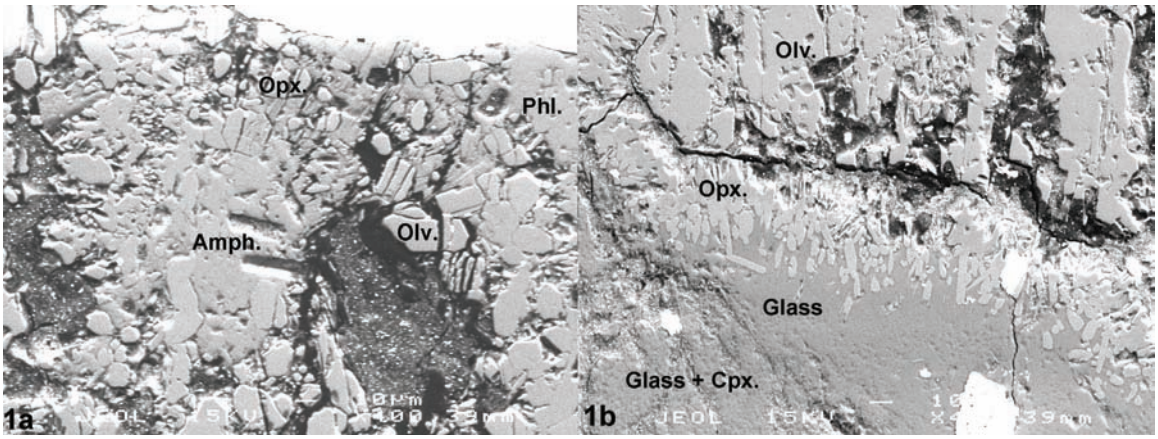

Fig.1. 1a. H_2O-rich mixed experiment showing anhydrous phases (Olivine, Orthopyroxene) and hydrous phases (Biotite, Amphibole) 1b. H_2O-rich layered experiment showing the contact zone between the olivine and the glass, forming an orthopyroxene layer.

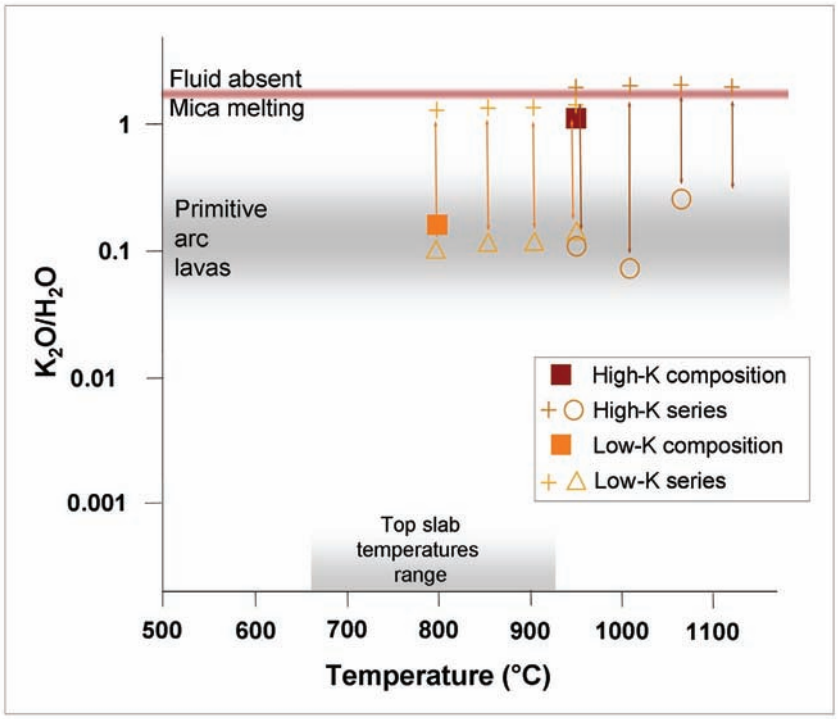

Fig.2. Composition of the different K-bearing phases of these sets of mixed experiments. Full squares are starting compositions; crosses are phlogopite K_2O/H_2O ratios; circles are quenched fluids and triangles give the amphibole composition.

Archean granitoid magmatism and the chemical evolution of the cratonic lithosphere

Robert Rapp[1], Herve Martin[2], Didier Laporte[2], and J-F. Moyen[3]

[1] *Research School of Earth Sciences, Australian National University, Canberra, ACT 0200, Australia*
[2]*Laboratoire Magmas et Volcans, Universite de Blaise Pascal, Clermont-Ferrand, France*
[3]*Department of Geology, University of Stellenbosch, Matteland, South Africa*

Although there is indirect evidence for the existence of continental crust on Earth more than 4.0 Ga ago (Harrison et al., 2005), no intact, preserved fragments of continents have been found. This begs the question when and how did the first truly "nondestructible" continents form? The development of deep (>200 km), old and chemically refractory roots to the continents in the underlying lithospheric mantle appears to be a critical stage in the physical and chemical evolution of Earth's cratons, the old and stable nuclei of the continents. Without roots in the underlying sub-cratonic lithospheric mantle, the preservation of large continental masses over billions of years may not have been possible. Ongoing experimental and field-based petrologic research over the past several years has led to an improved understanding of the genetic links between granitoid magmatism on the early Earth and the development of their roots in the cratonic lithosphere.

It is well established from studies of Archean (~2.5-4.0 Ga old) granite-greenstone and high-grade gneiss terranes around the world that the granitoid plutons comprising the "continental" component in these areas are dominated by rocks of the trondhjemite-tonalite-granodiorite (TTG) suite of granitoids. A number of experimental studies have previously shown that TTG "magmas" can be generated by low-moderate degrees of partial melting of hydrous "metabasaltic" crust in the garnet-amphibolite-eclogite facies (e.g., Rapp and Watson, 1995; Rapp et al., 2003), and thus tectonic processes that lead to overthickening or recycling (subduction?) of secondary basaltic (oceanic?) crust could also culminate in TTG-forming dehydration melting reactions. In the meantime, detailed field-based petrologic and geochemical studies in a number of granite-greenstone terranes (e.g., the Superior Province of Canada and the Pilbara of Australia; see Smithies and Champion, 2000) had identified another suite of Late Archean "post-kinematic" granitoid intrusives (the "sanukitoid" suite), that possessed "primitive" (i.e., mantle-like) characteristics overprinted onto an overall "TTG-like" geochemical signature, suggesting a hybrid lineage with a significant mantle contribution somewhere along the way.

In an effort to constrain the petrogenesis of sanukitoid magmas, we began a series of high-pressure laboratory experiments at 3-5 GPa in which TTG melts were allowed to react with (and assimilate) a peridotite mineral assemblage (Rapp et al., 1999). Our latest results show that primitive (high-magnesium) granitoids (andesites) comparable to Late Archean sanukitoids result from the equilibration of TTG melts with olivine-bearing mantle phase assemblages (Rapp et al., 2009). The resulting olivine-free garnet pyroxenite and garnet websterite reaction residues are currently being characterized in terms of their major- and trace-element compositions, for subsequent comparison with mantle xenoliths from the subcratonic mantle lithosphere.

Harrison, TM, Blichert-Toft, J, Muller, W, Albarede, F, Holden, P, Mojzsis, SJ (2005) Heterogeneous Hadean Hafnium: evidence of continental crust at 4.4 to 4.5 Ga. Science 310, 1947-1950.

Rapp, RP, Watson, EB (1995) Dehydration melting of metabasalt at 8-32 kbar: Implications for continental growth and crust-mantle recycling, *Journal of Petrology* **36**, 891-931.

Rapp, RP, Shimizu, N, Norman, MD, Applegate, GS (1999) Reaction between slab-derived melts and peridotite in the mantle wedge: experimental constraints at 3.8 GPa. *Chemical Geology* **160**, 335-356.

Rapp, RP, Shimizu, N, Norman, MD (2003) Growth of early continental crust by partial melting of eclogite. *Nature* **425**, 605-609.

Rapp, RP, Yaxley, GM, Norman, MD (2008) Genetic relations between Archean granitoid magmatsim and the chemical evolution of subcratonic lithospheric mantle: experimental constraints at 3-4 GPa. *Lithos* Special Volume: 9th International Kimberlite Conference (submitted).

Smithies, R.H. and Champion, D.C. (2000). The Archaean high–Mg diorite suite:

links to tonalite–trondhjemite–granodiorite magmatism and implications for Early Archaean crustal growth. *Journal of Petrology* **41**, 1653–1671.

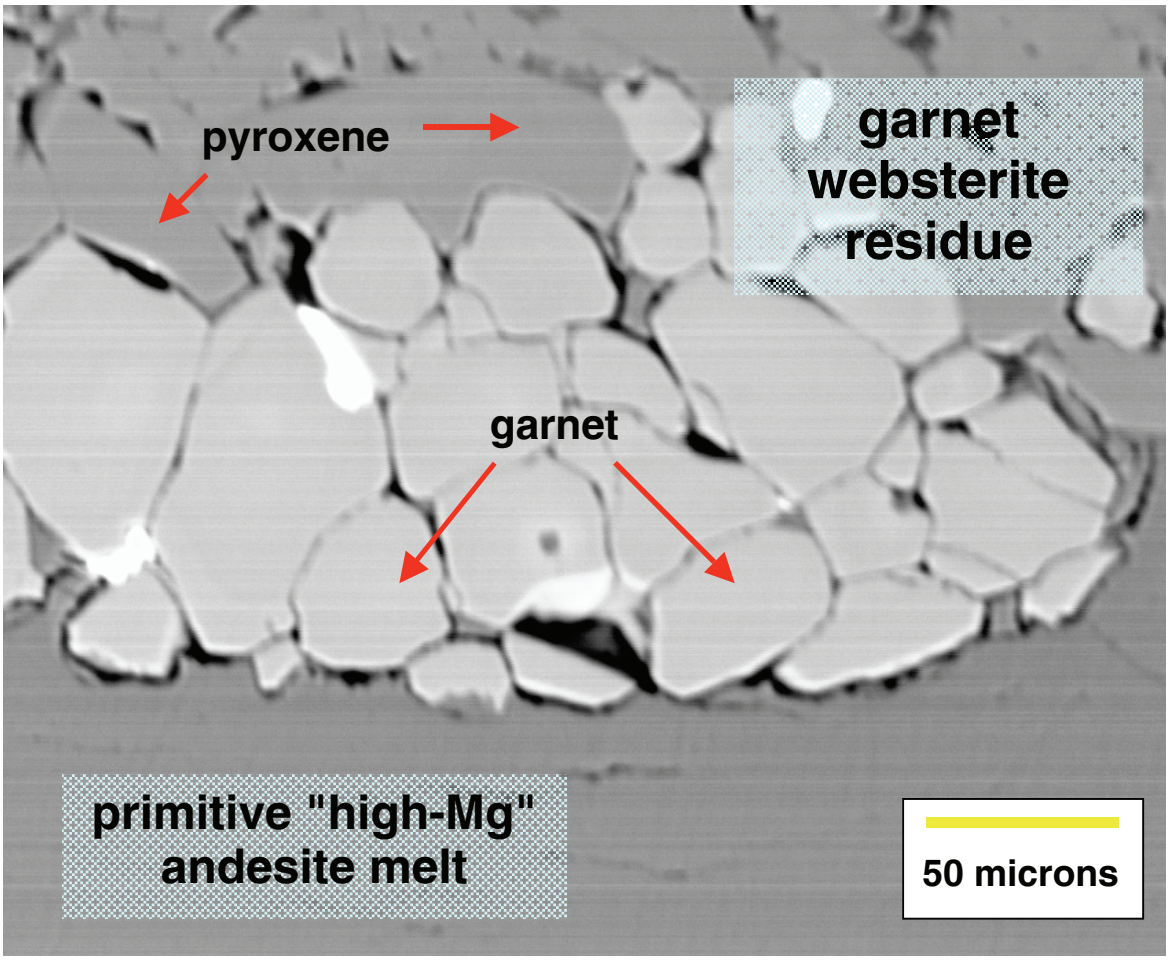

Synthesis and crystal structure of $CuZrTiO_5$: a new inorganic compound

Ulrike Troitzsch[1], Andrew G. Christy[1], David J. Ellis[1] and Anthony C. Willis[2]

[1] *Research School of Earth Sciences, Australian National University, Canberra, ACT 0200, Australia*
[2] *Research School of Chemistry, Australian National University, Canberra, ACT 0200, Australia*

A new inorganic compound, $CuZrTiO_5$, was discovered as a by-product of high-PT experiments with rutile [TiO_2] and baddeleyite [ZrO_2] that were fluxed with CuO. The compound was synthesized in pure form by sintering from the oxides at 1000°C under atmospheric pressure. It is bright green (Figure 1) and strongly pleochroic.

Its composition was confirmed with energy-dispersive x-ray analysis in the scanning electron microscope, and its crystal structure investigated with single-crystal and powder X-ray diffraction.

$CuZrTiO_5$ is orthorhombic, and crystallizes in space group $P2_12_12_1$, with unit cell dimensions a = 3.5871(3) Å, b = 6.6968(4) Å, c = 14.6679(9) Å, cell volume V = 352.35(4) Å, Z = 4, based on a single crystal refinement resulting in R = 0.032 and R_w = 0.079.

The crystal structure is topologically similar to that of In_2TiO_5 (*Pnma*) (Gaedwang et al.1993) but differs in space group and cation coordination (Figure 2). In $CuZrTiO_5$, the two types of In are replaced by Cu and Zr. While $CuZrTiO_5$ has relatively regular TiO_6 polyhedra (Ti-O = 1.84 - 2.18 Å), Zr is in 7+1 coordination (6 O at 2.10 - 2.27 Å and one at 2.811 Å) and Cu shows the 4+2 coordination characteristic of the Jahn-Teller effect. Four O surround Cu in an approximate square at 1.915 - 2.029 Å, while two more distant neighbours lie on opposite sides of the square at 2.565 and 2.591 Å.

In $CuZrTiO_5$, the cations are ordered into layers parallel to (001) of either pure Cu or alternating zigzag chains of Ti and Zr. This layered structure causes the distinct {001} cleavage of $CuZrTiO_5$ observed in the electron microscope (Figure 3).

Gaewdang T, Chaminade JP, Gravereau P, Garcia A, Fouassier C., Hagenmuller P, Mahiou R (1993) Crystal structure and luminescent properties of indium titanate. *Materials Research Bulletin* **28**:1051-1060.

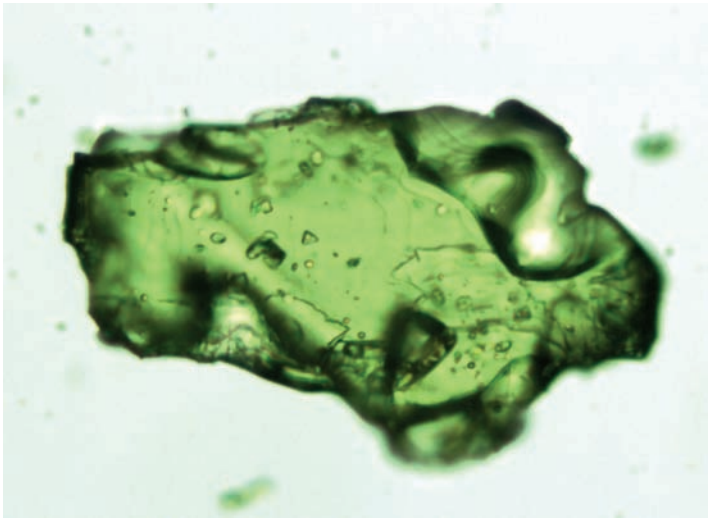

Figure 1.

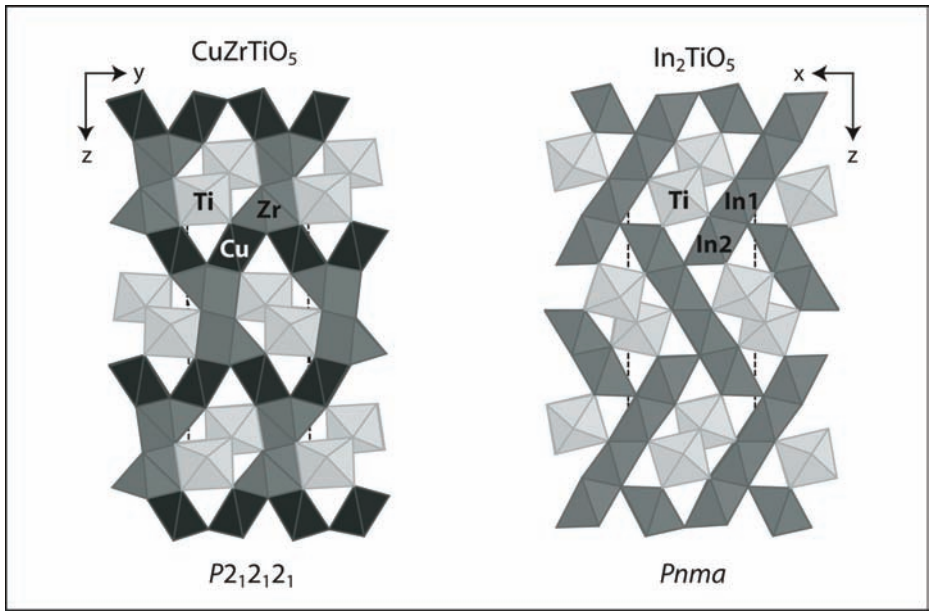

Figure 2.

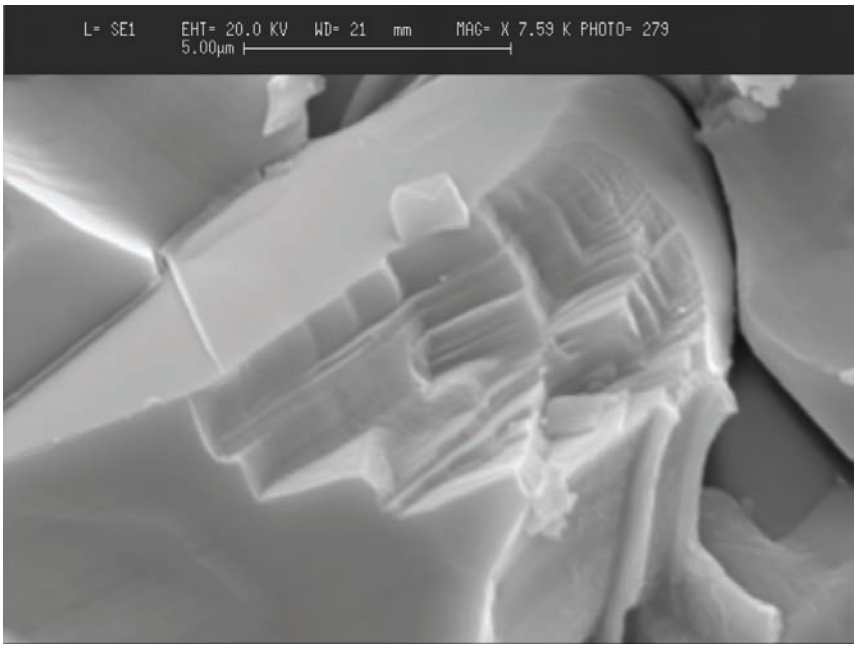

Figure 3.

Coupling between deformation processes and fluid flow in the Earth's crust

Stephen F. Cox

Research School of Earth Sciences, The Australian National University, Canberra, ACT, 0200

Experimental, field-based, microstructural and numerical modelling approaches are being used to explore several aspects of coupling between deformation processes, fluid transport and reaction, especially in fracture-controlled flow regimes.

In 2008, *field-based, modelling, microstructural and microchemical studies* are being used to further explore the growth of faults and fracture networks, and what factors lead to fluid flow becoming localised in certain parts of fracture controlled hydrothermal systems. The research has implications for understanding the localisation of hydrothermal ore deposits within fracture systems, and with minerals industry support, is providing new tools to help enhance exploration strategies. The work is also providing fundamental insights about the roles of reactive pore fluids in controlling fault mechanics and the growth of fracture networks.

Field and modelling studies, in the North Carlin gold systems in Nevada, have evaluated the role of co-seismic static stress changes in governing the distribution of aftershock activity in controlling localisation of fluid flow and related gold mineralisation within particular parts of fault networks.

A study of an Archaean, mesothermal gold system near Kambalda (WA), has shown how, during fault-valve behaviour near the base of the continental seismogenic regime, the relative rates of recovery of shear stress and pore fluid factors after slip events, impact on the internal structure of fault zones, as well as the nature and distribution of gold mineralisation.

In intrusion-related hydrothermal systems, the evolution of fluid pathways and the geometry, distribution, and other characteristics of vein systems, are governed by interactions between stress and fluid pressure states, and by the orientation of stress fields during and after magma emplacement. Stress states and the orientations of stress fields within active intrusive systems respond very dynamically to repeated cycles of inflation and deflation of fluid pressures due to migration of magma and hydrothermal fluids. Repeated variations in stress magnitudes and orientations can also be driven by sudden co-seismic stress relief and more gradual interseismic stress recovery associated with episodic, large earthquakes in convergent margin settings. Additionally, geodetic and seismological studies have demonstrated that episodic fluid migration, as well as cyclic changes in the orientations and magnitudes of stresses, occur on time-scales of years to decades in contemporary magmatic systems. This occurs especially in response to eruption cycles, emplacement of dyke swarms, and effects of nearby earthquakes. Indeed, stress change due to magma migration is likley to be a major driver of seismicity, and associated development of fracture-controlled fluid pathways, up to 15 km from the sites of magma movement. Small dynamic stress changes associated with remote, but large, earthquakes can also trigger microseismicity and attendant fracture propagation and fluid movement in magmatic systems.

A new project, as part of the ANU node of the Centre of Excellence in Ore Deposits, is using this modern understanding of the dynamics of magmatic systems as a basis for undertaking structural, microstructural and alteration studies to analyse the evolution of stress and fluid pressure states during the development of vein systems and faults in intrusion-related hydrothermal systems. The broad goal is to understand how the dynamic evolution of fracture-controlled fluid pathways impacts on the styles of flow

and ore deposition, as well as the distribution of mineralisation. In 2008, attention has focussed on the giant Porgera gold deposit (in the far western PNG highlands). Projects on other intrusion-related systems are being developed for subsequent years. A key early result is that fluid flow, in such fracture-controlled hydrothermal systems, is probably controlled by episodic breaching of substantially overpressured, magmatic fluid reservoirs at depth. Fluid pressure fluctuations are associated with repeated cycles of reservoir breaching and episodic, fluid-driven growth and sealing of fracture networks. These processes have important implications for ore deposition. In particular, large, transient hydraulic gradients promote rapid flow and potentially severe chemical disequilibrium in the ore fluid.

The mechanical and fluid pressure evolution of the Argo fault zone, St Ives goldfield, Western Australia: an example of an Archaean, shear-hosted, mesothermal gold system

Matthew A. Crawford[1] and Stephen F. Cox[1]

[1]*Research School of Earth Sciences, The Australian National University, Canberra, ACT, 0200*

The development of low displacement, moderate to high-angle reverse faults during the formation of the Argo gold deposit, within a tholeiitic gabbro host-rock, involved a four stage evolution of deformation and associated hydrothermal alteration. Fault zone evolution and Au mineralization were associated with high fluid flux, fault-valve behaviour in a severely-misoriented fault zone. The far-field maximum principal stress was approximately east-west and horizontal, and the far-field minimum principal stress was sub-vertical. The fault system developed at approximately 400°C in a transitional brittle-ductile regime, near the base of the continental seismogenic regime. Initial Stage 1 deformation involved ductile shear and the development of potassic (biotite-rich) alteration assemblages and associated reaction-weakening in shear zones; few quartz extension veins were formed. Stage 2 is marked by onset of predominantly brittle shear failure at elevated pore fluid factors, and was associated with widespread development of matrix-supported, dilational breccias in fault zones, and a change to sodic (albite-carbonate-quartz) alteration styles. Extension veins have limited development. Stage 3 is also dominated by brittle shear failure, and characterized by a change to quartz-carbonate assemblages in fault-fill veins and breccias. In contrast to Stage 2, large arrays of extension veins are well-developed adjacent to faults. In Stage 4, widespread sub-horizontal quartz-carbonate-biotite extension veins were developed, but shear failure was limited.

Failure mode diagrams in pore fluid factor ~ differential stress space (Figure 1) illustrate how the structural evolution and styles of mineralisation in the Argo fault system reflect a response to progressive changes in relative rates of change of pore fluid factor and differential stress during individual fault-valve cycles. High fluid fluxes and rapid rates of recovery of fluid pressures, relative to rates of recovery of shear stress after slip events, have maintained the system at near-lithostatic fluid pressures and very low differential stresses during gold mineralization.

The structural and rock mechanics study has been complemented by detailed microstructural, microchemical and stable isotope studies of hydrothermal alteration and vein mineral assemblages to characterise variations in the intensity and style of alteration in space and time in the Argo shear system. This work, together with analysis of gold grade distribution, is providing new insights about structural and geochemical controls on gold deposition at scales ranging from the deposit scale, down to metre-scales.

Laboratory studies of Dislocation Damping

Robert Farla[1], Harri Kokkonen[1], John Fitz Gerald[1], Auke Barnhoorn[1,2], Ulrich Faul[3] and Ian Jackson[1]

[1] Research School of Earth Sciences, Australian National University, Canberra, ACT 0200, Australia
[2] Now at Department of Earth Sciences, Utrecht University, 3508 TA Utrecht, The Netherlands.
[3] Department of Earth Sciences, Boston University, Boston, MA 02215, USA

Last year we presented some preliminary results on dislocation annealing in fine-grained synthetic olivine [1]. Since analyses of these results showed that dislocations can be preserved over laboratory timescales, the first experiments to search for dislocation damping in polycrystals have now been conducted.

Two similar deformed synthetic olivine specimens have been investigated so far. The first specimen, 6618, has been deformed in compression up to 2.3% strain, the second, 6646, to 22%. The resulting dislocation densities are 2.3 and 3.6 μm^{-2} respectively. The specimens were exposed to a maximum temperature of 1100°C, and to oscillating torques of 1 – 1000s periods at each temperature decrement, generating maximum shear strains of around 10^{-5}. The strains are sensed from displacements measured with parallel-plate capacitance transducers.

The first attenuation experiment in torsion on specimen 6616 yielded a surprise null result. This led to some calculations for resolved shear stresses in relation to deformation in compression or torsion and assuming that, at high temperatures, the dominant slip system for olivine involves slip in the [100] direction on the (010) glide plane. The main results are shown in figure 1 for [100](010) slip in a single crystal olivine. The two panels (a) and (b) represent deformation in compression and torsion respectively. The parameters α, and β (and γ) are the direction cosines relative to the crystal axes [α,β,γ] and some major crystal directions are labelled. In uniaxial compression, the resolved shear stress as indicated by the contours in (a) has its maximum value of 0.5 for compression parallel to $[110]_c$. The contours in panel (b) describe the azimuth-dependent resolved shear stress for different torsion axes. Note that torsional deformation around the $[110]_c$ is the least favoured orientation for stressing [100](010). In contrast, a cylinder axis parallel to $[111]_c$ (ie making equal angles with all 3 principal unit-cell axes) is a good trade-off if a single crystal were to be deformed in compression then transferred to attenuation measurements in torsion. For the case of polycrystalline olivine, preliminary calculations show that prior torsional deformation should increase the anelastic strain by 6-fold relative to prior compressional deformation.

Figure 2 shows measurements of Q^{-1} for both deformed specimens with different dislocation densities in comparison to a similar synthetic but undeformed olivine specimen. Only specimen 6646 with the higher dislocation density shows enhanced attenuation and only at the highest temperatures (> 1000°C). In nature, dislocation density should be in equilibrium with the prevailing tectonic stresses in the upper mantle. Dislocation damping will become progressively more important as the grain-boundary dissipation decreases with increasing grain size. Accordingly, dislocation damping could dominate in melt-free material under upper-mantle conditions.

Since the resolved shear stress calculations indicated the need, prior torsional deformation experiments will be done through a collaboration with the University of Minnesota in 2009. Also for single crystals we plan to investigate the possibility of deforming along $[111]_c$ in compression. For both materials, subsequent measurement of the forced torsional behaviour will proceed at ANU.

[1] Farla RJM, Kokkonen H, Fitz Gerald JD, Barnhoorn A, Faul UH and Jackson I (2008) Dislocation recovery in fine-grained synthetic olivine. In preparation for submission to *Physics and Chemistry of Minerals.*

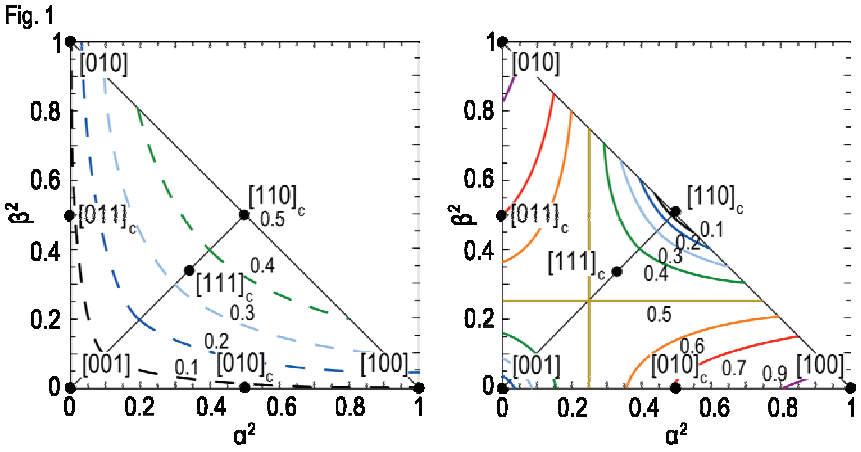

Figure 1. *Calculations showing the resolved shear stress (contours) for uniaxial compression (left) and torsion (right}*

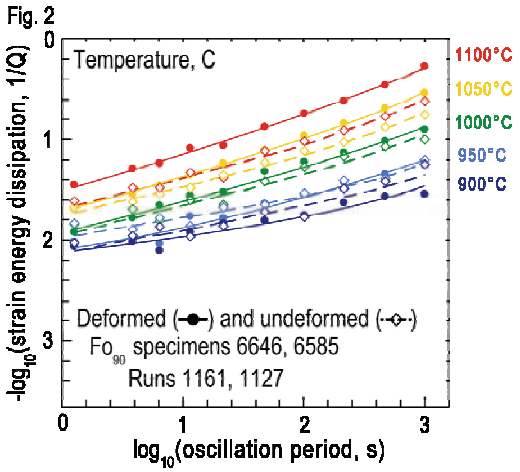

Figure 2: *Q^{-1} data for a deformed (6646) and undeformed specimen (6585).*

Development of fracture-controlled flow regimes and gold mineralisation, Porgera gold deposit, PNG

Angela Halfpenny[1] and Stephen F Cox[1]

[1]*Research School of Earth Sciences, The Australian National University, Canberra, ACT 0200*

Within the framework of the rapidly developing understanding of the dynamics of stress and fluid pressure regimes in contemporary, active magmatic systems, this project is exploring how stress states, stress field orientations and fluid pressures evolved during the development of the large, intrusion-related, hydrothermal gold system at Porgera in the highlands of Papua New Guinea. Fieldwork is being used to document the geometries and styles of vein systems, their overprinting relationships, and relationships to growth of fault networks. This is allowing us to examine how stress states, fluid pressure regimes, and the orientations of stresses evolved during the multi-stage evolution of the hydrothermal system. We are also evaluating what processes drove the growth of fracture-controlled flow networks and the evolution of fluid pathways. A key goal is to understand how the evolution of fracture-controlled fluid pathways and reactions impacts on the distribution of economic mineralisation in multi-stage, intrusion-related hydrothermal systems.

Work in 2008 has focussed on developing a 4D understanding of the evolution of vein distribution, geometries and internal textures during five distinct stages of vein development. The Porgera gold deposit exhibits at least two gold-bearing vein formation stages. The development of the richest vein-hosted Au mineralisation is associated with the growth of several low-displacement faults, which exhibit a complex kinematic evolution involving both dextral and normal slip histories during mineralisation.

The varied internal structures of Au-bearing veins and fault zones, such as textural and mineralogical zoning, in some cases provide evidence for multiple opening and sealing events (Figure 1). Flow in such fracture-controlled hydrothermal systems is unlikely to have been continuous. Instead, flow is interpreted to have occurred as numerous, episodic pulses associated with repeated cycles of breaching of the overpressured, magmatic fluid reservoir by failure events. Breaching events are followed by propagation of fracture arrays driven by migration of a fluid pressure pulse, then progressive sealing of fractures as flow rates decay. Ongoing work is focusing on defining the architecture of major, ore-producing fluid pathways.

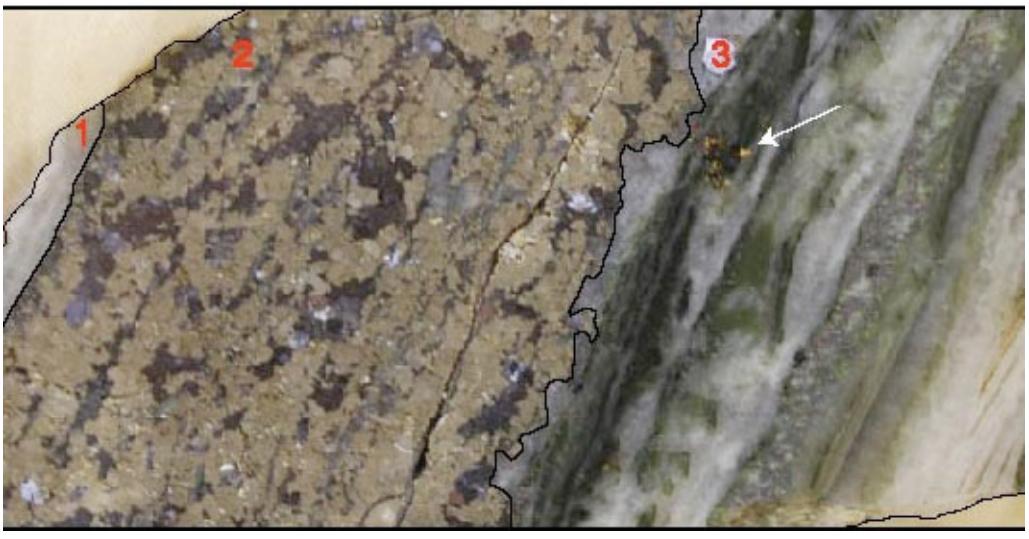

Figure 1. *a. The internal structure of a composite Stage 1 and Stage 2 vein. Section 1 and 3 represent the Stage 2 mineralisation, which exhibits crustiform quartz interlayered with roscoelite-rich layers. The gold is associated with the roscoelite-rich bands and a patch of gold is marked by the white arrow. Section 2 shows the Stage 1 vein.*

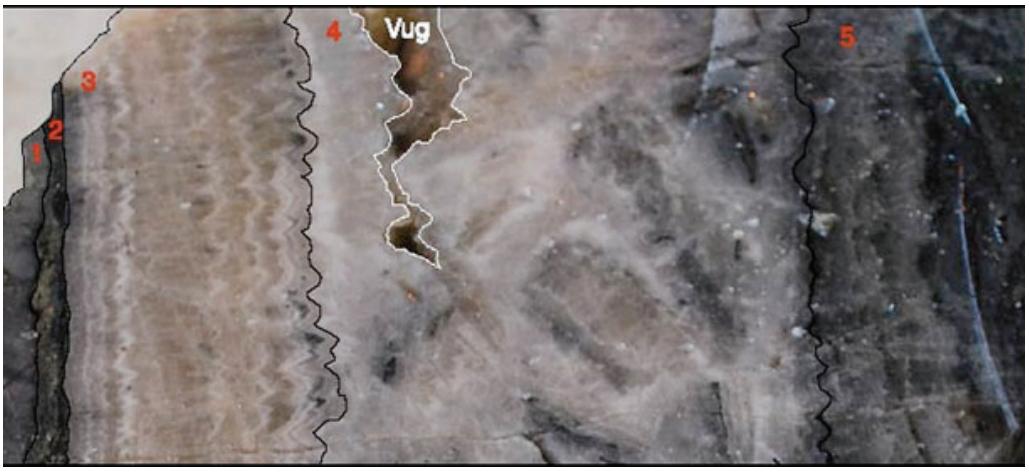

Figure 2. *Internal texture of a complex Stage 2 vein. Section 1 shows the wall rock. Section 2 is a pyrite-rich layer. Section 3 exhibits quartz-rich, crustiform banding which grades out into section 4 which shows a dilatational breccia containing wall-rock and quartz-rich clasts with a crustiform overgrowth. Section 4 also exhibits a vuggy centre to the vein. Section 5 exhibits crustiform banding and was in contact with the wall rock.*

Viscoelasticity, poroelasticity and seismic properties

Ian Jackson, John Fitz Gerald, Robert Farla, Harri Kokkonen, Hayden Miller

Research School of Earth Sciences, Australian National University, Canberra, ACT 0200, Australia

At sufficiently high temperatures in the Earth's interior, the mechanical behaviour changes from elastic to viscoelastic with profound implications for mantle rheology and also seismic wave speeds and attenuation. Such viscoelastic behaviour results from the stress-induced migration of vacancies and dislocations (extended defects reflecting prior or current deformation: see also Farla et al.). Equally, the stress-induced flow of fluids within cracked/porous media results in departures from elastic behaviour, termed poroelasticity. The following are highlights for 2008 of our ongoing study of rheology and seismic properties:

Hot-pressing and high-temperature deformation of titaniferous olivines (with U.H. Faul of Boston University): Work has continued this year towards an understanding of the influence of trace impurities on the rheology of fine-grained polycrystalline olivine. Specimens have been hot-pressed at 1300°C from sol-gel-derived Fo_{90} olivine precursors containing 0.1 wt % each CaO and TiO_2, and deformed at 1200-1300°C in compressive creep tests at progressively higher stress reaching ~300 MPa. Preliminary indications are that these materials (Fig. 1) undergo much more rapid grain growth than their Ti-free counterparts and are significantly weaker.

Seismic-wave dispersion and attenuation (with U.H. Faul, S.J.S. Morris of UC Berkeley, and D.R. Schmitt of the Univ. of Alberta): Our torsional forced-oscillation method for the study of high-temperature viscoelastic relaxation has recently been refined to take account of (i) compliance associated with frictional coupling between the specimen and neighbouring torsion rods, and (ii) significantly viscoelastic behaviour of the alumina control specimen [1]. Our published data concerning the shear modulus G and dissipation 1/Q for fine-grained melt-free and melt-bearing olivine have been re-processed with this improved strategy. Allowance for the compliant frictional coupling results in systematically higher G and lower 1/Q - especially for relatively coarse-grained (low-loss) materials tested at the highest temperatures (≥1200°C) and longest periods (>100 s). These effects are offset to some degree by allowance for the appreciably viscoelastic behaviour of the high-grade polycrystalline alumina control specimen. The interim result is an enhanced grain-size sensitivity of the viscoelastic relaxation (Fig. 2) meaning higher wavespeeds and lower attenuation on extrapolation to upper-mantle grain sizes. Additional experimental data for medium-coarse-grained materials are needed to underpin more robust extrapolation. Planned changes to the experimental procedure involving more active gripping of the cylindrical specimen and use of a single-crystal alumina control specimen may increase the signal/noise ratio for such low-loss materials. In a new initiative, our 'attenuation apparatus' is currently being modified to allow forced-oscillation measurements in extension/flexure, as well as torsion. Such measurements will allow the probing of poroelastic effects in cracked and fluid-saturated media that are analogues for upper-crustal rocks.

Modelling of elastic properties and equation of state (with B.L.N. Kennett): The thermodynamically consistent finite-strain model of Stixrude and Lithgow-Bertelloni (*GJI*, 2005) provides an attractive framework for the assessment and assimilation of experimental data concerning elastic properties and equation of state. The model requires the specification of 9 parameters: molar volume, (isotropic) bulk and shear moduli and their pressure derivatives, the effective Debye temperature, and the Grüneisen parameter and its volume and shear strain derivatives. We have explored the feasibility of using Sambridge's Neighbourhood Algorithm strategy (*GJI*, 1999) to undertake a guided search of the model space that is constrained simultaneously by

diverse experimental datasets as an alternative to iterative least-squares fitting. This approach has been tested on data for MgO including measurements of specific heat and thermal expansion, static and shock compression, and the pressure and temperature dependence of elastic wavespeeds. The search converged on a unique model that adequately represents most of the experimental data, but not before revealing tensions between marginally incompatible datasets.

[1] Jackson, I, A. Barnhoorn, Y. Aizawa and C. Saint. Improved experimental procedures for the study of high-temperature viscoelastic relaxation, *Phys. Earth Planet. Interiors* (in press).

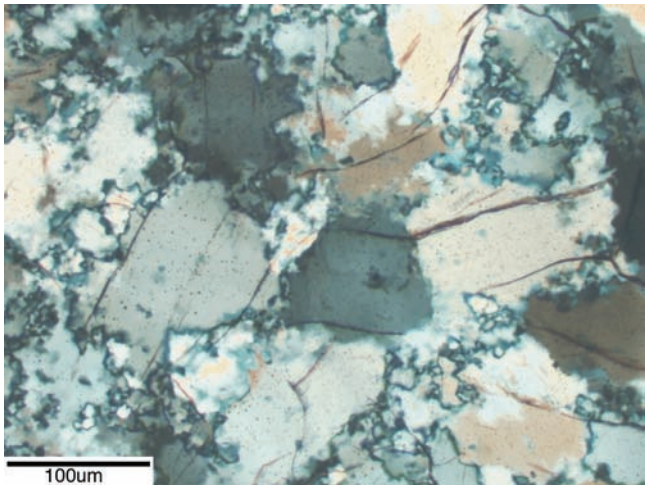

Figure 1

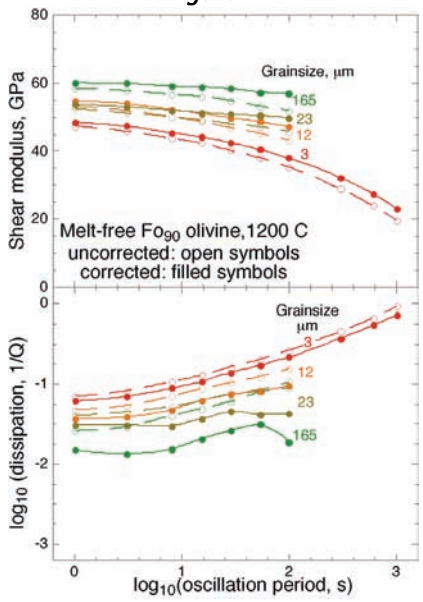

Figure 2

Exploration potential of stress transfer modelling in fault-related mineral deposits

Steven Micklethwaite[1,2], Stephen F. Cox[1]

[1] *Research School of Earth Sciences, Australian National University, Canberra, ACT 0200, Australia*
[2] *Now at: CODES, Private Bag 126, University of Tasmania, Hobart, TAS 7001, Australia*

This project applies the principles of the triggering mechanisms and triggering effects of active fault systems to understand gold mineralisation in ancient fault systems. Earthquakes generate small elastic stress changes, which in turn trigger other earthquakes and many thousands of aftershocks. Each aftershock is a fault slip event that enhances the permeability of the crust and high-frequencies of aftershocks tend to occur on faults with the same dimensions as those faults that host gold mineralisation in Australian gold camps. Previously, we have shown that at crustal depths of 10-20 km, orogenic-type gold deposits occur where co-seismic stress changes around a fault are likely to have triggered clusters of aftershocks (Micklethwaite and Cox, 2004, 2006; Micklethwaite, 2007). Therefore Stress Transfer Modelling helps us understand the dynamics of ancient fault systems and acts as a valuable predictive tool for the exploration industry.

Stress Transfer Modelling is now being extended to gold mineralised fault systems that developed in near-surface crustal environments (1-6 km) during episodes of normal faulting and high geothermal gradients, such as the Carlin-type gold deposits.

Both earthquakes and intrusive events generate small elastic stress changes in the crust, which have been linked to the triggering of thousands of aftershocks and the enhancement of permeability. We developed stress transfer modelling (STM) to understand the dynamics of ancient fault systems and act as a valuable predictive tool for the exploration industry (Micklethwaite and Cox, 2004, 2006; Micklethwaite, 2007). We have also been able to link co-seismic stress changes to wall rock damage generation and permeability, using Damage Mechanics Theory (Sheldon and Micklethwaite, 2007).

In 2008, we applied STM to near-surface hydrothermal environments (0.5-2 km; Carlin goldfield, Nevada), and deep hydrothermal environments (15-25 km; Agnew goldfield, West Australia). In the Carlin goldfield, mineralisation is broadly stratiform but also related to the upper tips of ~5 km-long normal dip-slip faults. Debate exists as to whether fluid migration was controlled by active fault processes, reaction-enhanced porosity generated in specific lithologies, or convection through fracture networks that were indefinitely open due to the low confining stresses of near-surface environments. In the Agnew goldfield, mineralisation forms a linear trend of pod-like bodies on the western limb of a regional fold. Fault rocks containing ore-grade mineralisation are dominated by ductile shear textures, with only small percentages of brittle deformation textures such as breccias and veins. Metamorphic grades suggest the goldfield formed in the mid-crust possibly at the base of a structure, but it was not clear whether visco-elastic creep processes, or co-seismic damage controlled fluid migration and mineralization.

In both case studies, STM predictions were made in three dimensions, and it was demonstrated that mineralization could be matched by the unique stress patterns generated at the tips of fault ruptures; indicating co-seismic elastic stress changes are a first-order control on permeability enhancement and mineralisation. This potentially represents a breakthrough for Carlin-related research and promises to resolve a long-standing debate.

Micklethwaite, S. and Cox, S.F., 2004. Fault segment rupture, aftershock-zone fluid flow, and mineralization. *Geology*, 32, 813-816.
Micklethwaite, S. and Cox, S.F., 2006. Progressive fault triggering and fluid flow in aftershock domains. *Earth and Planetary Science Letters*, 250, 318-330.
Micklethwaite, S., 2007. The significance of strings and clusters of fault-related mesothermal lode gold mineralization. *Economic Geology*. 102, issue 6, 1157-1164.
Sheldon, H.A. and Micklethwaite, S., 2007. Damage and permeability around faults: Implications for mineralization. *Geology,* 35, 903-906.

Mineralisation

Marie-Aude Bonnardot[1], Gordon Lister[1], Joe Kurtz[1] and Marnie Forster[1]

[1] *Research School of Earth Sciences, Australian National University, Canberra, ACT 0200, Australia*

Tectonic plate boundaries are the preferred location for economic mineralization, which appear to have been emplaced at specific time. This two-folded project proposes to re-examine tectonic evolution of the lithosphere along convergent and divergent boundaries. This project involves the development and application of the tectonic reconstruction tool, *Pplates*, in collaboration with Joe Kurtz and is also undertaken with the support from the DeBeers group.

Along convergent margins, subduction of lithospheric anomalies like seamount chain or oceanic plateau has the potential to vastly impact on the motion of tectonic plates. A famous example is the collision of the Ontong Java oceanic plateau along the New Guinea subduction zone to the north of Australia, which induced a drastic plate reorganisation involving subduction reversal in the SW Pacific. Based on previous works (Bonnardot et al., 2008), the first part of the project focuses on understanding the 3D geometry of slabs related to seafloor heterogeneities subduction and in particular, it focuses on the identification of slab tears, which may have a fundamental effect on the upper plate tectonic regime and on the porphyry deposits emplacement. We are currently revising the slab geometry in the Tonga, Sumatra and the South America subduction zones in regards to the tectonic evolution of the overriding plate, based on the analyse of the seismicity distribution and the stress regime within the involved lithospheric plates.

The second part of that project focuses on intracontinental rifting processes and aims at understanding the tectono-magmatic structures associated with anorogenic alkaline trends, for instance the relationship between transform faults/structural pattern of the mid-oceanic ridge and kimberlite emplacement.
Outcomes will allow refining plate motion in global tectonic reconstruction, as it will result in better quantifying the intraplate deformation that occurs during rifting initiation.

Bonnardot M.-A., Régnier M., Christova C., Ruellan E., Tric E. 2008. Seismological evidence for a slab detachment in the Tonga subduction zone. *Tectonophysics*, doi:10.1016/j.tecto.2008.10.01

Tectonic mode switches and the nature of orogenesis

Gordon Lister and Marnie Forster

Research School of Earth Sciences, Australian National University, Canberra, ACT 0200, Australia

The birth and death of many mountain belts occurs in lithosphere that over-rides major subduction zones. Roll-back creates a gravitational potential well into which the orogen collapses. This motion, coupled with stress guides, can "pull" an orogen apart. A slowing of roll-back (or of hinge retreat) means that the subduction flexure may subsequently begin to be "pushed back" or be "pushed over" by the advancing orogen. The consequence of such changes in relative motion is that orogenic belts are affected by abrupt tectonic mode switches. The change from "push" to "pull" leads to a sudden change from horizontal extension to horizontal shortening, potentially throughout the entire mass of the orogenic lithosphere that over_rides the subducting slab. The sequencing of these tectonic mode switches affects the thermal evolution of the orogen, and thus fundamentally determines the nature of orogenesis. In consequence high pressure metamorphic rocks are found in orogens characterized by push-pull sequences while high temperature metamorphic rocks are found in orogens characterized by pull-push sequences (Lister and Forster, 2008).

However the real complexity evident in the evolution of any orogen begins to emerge once we begin to consider movement in three dimensions. Motion orthogonal to an arcuate mountain front is typical of the geometry of collapse, where the orogen has spread over or been pushed over the adjacent foreland. For example it can reasonably be inferred that the Tibetan crust collapsed southward to create the modern arcuate shape of the southern boundary of the Himalayan mountain chain (see Figure below). In fact the mountain front defines an almost perfect small circle, with a radius of 1696 $\pm$ 55 km (Bendick and Bilham, 2001). GPS measurements suggest this flow is still occurring: present day movement is taking place in directions orthogonal to the modern arc (Jade et al., 2004). England and Molnar (2005) provide a convincing argument that crustal flow in Tibet is driven by the gravitational potential energy of the collapsing orogen: in their words, the orogen behaves more like a 'fluid' than a 'plate'. Forward motion of the Indian indentor is accommodated in the west by the left-lateral Chaman fault zone on the boundary between Afghanistan and Pakistan, and in the east (in Myanmar) by the right-lateral Sagaing fault zone.

The main focus of the India-Asia collision is now in the NW, under the ranges of the Hindu Kush. The impact of an indentor can be inferred from the paired clusters of strike-slip faults. In the South, the small-circle geometry of the Himalayan mountain front is diagnostic of the fluid-like behaviour of this collapsing orogen, reflecting the impact of radiating viscous flow driven by the gravitational potential energy of the collapsing Tibetan Plateau. Thrusts radiate orthogonally from the orogenic welt defined by the Tibetan plateau, southward, northward, and eastward. The effects of eastward flow of the collapsing Tibetan Plateau is particularly evident in the fold and thrust belt in Sichuan Province, the locus of several catastrophic earthquakes (yellow dots in Figure).

In contrast, in the Myanmar crust, there are two almost orthogonal competing movement patterns. Shortening occurs in the foreland fold and thrust belt because this zone accommodates WSW directed motion of crust flowing out from the Myanmar hinterland. The Sagaing wrench fault zone marks the locus of accumulating right-lateral offsets, periodically accommodating distortions caused by relative plate motion. At the same time concentric left-lateral strike-slip faults accommodate flow around the eastern syntaxis, causing distortion of the Sagaing Fault. These concentric

left-lateral strike-slip faults are most evident in the green lines that show the trend of fault plane slip vectors associated with left-lateral strike-slip earthquakes. As we move from north to south in a semicircle around the eastern syntaxis the movement direction associated with these earthquakes changes from towards ~90° to towards ~250°. This is a movement pattern that suggests mass flow in the deeper crust driven by the WSW-directed roll-back of the tearing Myanmar slab that lies beneath this zone.

Bendick, R., Bilham, R., 2001. How perfect is the Himalayan arc? Geology 29, 791-794, doi:10.1130/0091-7613(2001)029<0791:HPITHA>2.0.CO;2

England, P., Molnar, P., 2005. Late Quaternary to decadal velocity fields in Asia. Journal of Geophysical Research _110, B12401, doi:10.1029/2004jb003541.

Jade, S., Bhatt, B.C., Yang, Z., Bendick, R., Gaur, V.K., Molnar, P., Anand, M.B., Kumar, D., 2004. GPS measurements from the Ladakh Himalaya, India: preliminary tests of plate-like or continuous deformation in Tibet. Geol. Soc. Amer., Bull. 116, 1385–1391, doi:10.1130/B25357.1

Lister, G. and Forster, M. 2008. Tectonics mode switches and the nature of orogenesis. Lithos, in press.

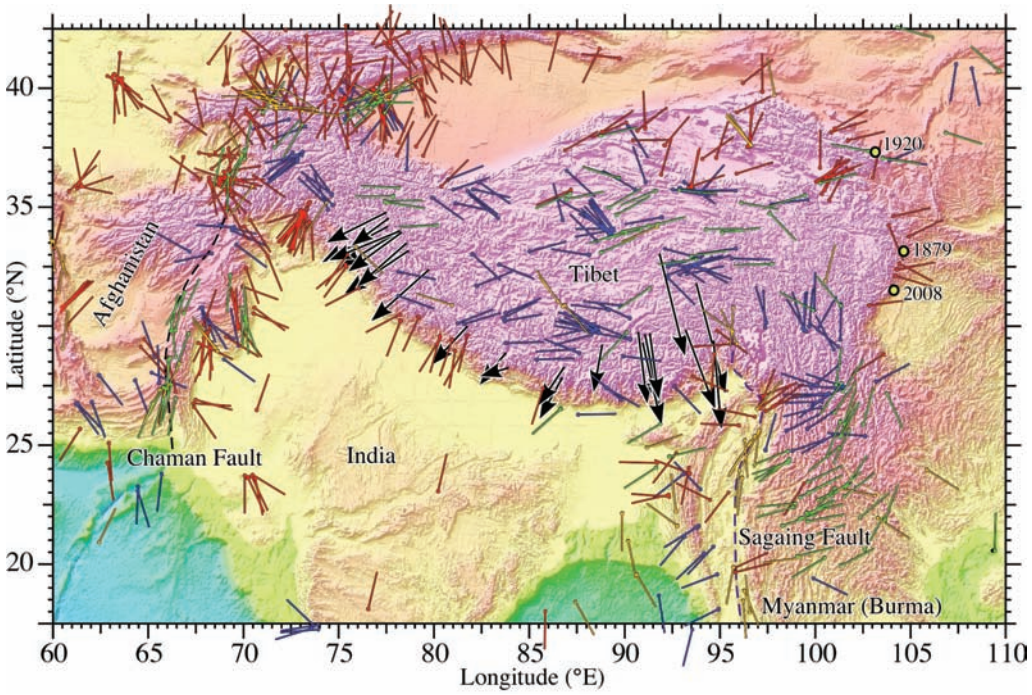

Figure 1. Geometry of a mountain front reflecting the impact of collapse driven by the gravitational potential energy of the orogen. Arrows show GPS motions relative to India (after Jade et al., 2004). The coloured slip lines stem from epicenters of 575 earthquakes in the period 1976-2006 in the depth range 0-60 km, as recorded in the Harvard Centroid Moment Tensor database (http:/ www.seismology.harvard.edu/CMTsearch.html). Map produced using Program eQuakes superimposed on images derived from NOAA (http://ibis.grdl.noaa.gov/cgi-bin/bathy bathD.pl). Each slip line shown represents a choice of one of two conjugate fault plane solutions derived from the centroid moment tensor: each choice based on details of the local geology. Thrusts (red), normal faults (blue), left-lateral strike-slip faults (green) and right lateral (yellow). Motion orthogonal to the mountain front is typical of the geometry of collapse where the orogen has spread over, or been pushed over the adjacent descending slab. Left-lateral Chaman fault zone (dashed) in the west (a). Right-lateral Sagaing fault zone (dashed) in the east (b).

Episodic emplacement of the Ladakh and Karakoram Batholiths

Lloyd White[1], Gordon Lister[1], Marnie Forster[1], Talat Ahmad[2] and Trevor Ireland[1]

[1] *Research School of Earth Sciences, Australian National University, Canberra, ACT 0200, Australia*
[2] *Department of Geology, University of Delhi, India*

Preliminary U-Pb SHRIMP dating of zircon grains from the Ladakh and Karakoram batholiths confirms some of the previously published ages for the two batholiths, but also indicates that older crust (possibly associated with the Tibetan slab) may have been involved with the Karakoram Bathoiith.

Samples of the Ladakh Batholith were collected from Khardung La and Chang La in Ladakh, NW India. These samples obtained an age of circa 58 Ma, similar to the age data published by earlier workers (e.g. Singh et al. 2007). This confirms that there was a strong phase of magmatism in the Ladakh Batholith at approximately 58 Ma.

Samples of the Karakoram Batholith were collected near Tangste Gompa and obtained an age of circa 32 Ma. One zircon grain from this sample also gave a late Permian age, which could indicate that older crust is associated with the Karakoram Batholith. One sample of a cross-cutting dyke collected in the Tangste Gorge (Figure 1 and 2) gave an age of circa 18 Ma. This is consistent with earlier published data that was associated with movement on the Karakoram Fault. Another sample of the Karakoram Batholith obtained an age of circa 102 Ma. Again, this is consistent with a date published for the same Batholith in Pakistan.

This study confirms many of the earlier published dates of the Ladakh and Karakoram batholiths. However, our preliminary work also shows that attention must be paid to younger phases of magmatism that cross-cut older phases of magmatism.

Singh, S. Kumar, R., Barley, M. E., Jain, A. K. 2007. SHRIMP U-Pb ages and depth of emplacement of Ladakh Batholith, Eastern Ladakh, India. *Journal of Asian Earth Sciences* **30**: 490-503

Figure 1. Aplite dyke cross-cutting an earlier migmatitic phase of the Karakoram Batholith, Tangste Gorge, Northwest India.

Figure 2. Tangste Gorge, Ladakh, Northwest India

Earth Physics

Research into the structure and dynamics of the Earth uses a range of physical and mathematical techniques and is grouped into the three main themes of Seismology and Mathematical Geophysics, Geophysical Fluid Dynamics, and Geodynamics and Geodesy. The work spans observational, theoretical, laboratory, computational and data oriented studies, all directed towards understanding the structure and physical processes in the earth's interior, the crust or the earth's fluid envelope.

Two members of the Earth Physics academic staff received awards this year. Prof B.L.N. Kennett received the Gold medal in Geophysics from the Royal Astronomical Society, London, for his work in seismology and the Peter Baume Award from ANU for his exemplary record of research achievement and leadership. Prof K. Lambeck contributed to the award of the Nobel Peace Prize for 2007 to the Intergovernmental Panel on Climate Change (IPCC), as a substantial contributor to the IPCC since the inception of the organization.

PhD theses were submitted by T. Prastowo ("Mixing in buoyancy-driven exchange flows"), M. Coman ("Convective circulation forced by horizontal gradients in heating"), J.Dawson ("Satellite radar interferometry with application to the observation of surface deformation in Australia")and G. Estermann ("Contribution of mountain glacier melting to sea-level changes: Recent past and future"). New Postdoctoral academic staff commencing during 2008 include M. Ward in ocean modeling, S. Pozgay and A. Coffey in seismology, G. Luton on geodesy and S. Bonnefoy in computational geophysics.

RSES is taking a major role in Component 13 of the National Cooperative Research Infrastructure Strategy (NCRIS): "Structure and Evolution of the Australian Continent", which is managed through 'AuScope'. RSES hosts activities in Earth Imaging through support of portable instrumentation and transects, Geospatial through gravity measurements and testing of portable equipment for satellite laser ranging, and Simulation & Modelling through 'pPlates' software for tectonic reconstruction. As a linked activity between three AuScope components (Imaging, Geospatial and Access and Interoperability), the Terrawulf II cluster computer at RSES provides capability in geophysical inversion and the computation reduction of observational data.

Acting Director Prof. Ross Griffiths launching the Terrawulf II computational facility in June at RSES. TII is the latest in a long line of Geoscience computational facilities at RSES stretching back 30 years. Projects initiated in 2008 range from atmospheric effects in GPS, through ocean modeling to studies of the Earth core and geodynamo.

Centre for Advanced Data Inference

In the Centre for Advanced Data Inference a new, more powerful compute cluster, Terrawulf II, was commissioned early this year. The new cluster was made possible by NCRIS funding combined with support from RSES. Terrawulf II consists of 96 dual processor dual core 2.8GHz Opteron systems with 8GB of memory per node, connected with Gigabit Ethernet. Half of the nodes are also connected through higher bandwidth switches, which significantly extend the range of potential applications of the cluster to both `tight' and `loosely' coupled codes. The Terrawulf II cluster is integrated into the AuScope grid and used for a broad range of geoscience data processing as well as continuing development of state of the art inversion and data inference software.

Geodynamics and geodesy

The geodynamics group within Earth Physics is involved in the Geospatial component of AuScope. NCRIS funding in this strand has enabled investment in geodetic infrastructure throughout Australia, including three new Very Long Baseline Interferometry (VLBI) sites, a national Global Navigation Satellite System (GNSS), terrestrial gravimeters, a test of a mobile Satellite Laser Ranging (SLR) system and a contribution towards the new Terrawulf II compute cluster. Members of the geodynamics group are involved in the AuScope Executive Committee, the Geospatial Steering Committee as well as the gravity, VLBI and Grid Computing subcommittees charged directly with the acquisition and deployment of the infrastructure. The ANU component of the above equipment includes an FG5 absolute gravimeter (acquired in April 2008), a relative gravimeter (acquired in July 2008), a gravity technician and a SLR technician. Dr Jason Zhang, the SLR technician, was involved in instrument testing at Burnie, Tasmania early in 2008 while Mr Geoff Luton has been involved in FG5 observations in Melbourne, Hobart and Western Australia.

The InSAR analysis of small, shallow earthquakes in Western Australia demonstrated the capability of the technique to not only estimate fault plane location, orientation and depth but also to estimate the distribution of slip on the fault plane (Dawson et al., 2008). The stress drop for the Mw=4.7 Katanning earthquake was found to be 14-27 MPa, significantly smaller than expected for such as small event. This suggests that the seismic hazard of small earthquakes might be higher than previously thought.

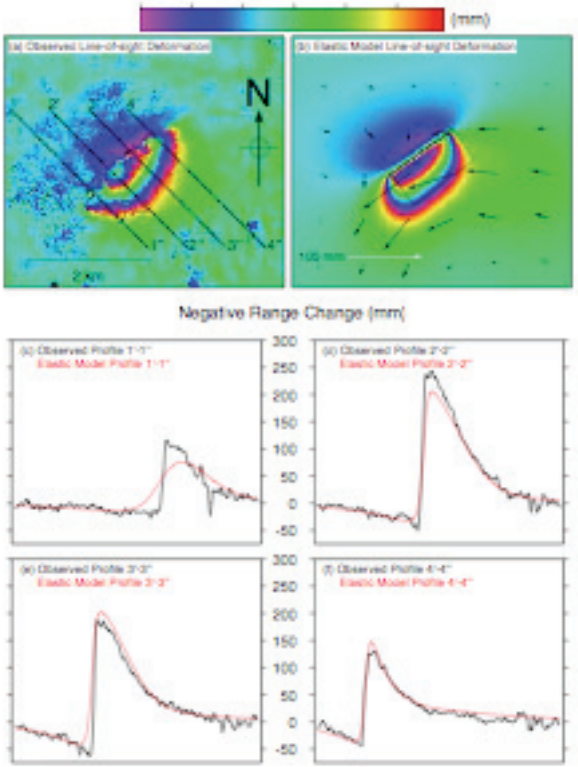

Observed and modelled interferograms of deformation caused by the Katanning earthquake. Observed and modelled changes in ground-satellite distance is shown across four different profiles (Dawson et al., 2008).

A combination of surface deformation from GPS and inferred deformation from changes in the Earth's gravity field from the Gravity Recovery and Climate Experiment (GRACE) have been undertaken to separate short-term hydrological variations from longer-term glacial isostatic adjustment as a result of melting of polar ice sheets since the Last Glacial Maximum. Coupled with continued advances in the analysis strategies of the raw GPS observations, these studies have revealed that both the GPS and GRACE estimates of surface deformation agree at the 1-2 mm level and mm/yr level, enabling highly accurate estimates of crustal deformation to be made.

Successful field experiments have been undertaken using the new gravimeters in Melbourne, Hobart and several sites in Western Australia. The GPS field programme in Papua New Guinea concluded this year while coral sampling in the Ningaloo Reef region continued in order to understand past levels of relative sea level.

Geophysical fluid dynamics.

Highlights of work in geophysical fluid dynamics this year included laboratory and theoretical fluid dynamics studies modelling lava flows, where cooling, solidification and yield-strength are important factors. Experiments have focused on the flow of yield-strength fluid that is also cooling and solidifying as it flows down a sloping channel. A variety of inertial, viscous, plastic and cooling-controlled flow regimes have been found.

The geophysical fluid dynamics laboratory has also seen a renewed effort to understand the three-dimensional flow in mantle subduction zones, including the influences of an over-riding plate, back-arc spreading, the effects of a thick keel on the over-riding plate, and the behaviour of a hot mantle plume ascending under the over-riding plate. This work relied on an extended visit by Prof Kincaid and a student from the University of Rhode Island. The interaction of ascending mantle plumes and subduction zones is being examined with a view to explaining the distribution and ages of the Columbia River Basalts and volcanism of the Yellowstone hotspot. The work has shown that previously unsuspected patterns of volcanism can be produced and many aspects of the volcanism, including the age distributions, around Yellowstone and the Lava High Plains of the northwest USA can be explained by interaction of a plume and subduction zone.

Lessons learnt from several years of numerical modelling of the combined chemical and thermal evolution of the mantle are now bearing fruit in two directions. The models are being extended to Venus' mantle to test whether the 'basalt barrier' mechanism, reported last year, can explain the outburst of volcanism that completely resurfaced Venus about 500 Myr ago. Initial results are promising.

The insights from the numerical modelling have also fed into a new hypothesis to reconcile mantle chemistry with mantle dynamics. The idea is that only a fraction of the melt generated under a mid-ocean ridge actually reaches the surface. The remaining melt is trapped in the mantle, and carries the so-called incompatible elements. This hypothesis removes the need for a postulated deep, hidden reservoir containing 'missing' incompatible elements. It can also explain the presence of enigmatic 'unradiogenic' helium and other noble gases that emanate from some hotspot volcanos.

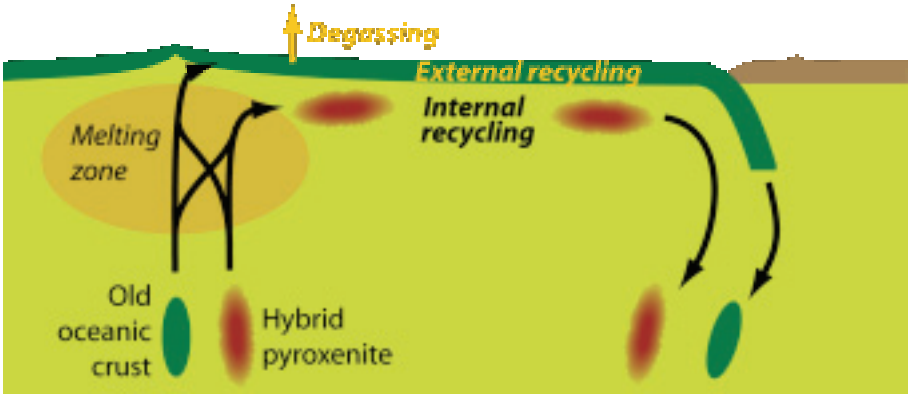

Cartoon of how noble gases may be partially retained in the mantle despite losses due to melting under mid-ocean ridges. Some of the melt is trapped, in the form of hybrid pyroxenite, and recycled internally without losing its gases. The melt that reaches the surface forms oceanic crust that degasses.

Studies of the fundamental dynamics of the ocean's meridional overturning circulation continued in the geophysical fluid dynamics laboratory. A new approach to the energetics of the circulation developed this year has elucidated the way in which energy supplied to irreversible turbulent mixing from the winds and tides must be in balance with the available potential energy supplied by the surface buoyancy fluxes. The two are closely tied, the buoyancy fluxes providing the driving force while the turbulent mixing maintains the stratification, and hence the strength of the forcing and the consequent rate of overturning. Numerical solutions have revealed the presence of significant internal gravity wave activity generated by the convection. It will require further work to determine whether there is likely to be substantial wave generation under oceanic conditions, and whether the wave energy can contribute to the vertical mixing. The steady-state dynamics were also examined in experiments with the case of a large ocean basin connected to a marginal sea by flow over a topographic sill. The exchange flow can influence the circulation and stratification in the ocean.

A video clip (available on-line) of flow in the laboratory convection model, in which the base is heated near both ends and cooled over the central half. The right hand section of the base is heated by an applied heat input 10% smaller than that applied to the left hand section of the base. Hence the plume at the left hand end is stronger than that at the right end and fills the top of the box. In the oceans this is analogous to the strongest sinking region producing the bottom waters.

In other experiments the response to small changes in the surface boundary conditions, such those as implied by global warming, has been investigated. The conditions leading to a potential shutdown of the deep sinking leg of the overturning circulation in simplified cases have been outlined. A first set of experiments with periodic oscillatory surface forcing is also providing insights into whether the global circulation is influenced by fluctuations having periods from the annual seasonal cycle (which is known to force variations in the deep sinking of cold waters) to millennia (which is the time scale for complete equilibration of the stratification to new surface conditions).

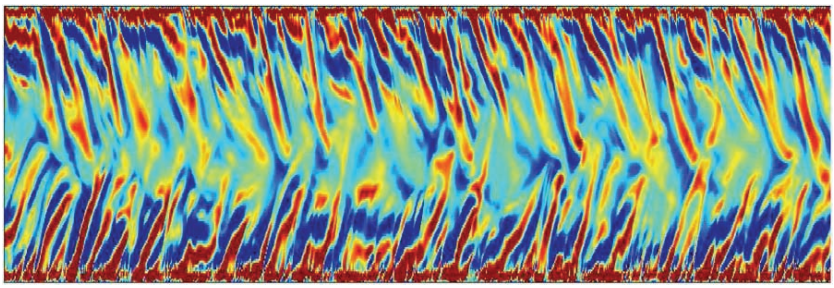

Hovmöller plot of the vertical velocity along a horizontal section at mid-depth from a 2-D numerical simulation of horizontal convection. Time increases upwards; blue represents upwelling motion, green approximately no motion, and red downwelling motion. Regions of high latitude sinking are situated in this case at both the left and right hand ends of the horizontal section, and excite strong wave modes that propagate towards 'low latitudes' at the centre of the section. These waves and their interactions appear to be responsible for much of the variability in the circulation.

In another laboratory study, the dynamics of wakes behind islands and headlands were shown to be sensitive to eddy disturbances or turbulence carried from upstream of the topographic feature. The incident disturbances cause a faster dissipation of wake instabilities with distance downstream, hence a smaller recirculation region. This study is currently being extended to a practical application involving the dispersion of wastewater released into a major estuary in which there is a separation of the flow in the main channel and a relatively slow flushing of a shallow region to one side. Preliminary experiments in a water flume are exploring the roles of wastewater outflow location and tides on the flushing time.

Seismology.

2008 was an eventful year for seismic experiments, with the deployment of two new arrays, and the continued maintenance of the SEAL3 array which was deployed in late 2007. SEAL3 comprises 57 3-component short period stations distributed throughout southeast New South Wales at a spacing of approximately 50 km. With a recording period in excess of 1 year, this study has substantially contributed to the cumulative coverage of passive seismic data in southeast Australia. To date, nearly 400 sites have been occupied in Tasmania, Victoria, South Australia and New South Wales. Teleseismic tomography, ambient noise tomography, receiver functions and core phase studies are currently in progress using SEAL3 and pre-existing data.

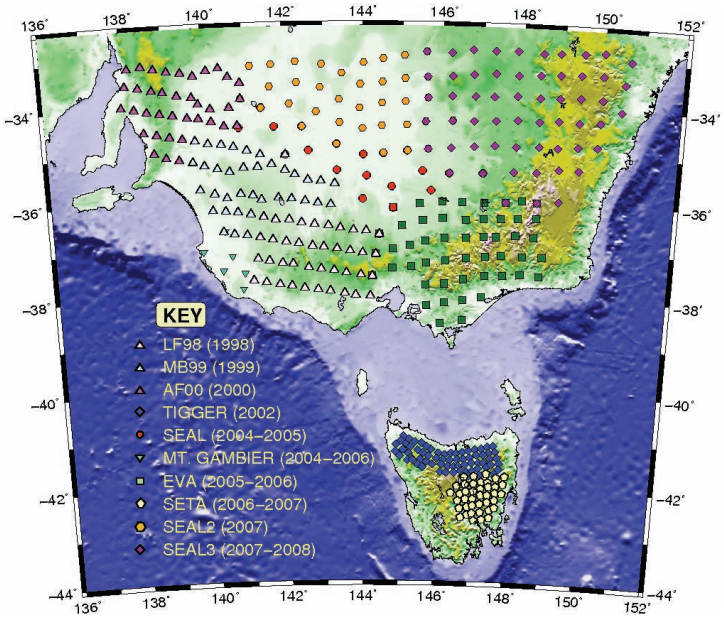

Location of all short period seismic arrays deployed in southeast Australia over the last 10 years.

In order to determine the nature of the transition at lithospheric depths between the northern and southern Australian cratons, a transect of 25 broadband seismic stations was deployed between the Eyre Peninsula in South Australia and Tennant Creek in the Northern Territory. The installation took place in August-September 2008, with all stations expected to remain in operation for at least one year. With a site spacing of between 60-90 km, receiver functions, shear wave splitting and traveltime inversion can be utilized to help address fundamental questions relating to the anomalously slow velocities beneath the central Australian intercratonic structures, and how they propagate with depth.

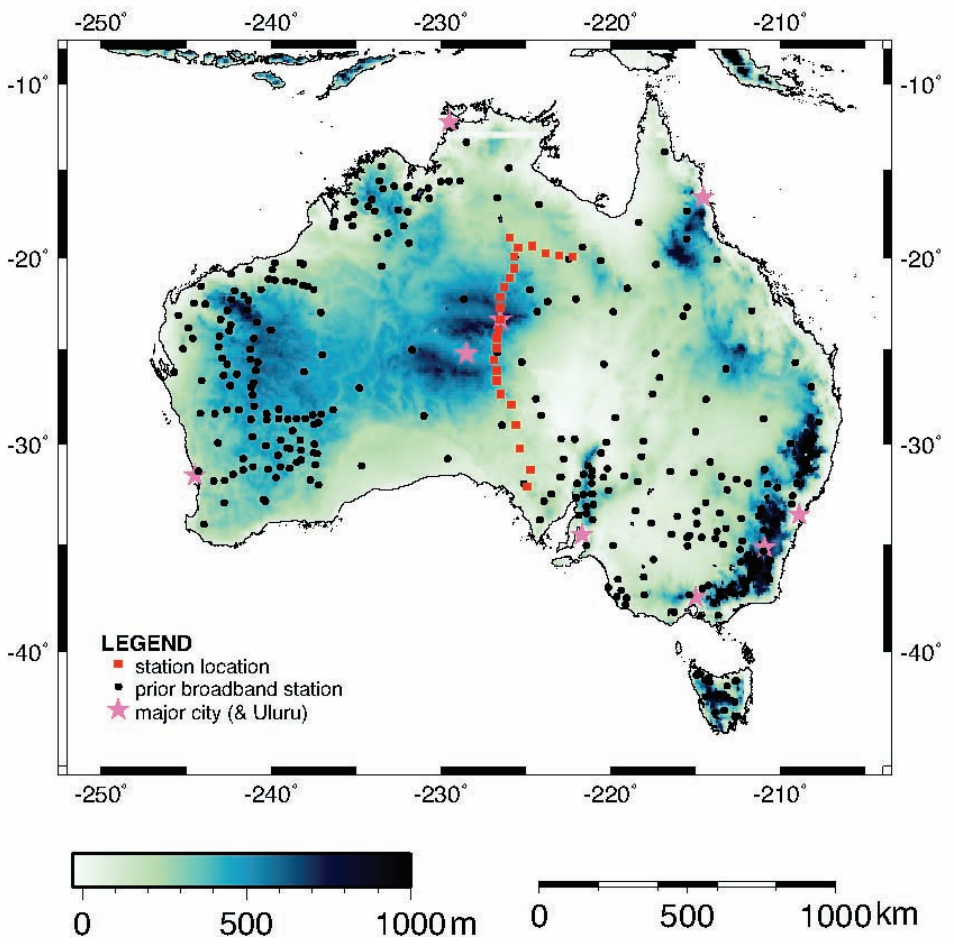

Bilby array comprising 25 boradband seismometers deployed in central Australia.

In June-July 2008, an array of 35 short period seismometers was installed across the Gawlor Craton in South Australia for an eight month period. Station spacing is approximately 50 km and the area covered runs from Port Lincoln in the Eyre Peninsular to Leigh Creek just west of the Flinders Ranges. The primary aim of this array is to increase passive data coverage in this part of Australia for seismic imaging, which includes teleseismic tomography and receiver function analysis. Local earthquakes, which are relatively plentiful in this part of Australia, will also be exploited to improve structural constraints. The eastern edge of the Gawler craton is currently of particular interest for the supply of geothermal energy and there are many ongoing industry projects in the area. Geoscience Australia completed a deep seismic reflection transect across the top of the Eyre Peninsular just prior to the deployment of the Gawler array. This array will provide broad scale earth imaging required for more detailed studies.

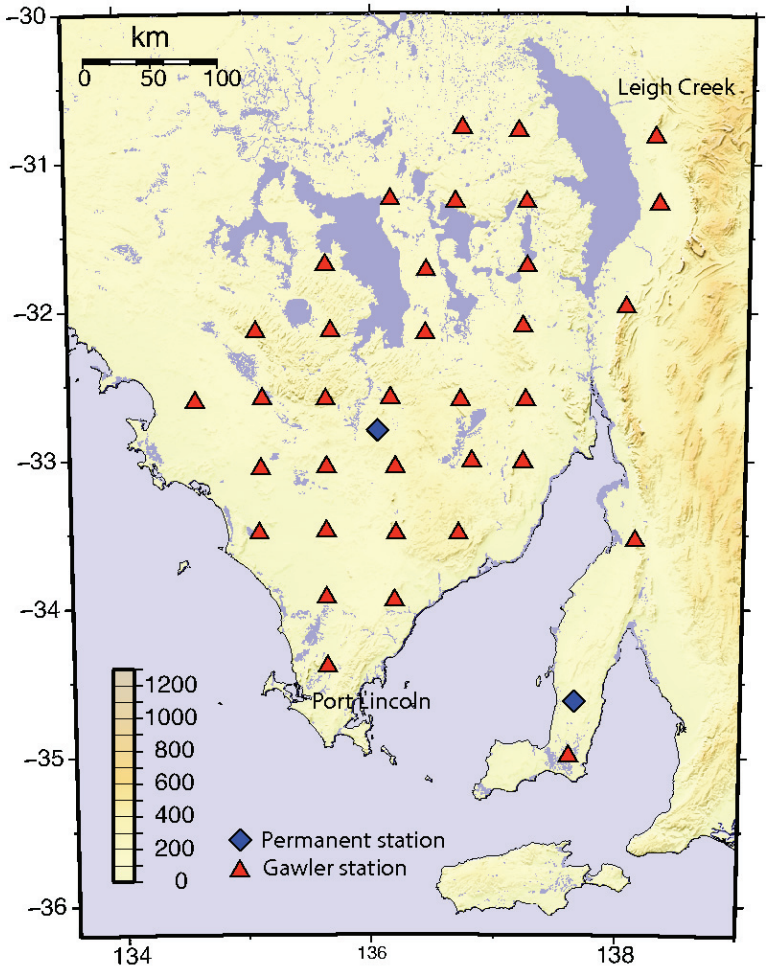

Short period array deployed across the Gawler craton in mid 2008.

In 2008 the conversion of a large portion of our seismic data from past experiments to an international standard format called "miniseed" was accomplished. This is the first step in building a continuous archive of data, which is now easily accessible by local researchers through a java acquisition tool called Seismic Data Centre (SDC). About one half of our data has been converted and it is a work in progress. In other projects it was shown that it is not feasible to use 1D structural model for Australia when inverting for source parameters of large earthquakes surrounding Australia, and that a 3D model will be needed for the computation of Green's functions. This work is important in the context of the Tsunami warming for Australia. Work also commenced on the lithospheric structure of the Balkans peninsula using receiver functions, and an interactive tool (java) for forward modelling of receiver functions was completed. A large dataset from Antarctica was used to examine current hypotheses about the core anisotropy and structure showing in particular that the Antarctic data do not support the existence of significant heterogeneity in the outer core Taylor cylinder.

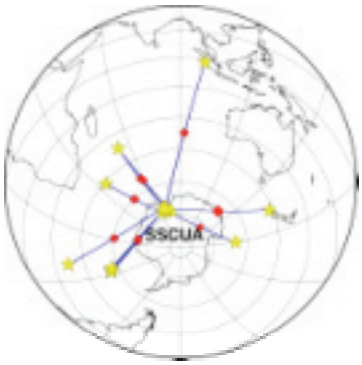

Distribution of events (stars) with clear PcP arrivals recorded at SSCUA stations in Antarctica (triangles). The red diamonds are bouncing points of the PcP waves at the CM

Ambient noise tomography in Southeast Australia

Pierre Arroucau[1], Nick Rawlinson[1] and Malcolm Sambridge[1]

[1] *Research School of Earth Sciences, Australian National University, Canberra, ACT 0200, Australia*

Previous studies have demonstrated that the Green's function of the medium between two stations can be extracted from the cross-correlation of the seismic ambient noise wavefield recorded at these stations. This class of technique is now progressively becoming a standard seismic investigation tool and has successfully been used for tomographic imaging purpose in many parts of the world. Saygin (2007) obtained encouraging results for the Australian continent using broadband records, and showed that Rayleigh wave group velocity contrasts within Australia correlated well with its major geological units.

In the last decade, dense rolling short-period seismic array deployments have been carried out by RSES in Southeast Australia (WOMBAT-SE). With an interstation distance of a few tens of km, several months of continuous records and a cumulative total of approximately 400 stations, these temporary arrays provide an unique opportunity for high-resolution ambient noise imaging in the region, which can address fundamental questions regarding the structure and tectonic evolution of the Lachlan and Delamarian orogens, which underpin the southern half of Palaeozoic eastern Australia.

Dispersion curves constructed form the cross-correlation of the vertical component, by means of frequency-time analysis for periods ranging between 1 to 20s, have been used to extract Rayleigh wave group traveltimes. An iterative non-linear tomographic scheme based on the fast marching method, a grid-based eikonal solver, and a subspace inversion method, was used to map the traveltimes as variations in Rayleigh group wavespeeds at different frequencies.

Saygin, E, (2007) Seismic Receiver and Noise Correlation Based Studies in Australia. *PhD Thesis, The Australian national university*, 175p.

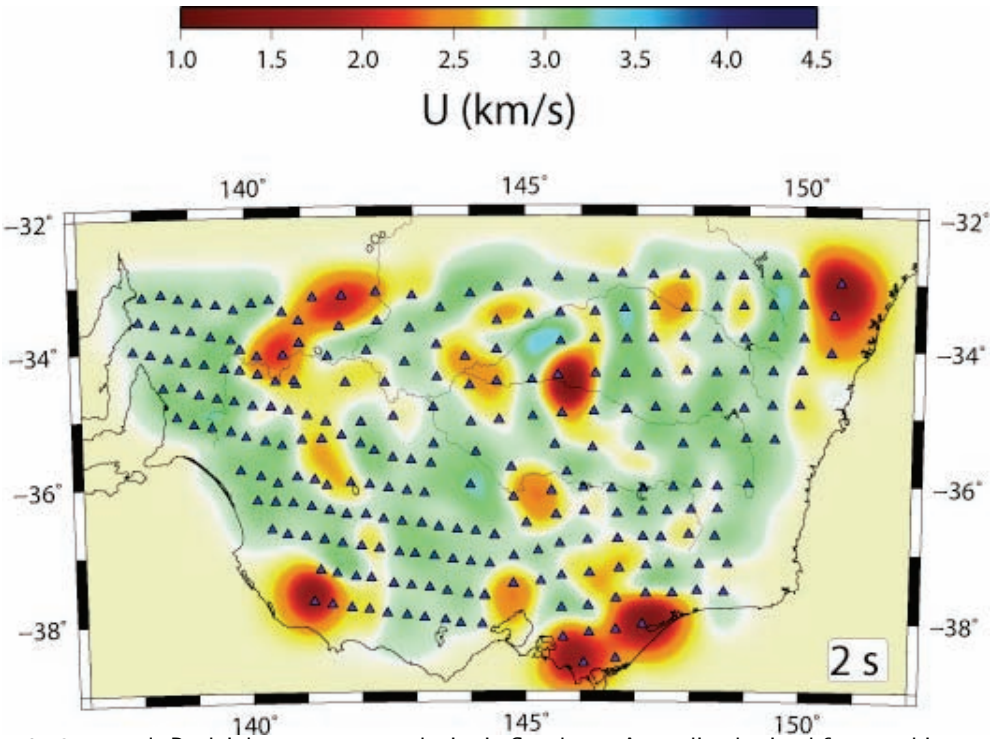

Figure 1. 2-seconds Rayleigh wave group velocity in Southeast Australia obtained from ambient noise cross-correlation of the vertical component for simultaneously recording pairs of stations. The stations used belong to 10 temporary arrays of short-period instruments deployed in the last decade.

Seismic Tomography With a Transdimensional Markov Chain

Thomas Bodin, Malcolm Sambridge[1]

[1] *Research School of Earth Sciences, Australian National University, Canberra, ACT 0200, Australia*

In seismic tomography, the Earth's interior must be parametrized in some fashion. This is typically done using uniform local cells, and the inversion process consists of finding seismic wave speeds within each cell. The number of cells (and size) has to be chosen according to a compromise between model resolution and model uncertainty. Usually, seismologists choose to have a large number of cells and then face the problem of non-uniqueness by imposing constraints on the solution that are independent of the observations, i.e. by employing regularization procedures like spatial smoothing and norm damping. The type and weighting applied to regularization terms often forms a subjective choice of the user. Another aspect is that the strength of damping and smoothing is determined globally which raises the possibility that, while the ill-constrained regions are being suitably damped, the well constrained regions may be over-smoothed with resulting loss of information from the data.

Our work this year has been devoted to using some new ideas in nonlinear inversion to determine the model dimension (i.e. the number of cells) during the inversion. Treating the number of unkowns as an unknown itself has received little attention in geophysics. However, for more than 10 years, Markov chain Monte Carlo (MCMC) methods that admit transitions between states of differing dimension have been actively developed in the area of Bayesian statistics.

We have developed an approach which uses Voronoi cells instead of a regular mesh for an Earth parametrization (see Figure 1). The Voronoi cells are defined by their centres which are able to move. That is, the number and the position of the cells defining the geometry of the velocity field, as well as the velocity field itself are unknowns in the inversion. The inversion is carried out with a fully non-linear parameter search method based on a trans-dimensional Markov chain.

At each step of the chain, a change from the current model is proposed : we either change the velocity or the position of one random cell. The algorithm also allows jumps between dimensions by adding or removing random cells. The forward problem is computed and provides new estimated travel times. The new misfit to observed travel times is compared to that of the current model. The proposed model is either accepted or rejected using a predefined probabilistic threshold.

The Markov chain produces an ensemble of models with different dimensions which carries relevant statistic information about the unknown velocity field. The method takes as a solution the average of this family of models. Each model in the ensemble has a different parametrization but the average is continuous without obvious 'parametrization' artefacts. The standard deviation of the ensemble forms a continuous map and can be used as a proxy for the error for the solution model.

The method has been tested on synthetic situations where the ray coverage is not uniform and where the parametrisation is an issue (see Figure 2). A major advantage is that explicit regularisation of the model parameters is not required, thus avoiding global damping procedures and the need to find an optimal regularisation value. The technique has also been tested on real data and gives promising results.

Figure 1: Voronoi cells about 30 pseudo random points on the plane. The cell nuclei have been drawn from a 2-D uniform distribution over the spatial domain delimited by the red rectangle. The cell boundaries are defined as the perpendicular bisectors of pairs of nuclei. Any point inside a cell is closer to the nucleus of that cell than any other nucleus.

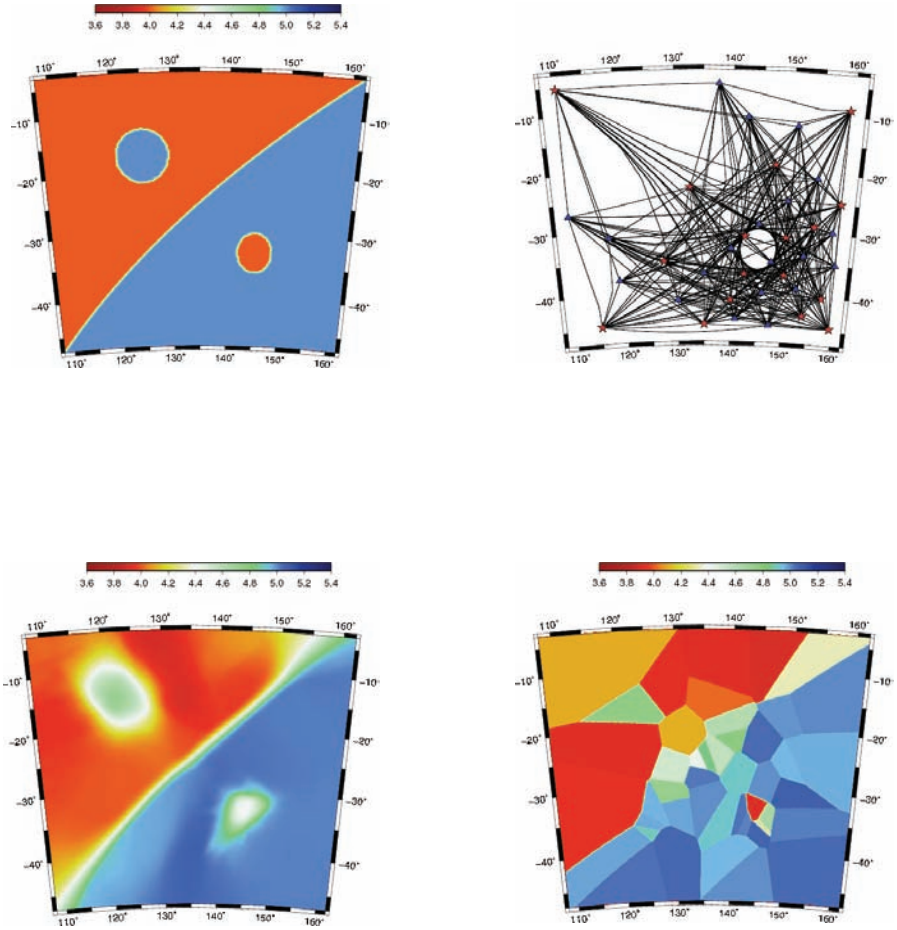

Figure 2 : Upper left map shows the true model. The upper right map shows the ray geometry. The lower left map shows the model sampled with the best fit to the data and the lower right map shows the average estimated solution.

Terrawulf II

Malcolm Sambridge[1], Herb McQueen[1], Shinta Bonnefoy[1]

[1] *Research School of Earth Sciences, Australian National University, Canberra, ACT 0200, Australia*

TerraWulf is a networked cluster of computers set up in RSES to provide convenient high end computing power for a range of demanding geoscience problems. A major upgrade of the TerraWulf compute cluster was recently made possible by funding support from the National Collaborative Research Infrastructure Strategy (NCRIS) under the AuScope umbrella. Contributions from the AuScope Geospatial, Imaging and Structure, and Access and Interoperability components combined with support from RSES have enabled the construction of a new and more powerful cluster. The hardware was delivered and assembled in 2007 and commissioning and benchmarking continued through the first half of 2008.

On Friday 27th June 2008 TerraWulf II was launched at the Research School of Earth Sciences by Acting Director Prof. Ross Griffiths. It has a total of 24 Tb of disk storage and 1Tb of RAM and was built to tackle large complex computational problems in the Earth Sciences using parallel processing techniques. 'TII', is the latest in a long line of Geoscience computing platforms at the RSES which stretch back more than 30 years. Projects initially identified for TII include applications in seismic imaging of Earth structure, geospatial data analysis and mathematical geophysics. TII is open for access by the Australian Earth Science community for projects consistent with the AuScope vision to '...characterise the structure and evolution of the Australian continent from surface to core in space and time.' It is accessible directly through a local account and via the AuScope grid.

The main cluster consists of 96 nodes (384 processor cores) connected through Gigabit and Infiniband switches which support a range of potential applications of the cluster including both `tight' and `loosely coupled' codes. Each node is an IBM System x3455 with 2 AMD Opteron Dual-core 2.8 GHz processors, 160 GB local disk and 9GB to 17GB RAM. All the nodes are interconnected through SMC8848 Gigabit Ethernet switches, and half of the cluster is also inter-connected via three 24port Voltaire ISR9024S Infiniband switches providing 10Gbit inter-process communication. Compute nodes are configured with Open SUSE 10.3 and two kinds of MPI environment, MPICH2 and VLTMPI, have been installed to enhance paralled processing applications. It is accessible directly through a local account and via the AuScope grid.

The TerraWulf II cluster is now running a variety of geoscience data processing, technique development, simulation and analysis codes. Current projects include studies of atmospheric effects in GPS analysis, ocean overturning circulation and Earth's inner core structure & geodynamo, as well as multi-arrival wavefront tracking seismic tomography, inversion of airborne electromagnetic data, development of nonlinear inversion methods, implementation of earthquake source parameter inversion, and high-resolution ambient noise tomography.

Figure 1.

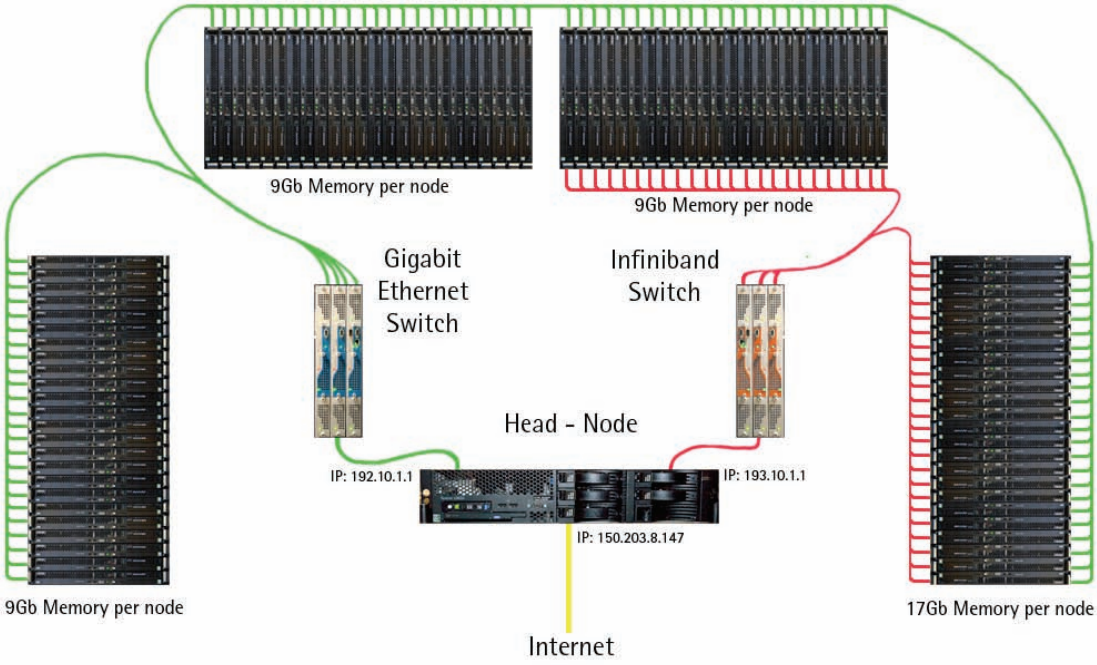

Figure 2.

Holistic inversion of time-domain airborne electromagnetic data

Ross Brodie[1] and Malcolm Sanbridge[1]

[1] *Research School of Earth Sciences, Australian National University, Canberra, ACT 0200, Australia*

Since the research on this project resumed in August 2008 we have been investigating the feasibility of applying our holistic inversion technique to time-domain airborne electromagnetic (AEM) data. Holistic inversion was originally developed to invert frequency-domain AEM data to solve for continuous 3D survey wide conductivity model while simultaneously solving for systematic calibration errors (e.g., scaling effects, phase shifts and zero-level bias) which often degrade frequency-domain data (Brodie and Sambridge, 2006).

One of the challenging 'calibration' issues in fixed-wing time-domain AEM is the fact that the position and attitude of the receiver coils, which are towed ~120m behind and ~40m below the aircraft, cannot be accurately measured under normal operating conditions. This receiver geometry information is a critical input into quantitative modelling and inversion routines. Conventionally the receiver coils' position are estimated from the measured AEM data during the routine data processing. However this requires assumptions to be made about the conductivity of the subsurface and the attitude of the receiver coils. When these assumptions are poor the estimated receiver position is not accurate, which results in the data not being able to be fitted and/or inaccurate conductivity models being estimated from subsequent inversions. More recently it has been demonstrated that a better approach is to simultaneously invert for the system geometry and the conductivity model (Lane et al., 2004).

The fixed-wing time-domain holistic inversion we improve on this by inverting not just one sample of AEM data at a time but a whole flight line of data. Figure 1 shows a schematic outline of the elements of the inversion formulation. We solve for layer conductivities, the transmitter to receiver in-line (D_x) and vertical separations (D_z), and the receiver pitch (R_p). All of these are parameterized as along line 1D cubic B-splines. Splines are an ideal choice because they are able to naturally represent the smooth and continuous along line variation of receiver geometry that occurs in reality. In doing so we are able to exploit the along line coherency, which is not accessible to the conventional sample by sample inversion, to improve upon the accuracy and stability of the inversion.

As a demonstration of the improvement that the new method offers, we have inverted a flight line of data that was acquired with the TEMPEST system using the two techniques. Figure 2 shows the results using a conventional inversion in which we solve for the layer conductivities independently for each airborne sample point and stitch the results together post-inversion to form a conductivity section. We did not solve for the receiver geometry. Figure 3 shows the results for the holistic method where we inverted the whole line at once to solve for the layer conductivities and three receiver geometry parameters, each parameterized as along line splines.

In the holistic inversion the data was able to be fitted to the expected misfit value of 1. However they were not able to be fitted in the conventional inversion due to inaccurate receiver geometry estimates made during the data processing. The holistic inversion conductivity section does not have the numerous vertical artefacts that are apparent in the conventional inversion section. This makes it more geologically realistic and continuous, and thus easier to interpret/trace subtle features. As a means of gauging the relative accuracy of the methods via independent ground truth two downhole conductivity logs (GW800232 and LMQ03) are plotted over the conductivity sections in the same color lookup scheme. It can be seen that in the vicinity of both logs the holistic inversion more accurately reproduces the downhole logs.

Brodie RC, Sambridge M (2006) A holistic approach to inversion of frequency-domain airborne EM data. *Geophysics* **71:** G301–G312

Lane R, Brodie RC, Fitzpatrick A (2004) Constrained inversion of AEM data from the Lower Balonne Area, Southern Queensland, Australia. *CRC LEME open file report* **163**

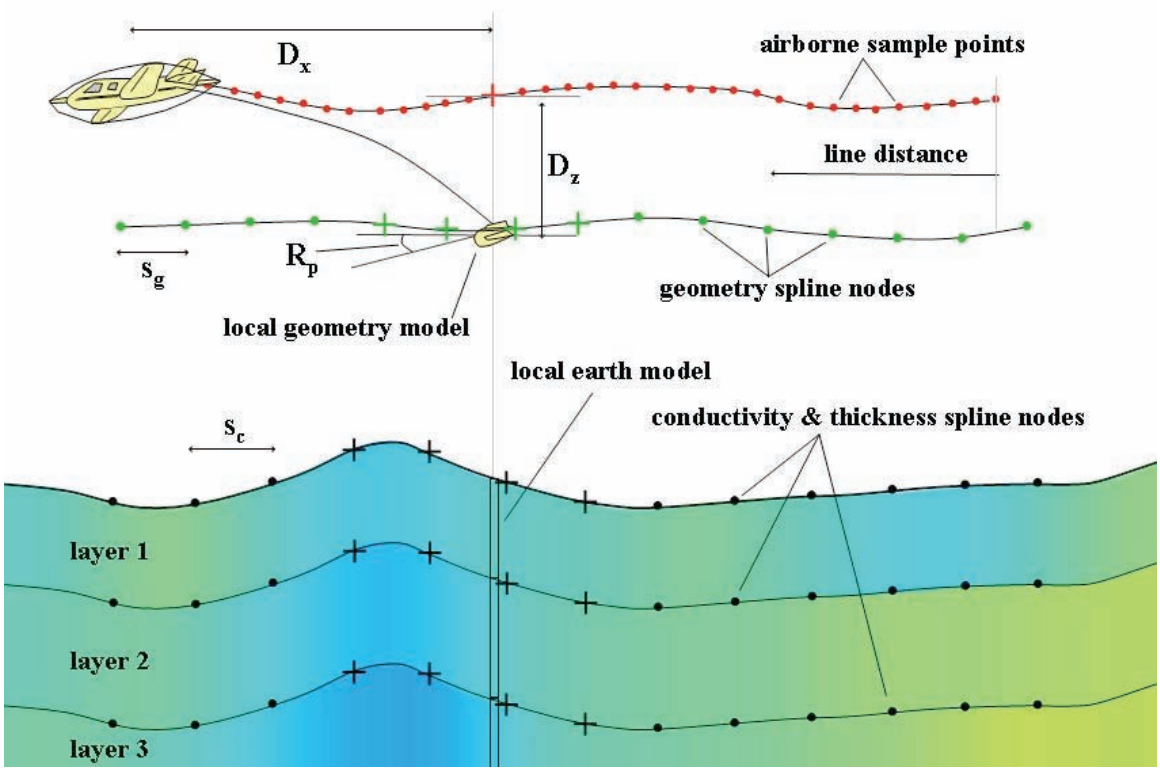

Figure 1.

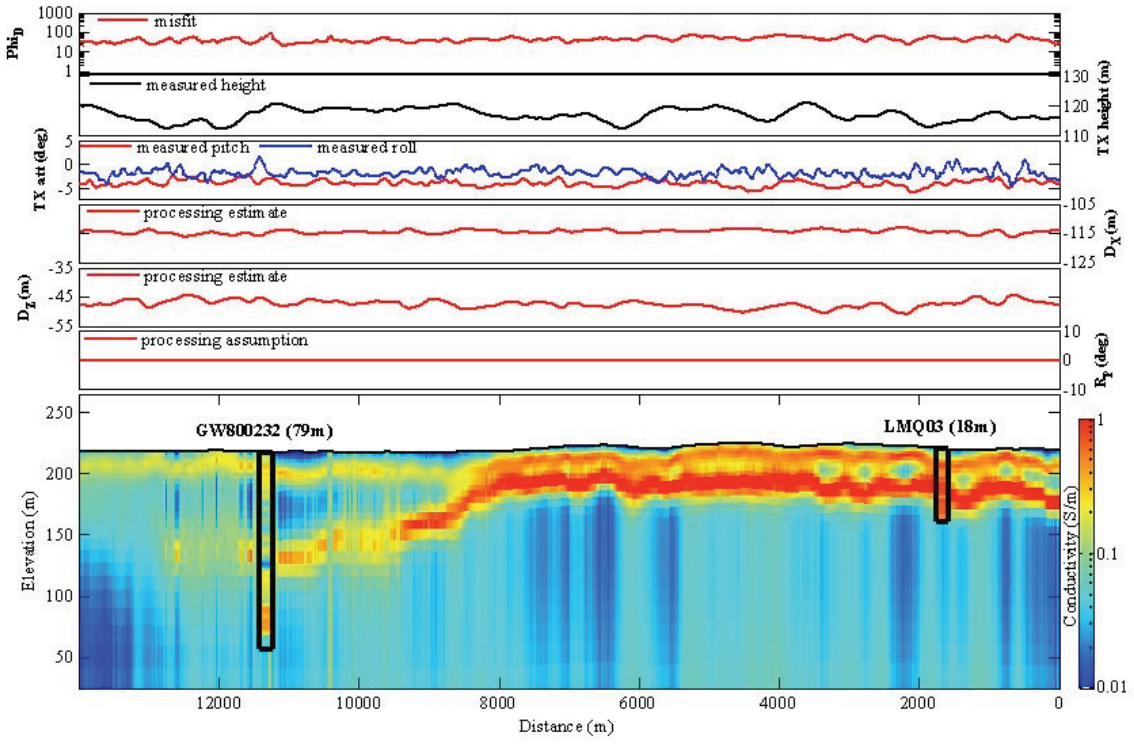

Figure 2.

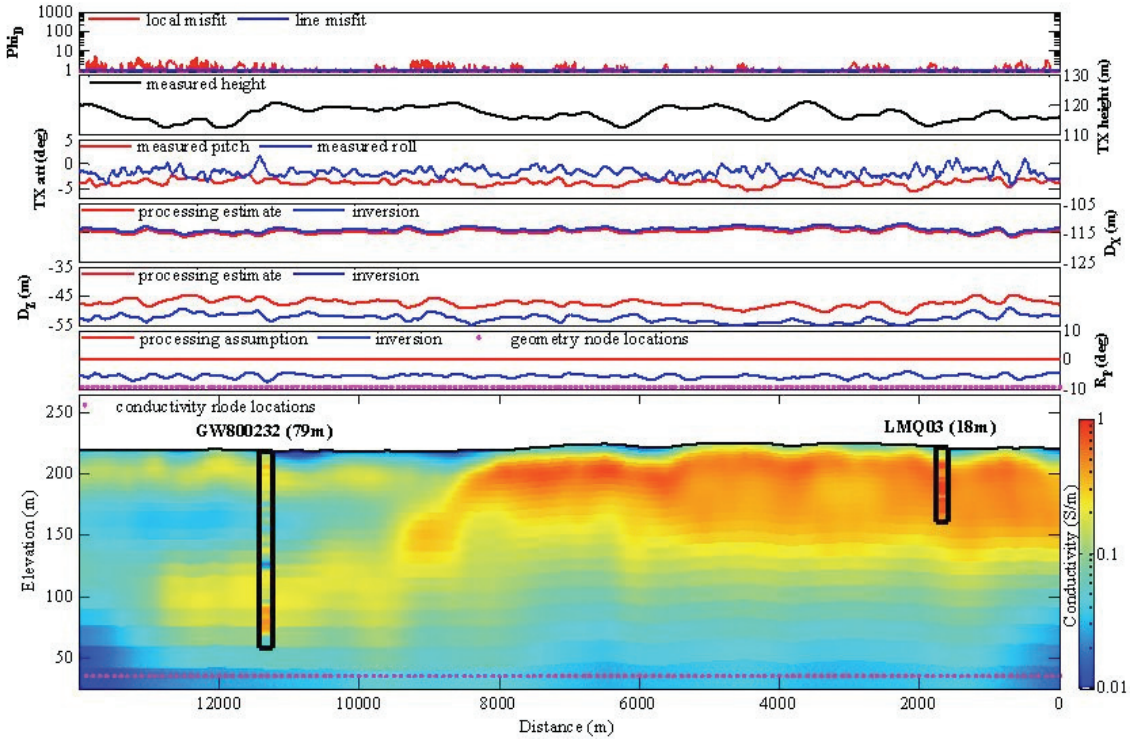
local misfit
line misfit
measured height
measured pitch
measured roll
processing estimate
inversion
processing estimate
inversion
processing assumption
inversion
geometry node locations
conductivity node locations
GW800232 (79m)
LMQ03 (18m)
Elevation (m)
Distance (m)
Conductivity (S/m)
TX height (m)
TX att (deg)

Figure 3.

Mantle Evolution, Dynamical and Chemical, Earth and Venus

Geoffrey F. Davies and Andreea Papuc

Research School of Earth Sciences, Australian National University, Canberra, ACT 0200, Australia

Numerical modelling of mantle dynamics is leading to important insights into the history of Earth and Venus.

A series of studies of how mantle convection stirs chemical tracers has established a quantitative basis for a new hypothesis regarding the abundance of trace elements in the mantle, including the enigmatic noble gases. Because the mantle is heterogeneous, being a mixture of subducted oceanic crust and peridotitic mantle, the extraction of melt at mid-ocean ridges is expected to be inefficient. A cartoon of melting under ridges is shown in the Figure. The inefficient extraction implies that the abundance of incompatible trace elements in the mantle is higher than has been estimated in the past. Geophysical constraints indicate the abundance is 2-3 times previous estimates. This removes the need for a 'hidden' reservoir, clarifies the relationship between continental crust and the mantle, and helps to resolve a discrepancy between estimates of radioactive heating and models of the thermal evolution of the mantle.

The source of 'unradiogenic' helium, i.e. helium that has a low $^4He/^3He$ ratio, from Hawaii and other hostpots has been an enduring puzzle for which the new hypothesis offers a resolution. Melting of the heterogeneous mantle is expected to produce a 'hybrid pyroxenite' that contains much of the mantle's complement of incompatible elements, including the noble gases. It is also likely to be denser than average mantle, like subducted oceanic crust. Numerical models have shown that such denser components tend to partially settle to the bottom, plausibly explaining the seismological D" region at the base of the mantle. Whereas subducted oceanic crust is expected to contain little noble gas, the hybrid pyroxenite should contain substantial noble gas. Furthermore the material in D" has a longer residence time, according to the numerical models, so it will degas more slowly, meaning the content of primordial ^3He will be higher. D" is already believed to be the source of mantle plumes, so the new hypothesis offers a straightforward explanation of mantle helium observations. A simple quantitative model, based on results from numerical models, then successfully explains the helium, neon and argon observations from mid-ocean ridge basalts and oceanic island basalts.

These results, if substantiated, go far to reconciling mantle geochemistry with the dynamical picture of the mantle based on geophysical evidence and numerical modelling. It has been unclear for at least three decades how this could be achieved.

Work reported last year on numerical models that yield episodic layering and overturns in Earth's early mantle is now being extended to Venus. Venus was volcanically resurfaced about 500 Myr ago. PhD student Andreea Papuc's project is to investigate whether conditions in Venus' mantle today are conducive to layering and overturn, as Earth's mantle was early in Earth history. Layering occurs because of the 'basalt barrier' mechanism, in which subducted oceanic crust tends to accumulate at 660 km depth because it is buoyant between 660 and 750 km depth, but negatively buoyant at other depths. Initial results show that overturns are indeed still likely in Venus, mainly because of its hotter surface and lack of plate tectonics. Venus' slightly smaller size, gravity and mantle density also seem to favour layering, though it is not yet clear why. The effects of different lithosphere strengths are yet to be investigated, and the goal is to do evolutionary models of Venus. It will be important for understanding Venus' atmosphere and geochemistry to know whether and how often earlier resurfacing events might have occurred.

Davies, G. F. (2008) Inefficient melt extraction from a heterogeneous, mildly depleted mantle: no hidden reservoir, Earth Planet. Sci. Lett., submitted.

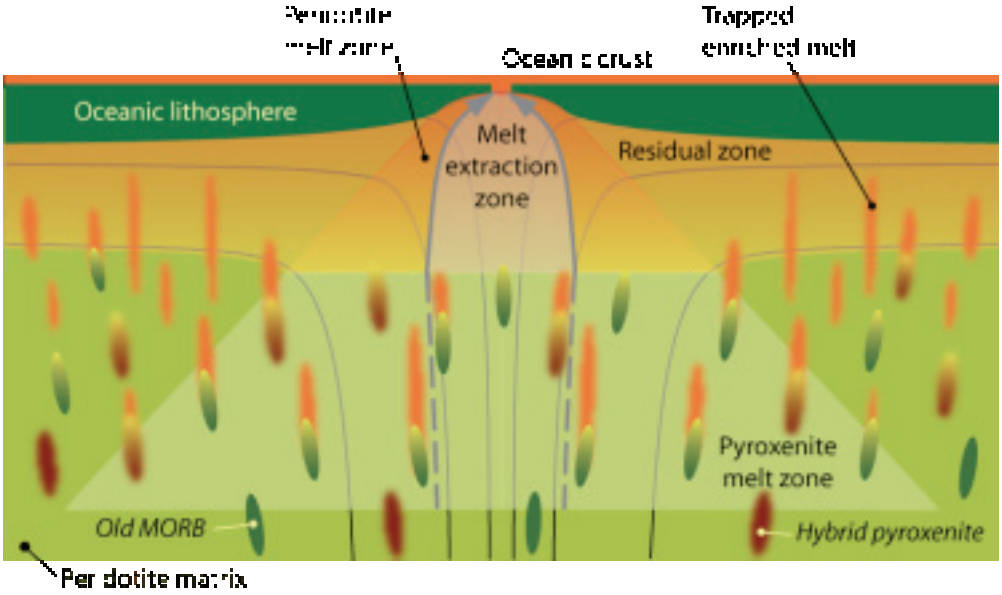

Figure 1. Melting under a mid-ocean ridge in a heterogeneous mantle.

Detecting Australian Earthquakes with InSAR

John Dawson[1,2] and Paul Tregoning[1]

[1] *Research School of Earth Sciences, Australian National University, Canberra, ACT 0200, Australia*
[2] *Geoscience Australia, Canberra, Australia.*

Analysis of Interferometric Synthetic Aperture Radar (InSAR) images has detected two shallow, intraplate earthquakes over the past three years. Each of these small earthquakes occurred in the top ~1 km of the crust and caused sufficient surface deformation that the location and fault parameters (orientation, dip, slip direction) could be estimated. These are the smallest magnitude earthquakes ever imaged by the InSAR technique (Dawson et al., 2008).

The Mw 4.7 October 2007 Katanning earthquake ruptured ~1 km2 with an average slip of ~ 42 cm. This implies a static stress drop of 14-27 MPa which is much higher than previously expected for such a small event. The quality of the InSAR deformation estimates is sufficiently high that the depth of the event can be estimated with a precision of ~10 m. It was even possible to invert for the distribution of slip on the fault plane – the first time that this has been achieved for such a small event. These results have been published by Dawson et al. (2008).

The fine spatial resolution and accuracy that InSAR analysis can provide to the study of earthquakes in Australia opens up exciting new possibilities. Given the vastness of the Australian continent, it is likely that most earthquakes will not occur close to a seismic station. Therefore, the accuracy with which seismic data can be used to locate earthquakes is limited. Given that InSAR observations are made remotely from space platforms, the deformation from any shallow earthquake (ie < 5 km depth) can be captured by InSAR provided an image of the region exists prior to the earthquake. It is even conceivable that the highly accurate locations estimated by InSAR could be used as constraints in seismic inversions for crustal rheology modelling and/or as master event locations in a bootstrapping process to relocate other Australian earthquakes.

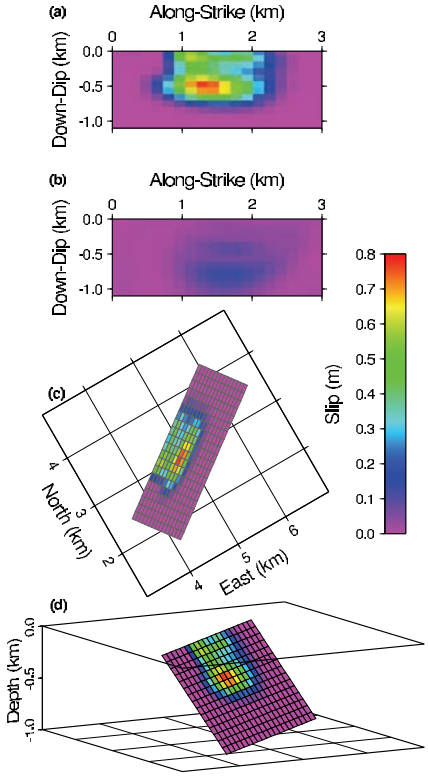

Dawson, J., P. Cummins, P. Tregoning, and M. Leonard, 2008. Shallow intraplate earthquakes in Western Australia observed by InSAR, *J. Geophys. Res.* 113, B11408, doi:10.1029/2008JB005807.
.

Figure 1. Slip distribution estimate of the Katanning earthquake, October 2007. A) Estimated slip. View is normal to the fault plane. b) 1_ uncertainties of the slip. c) Plan view of the rupture in an arbitrary local coordinate system. d) Viewing azumuth and elevation is 210° and 10°, respectively (Dawson et al., 2008).

Relative sea-level changes due to ocean bottom pressure changes caused by thermal expansion

Gisela Estermann[1,2], Kurt Lambeck[1,2] and Herb McQueen[1]

[1] *Research School of Earth Sciences, Australian National University, Canberra, ACT 0200, Australia*
[2] *Antarctic Climate & Ecosystems, Cooperative Research Centre, Hobart, Tasmania 7001, Australia*

Ocean thermal expansion does not alter the total global ocean mass but can nevertheless result in relative sea-level changes. The heat uptake by the ocean (in the case of a warming climate) varies locally both horizontally and in depth. In a simplified model the total water column in the deep ocean tends to expand more than in shallow areas (illustrated with arrow 1 in Figure 1). In order to maintain an equipotential surface, water has to flow from the deep ocean to the shallow areas. This redistribution of water (illustrated with arrows 2 in Figure 1) consequently results in a spatial change in ocean bottom pressure. These ocean bottom pressure changes result in relative sea-level changes.

Atmospheric CO_2 concentrations and projected global sea-level rise over the period from 1860 to 2200 used here are based on IPCC scenario simulations (see Figure 2 in Landerer et al., 2007). Landerer et al. (2007) calculated ocean bottom pressure changes caused by secular oceanic mass redistribution due to thermal expansion. They developed a numerical model for the mass transfer from deep open water to coastal (shallow) areas. A data set of ocean bottom pressure changes produced by this model has been provided by Felix Landerer. The variations are expressed as changes of mass load in meters of water and are given on an annual basis from 1860 to 2200 on a 1° x 1° grid. Three examples of 10-year averages are shown in Figure 2. The plots show an increase in intensity of the redistribution of mass particularly from 2000 onwards.

The plots in Figure 2 show the overall transfer of mass from the southern to the northern hemisphere. In particular, the Arctic Ocean shelves experience an above-average increase in mass load. It appears that there is a good correlation between ocean bottom pressure changes and ocean bathymetry. For the IPCC scenario simulations used here, positive loads of up to 0.4 m by the end of the 21st century and 0.8 m by the end of the 22nd century are projected mostly for the Arctic Sea, while the deeper oceans (especially in the southern hemisphere) experience negative loads of _0.2 m and _0.4 m by 2100 and 2200, respectively. These results represent the redistribution of mass assuming a rigid Earth. Hence, the so-called second order relative sea-level changes as a result of the viscoelastic response of the Earth to the redistribution are now calculated. Since only thermal expansion is considered here, no mass is added or taken away from the ocean and the total change in mass over the oceans is zero.

The bottom pressure changes, expressed as water-mass loads, have been implemented in a sea-level program (the calsea program; Johnston 1993a,b; Lambeck et al., 2003). The resulting relative sea-level changes for 10-year averages are shown in Figure 3. Changes in relative sea level from this source are negligible until the beginning of the 21st century. By the end of the 22nd century, relative sea-level rise reaches a maximum of approximately 60 mm in the Arctic. This value is expressed relative to the mean of the period 1860-1869, which is assumed to be an unperturbed period. As the spatial distribution of relative sea-level changes (Figure 3) correlates with the spatial distribution of ocean bottom pressure changes (Figure 2), a rise in second order relative sea level is predicted mostly in coastal areas, in particular in the Arctic Ocean, whereas second order relative sea level falls in deep ocean areas.

Assuming this climate scenario adequately represents future thermal expansion, relative sea-level changes due to the redistribution of water caused by secular ocean mass redistribution are amplified by about 10% due to these ocean bottom pressure changes.

While there is a variety of uncertainties in thermal expansion models (e.g. size of the surface warming, the effectiveness of heat uptake by the oceans for a given warming, and the expansion resulting from a given heat uptake; see Section 11.5 in Church et al., 2001), predicted future sea-level changes will have to be increased by 10% to account for the redistribution of ocean water following thermal expansion.

Church, J. A., Gregory, J. M., Huybrechts, P., Kuhn, M., Lambeck, K., Nhuan, M. T., Qin, D., and Woodworth, P. L. (2001). Changes in Sea Level. In Houghton, J. T., Ding, Y., Griggs, D. J., Noguer, M., van der Linden, P. J., Dai, X., and Johnson, C. A., editors, Climate Change 2001: The Scientific Basis. Contribution of Working Group I to the Third Assessment Report of the Intergovernmental Panel on Climate Change, chapter 11. Cambridge University Press, Cambridge, United Kingdom and New York, NY, USA.

Johnston, P. (1993a). Deformation of the earth by surface loads. PhD thesis, The Australian National University, Canberra.

Johnston, P. (1993b). The effect of spatially non-uniform water loads on prediction of sea-level change. Geophysical Journal International, 114, 615–634.

Lambeck, K., Purcell, A., Johnston, P., Nakada, M., and Yokoyama, Y. (2003). Water-load definition in the glacio-hydro-isostatic sea-level equation. Quaternary Science Reviews, 22, 309–318.

Landerer, F. W., Jungclaus, J. H., and Marotzke, J. (2007). Ocean bottom pressure changes lead to a decreasing length-of-day in a warming climate. Geophysical Research Letters, 34 (L06307).

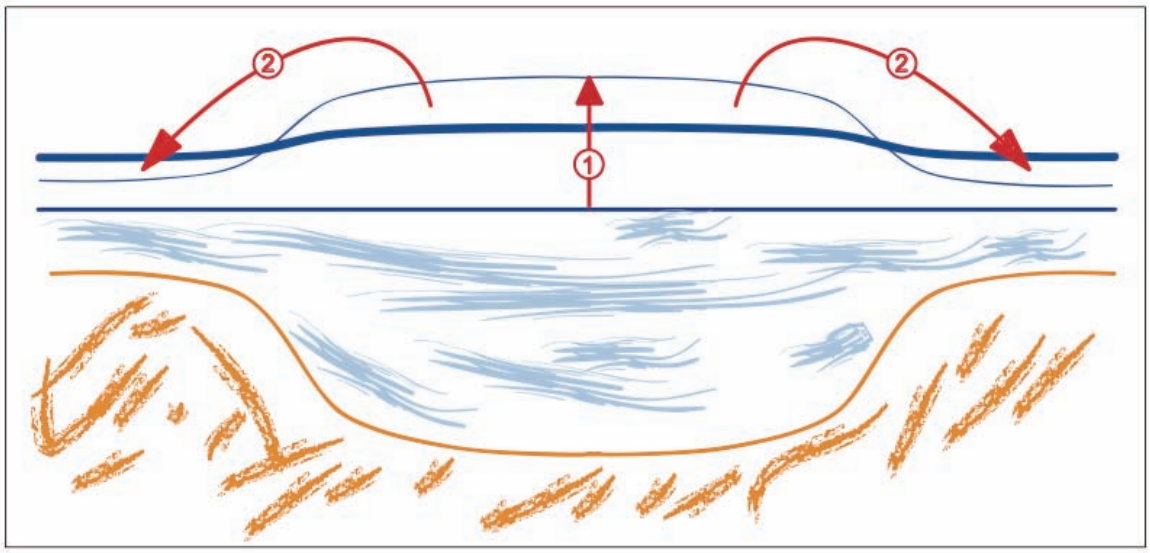

Figure 1.

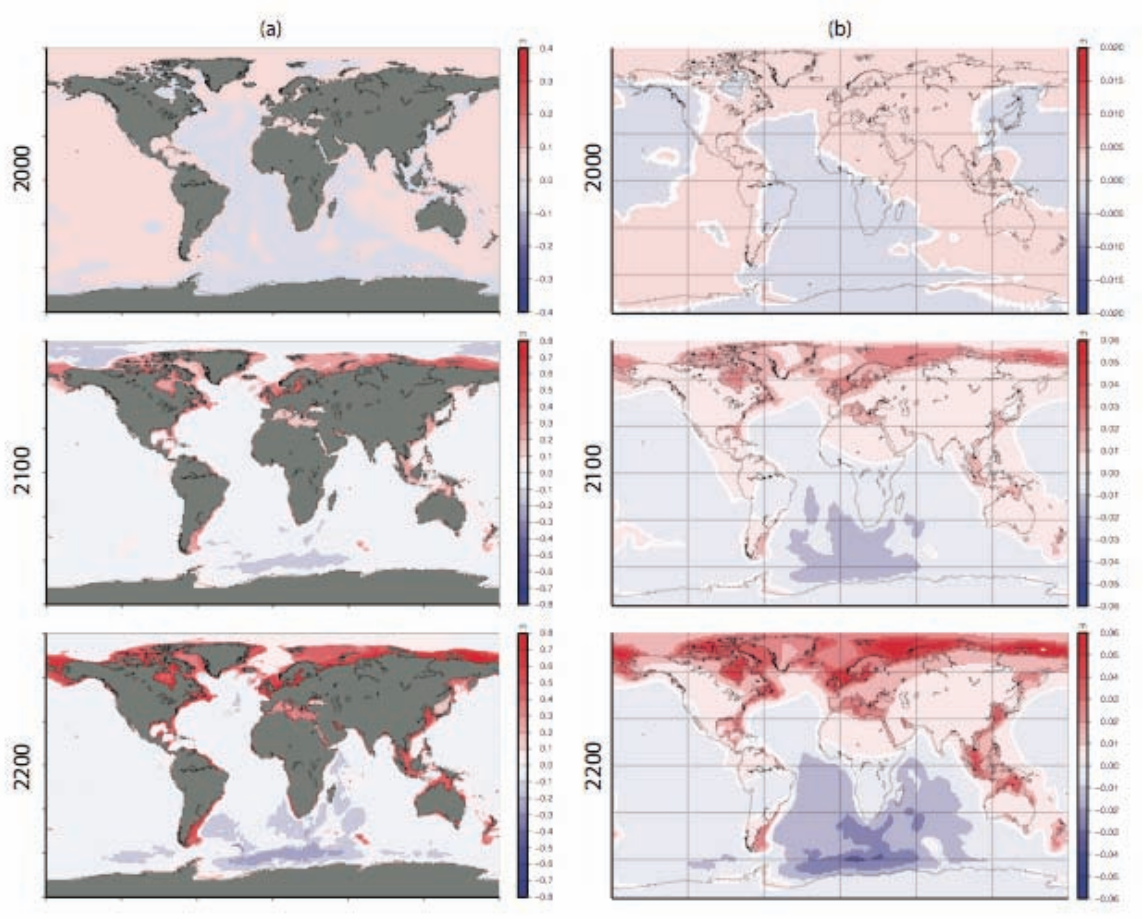

Figure 2.

The roles of bottom topography and internal gravity waves in horizontal convection

Ross W. Griffiths[1], Graham O. Hughes[1], Melissa A. Coman[1], Kial D. Stewart[1]

[1] *Research School of Earth Sciences, Australian National University, Canberra, ACT 0200, Australia*

Horizontal convection is the flow generated by heating and cooling along one horizontal boundary of a box. Studies of this form of convection have yielded much insight into the fundamental dynamics governing the ocean overturning circulation. In particular, equatorial surface waters are heated and high latitude surface waters are cooled, and analogies with horizontal convection allow us to investigate the role of surface buoyancy forcing in the overturning circulation. We have examined the progress in this field in a major review article published this year (Hughes and Griffiths, 2008).

In 2008 we have built on our previous studies of horizontal convection, and work has progressed on two main fronts. Firstly, we have studied the role of bottom topography in restricting flows between ocean basins, and thus in controlling the rate of overturning circulation. Secondly, we have discovered the spontaneous generation of internal gravity waves in the convective flow.
Laboratory experiments (figure 1) have shown that the introduction of bottom topography blocks the circulation, isolating waters in adjoining basins below the level of the sill. The circulation is most strongly affected when the depth of the sill is comparable with the depth to which the surface thermal boundary layer extends (i.e. the thermocline). In this regime, the range of densities in the flow increases markedly and the rate of overturning decreases. On this basis we expect the Denmark Straits and Faroe Bank Channel in the North Atlantic and the Weddell Sea ice shelf overflow in the Southern Ocean to influence the global overturning circulation.

Numerical simulations of horizontal convection have revealed the existence of coherent propagating waves (figure 2). Further investigation has shown that highly localized sinking plumes (as in figure 1) perturb the density stratification and excite a spectrum of internal gravity waves. We have been able to identify interaction of these wave modes as a source of strong variability in the circulation. Further work is required to assess the importance of this phenomenon in the ocean overturning circulation.

Hughes, G.O. and Griffiths, R.W. (2008) Horizontal convection. *Annu. Rev. Fluid Mech.* **40**, 185–208.

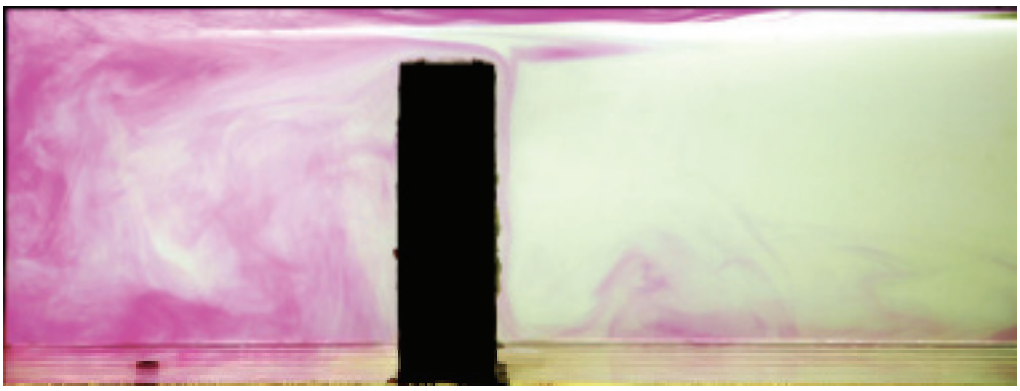

Figure 1. Dye visualization of a horizontal convection experiment with bottom topography (the field of view includes only the left-hand half of the box). The overturning circulation is forced by surface cooling at the left-hand end of the box ("polar latitudes") and surface heating over the right-hand end ("equatorial latitudes"; not visible). The dye reveals that relatively warm surface waters flow from right to left above the sill, where they subsequently become very cold, sink, and are trapped on the left of the topography at levels below the sill. This trapped water eventually fills the left-hand basin and can be seen leaking across the top of the sill (from right to left), whence it enters the main basin as a highly localized sinking plume.

Figure 2. Hovmöller plot of the vertical velocity along a horizontal section at mid-depth from a 2-D numerical simulation of horizontal convection. Time increases upwards; blue represents upwelling motion, green approximately no motion, and red downwelling motion. Regions of high latitude sinking are situated in this case at both the left and right hand ends of the horizontal section, and excite strong wave modes that propagate towards 'low latitudes' at the centre of the section. These waves and their interactions appear to be responsible for much of the variability in the circulation.

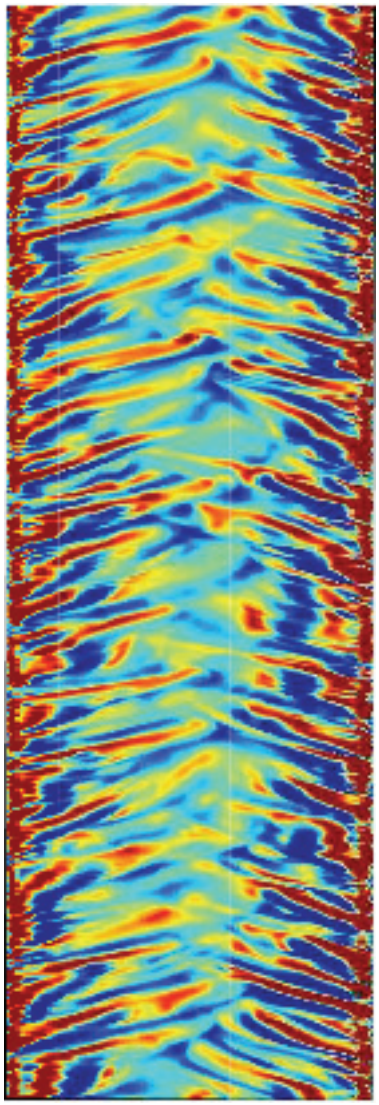

Multi arrival tomography

Juerg Hauser[1], Malcolm Sambridge[1] and Nicholas Rawlinson[1]

[1] *Research School of Earth Sciences, Australian National University, Canberra, ACT 0200, Australia*

In seismic imaging the focus has largely been on first arrivals, with a wide variety of schemes developed for their calculation. However, later arrivals often contribute to the length and shape of a recorded wave train, particularly in regions of complex geology. They are likely to contain additional information about seismic structure as their two point paths, differs from that of the first arrival. If they can be used in seismic tomography, improved images should result. Here we use the wavefront construction principle as the basis of a new scheme for computing travel times for first and later arrivals that arise from smooth variations in both velocity structure and interface geometry.

To investigate the possibility of using later arrivals to improve seismic imaging a numerical test is performed. We compare the results of first and multi arrival tomography, when recovering a two layered crustal scale structure characterised by two low velocity anomalies and a u-shaped valley in the interface. The inversion is performed simultaneously for interface and velocity structure. There are sources above and below the interface and two incoming plane waves are also simulated. Figures 1.a and 2.a show the ray path coverage of the structure, which we will try to recover using travel times. Clearly the later arrivals not only contain additional information about the two low velocity anomalies but also about the shape of the valley in the interface. Figure 1.b shows the difference between the inversion result and the true structure when only first arrivals are used in the inversion. The trade off between interface geometry and velocity anomaly is clearly not as well resolved compared to when both first and later arrivals are used (figure 2.b).

This example demonstrates that multi arrival tomography has the potential to lead to an improved recovery of structure. An important difference between first and later arrivals is that the existence of a later arrival is a function of the structure. This means that during the iterative inversion procedure, the number of ray paths and hence data is not constant. Using later arrival therefore makes the inverse problem much more non-linear, which means that care must be taken to avoid instabilities in an iterative non-linear approach.

Potential applications of multi arrival tomography include surface wave tomography, where observations of multipathing has been a long recognised phenomenon, with measurements and analysis using earthquake sources dating back many decades.

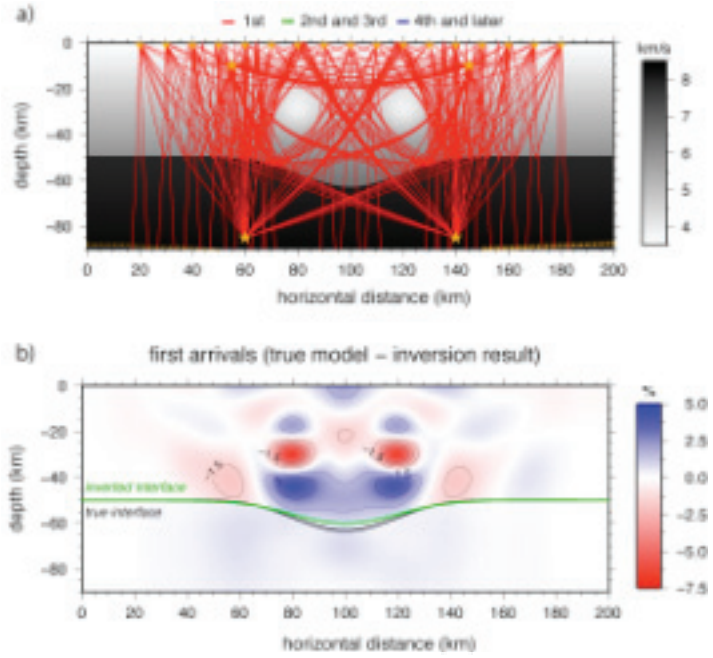

Figure 1. a) Layered velocity model and associated first arrival paths used in the inversion test. Point sources are denoted by stars and receivers by triangles. Note that paths also emanate from two impinging plane waves. b) Relative error in percent between the true model and the inversion result. Contour lines are plotted at 1.5% intervals.

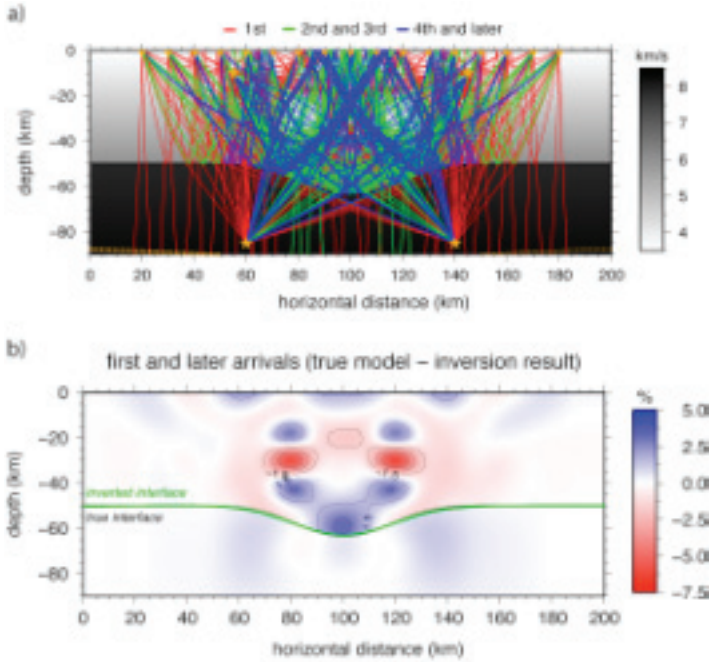

Figure 2. a) Layered velocity model and associated first and later arrival paths used in the inversion test. Point sources are denoted by stars and receivers by triangles. Note that paths also emanate from two impinging plane waves. b) Relative error in percent between the true model and the inversion result. Contour lines are plotted at 1.5% intervals.

The effects of mesoscale ocean-atmosphere coupling on the large-scale ocean circulation

Andrew McC. Hogg[1], William K. Dewar[2], Pavel Berloff [3,4], Sergey Kravtsov[5] and David K. Hutchinson[1]

[1] *Research School of Earth Sciences, Australian National University, Canberra, ACT 0200, Australia*
[2] *Department of Oceanography, Florida State University, Tallahassee, USA*
[3] *Woods Hole Oceanographic Institution, USA*
[4] *Cambridge University, UK*
[5] *University of Wisconsin, Milwaukee, USA*

Recent satellite measurements of wind stress at the ocean-atmosphere interface have pointed to large variations in stress on very fine scales. These fine scales are set by ocean mesoscale dynamics, and the variations in stress occur due to coupled interaction between the ocean and atmosphere. Given that wind stress drives the ocean circulation, there is a realistic possibility for coupled feedback acting to alter ocean currents.

We model this ocean-atmosphere interaction using high-resolution ocean model, coupled to a dynamic atmospheric mixed layer. The goal is to answer the question: Do small-scale variations in stress alter the large-scale ocean circulation?

The model results show that, despite the small spatial scale of the forcing anomalies, mesoscale coupling reduces the strength of the large-scale ocean circulation by approximately 30-40%. This result is due to the highest transient wind stress curl (or Ekman pumping) anomalies (see Fig. 1) destabilising the flow in a dynamically sensitive region close to the western boundary current separation.

These results indicate the complexity involved in migrating ocean models to eddy-resolving scales. The next generation of ocean models need to resolve atmospheric boundary layer processes at the same resolution as the ocean model.

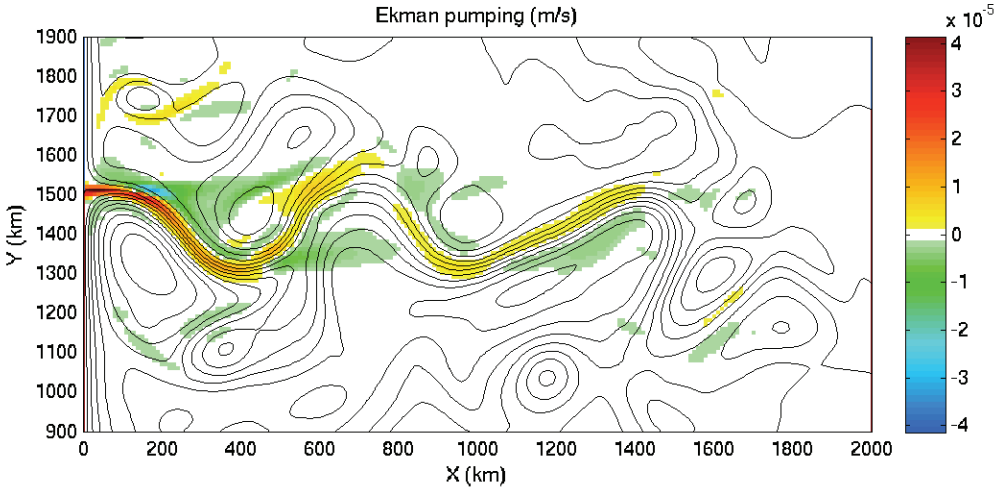

Figure 1. Snapshot of wind stress curl (or Ekman pumping) in colour, with contours of streamfunction superimposed. The streamfunction shows a western boundary current separating from the boundary, and forming a meandering zonal jet in the interior. This jet is accompanied by strong sea surface temperature gradients, which interact with the atmospheric boundary layer to produce large values of wind stress curl over the core of the jet. This extra forcing, somewhat paradoxically, acts to reduce the circulation by destabilizing the mean flow.

Energetics of the global ocean overturning circulation

Graham O. Hughes[1], Andy McC. Hogg[1], Ross W. Griffiths[1]

[1] *Research School of Earth Sciences, Australian National University, Canberra, ACT 0200, Australia*

The overturning circulation of the global oceans regulates Earth's climate, and oceanographers have been interested in which energy sources maintain that circulation. Energy input from surface winds and tides is important, but whether or not surface heating and cooling also contribute has been the subject of considerable debate. An understanding of the energetics is essential in addressing problems such as the response of the overturning circulation to forcing changes and in highlighting processes that need to be addressed in the development of general circulation models and climate models.

This year we have developed a theoretical framework that can be used to study the energy budget of the ocean overturning circulation. The concept of available potential energy, which is a measure of how far the density field is from equilibrium, underpins this framework. We have demonstrated that surface buoyancy forcing generates available potential energy, and is indeed an important energy source for the overturning circulation. In particular, only mixing and surface buoyancy forcing act to change the density of waters and, in a steady circulation, the energy transports associated with these two processes must balance. We have further clarified how the sources of kinetic energy associated with the winds and tides are simultaneously necessary to maintain the observed ocean overturning circulation.

We have in conjunction with our theoretical work undertaken a series of high-resolution numerical computations using a general circulation model of an ocean basin (figure 1). The results confirm our theoretical findings. Importantly, they also show that deductions regarding the energy budget of the ocean overturning circulation are strongly influenced by parameterizations of small-scale processes that are in common use in numerical models.

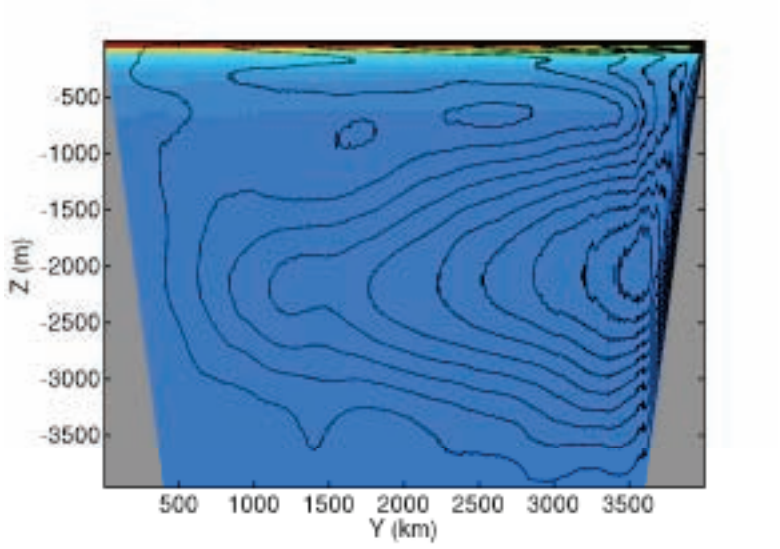

Figure 1. The time-averaged overturning circulation obtained in 2-D numerical simulations of a model ocean basin forced only by surface heating and cooling (varying smoothly from 200 W/m^2 at the left end to −200 W/m^2 at the right end, but with no net heat input to the basin). The simulation was non-hydrostatic, was conducted at high resolution (10–75 m vertical resolution and 0.75 –7.5 km horizontal resolution), and was run with a vertical diffusion coefficient of 10^{-4} m^2/s. The coldest waters are coloured blue and warmer waters towards the surface are shown as yellows and reds. The maximum overturning streamfunction is 28 x 10^3 kg/s per unit width.

Effect of thermal diffusion on the stability of strongly tilted mantle plume tails

Ross Kerr[1], John Lister[2] and Catherine Mériaux[3]

[1] *Research School of Earth Sciences, Australian National University, Canberra, ACT 0200, Australia*
[2] *Institute of Theoretical Geophysics, Department of Applied Mathematics and Theoretical Physics, University of Cambridge, Cambridge CB3 0WA, United Kingdom*
[3] *School of Mathematical Sciences and MC², Monash University, Victoria 3800, Australia*

Mantle plumes are produced by heat conducted into the Earth's mantle from the underlying core. This heating forms a thermal boundary layer of hot, low viscosity fluid, which focuses into narrow plumes that rise through the mantle. At the Earth's surface, partial melting of the plumes produces flood basalts from plume heads and volcanic island chains from plume tails.

As plume tails rise through the mantle, they are deflected by large-scale convection driven by the subduction of cold lithospheric plates. Last year, we reported a series of laboratory experiments that investigated the effect of thermal diffusion on the gravitational stability of these plume tails when they have been strongly tilted. This year, we examined this instability using a series of numerical calculations (Figure 1).

At large viscosity ratios, we conclude that the instability is unaffected by thermal diffusion when the Rayleigh number *Ra* is greater than about 300. When *Ra* is less than 300, thermal diffusion significantly increases the time for instability, as the rising fluid region needs to grow substantially by entrainment before it becomes unstable. When *Ra* is less than about 140, and the rise height available is less than about 40 times the cylinder radius, the rising region of fluid is unable to grow sufficiently and instability is prevented. When our results are applied to the Earth, we predict that thermal diffusion will stabilize plume tails in both the upper and lower mantle (Kerr, Mériaux and Lister 2008). We also predict that some of the buoyancy flux in mantle plumes is lost during ascent to form downstream thermal wakes in any larger scale mantle flow.

Kerr RC, Mériaux C, Lister JR (2008) Effect of thermal diffusion on the stability of strongly tilted mantle plume tails. *Journal of Geophysical Research* **113**: B09401, doi:10.1029/2007JB005510

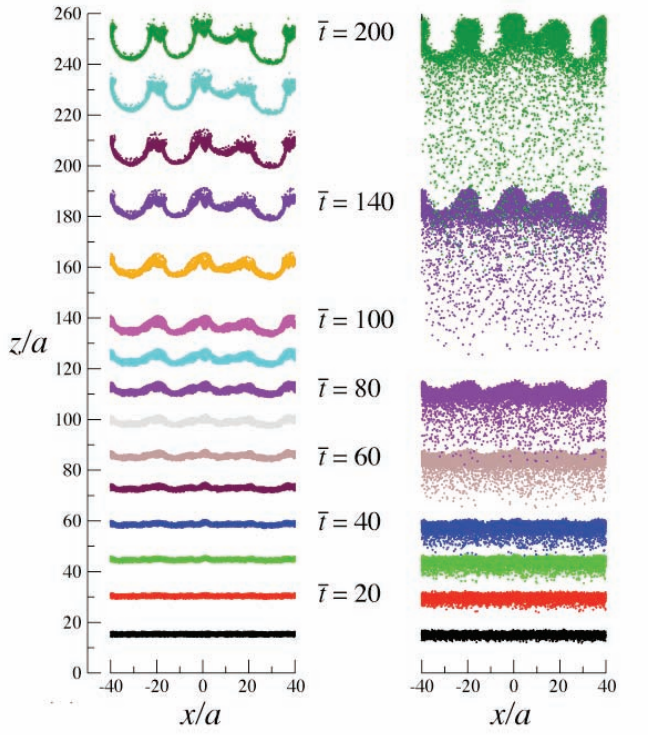

Figure 1. Numerical calculations showing the rise and eventual instability of a cylinder of buoyant fluid, as a function of dimensionless time. The cylinder has an initial radius *a*, and a Rayleigh number of 80. The side views show the distribution of tracers (left) and buoyancy (right).

Testing the Plume Hypothesis: Laboratory models of Subduction-plume interaction for the Cascades and Tonga-Lau Convergent Margins

Chris Kincaid[1], Ross Griffiths[2], the High Lava Plains Working Group[3] and the Somoan Plume working group[4].

[1] *Graduate School of Oceanography, University of Rhode Island, Narragansett, RI, USA*
[2] *Research School of Earth Sciences, Australian National University, Canberra, ACT 0200, Australia*
[3] *Richard Carlson & David James (Carnegie Inst. Of Wash.), Tim Grove (MIT), William Hart (Miami Univ.), Anita Grunder & Robert Duncan (Oregon State Univ.), Matt Fouch (Ariz. State Univ.), Randy Keller (Univ. of Oklahoma), Steve Harder (Univ. of Texas), Maureen Long (Yale Univ.).*
[4] *Stan Hart, Mark Behn & John Collins (Woods Hole), Greg Hirth (Brown Univ.), Magali Billen (Univ. of California, Davis).*

Subduction of lithospheric plates back into the mantle at subduction zones (ocean trenches) provides the dominant driving force for plate tectonics and causes thermal and chemical exchange with the Earth's interior. We have developed a laboratory apparatus for modeling 3D aspects of flow in subduction zones in response to various modes by which plates move and subduct into the mantle. These include slab rollback, when the slab sinks with a backward retreating or horizontal component of motion, and periods where the angle of descent (slab dip) either increases or decreases with time. Previous work has documented the importance of these modes of plate motion on 3D shallow mantle return flow and both slab and mantle wedge temperatures (Kincaid and Griffiths, 2003; 2004).

Kincaid and Griffiths are involved with two NSF funded projects to look at aspects of plume vs. non-plume models for reconciling patterns in geophysical and geochemical data collected within subduction zones. One project (the High Lava Plains project) involves a combination of efforts (seismology, geology/geochemistry and geodynamics) to better understand the evolution of the Cascades subduction system, spatial–temporal patterns in melt production and continental growth in the northwestern USA. In addition to field geology, this effort involves an a spatially detailed broadband seismic experiment coupled with a recent large scale active source seismic experiment. In terms on modeling, Kincaid and Griffiths are exploring aspects of 3D mantle flow and both thermal and compositional evolution of the mantle, and spatial-temporal patterns melt production for a subduction zone with representative plate motions for the Cascades-Pacific northwest USA system.

Plume-subduction interaction experiments show that plumes can be strongly deformed by rollback subduction and can be efficiently drawn into the arc wedge corner over large horizontal distances (~1000 km). The combination of rollback subduction and backarc extension deform the plume head and tail in a way that produces an early, circular large volume melt feature and two subsequent linear melt production features which are offset in space and time (~15 Ma). Two tracks are formed with time-transgressive rhyolite melting (e.g. reheating of the plate) and basaltic melt production, which trend in opposite directions. One is similar to the High Lava Plains in central Oregon, and the other is similar to the Snake River Plain. The initial, circular magma production feature is offset from the linear features by 300-400 km in a trench-parallel direction. The style of back-arc spreading changes the offsets and orientations of these three basic features. The influence of plate steepening is to deform the plume material into a very narrow feature. The severe, rapid deformation of plume material works to limit rise rates, essentially trapping much of this material deep in the wedge. The combined effects of increased diffusion and small length scales, partial melting and severe distortion in 3D, will make these remnant plume features difficult to image with seismic techniques.

In 2008 a URI PhD student, Ms Kelsey Druken, is working to extend these models of Cascades subduction system, including the effect of a keel-like morphology (Figure 1a) for the base of the overriding plate. An important part of the project is to also test

non-plume models. Three-dimensional flow-fields (Figure 1) are being analysed in combination with temperature data and a melt production model to calculate spatial patterns in vertical heat and melt flux through time for non-plume cases. In addition, finite strain is being observed within the flow through the use of whiskers. These act as a proxy for olivine alignment within the upper mantle and are being compared with seismic anisotropy data collected from the High Lava Plains.

Kincaid, C., and R. W. Griffiths (2003) Thermal evolution of the mantle during rollback subduction, *Nature*, 425, 58-62

Kincaid, C. and R. W. Griffiths (2004) Variability in mantle flow and temperatures within subduction zones. *Geochem. Geophys. Geosyst.*, 5, Q06002, doi:10.1029/2003GC000666

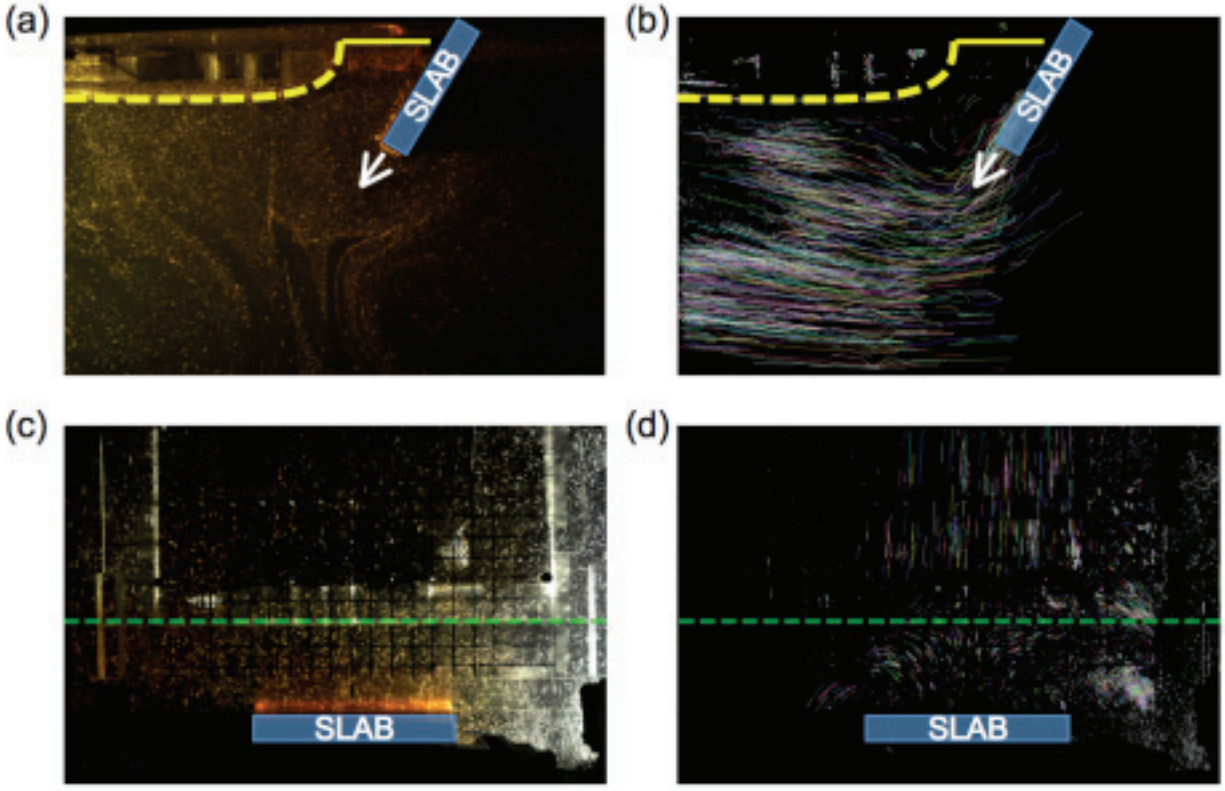

Figure 1: Top- and side-view images of the non-plume modelling of the Cascades using the 3D subduction system. that includes down-dip slab motion (5 cm/Ma), rollback slab motion (2.8 cm/Ma) and westward drift of the overriding plate (OP) at 1.4 cm/Ma. The combination of trench rollback and OP westward motion give a net extension rate about the spreading center (green dashed line) of 1.4 cm/Ma. Vertical and horizontal slices are imaged to produce 3D flow fields using particle tracking velocimetry (PTV) in FluidStream (developed by R. Nokes) (a) Side-view slice 4.5 cm (225 km scaled) along trench from plate centerline illustrating the subducting slab and the keel-like morphology of the over-riding plate (dashed yellow line) (b) Path-lines from PTV on the side-view slice using FluidStream. (c) Top-view slice at 2 cm (100 km scaled) depth where the back-arc spreading center (green dashed line) marks the start of the thickened morphology of the over-riding plate. (d) Path-lines for the top-view image using FluidStream PTV analysis.

Seismic Investigations of Lithospheric Transitions between the Northern and Southern Australian Cratons (BILBY)

Sara H. Pozgay[1] and Brian L.N. Kennett[1]

[1] *Research School of Earth Sciences, Australian National University, Canberra, ACT 0200, Australia*

We aim to determine the nature of the transition at lithospheric depths between the northern and southern Australian cratons. What are the controlling factors of the regions with anomalously slow velocities beneath the central Australian intercratonic suture zones? Do these intercratonic transitions propagate with depth and, if so, in what manner? To answer these questions, 25 broadband seismic stations were deployed in August-September 2008 and will remain operational for approximately one year.

Much of the Australian continent is an amalgamation of several smaller cratons and multiple orogenic events. The transitions between any two cratonic regions, however, do not necessarily reflect the same processes. Beneath the Capricorn Orogen (connecting the Yilgarn and Pilbara cratons), seismically fast wavespeeds (relative to a reference earth velocity model) and low attenuation are relatively continuous from 75 to >300 km depth. These large-scale observations suggest that a simple thermal origin is a likely explanation for the seismic signature of the orogen. However, much of central Australia is different; the central intercratonic belt regions exhibit low attenuation as for the case of the Capricorn Orogen, but slow wavespeeds persist at ~75 km depth. Only 25 km deeper, wavespeeds are fast and become relatively continuous at ~125 km depth. These observations suggest that the physical mechanism responsible for the observed seismic signature is more complex than simple thermal variations would predict.

What is the nature of this slow wavespeed region around 75 km depth beneath these intercratonic suture belts? Do the transitions between them extend through the whole lithosphere, as suggested by prior studies of the central Australian (Arunta Block) region? Several orogenic events should have made a lasting imprint through the whole lithosphere (e.g. the Alice Springs Orogeny 400-300 Ma), however these effects have yet to be imaged at the appropriate resolution to determine the nature of different lithospheric sections. Prior seismic deployments in the region were largely designed to image either crustal fault systems or deep lithosphere and upper mantle structures and, therefore, can provide only first-order constraints on the intercratonic suture belts.

We deploy an ambitious seismograph station configuration to image these lithospheric transitions between the northern and southern Australian cratonic regions and across parts of the intercratonic suture belts. The experiment configuration is designed specifically to connect the Gawler Craton in the south to components of the North Australian Craton - specifically, through the Musgrave Block and to the northern side of the Arunta Block, and to connect the Arunta Block with the Mt. Isa Block. A combination of rigorous analysis tools, such as velocity and attenuation tomography coupled with receiver functions, will help to provide a comprehensive understanding of the amalgamation of continental cratons and the associated intercratonic transitions. In addition, a significant amount of information will be added to the present understanding of intercratonic suture belts and further constraints on the Australian lithospheric structure and overall continental amalgamation will be realised.

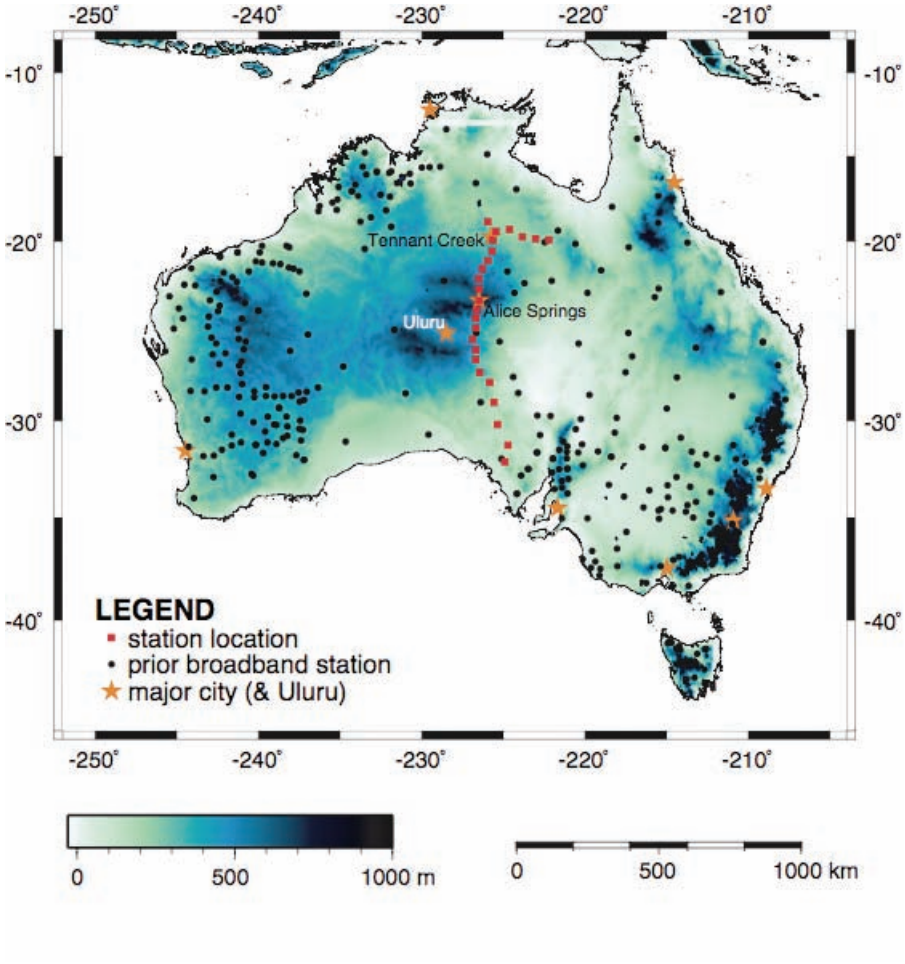

Figure 1. BILBY station map. Red squares indicated proposed station locations; black circles are prior broadband instrumentation; orange stars are major landmarks. Topography scale (in meters) shown at bottom.

Figure 2. Station near Alice Springs.

Exploring deep Australia with the WOMBAT array

Nick Rawlinson, Brian Kennett and Hrvoje Tkalcic

Research School of Earth Sciences, Australian National University, Canberra, ACT 0200, Australia

In the last decade, a dense rolling array of short period seismometers has been used to achieve a cumulative coverage of over 400 sites throughout southeast Australia (see Figure 1). This experiment, known as WOMBAT-SE, has recorded large volumes of passive seismic data for use in teleseismic tomography, ambient noise tomography, receiver function analysis and array studies of deep mantle and core structure. Station spacings vary between approximately 15-20 km in Tasmania, and 30-50 km on mainland Australia. Deployment times of early experiments in western Victoria and southeast South Australia are approximately 4 months, but since EVA (Figure 1), they have been extended to 8-12 months. The majority of instruments used have been ANU solid state short period recorders connected to vertical component L4Cs (natural frequency of 1Hz), but since SETA (Figure 1), three-component Lennartz LE-3Dlite sensors (also with a natural frequency of 1Hz) have been deployed.

To date, a variety of studies have been carried out with the recorded data, including teleseismic tomography, joint inversion of passive and active source data, ambient noise tomography, and analyses of exotic core phases. In this report, early results from a combined inversion of teleseismic arrival time residuals will be featured. Figure 2 shows a tomographic image at 150 km depth produced by the inversion of EVA, LF98, MB99, SEAL and SEAL2 datasets. One of the clearest features in Figure 2 is the east to west change from slower to faster velocities from the Bendigo Zone to the Stawell Zone. It is tempting to interpret this as a change from Phanerozoic mantle lithosphere of oceanic origin to Proterozoic mantle lithosphere of continental origin. Expected changes in both composition and temperature between these two types of material make this a plausible argument. In addition, this approximate boundary has also been observed, albeit at lower resolution, using surface-wave tomography, which appears to clearly distinguish between cratonic western Australia and the younger orogens that characterise eastern Australia. However, it must remembered that recent overprinting effects, such as the hotspot-related Newer Volcanic Province in Victoria and magmatic processes related to the opening of the Bass and Otway basins and the Tasman Sea, may well have contributed significantly (via increased temperatures) to reduced wavespeeds observed in central and southern Victoria.

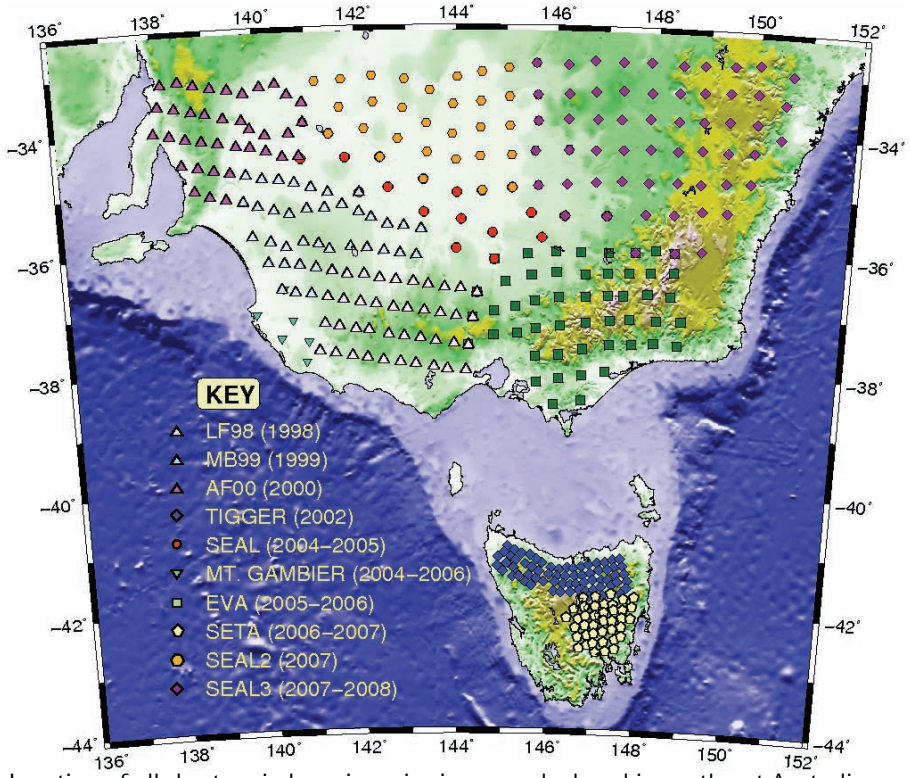

Figure 1. Location of all short period passive seismic arrays deployed in southeast Australia over the last decade

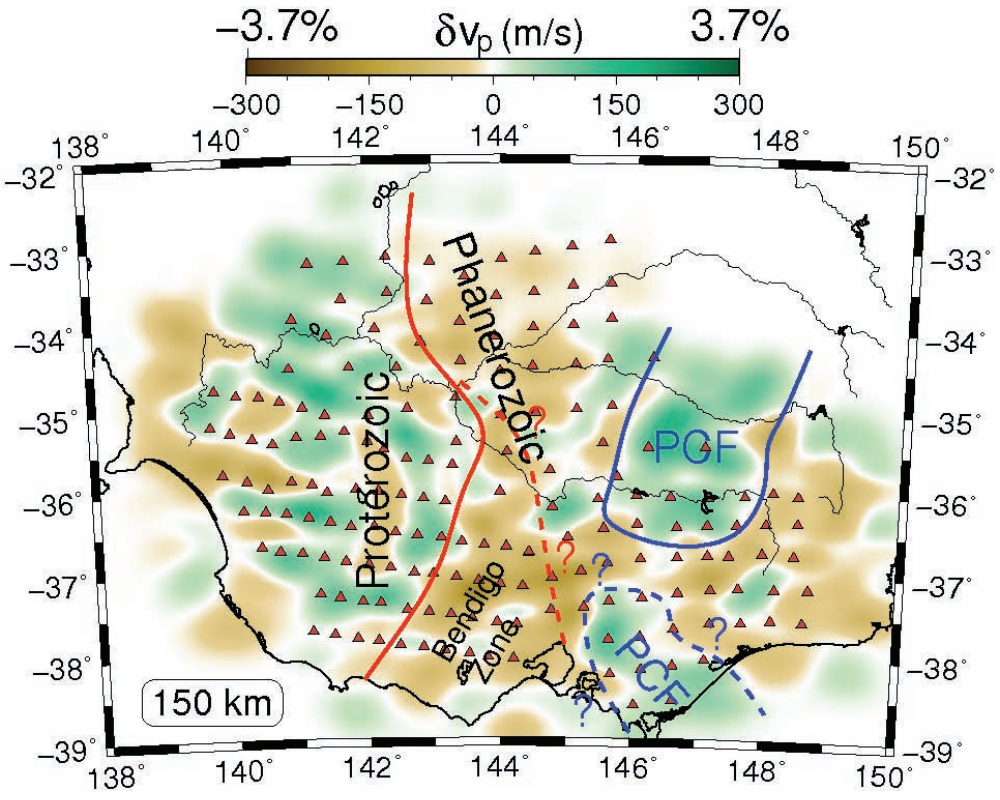

Figure 2: Preliminary image obtained from joint inversion of teleseismic arrival time residuals recorded at five arrays of the WOMBAT-SE project. PCF = Proterozoic Continental Fragment.

The dynamics of solidifying lava flows with a Bingham yield strength rheology

Jesse Robertson[1], Ross Kerr[1] and Ross Griffiths[1]

[1] *Research School of Earth Sciences, Australian National University, Canberra, ACT 0200, Australia*

Lava flows cover much of the Earth, the Moon, Mars, Venus, and several satellites of the outer planets. They vary greatly in their viscosities and eruption rates and form a wide range of flow types from long channel and tube flows to lava domes. Recent research in the GFD Laboratory has focused on surface crust formation, channel formation and flow morphology in Newtonian fluids subject to surface cooling (Griffiths et al. 2003; Kerr et al. 2006). This work predicts the behaviour of crystal-poor lava flows with a Newtonian rheology, such as some proximal basaltic flows on Kilauea Volcano, Hawaii and submarine lava flows near submarine spreading ridges. However, many lava flows contain sufficient crystals for the lava to have a viscoplastic rheology with a substantial yield strength, including those typical of distal Hawaiian channels and most Mt Etna flows. The yield strength can have a significant effect on the velocity distribution in a channel flow, and hence should have a major impact on the very complex interaction between convection and surface solidification seen in solidifying channel flows.

Experiments carried out this year have aimed to develop a quantitative understanding of solidification, cooling mechanisms, and tube formation in lava flows with a Bingham viscoplastic rheology. In these experiments, slurries of polyethylene glycol and kaolin flowed down a long sloping channel under water. We systematically varied flow rate, slope and channel width for flows with no cooling, flows with cooling but no solidification, and flows with cooling and solidification (Figure 1). This data set will allow us to determine the roles of yield strength, flow rate, cooling rate, slope and aspect ratio in governing surface crust distribution, the critical conditions for transition from open channel to lava tube flow, and the thermal efficiency of the flows.

Griffiths RW, Kerr RC, Cashman KV (2003) Patterns of solidification in channel flows with surface cooling. *Journal of Fluid Mechanics* **496**: 33-62

Kerr RC, Griffiths RW, Cashman, KV (2006) The formation of channelized lava flows on a slope. *Journal of Geophysical Research* **111**: B10206, doi:10.1029/2005JB004225

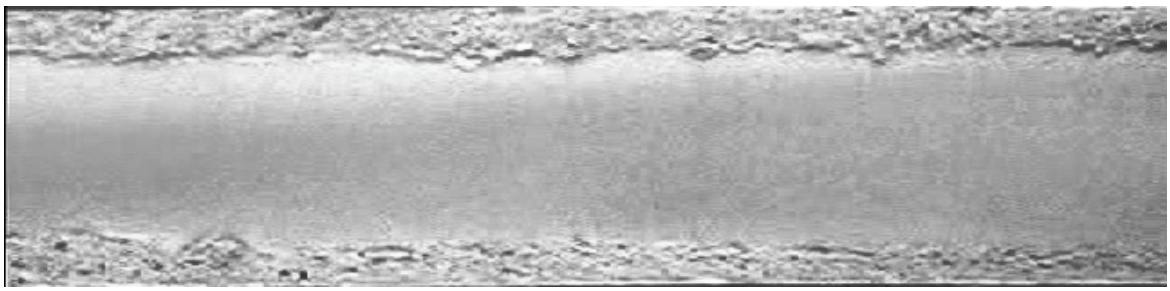

Figure 1. Overhead photograph of a slurry of polyethylene glycol and kaolin, flowing from right to left down a 8 cm wide sloping rectangular channel. The flow is overlain by cold water, and freezes to form a central raft of smooth solidified crust, separated from the walls by two shear layers.

Gawler Craton Array

Michelle Salmon[1], Brian Kennett[1]

[1] *Research School of Earth Sciences, Australian National University, Canberra, ACT 0200, Australia*

As part of a wider AUSCOPE project 35 short-period seismometers have been deployed across the Gawler Craton in South Australia. Station spacing is approximately 50 km and the area covered runs from Port Lincoln in the Eyre Peninsular to Leigh Creek just west of the Flinders Ranges (figure 1.). Stations will record continuous three component data for a period of 8 months. The primary aim of this array is to increase data coverage in this part of Australia for seismic imaging. There are only two permanent seismographs in the region covered by this array. Data from this array will eventually be publicly available providing the information required to build basic images of the earth structure in the region.

The instruments are capable of recording data from both local and distant earthquakes. This area of South Australia is seismically active and local earthquake data recorded on this array (figure 2.) will help improve our ability to locate and characterize these events. Distant earthquakes will be used to produce tomographic images of the crust and upper mantle in the region. Receiver functions constructed from the three component data can will also be used to locate seismic discontinuities such as the crust-mantle boundary.

The eastern edge of the Gawler craton is currently of particular interest for the supply of geothermal energy and there are many ongoing industry projects in the area. Geoscience Australia completed a deep seismic reflection transect across the top of the Eyre Peninsular just prior to the deployment of the Gawler array. This array will provide broad scale earth imaging required for more detailed studies.

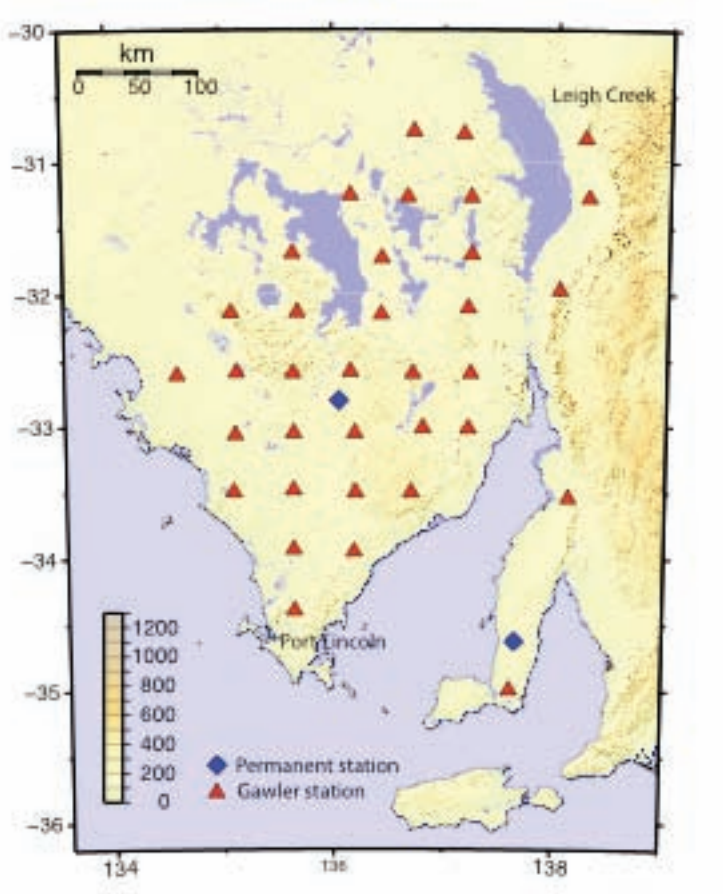

Figure 1.

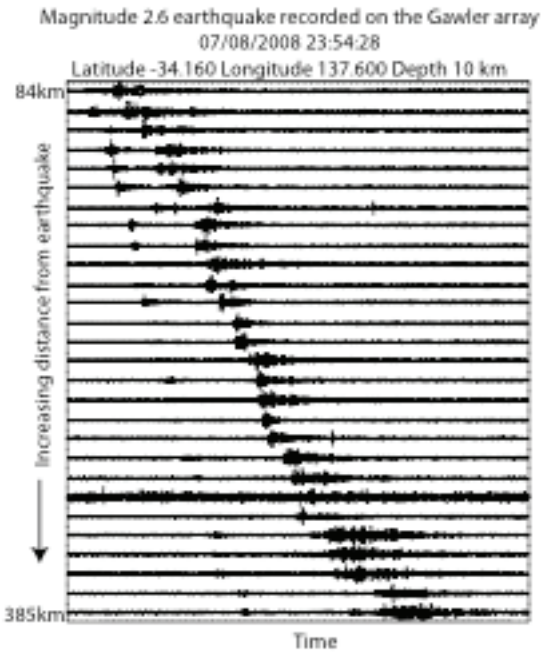
Magnitude 2.6 earthquake recorded on the Gawler array
07/08/2008 23:54:28
Latitude -34.160 Longitude 137.600 Depth 10 km
84km
Increasing distance from earthquake
385km
Time

Figure 2.

Dynamic objective functions in seismic tomography

N. Rawlinson[1], M. Sambridge[1] and E. Saygin[2]

[1]*Research School of Earth Sciences, Australian National University, Canberra, ACT 0200, Australia*
[2]*Geoscience Australia, Symonston ACT 2609, Australia*

A new technique designed for generating multiple solutions to seismic tomography problems using gradient based inversion has been developed. The basic principle is to exploit information gained from previous solutions to help drive the search for new models. This is achieved by adding a feedback or evolution term to the objective function that creates a local maximum at each point in parameter space occupied by the previously computed models (Figure 1). The advantage of this approach is that it only needs to produce a relatively small ensemble of solutions, since each model will substantially differ from all others to the extent permitted by the data. Common features present across the ensemble are therefore likely to be well constrained.

A synthetic test using surface wave traveltimes and a highly irregular distribution of sources and receivers shows that a range of different velocity models are produced by the new technique. These models tend to be similar in regions of good path coverage, but can differ substantially elsewhere. A simple measure of the variation across the solution ensemble, given by one standard deviation of the velocity at each point, accurately reflects the robustness of the average solution model. Comparison with a standard bootstrap inversion method unequivocally shows that the new approach is superior in the presence of inhomogeneous data coverage that gives rise to under or mixed-determined inverse problems. Estimates of posterior covariance from linear theory correlate more closely with the dynamic objective function results, but require accurate knowledge of *a priori* model uncertainty.

Application of the new method to traveltimes derived from long term cross-correlations of ambient noise contained in passive seismic data recorded in the Australian region demonstrates its effectiveness in practice, with results well corroborated by prior information (Figure 2). The dynamic objective function scheme has several drawbacks, including a somewhat arbitrary choice for the shape of the evolution term, and no guarantee of a thorough exploration of parameter space. On the other hand, it is tolerant of non-linearity in the inverse problem, is relatively straightforward to implement, and appears to work well in practice. For many applications, it may be a useful addition to the suite of synthetic resolution tests that are commonly used.

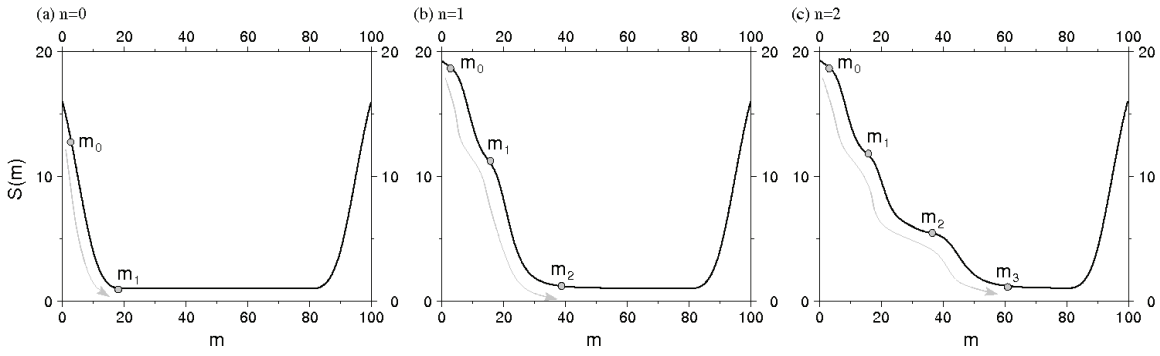

Figure 1: Schematic diagram demonstrating the principle of the dynamic objective function method. When each new solution is located by the gradient based method, a "hump" is introduced in model space at that point to disuade future solutions from investigating this region.

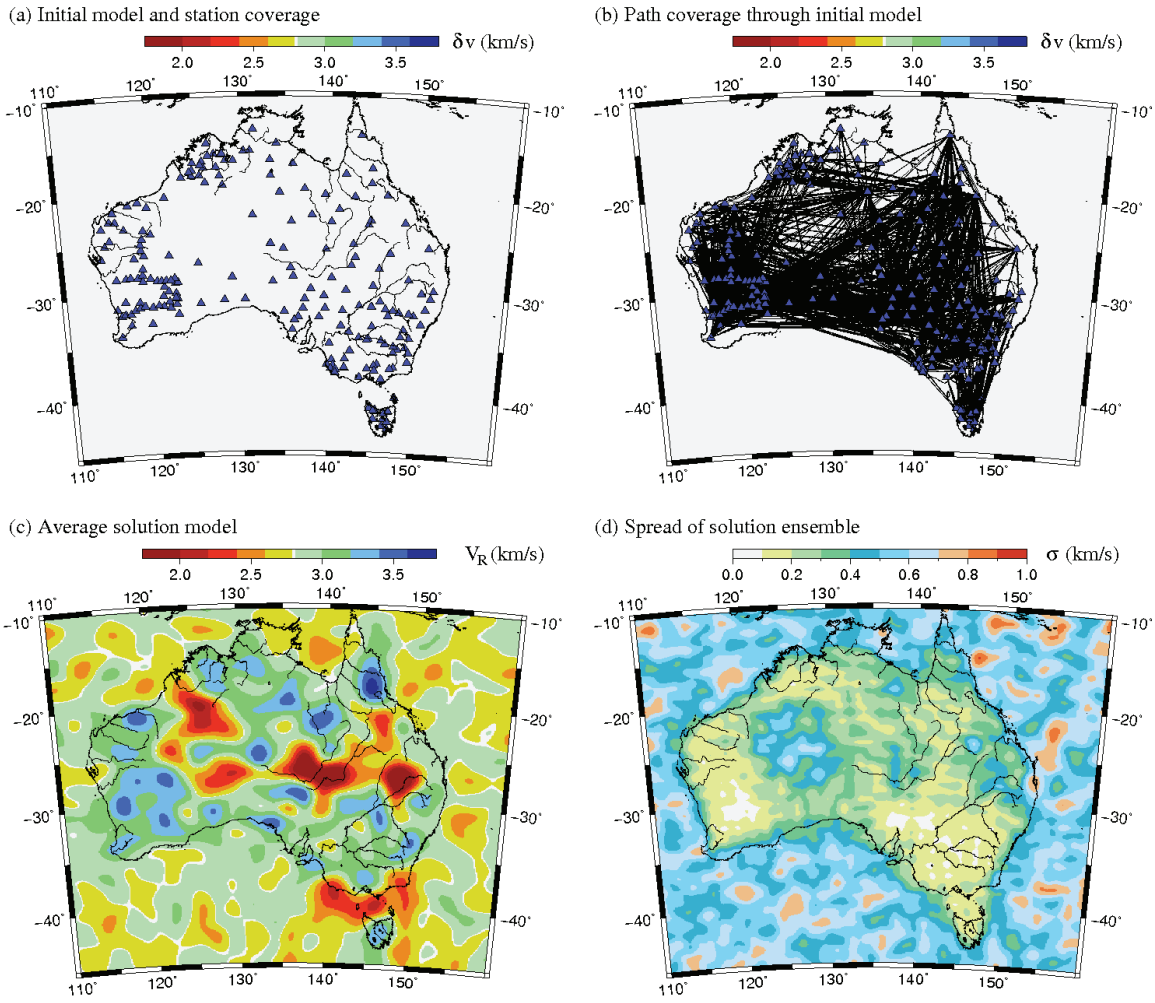

Figure 2: (a) Stations used in the cross-correlation of ambient noise data; (b) *path coverage through the initial model; (c) average solution model computed from an ensemble of 25. V_R denotes Rayleigh wave group velocity; (d) variation of the model ensemble as represented by one standard deviation of the distribution.*

On The Inner-Outer Core Density Contrast From New PKiKP/PcP Amplitude Ratios And Uncertainties Caused By Seismic Noise

Hrvoje Tkalčić[1], Brian L. N. Kennett[1] and V. F. Cormier[2]

1 Research School of Earth Sciences, Australian National University, Canberra, ACT 0200, Australia
2 Department of Physics, University of Connecticut, Storrs, 06269 – 3046United States

The inner core boundary of the earth is characterised by a discontinuous change in elastic properties between the liquid outer and solid inner core. In the ray theory approximation, a measure of the density contrast at the inner core boundary is given by the amplitude ratio of P waves reflected from the core-mantle boundary (PcP waves) and the inner core boundary (PKiKP waves), since that ratio conveniently appears in an explicit form in the transmission/reflection coefficient equations. The results for inner-outer core density contrast derived from direct amplitude picks of these waves in the time domain have varied significantly among different authors.

The transmission/reflection coefficients on the liquid-solid and solid-liquid boundaries derived from ground displacements enable a direct comparison between the amplitude measurements on displacement seismograms in the time domain and theoretical values. A new approach is proposed and applied to integrate effects of microseismic and signal-generated noise with the amplitude measurements, thus providing a direct maximal uncertainty measure. To suppress the effects of varying radiation pattern and distinctively different ray-paths at longer epicentral distances, this new method was applied to high-quality arrivals of PcP and PKiKP waves from a nuclear explosion observed at epicentral distances 10° to 20° from recording stations. The resulting uncertainties are high precluding precise estimates of the inner core boundary density contrast, but provide a robust estimate of an upper bound from body waves of about 1100 kg/m^3.

Median values of two amplitude ratios observed around 17° epicentral distance indicate a small density contrast of 200-300 kg/m^3 and suggest the existence of zones of suppressed density contrast between the inner and the outer core, a density contrast stronger than 5000 kg/m^3 at the core-mantle boundary, or a combination of both (Figure 1). Such a small estimate of the density contrast across the inner-core boundary from body waves could still produce the desired effect on the compressional velocity profile in the thermo-chemical boundary layer at the bottom of the outer core and return a modest heat flux from the inner core with a substantial inner core age, but only if accompanied by a small estimate of the density contrast of about 400 kg/m^3 from normal modes. If the inner-core boundary is characterized with such a mosaic of variable density contrast to which seismic body waves are sensitive, it is more likely that the density fluctuations are restrained to the top of the inner core. It has been argued that at least the top of the inner core is a dendritic mushy zone, in which interdendritic fluid pockets likely coexist to explain the observed nature of attenuation and attenuation in anisotropy of body waves. If PKiKP waves reflect from the inner core at the places where less dense features at the top of the inner core reduce the density contrast, than this could explain the observed lower values for stations at around 17° (Figure 1).

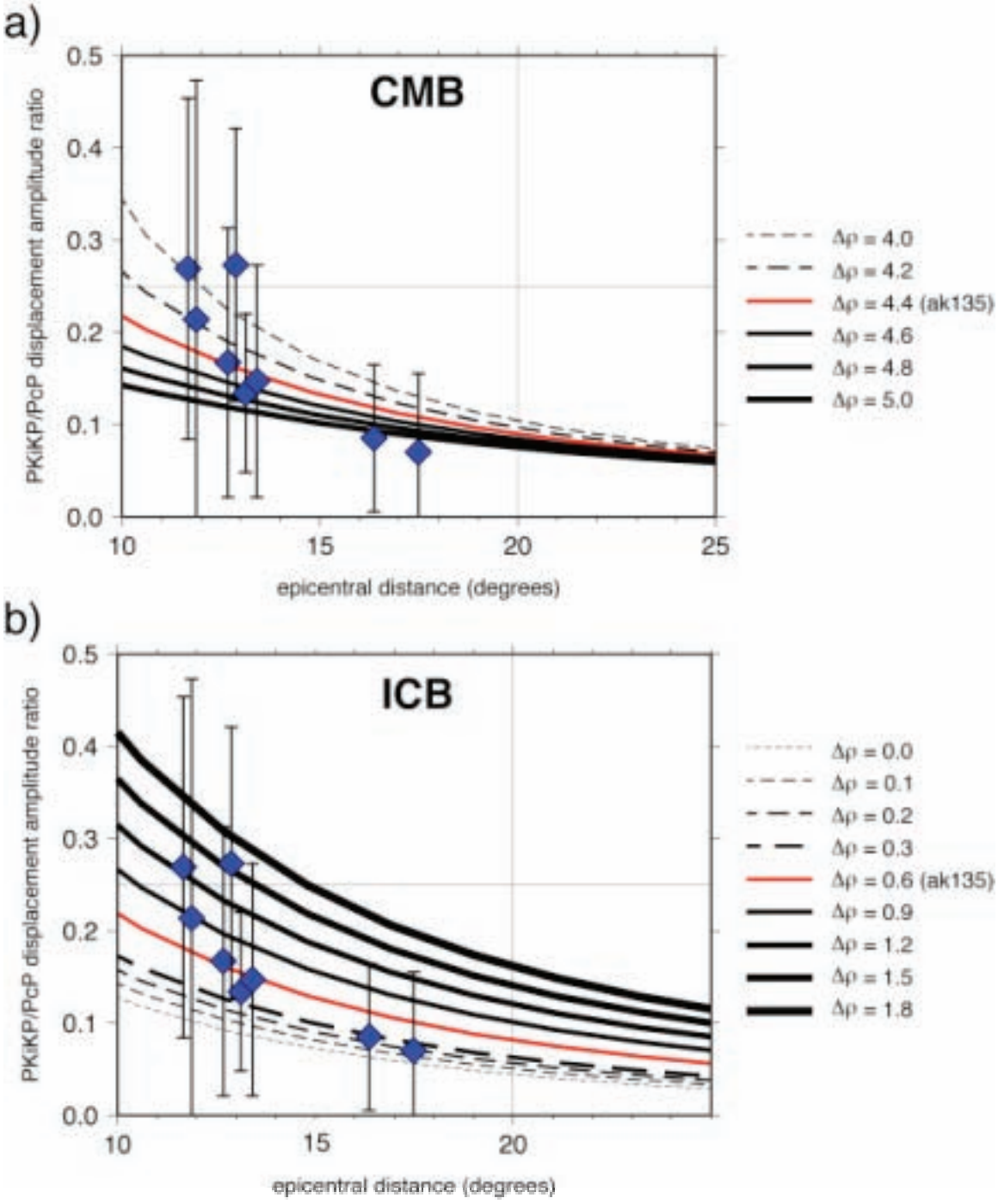

Figure 1. PKiKP/PcP amplitude measurements and their uncertainties (the median values are shown by diamonds, and the uncertainties are shown by error bars) plotted as a function of epicentral distance for: a varying density contrast at the inner core boundary (top) and the core mantle boundary (bottom). Theoretical values are indicated with lines of various thicknesses. Red line indicates the theoretical ratio from the ak135 model.

Drought in the Murray-Darling Basin

Paul Tregoning[1], Marc Leblanc[2] and Guillaume Ramillien[3]

[1] *Research School of Earth Sciences, Australian National University, Canberra, ACT 0200, Australia*
[2]*School of Earth and Environmental Sciences, James Cook University, Cairns, Australia.*
[3]*Groupe de Recherche en Géodesie Spatiale, CNRS, Toulouse, France.*

The Murray-Darling Basin (MDB) is experiencing one of the most severe droughts in recorded history, driven by record high temperatures and several years of rainfall deficit. The multi-year drought has seen an almost complete drying of surface water resources, water that is required for agriculture and domestic use.

It has always been difficult to quantify total water storage in drainage basins because of the difficulty of measuring and monitoring water retained as soil moisture and in groundwater reservoirs. With the launch of the Gravity Recovery and Climate Experiment (GRACE) space gravity mission in 2002, it is now possible to estimate basin-scale total water storage. GRACE detects changes in the Earth's gravity field – more precisely, changes in potential between the centre of the Earth and the satellites. Making the assumption that the changes in potential are due entirely to changes in water volume, it then becomes possible to estimate the spatial and temporal variations in water integrated across large regions.

Figure 1 shows the time series of changes in total water storage of the MDB since the beginning of the GRACE mission (*Leblanc et al.,* 2008) compared to groundwater, soil moisture and surface water variations. A significant loss of ~260 GTonnes of water can be seen between 2005 and 2007 in the GRACE estimates and the overall loss of total water storage correlates with groundwater losses. The meteorological drought (ie rainfall quantities) abated in 2007 and early 2008 with a return to average or above-average rainfall in the northern part of the basin. The drought actually began some years earlier; hence it is not possible to quantify the total loss of water caused by the current drought. Nonetheless, the GRACE total water storage data indicates that a substantial water deficit remains. Rainfall levels have declined below average values since March 2008.

Leblanc, M., P. Tregoning, G. Ramillien, S. Tweed and A. Fakes, Basin scale, integrated observations of the 21st Century multi-year drought in southeast Australia, *Water Resourc.. Res. in revision*.

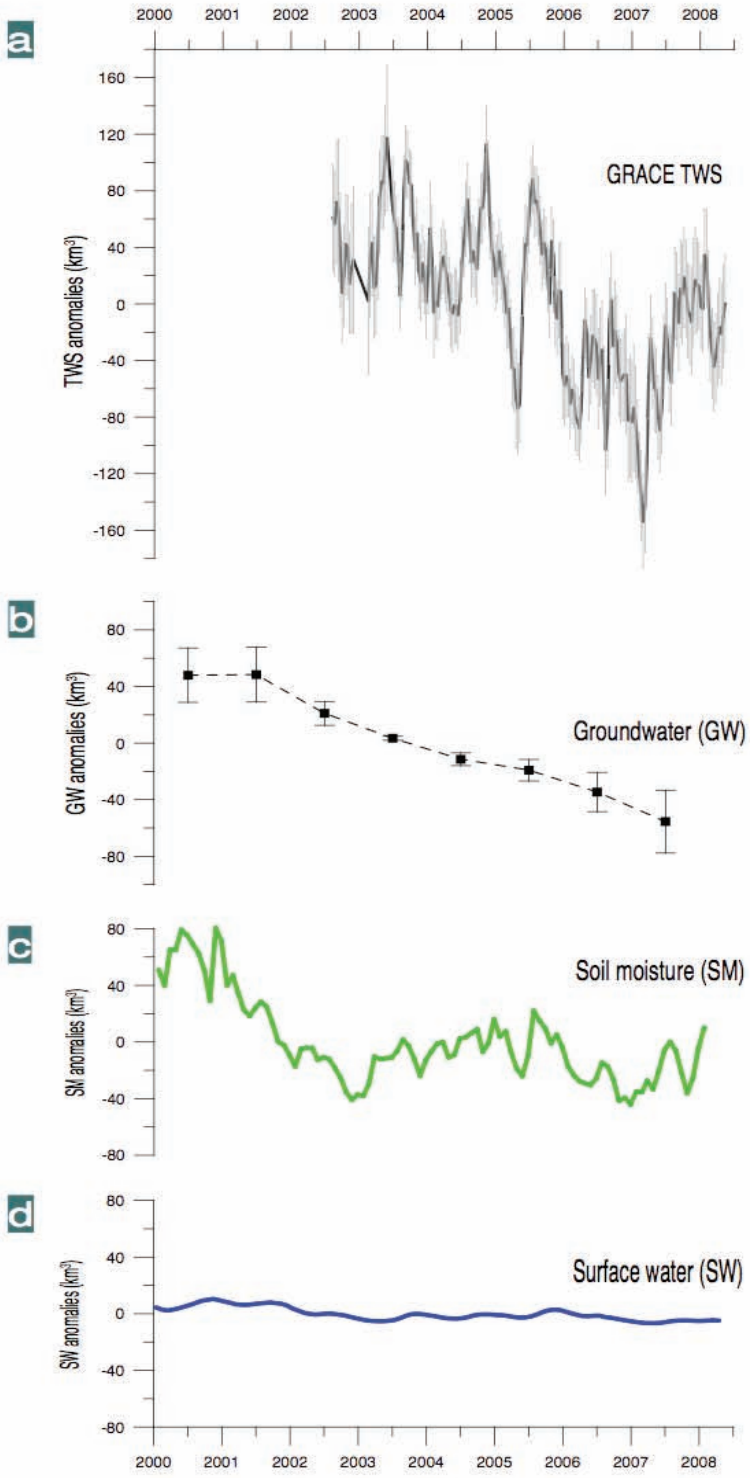

Figure 1. Change in water storage of the Murray-Darling Basin as estimated from a) GRACE space gravity observations b) groundwater borehole measurements c) GLDAS soil moisture model d) lake, river and reservoir level estimates (*Leblanc et al.*, 2008)

A global dataset of frequency-dependent body-wave travel times: towards a global finite-frequency tomography of the Earth's mantle.

Christophe Zaroli[1], Eric Debayle[1] and Malcolm Sambridge[2]

[1] *Institut de Physique du Globe de Strasbourg, Ecole et Observatoire des Sciences de la Terre, Centre National de la Recherche Scientifique and Université de Strasbourg, France*
[2] *Research School of Earth Sciences, Australian National University, Canberra, ACT 0200, Australia*

With the growth in the number of seismic stations, the increase in computational power and the development of new analysis tools that extract more information from seismograms, the resolution of global seismic tomographic models has improved significantly in the last 25 years. For example the lateral resolution of surface wave velocity and anisotropy models of the upper mantle has decreased from 5000 km (Woodhouse and Dziewonski (1984), Nataf et al., 1984) to about 1000 km in the most recent seismic models, allowing the anisotropic behaviours between continents to be distinguished (Debayle et al., 2005).

Finite-frequency theory (Dahlen et al. 2000) incorporates single scattering into the formulation, and has been developed for long period body-waves. It is known that long period body waves are sensitive to the wave speed over a broad 3D volume surrounding the geometric ray. The corresponding 3D kernels have become known as "banana-doughnut" (BD) kernels because of their shape (See Figure 1).

The actual benefit of a finite-frequency theory remains controversial (Sieminski et al., 2004, de Hoop and van der Hilst, 2005a; Dahlen and Nolet, 2005; de Hoop and van der Hilst, 2005b; Montelli et al., 2006a; van der Hilst and de Hoop, 2006; Boschi et al., 2006). These authors suggest that the effect of the improved theory could be smaller than that of practical considerations such as the level of damping, the weighting of different data sets and the choice of data fit, especially when considering the relatively small amount of finite-frequency data (~90 000 long period body waves) compared with the large number (~1 500 000) of travel time data analysed with ray theory (e.g. van der Hilst et al. 2005).

Other limitations come from the travel-time datasets. Until now, most finite-frequency studies have been made using long period travel-times measured for ray theory applications. These travel times are not well suited for an inversion using Dahlen et al. (2000) kernels which are designed for travel-times measured by cross-correlation of a broadband seismic phase with a synthetic. To take a full advantage of Dahlen (2000) finite frequency theory, it is necessary to keep control of the frequency content of the waveform associated with a given travel-time, so that it can be associated with a finite-frequency kernel carrying the same frequency information. Secondly, by measuring finite frequency travel-times over different frequency ranges, it is possible to extract more information from each seismic phase. According to Dahlen et al., (2000), the width of a given BD kernel increases with the dominant period of the corresponding body waveform. Therefore, by measuring the travel-time of a seismic phase at several frequencies, there is a potential for increasing the amount of independent information in the inverse problem, as at each frequency, the waveform "senses" a different weighted average of the structure, through a different Banana Doughnut kernel.

If the debate about the real benefit of finite-frequency is still active, we believe that significant progress can be achieved by building a new dataset of massive long period body phases travel-times measured over a broad frequency range. To date, there is no such global database of frequency-dependent body-wave travel-time measurements.

A first result from this project is an automated approach for measuring long period body wave travel times at multiple frequencies. The approach has been designed to built a dataset for global finite-frequency SH or SV-wave tomography, but can be easily

extended to P-wave tomography. The travel times are computed by cross correlation and are fully compatible with the kernels provided by Dahlen, (2000). Currently, our approach allows us to measure in an automated way S, ScS, SS travel-times on SH components in different frequency-bands covering the period range 6-68 s. Frequency dependent crustal and attenuation corrections for WKBJ synthetics can also be incorporated.

The figures show the finite frequency kernels together with maps showing the coverage of the new data set. The automated procedure has been used to build a global dataset of finite frequency travel times, using 30 years of data from IRIS and GEOSCOPE networks. This will be the basis of future work on mantle imaging.

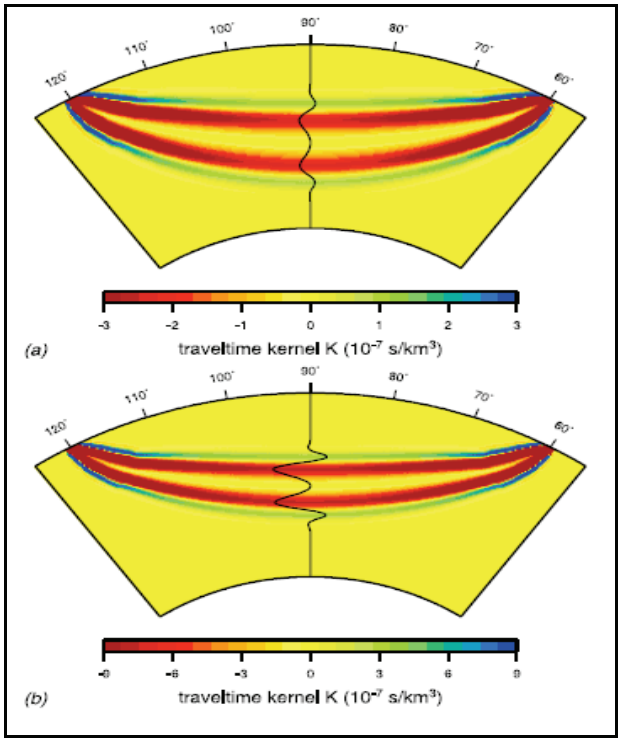

Figure 1. Fréchet Kernels at 20s period for a) P wave and b) S wave.

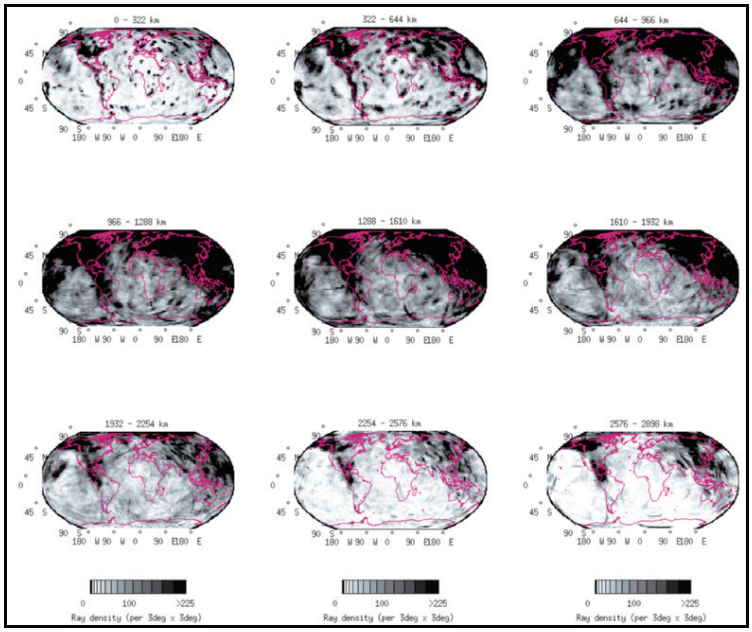

Figure 2. Ray density maps at different depth of the new dataset.

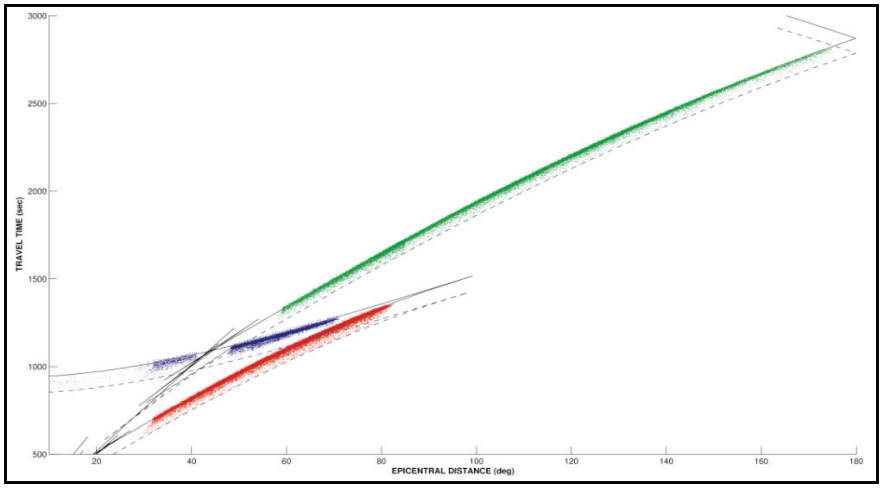

Figure 3. Arrival times of S, ScS and SS phases retained in the final dataset.

Australian trials of the French Transportable Laser Ranging System (FTLRS)

Jason Zhang[1] Chris Watson[2], Francis Pierron[3],
Richard Coleman[2,4,5], Paul Tregoning[1]

[1] *Research School of Earth Sciences, Australian National University, Canberra, ACT*
[2] *University of Tasmania, Hobart, Tasmania*
[3] *Observatoire de la Côte d'Azur, Grasse, France*
[4] *Centre for Australian Weather and Climate Research (CAWCR), Hobart, Tasmania*
[5] *Antarctic Climate and Ecosystems Cooperative Research Centre, Hobart, Tasmania*

The Bass Strait in-situ calibration site has been used in the calibration and validation of satellite altimeter data since the launch of TOPEX/Poseidon in 1992. The primary focus at the site has been the estimation of absolute bias in altimeter derived sea surface height (SSH) using a combination of oceanographic moorings, GPS buoy deployments, coastal tide gauge and land based GPS data. As the sole site of its kind in the Southern Hemisphere, the Bass Strait site provides important input into understanding various error sources in satellite altimetery.

With an objective of improving our understanding of any geographically correlated orbit errors present in altimeter orbits, the Bass Strait site was selected as part of a collaborative French/Australian project to trial the French Transportable Laser Ranging System (FTLRS). The FTLRS was operated in Tasmania over a five month period between 1 December 2007 to 17 April 2008 jointly by French and Australian staff. The FTLRS and temporary GPS were located within the city of Burnie beneath Jason-1 descending pass 088, several kilometers from the Burnie tide gauge/CGPS and inland CGPS sites.

During the Tasmanian FTLRS campaign, a total of 673overflights from 12 different satellites were observed and a total of 9200 normal points have been computed In this poster, we present initial results from our analysis of FTLRS data. Whilst building SLR capacity in Australia, we seek to highlight the influence of an additional tracking station in this area of the Southern Hemisphere. Our FTLRS based orbits will assist in quantifying regional or geographically correlated orbit errors present in satellite altimeter data, allowing any bias in altimetry derived SSH in this region to be estimated.

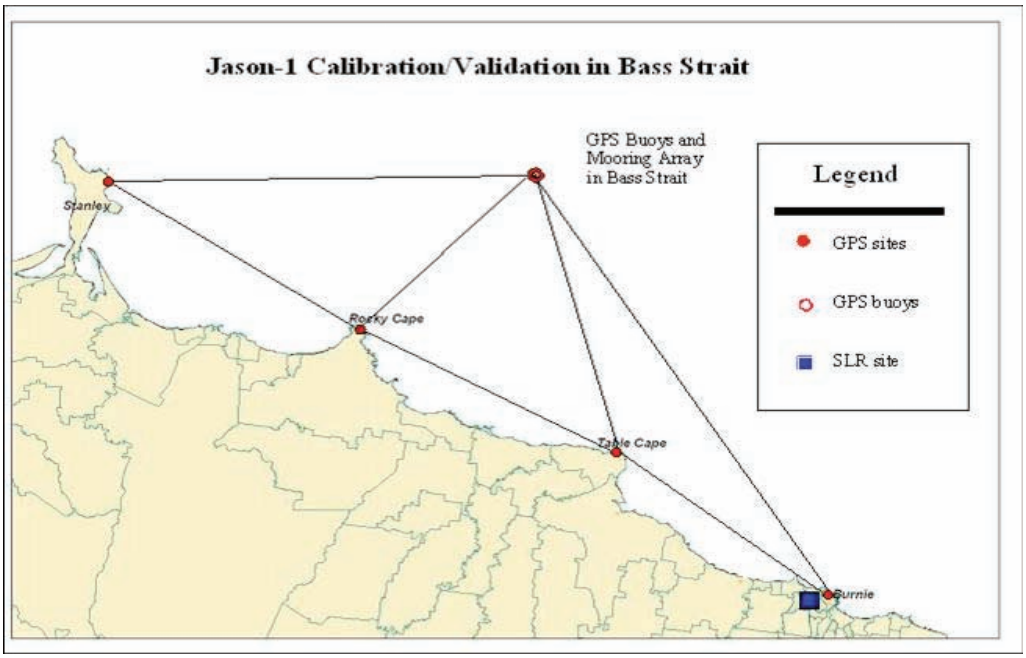

Figure 2. Sketch of the Bass Straite In-Situ Calibration Site

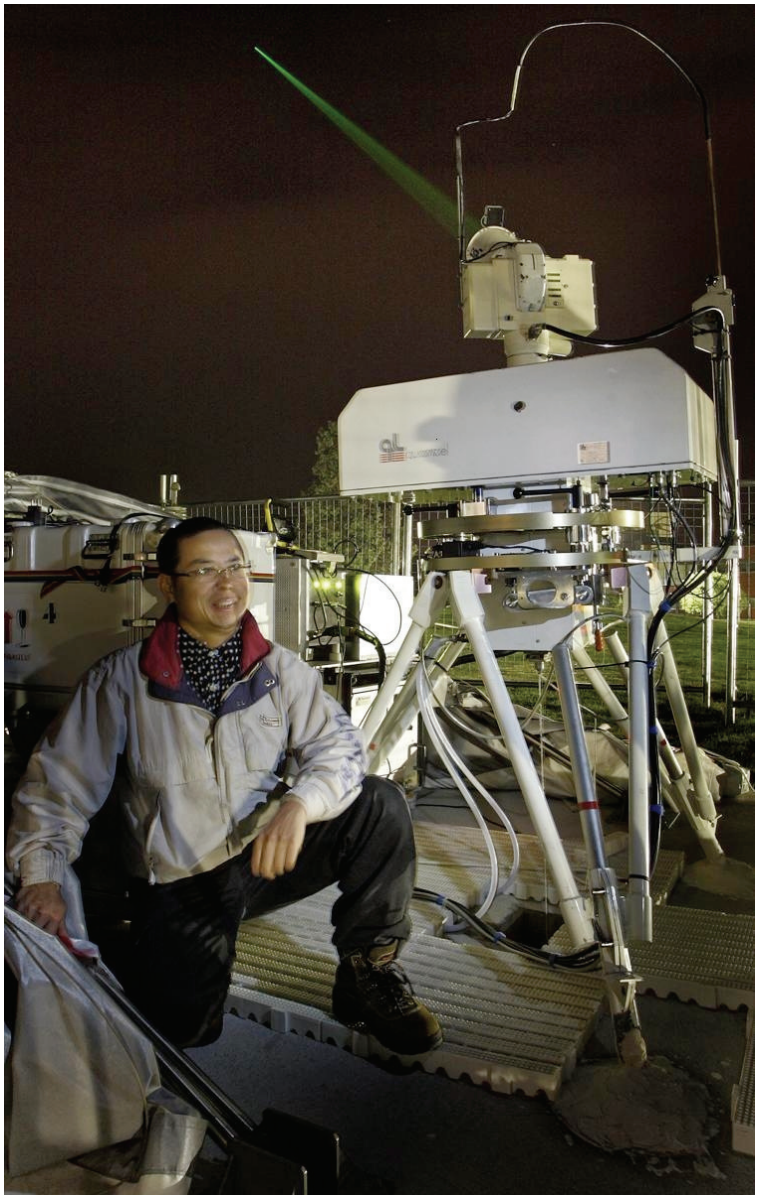

Figure 1. *FTLRS in night operation*

Integrated Ocean Drilling Program

Australia has joined the Integrated Ocean Drilling Program (www.iodp.org), which is the world's largest multinational geoscience program and includes almost all OECD countries. IODP carries out deep scientific coring around the world's oceans, and provides 'ground truthing' of global geoscientific theories that are often based largely on remote sensing techniques.

New technologies and concepts in geoscience are continuously being developed through IODP. IODP is a long-term program and membership will have important scientific outcomes for us. Australia was a highly successful member of IODP's precursor, the Ocean Drilling Program (ODP). The Research School of Earth Sciences hosts the Australian IODP Office (www.iodp.org.au) along with other National Facilities - AuScope and ANSIR.

Submarine plateaus off northeast Australia

Kinta Hoffmann[1], Neville Exon[2], Patrick Quilty[3], and Claire Findlay[4],

[1]Geological Survey of Queensland, 80 Meiers Rd, Indooroopilly, QLD 4068
[2]Research School of Earth Sciences, Australian National University, Canberra, ACT 0200.
[3]School of Earth Sciences, University of Tasmania, Hobart, TAS 7000;
[4]Canberra, ACT.

Mellish Rise and adjacent deep-water plateaus of northeast Australia: new evidence for continental basement from Cenozoic micropalaeontology and sedimentary geology. *In*: Blevin, J.E., Bradshaw, B.E. and Uruski, C. (Eds), *Eastern Australasian Basins Symposium III*, Petroleum Exploration Society of Australia, Special Publication, 317-323.

Widespread rifting and seafloor spreading replaced the compressional regime off eastern Australia from around 120Ma, in the Early Cretaceous. The magnetic anomalies in the newly formed oceanic crust indicate that spreading commenced in the south and migrated progressively northwards carving off large ribbon-like microcontinents. Gaina et al (1998) postulated from geophysical data that the Mellish Rise and other seafloor highs off northeast Australia might be microcontinental fragments but no geological evidence was available.

Two scientific cruises using R.V. *Southern Surveyor* (GA270 and GA274) obtained core and dredge samples, and seismic and bathymetric data, from the Kenn Plateau and Mellish Rise, and the Louisiade Plateau. A diverse suite of sedimentary rocks includes shallow and deep-water carbonates, siliciclastics, volcanogenic facies, deep-water siliceous lithologies, and some seawater precipitates. The carbonates have provided age dates from foraminiferal and calcareous nannofossil assemblages, which range in age from Paleocene to present day, and prevailing climate and palaeo-water have also been determined.

Some carbonates and siliciclastics contain quartz and mica grains and metamorphic lithic fragments indicating a continental provenance. Dredge sites located along the recently acquired seismic profiles indicate that the continental-derived lithologies correspond to isostatically buoyant basement blocks that have a uniform chaotic seismic reflection. The elevation of the basement blocks relative to oceanic crust in the intervening deep basins, coupled with the petrological properties of the grains and lithics, suggest that continental basement underlies the seafloor highs. The best evidence comes from a Late Eocene sandy glauconitic calcarenite on the southern Mellish Rise, which incorporates angular quartz grains. The age implies that deposition occurred subsequent to drifting and hence reflects a local source rather than contamination by terrestrial material from the continental shelf.

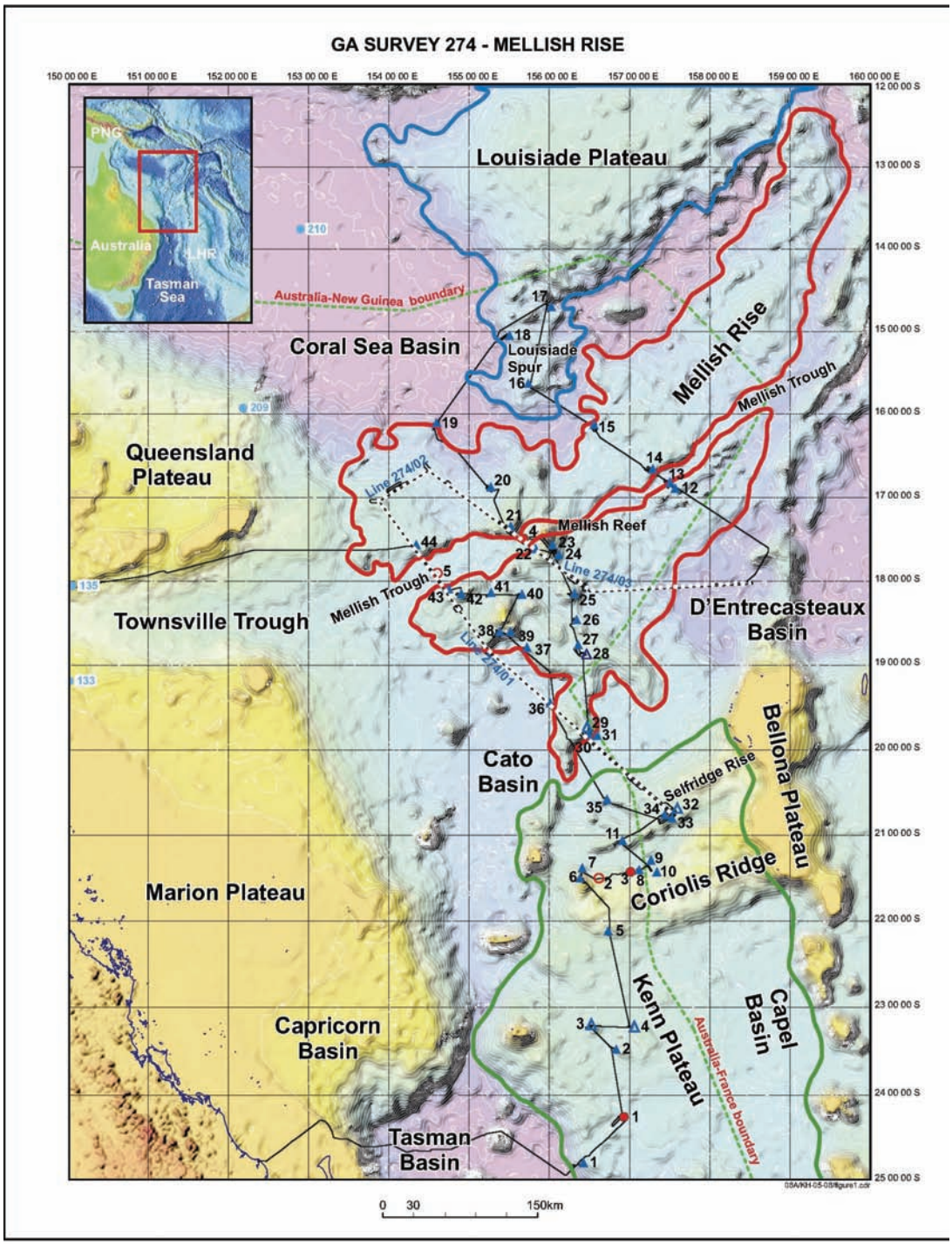

Figure 1. *Bathymetric map of offshore northeast Australia showing the Kenn Plateau, Mellish Rise (north and south segments), and Louisiade Plateau with the ship's tracks, dredge and gravity core sites from GA274 cruise. Legend: dredge sites (blue triangles), gravity core sites (red circles), ship's track (solid black line), seismic lines (dashed black line), and ocean drilling sites (numbered blue circles).*

PRISE

PRISE operates as a self-funded research group within the Research School of Earth Sciences, providing commercial and collaborative access to the Research School's specialised equipment and expertise in areas of geochronology, geochemistry and petrology. PRISE scientists also undertake their own research projects and supervise postgraduate students, both within the Research School and internationally.

All PRISE staff members are actively involved in wide-ranging collaborative research projects with academic colleagues throughout the world, as well as providing research and analytical skills to industry and Government agencies on a commercial basis. During 2008 PRISE hosted twenty-nine local and international visitors, most of whom undertook collaborative projects using the SHRIMP, Laser ablation- and solution ICPMS, electron microprobe and TIMS analytical facilities. PRISE staff also participated in a number of field-orientated studies in Australia, Africa, South America and Europe.

Some areas of current research include:

- Investigations of the origins of pyroxenite bodies in peridotite massifs of the Western Gneiss Region, Norway (PhD student A. Rosenthal)
- High pressure experimental investigations of kimberlite and carbonatite petrogenesis (PhD student K. Kiseeva)
- Impactor fluxes in the inner solar system from the ages and compositions of lunar glasses (PhD student S. Hui)
- Multi-isotopic and trace element zircon studies to constrain magmatic evolution of plate margins and continental reconstructions; combined U-Th-Pb, Lu-Hf, Ti geothermometry, trace and REE chemistry, and oxygen isotope studies.
- Development of in situ sulphur isotope analytical protocols for the SHRIMP
- Use of sulphur isotopes to aid in understanding the origin and conditions of formation of metal sulphides
- Chronology of the Archaean-Proterozoic transition and the rise of oxygen in the atmosphere
- Geological Connection between West Antarctica and Patagonia since the late Paleozoic: Tectonism, Paleogeography, Biogeography and Paleoclimate
- Placing realistic constraints on the timing of world-wide Neoproterozoic glacial events: a critical examination of the "Snowball Earth" hypothesis
- Bioarchaeology in early Cambodian populations and in situ oxygen and strontium analysis of human teeth
- Development of new mineralogical tools for diamond exploration
- Ages of granites and related mineralisation in NSW.
- Origin and evolution of plume magmas and Hawaiian volcanoes.
- Hydrochemistry of groundwater resources in the Sydney basin and Murrumbidgee Irrigation area of NSW.

Further developments in the *in situ* analysis of sulphur isotopes using SHRIMP II

Richard A. Armstrong, Peter Holden and Ian S. Williams

Research School of Earth Sciences, Australian National University, Canberra, ACT 0200, Australia

For several years the successful measurement of sulphur isotope ratios on the SHRIMP has been frustrated by the lack of suitable standards and the difficulty in producing reproducible, accurate and precise data through instrumental problems and idiosyncrasies. Establishing suitable standards is a difficult and time-consuming process, as internationally available material might be uniform on the bulk scales they were measured at, but might show some variation in composition at the 20 μm scale commonly measured on the SHRIMP. For analyses of sulphides, the early work by Eldridge et al. (1988, 1989) on SHRIMP I showed that matrix effects require the standards to be matched to the composition of the unknown sulphides. We have spent some considerable time in analysing available sulphide standards (e.g. those described by Crowe and Vaughan, 1996) and have managed to overcome many instrumental problems, enabling us to report consistent $d^{34}S/^{32}S$ isotope measurements with external precisions of ~2‰ in standards in a variety of sulphides. Figure 1 shows results from two different composition pyrites (Balmat and Ruttan) run in a single session on SHRIMP II. These results are in excellent agreement with the reported values for these standards.

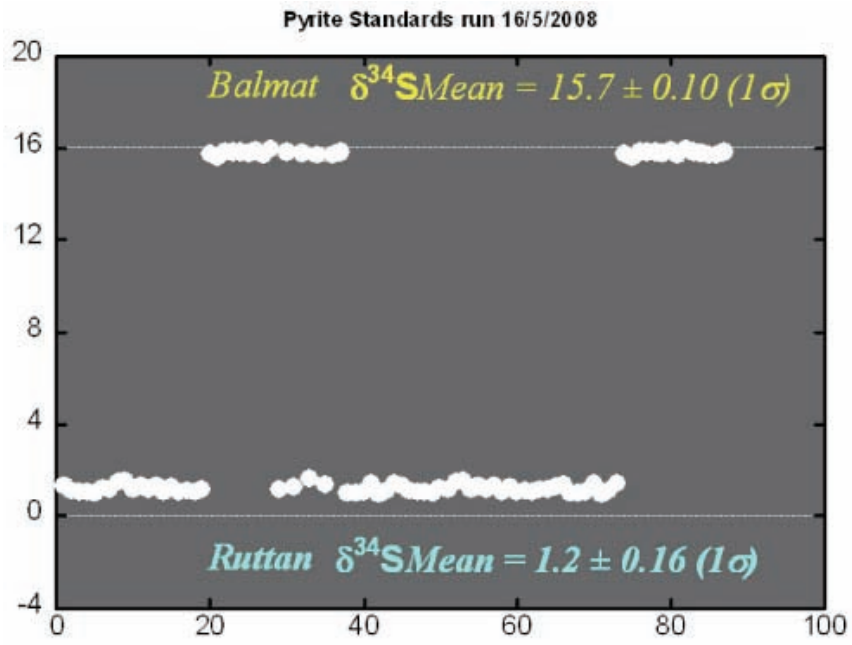

Figure 1. *Sulphur isotope compositions of two pyrite standards as measured on SHRIMP II during a single analytical session.*

Eldrige et al. (1988, 1989) were also able to show that isotope variations on the SHRIMP scale can be large and not necessarily comparable to bulk analyses in some ore deposits. Our investigations of a number of ore deposits from around the world have confirmed this finding. Detailed small-scale analyses within and across various types of pyrite grains from the Witwatersrand deposit show ranges up to 19‰ from core to rim. Many of these traverses show characteristic rhythmic saw-toothed changes in composition, suggesting a repeated process of formation in these particular concentric, structured grains. Figure 2 illustrates both the structure and isotope variation across a concentric Archaean pyrite grain from the Witwatersand sequence.

The successful development of this analytical capability on SHRIMP II will be extended to other more exotic applications, with an emphasis on establishing a routine for the added analysis of ^{33}S. This currently requires modifications to the mulitcollector configuration, but should be possible in the near future. This will extend our research capabilities, enabling us to assess and measure complex mass-dependent and mass-independent fractionation patterns relating to the early development of the Earth's atmosphere, as described by Farquhar and Wing, 2005.

Crowe, D.E. , Vaughn, R.G. (1996). Characterization and use of isotopically homogeneous standards of is situ laser microprobe analysis of $^{34}S/^{32}S$ ratios. Amercian Mineralogist, **81**: 187-193.

Eldridge, CS, Compston, W, Williams, IS, Both, RA, Walshe, JL, Ohmoto, H. (1988) Sulfur-isotope variability in sediment-hosted massive sulphide deposits as determined using the ion microprobe SHRIMP: 1. An example from the Rammelsberg orebody. Economic geology **83:** 443-449.

Eldridge, CS, Compston, W, Williams, IS, Walshe, JL, (1989) Sulfur isotope analyses on the SHRIMP ion microprobe. U.S. Geological Survey Bulletin **1890**: 163-174.

Farquhar, J, Wing, BA (2005) The terrestrial record of stable sulphur isotopes: a review of the implications for evolution of Earth's sulphur cycle. In: McDonald, I, Boyce, AJ, Butler, JB, Herrington, RJ, Poyla, DA (eds): Mineral Deposits and earth Evolution, Geological Society, London, Special Publication 248: 167-177.

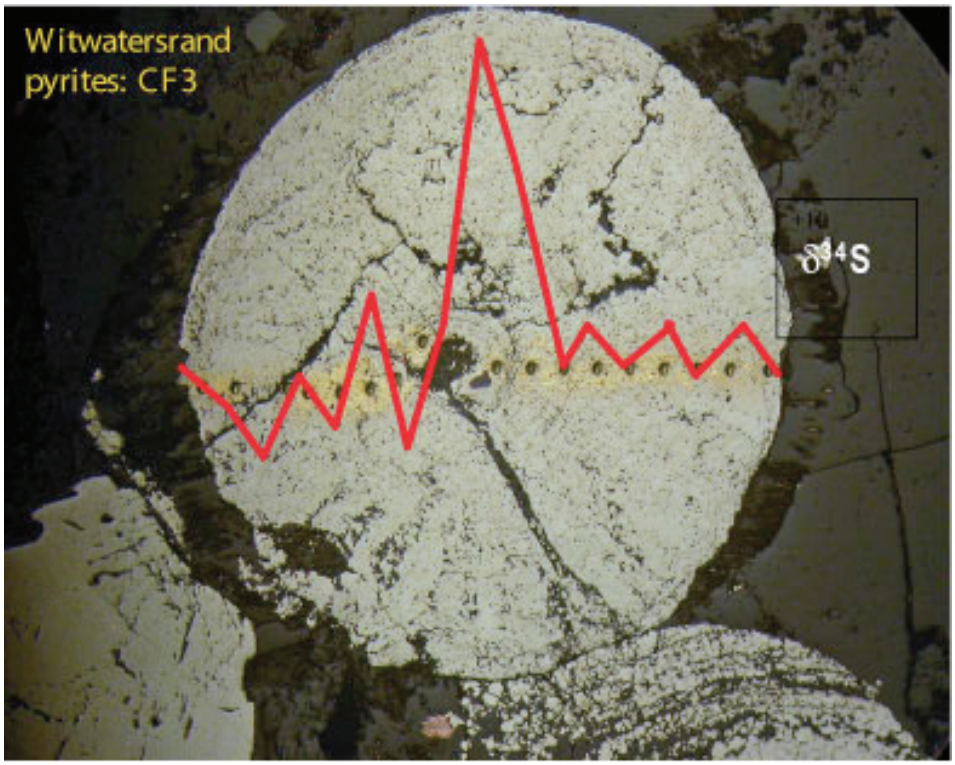

Figure 2. *A concentrically-grown pyrite grain from the Witwatersrand gold deposit, South Africa, showing a series of SHRIMP analytical spots across the grain. The SHRIMP spots are approximately 20 mm in diameter. Sulphur isotope compositions were measured across the growth bands and show a large range in values from +10‰ in the centre to ~-7‰ in one of the bands near the margin.*

Geochemistry and Analysis of Apollo 16 Lunar Impact Glasses

Simeon S. M. Hui[1] and Marc D. Norman[1]

[1] *Research School of Earth Sciences, Australian National University, Canberra, ACT 0200, Australia*

Lunar impact spherules are micron to centimetre sized glass particles formed during impact events where shock induced melting of the lunar regolith and impactor produce melt splashes that can be deposited locally or be ejected far beyond the point of impact. These particles can be found within the lunar soil and in microbreccias and are a medium from which we can study lunar chemistry and impact history.

We have separated over 900 lunar spherules, most of them likely to be from impact origins, from the Apollo 16 fines, 66031. Using new mounting and analysis techniques we aim to obtain major and trace element compositions while preserving the maximum amount of sample for ^{39}Ar-^{40}Ar dating on singular particles. Preliminary tests were conducted using shards of crushed USGS standard TB-1G which represents extremes in irregularity. Using wavelength-dispersive electron microscopy techniques to obtain major element compositions of the TB-1G shards, we are able to achieve errors of less than 5% relative.

Following this success, petrographic descriptions and dimensions were obtained for 272 lunar glasses greater than 75µm in diameter along with major element compositions. There are broad positive correlations between MgO vs. FeO and negative correlations between Al_2O_3 and CaO vs. FeO. The majority of the impact spherules have chemistry consistent with derivation of the glasses from the local regolith.

Most impact spherules are irregular and splash-like in shape, often with a coat of adhering grains while highly spherical forms are rarer but have cleaner surfaces. We also find that irregular shapes tend to be more internally heterogeneous in major element composition than the highly spherical forms. This may indicate that highly spherical forms cooled before contacting the lunar surface suggesting a more distant origin. However, rare exotic compositions are more likely to be irregularly shaped which might be due to fragmentation of the glass.

Results of this study were presented at the 8th Australian Space Science Conference, Canberra, Australia, 29th September-1st October 2008.

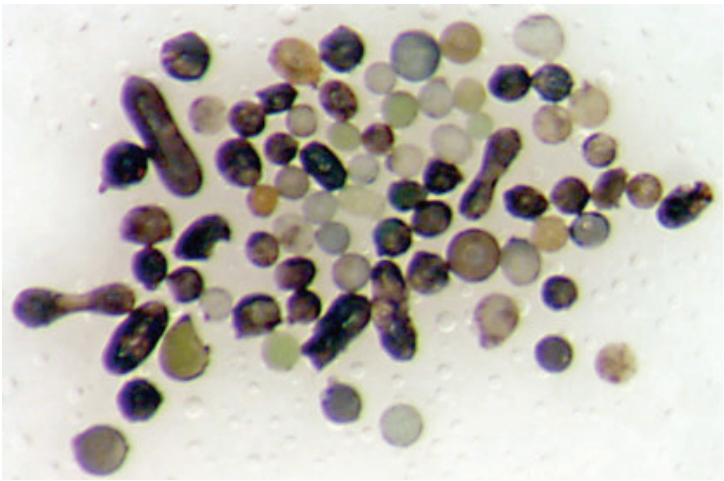

Figure 1.

The role of carbonated eclogite in kimberlite and carbonatite petrogenesis

Ekaterina S. Kiseeva[1], Gregory M. Yaxley[1] and Vadim S. Kamenetsky[2]

[1]Research School of Earth Sciences, The Australian National University, ACT 0200, Australia,
[2]CODES and School of Earth Sciences, University of Tasmania, Hobart, TAS, Australia

The exotic and rare rock types – kimberlites and carbonatites are undoubtedly of mantle origin and are sometimes considered to be genetically related, but the compositions of their parental melts and melting conditions are still widely debated. A component in the source of kimberlitic and carbonatitic melts may be carbonate-bearing eclogite, reflecting heterogeneity in the mantle derived from recycling during subduction of oceanic crust.

The aim of this study is to use high pressure experimental petrology to investigate the behaviour of carbonate-bearing eclogite in upper-mantle conditions and to test its possible involvement in the mantle sources of kimberlite and related magmas. The first part of our investigation aims to locate the solidus positions and partial melt compositions as functions of bulk compositional parameters such as SiO_2 and CO_2 contents, Ca/Mg, Na_2O/CO_2, etc.

Altered oceanic crust typically contains a few % calcite, formed during hydrothermal alteration. The starting experimental composition (GA1) is an average "altered" MORB composition. Ten % $CaCO_3$ was added to GA1 in the experiments to facilitate detection of carbonate in the runs. The second mix, Volga, is GA1 minus 6.5% SiO_2, to which 10% $CaCO_3$ was also added (Volga+10%cc). Experiments were run at 3.5 to 5.5 GPa and 1000-1400°C in piston-cylinder presses at RSES. The run results were analyzed with a HITACHI 4300 SE/N FESEM and JEOL 6400 at the ANU Electron Microscopy Unit, using EDS detectors for quantitative analysis of mineral phases.

Experimental runs after quenching contained the three main phases: garnet, clinopyroxene and melt (Fig. 1, A, B), and sometimes various accessory phases such as K-feldspar, rutile, coesite and carbonate.

Several types of melt were observed in our experiments. A large fraction (>30%) of silicate melt is present in higher temperature runs (T1250 °C). In these cases silicate melt segregated to a pool at one end of the capsule (Fig. 1, A). The totals are about 88-92%, suggesting 8-12% CO_2 dissolved in the melt. At T = 1150 to 1250 °C and 3.5 GPa in GA1+10%cc and 1100 to 1200 °C in Volga+10%cc experiments tiny particles of incompatible-element rich material (ie K-rich and P-rich) are distributed throughout much of the graphite capsules (Fig. 1, C, D) which was often vesiculated or fragmented, indicating decarbonation of a silicate-carbonate melt during quenching. Capsule piercing of some of these runs into a gas chromatograph detected significant CO_2-fluid. With decreasing temperatures at high pressures (4.5 and 5 GPa) carbonate-silicate melts formed small pools of melt within the graphite spheres. Interestingly, at near-solidus conditions in all the investigated pressure intervals two immiscible carbonate and silicate melts are formed. Potassium usually fractionates into the silicate melt, while phosphorous prefers the carbonate.

In sub-solidus conditions in GA1 + 10%cc 1050 °C and 3.5 GPa experiment apatite (Ap), potassium feldspar (K-Fspar), rutile (Ru) and carbonate were observed. At higher pressures potassium feldspar as well as apatite is no more stable and K and P presumably fractionate into the fluid. GA1 + 10%cc solidus at 3.5 GPa is at about 1075 °C, Volga + 10%cc solidus is at least 50 °C lower at all the studied pressures.

Carbonate-rich melts formed from a low degree of eclogite melting will infiltrate neighbouring peridotite, resulting in metasomatism and refertilization. Our next aim is

to investigate how these melts would interact with peridotite and compare the outcomes with melt compositions that may be parental to kimberlites.

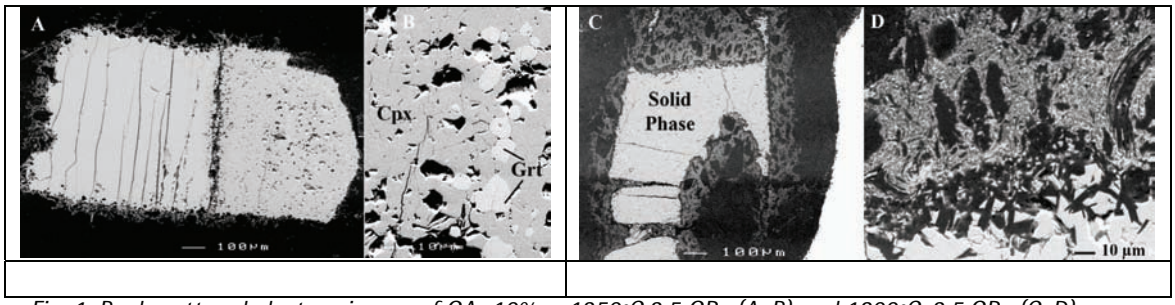

*Fig. 1. Backscattered electron image of GA+10%cc 1350°C 3.5 GPa (A, B) and 1200°C, 3.5 GPa (C, D) run material. **A**. Melt (left) and solid phase (right). **B**. Magnified view of part of the solid material in **A**, showing clinopyroxene (Cpx) and garnet (Grt) crystals. **C**. Solid phases represented by Grt and Cpx crystals. **D**. Magnified area of melt distributed within the capsule. Melt is in contact with residue.*

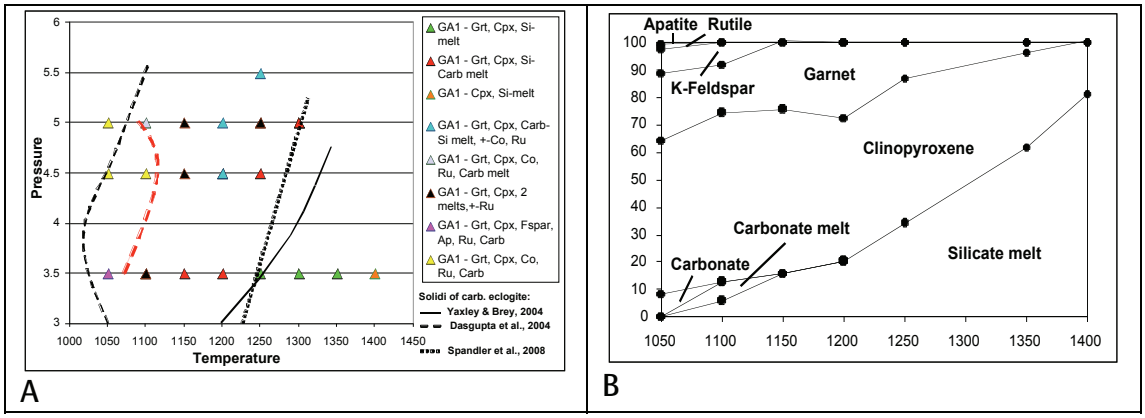

*Fig. 2. **A.** Results of experiments with GA1+10%cc. Approximate solidus is shown by the red dashed line. **B.** Phase proportions for GA1+10%cc at 3.5 GPa pressure. The sole liquidus phase is Cpx.*

The Lunar Cataclysm: Reality of Mythconception?

Marc Norman[1] and Robert Duncan[2]

[1] *Planetary Science Institute, Research School of Earth Sciences, Australian National University, Canberra, ACT 0200, Australia*
[3] *College of Oceanic and Atmospheric Sciences, Oregon State University, Corvallis, OR 97331 USA*

Understanding the early impact history of the terrestrial planets is a priority goal for solar system exploration. More specifically, ascertaining whether or not the Earth and Moon experienced a cataclysmic Late Heavy Bombardment of impacting planetesimals ~3.9 billion years ago remains an open question with significant implications for the dynamical history of the Solar System, environmental conditions on the early Earth, and the development of crustal structures on Mars.

The idea of a Late Heavy Bombardment is controversial. Lunar impact melt breccias have crystallisation ages that cluster between 3.8 and 4.0 Ga (Norman et al., 2006; Figure 1), corresponding to an episode of intense crustal metamorphism defined by U-Pb isotopic compositions of lunar anorthosites. The late cataclysm interpretation invokes a spike in the mass flux to the Earth and Moon at precisely the time when the Earth's oldest preserved continental crust was forming and life was emerging. Alternatively the age distribution of lunar impact melts may reflect a steadily declining flux of impactors, with the older record being erased by younger events.

Relating lunar surface deposits to specific basins is critical for assessing the reality (or otherwise) of the late cataclysm. An excellent example is the Descartes Formation, a regional unit of fragmental impact breccia that was sampled by the Apollo 16 mission in 1972. Taking advantage of recent improvements in mass spectrometry we measured high-precision ^{39}Ar-^{40}Ar ages and trace element composition of anorthositic clasts from two of the Descartes breccias. These measurements show that the breccias were deposited 3.866 $\pm$ 0.009 billion years, most likely as ejecta from the massive Imbrium basin, located some 1000 km to the NW of the Apollo 16 landing site (Fig. 2). The trace element compositions support this interpretation.

The significance of this discovery is that Imbrium is one of the youngest impact basins on the Moon. Previous interpretations linked the Descartes breccias to the older Nectaris basin, strongly supporting the idea of a late cataclysm. Our study pulls the pin on the cataclysm hypothesis by showing that age of Nectaris is effectively unconstrained by the sample data. Absolute ages of older basins will be necessary to define the pre-3.9 Ga impact history of the Earth and Moon.

Norman MD, Duncan RA, and Huard JJ (2006) Identifying impact events within the lunar cataclysm from 40Ar-39Ar ages and compositions of Apollo 16 impact melt rocks. *Geochimica et Cosmochimica Acta* **70**: 6032-6049.

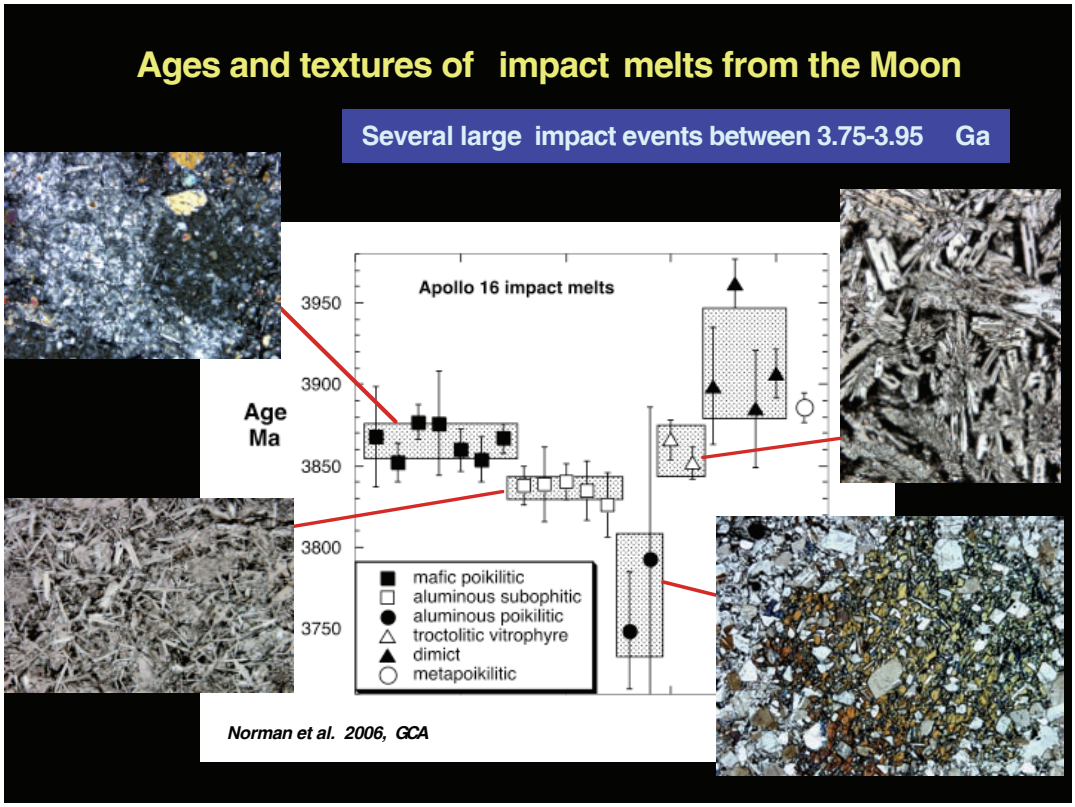

Figure 1.

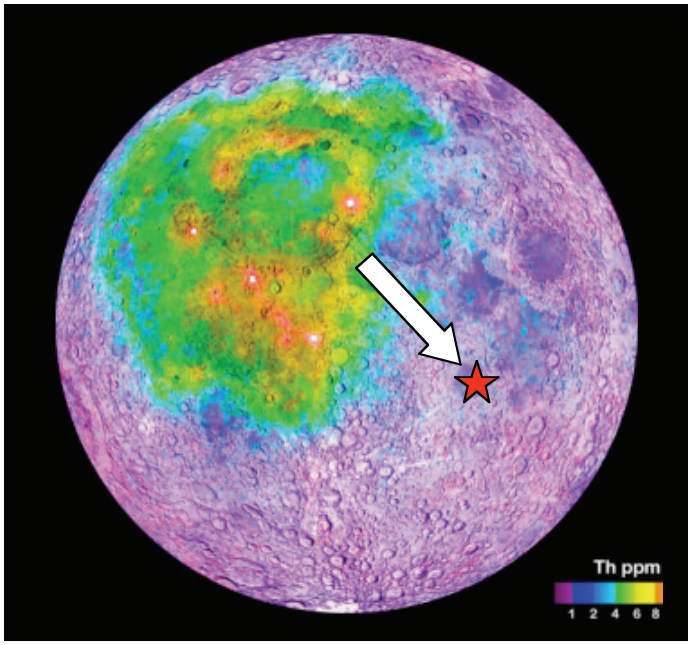

Figure 2.

Melting of residual eclogites with variable proportions of quartz/coesite

Anja Rosenthal[1], Gregory M. Yaxley[1], David H. Green[1], Jörg Hermann[1] and Carl S. Spandler[2]

[1] *Research School of Earth Sciences, Australian National University, Canberra, ACT 0200, Australia*
[2] *School of Earth and Environmental Sciences, James Cook University, Townsville, Australia*

Eclogite and pyroxenite layers and veins within the peridotitic mantle may be important in genesis of many magmas. Understanding high pressure melting of residual eclogites with varying amounts of quartz/coesite (qz/co) will improve understanding of the melting behaviour of heterogeneous mantle assemblages.

We are investigating the phase and melting behaviour of a residual eclogite composition, which crystallizes garnet (grt) + clinopyroxene (cpx) at 3.0 & 4.0 GPa with no qz/co (REC). The melting behaviour of REC reveals the anhydrous solidus of a coesite-free eclogite.

The subsolidus phases of REC are garnet (grt) and clinopyroxene (cpx) at 3.0 & 4.0 GPa. The solidus is at 1325±25°C at 3.0 GPa, and at 1475°C±25°C at 4.0 GPa. Melt compositions and proportions with cpx > grt are controlled by grt-cpx cotectics. At 3.0 GPa, cpx/grt ratios decrease with increasing % melting. At 4.0 GPa, cpx/grt ratios are lower at a given % melting than at 3.0 GPa.

We are also studying eutectic-like melting in coesite-bearing eclogites with varying proportions of qz/co. REC10 and REC20 are identical to REC, but have 10% and 20% higher SiO_2 contents, respectively.

Both REC10 & 20 crystallise sub-solidus as grt + cpx + qz/co at 3.0 GPa. The solidi of both are similar at 3.0 GPa, at 1275±25°C. Low-% melting (<20%) is eutectic-like until qz/co melts out. Like REC, grt-cpx cotectics control high degree melting for all compositions, with cpx abundance always exceeding grt. However, for REC, the proportion of cpx always exceeds those in REC10 & 20, but the % melt is always lower than for REC10 & 20 at given temperature.

Melts vary with increasing % melting from andesitic to basaltic for REC & REC10, but from dacitic to basaltic-andesitic for REC20. At <25% melting, melt in REC has lower Mg# at given % melting than melt in REC10 & 20. The contrary is observed at higher % melting.

Garnet and cpx in REC have higher Mg# at a given % melting than grt and cpx in REC10 & 20. Towards higher % melting (>25% melting), variations in cpx Mg# diminish.

These variations of residual grt and cpx Mg# and melt Mg# are principally because melts from REC (qz/co-free) are more mafic at a given % melting.

These outcomes reveal the strong dependence of Mg# of residual mineral phases & melt on the presence or absence of qz/co in melting of eclogites.

Rosenthal A, Yaxley GM, Green DH, Hermann J, Spandler CS (2008) Melting of residual eclogites with variable proportions of quartz/coesite. Geochimica et Cosmochimica Acta 72 (12): A806

Advancing diamond exploration – novel techniques for the interpretation of diamond indicator minerals

Greg Yaxley[1], Hugh O'Neill[1] and Andrew Berry[2]

[1] Research School of Earth Sciences, Australian National University, Canberra, ACT 0200, Australia
[2]Department of Earth Science and Engineering, Imperial College, London, UK

We have developed new mineralogical tools applicable to the search for diamonds in Australia and overseas. This project was an ARC Linkage Project with industry partners BHP-Billiton, de Beers and Rio Tinto Exploration, through AMIRA International.

Techniques of high-pressure experimental petrology were used to develop mineral thermometers based on partitioning of Zn and Mn between upper mantle minerals. A new synchrotron-based technique for determining the redox state of the upper mantle is also being developed. These tools are being applied to fragments of garnet peridotite transported from the deep lithosphere to the surface by deeply-derived, occasionally diamondiferous kimberlite magmas. The resulting temperature and redox information will provide fundamental constraints on lithospheric diamond stability, and will be important in diamond exploration programs at a strategic level for targeting cratonic lithospheric domains more likely to contain high grades of diamonds, and at a more local level for targeting particular kimberlites for grade assessment by expensive bulk sampling techniques.

High-pressure experiments, focussing on Mn partitioning between garnet and olivine under upper mantle pressure-temperature conditions, have been completed. Algorithms for a Mn partitioning thermometers based on statistical fitting of experimental Mn-Mg and Fe-Mn exchange data between garnet and olivine have been determined. Experiments measuring Zn partitioning between Cr-spinel and olivine were also conducted and an olivine-spinel Zn-based thermometer was developed. These thermometers were applied to a comprehensive range of natural garnet ± spinel peridotite xenoliths samples from kimberlites erupted through the Kaapvaal and Slave Cratons. They performed extremely well in most cases, when compared with conventional thermometers (eg two-pyroxene thermometry etc).

The calibration of a synchrotron-based, X-ray Absorption Near Edge Structure Spectroscopy (XANES) method for determining Fe^{3+} contents of mantle garnets has proved unexpectedly challenging, despite a promising start (Figure 1), due to complexities relating to the compositional variations of natural garnets. We therefore adopted the alternative approach of obtaining the Fe^{3+} data by conventional Mössbauer Spectroscopy in collaboration with Prof Alan Woodland (Uni of Frankfurt) and by the newly developed electron microprobe based Flank Method in collaboration with Dr Heidi Höfer (Uni of Frankfurt). This will still allow determination of the oxygen-fugacity depth profiles through the lithospheric section represented by the garnet peridotite xenoliths supplied by the sponsor companies. These calculations are currently underway.

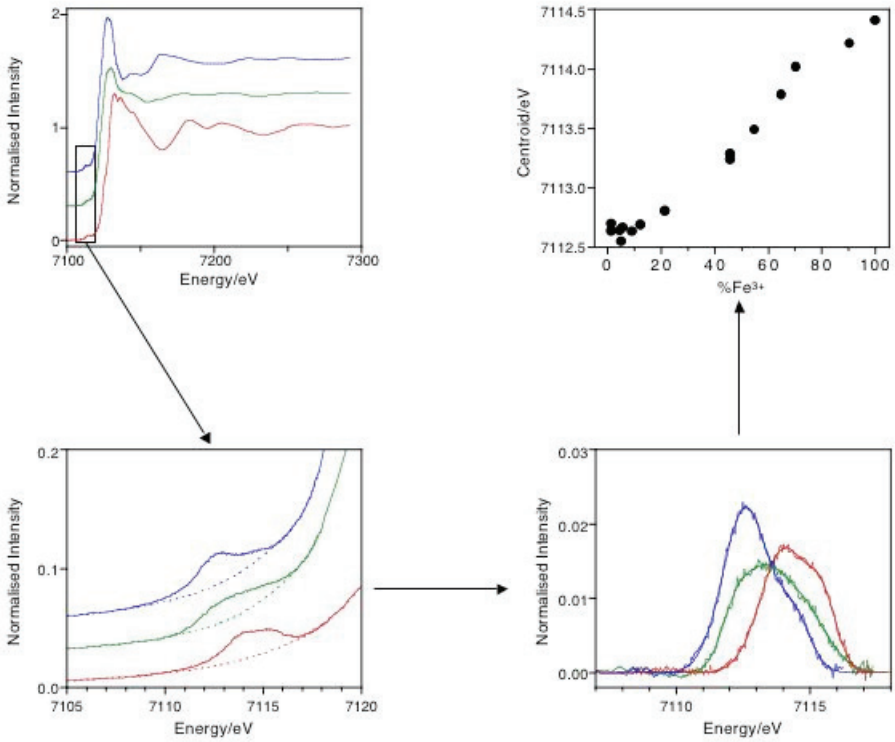

Figure 1*: Top left panel: Representative raw XANES spectra for synthetic garnets with Fe^{3+}/Fe = 1.0, 0.46 and 0.01 (red, green, blue respectively – compositions known from stoichiometry of skiaigite - almandine - andradite series, kindly supplied by Prof. Alan Woodland, University of Frankfurt) showing Fe K-edge and near edge structure in inset. Data was collected on the Australian National Beamline Facility, KEK, Tsukuba, Japan; Bottom left panel: Expanded view of inset in A, showing pre-edge spectral features with backgrounds (dashed lines); Bottom right panel: Pre-edge peaks after background subtraction and best fit from fitting a number of Gaussian components; Top right panel: Pre-edge peak centroids as a function of Fe3+/Fe, showing linear correlation, the basis of the calibration.*

Visiting Fellows' Research in 2008

The Electronic Geophysical Year 2007-2008

Charles E. Barton[1] , Daniel N. Baker[2] and William K. Peterson[2]

[1] Research School of Earth Sciences, Australian National University, Canberra, ACT 0200, Australia
[2] Laboratory for Atmospheric and Space Physics, University of Colorado, Boulder, USA

A worldwide revolution is taking place in the way we store, access, and analyze data and information. For the geosciences, our ability to gather data about the Earth and its space environment is unprecedented. Data acquisition rates of a petabytes per day no longer cause surprise and real-time access to data is becoming widespread. We can obtain data and services via the internet and grid systems from anywhere in the world, we can store and serve data with true interoperability, we can deal with real-time data applications, assimilate data into models, build virtual observatories, and more.

The challenges of organizing, providing ready access to, and using data effectively expand as data volumes, data complexity, and interoperability requirements increase. Meeting these challenges demands investment of time and resources as well as new skills. The onset of these demands has been rapid and novel.

The Electronic Geophysical Year of 2007–2008 (eGY – see www.egy.org) has served to build an international foundation for capitalizing on the new opportunities, The objective is to raise awareness of, and promote informatics capabilities in Earth and space science research; to advance towards the goal of a geoscience information commons in the spirit of the International Geophysical Year fifty years ago; to accelerate the development and adoption of virtual observatories and similar cyber-based systems for dealing with the large, diverse data and information requirements of modern research, and to promote better data management policies and practices. The formal themes of eGY are data access, data discovery, data release, data preservation & rescue, reducing the Digital Divide, and education and outreach.

The central outcome of eGY, which ends in December 2008, has been a heightened awareness among scientists and their professional bodies such as ICSU, IUGG, IUGS, COSPAR, AGU, GSA, and EGU, of the role of infomatics in science.

Microbialtes of Hamelin Pool and Lake Clifton, Western Australia

Robert Burne[1], Murray Batchelor[2]B, Gumpei Izuno[3] and Linda Moore[4]

[1] *Research School of Earth Sciences, Australian National University, Canberra, ACT 0200, Australia*
[2] *Department of Theoretical Physics, , Research School of Physical Sciences & Engineering and Mathematical Sciences Institute, Australian National University, Canberra, ACT 0200, Australia*
[3]*Coastal Environment Laboratory, Department of Socio-Cultural Environmental Studies, Graduate School of Frontier Sciences, The University of Tokyo, Japan*
[4]*Department of Microbiology, University of Western Australia*

The Hamelin Pool stromatolites show great morphological variation and extend from the high intertidal zone to subtidal depths of about 2 metres. Analysis of variation in stromatolite height shows that the tallest structures occur in the shallow subtidal zone, and that stromatolite relief decreases toward both the upper intertidal zone and toward the deeper subtidal limit of occurrence. Stromatolites at similar depths all have similar relief. The shape of the stromatolites also varies consistently depending on the position relative to present sea-level. Flat forms dominate the high intertidal zone, cauliflower-shaped stromatolites are found in the lower intertidal zone, columnar-shapes dominate in shallow subtidal environments and the deepest examples are all small domes.

Several authors have related variation in stromatolite shape to the occurrence of different types of microbial communities at different elevations. Burne (1991-1992) suggested that stromatolite growth was initiated in subtidal environments, and the present distribution is the result of falling sea levels and modification by intertidal microbial communities.

We have now (a) precisely surveyed the distribution of stromatolites in Hamelin Pool, and (b) modelled stromatolite growth variation by stipulating depth limits for stromatolite growth; suggested stromatolite growth rates; likely rate and direction of sea-level change; and period of time of that conditions for stromatolite growth have existed. We conclude that the morphological variation of stromatolites in Hamelin Pool can be accounted for by a model in which principal growth occurs only between mean low sea level and a depth of 2 metres, growth rate is 5 mm/decade, conditions suitable for stromatolite growth commenced 1,500 years ago, and relative sea level has fallen by 2 metres in the past 4000 years.

In 2007 research on Lake Clifton, a RAMSAR wetland south of Perth was resumed. Despite the recognised significanceand importance of Lake Clifton and its protection as part of a National Park (Burne and Moore 1987, Moore and Burne 1994), there has been very serious environmental degradation over the past 15 years. There appear to have been three major causes of environmental degradation –

Nutrient levels in the Lake - The naturally low nutrient levels of Lake Clifton were essential for the health of the thrombolite-based ecosystem. Despite the importance of monitoring of nutrient levels and limiting nutrient input to the Lake being emphasised by the Scientific Advisors in the Management Plan for the Lake, no monitoring appears to have been undertaken and nutrient levels appear to have risen considerably, possibly as a consequence of sub-division of the Lake's eastern border.

Introduction of Black Bream into Lake Clifton - The introduction of Black Bream into Lake Clifton by a Mandurah resident has had a devastating impact on the water quality, biota and microbial communities of the LakeResearch is being undertaken on the nature of possible remedial action that might be implemented.

Freshwater aquifer depletion - It appears that the construction of the Dawesville Cut involved pumping of the groundwater aquifer and discharge of the fresh groundwaters into the sea. This channel was constructed as an ecologically questionable engineering solution aimed at dealing with the environmental degradation of the Peel Harvey Estuary. The coincidence between the excavation of the Dawesville Cut and elevated salinity of Lake Clifton lake water suggests that this groundwater pumping severely impacted the fresh groundwater aquifer running along the eastern boundary of Yalgorup Lakes. This may account for the salinisation of the aquifer, the reduction in carbonate and fresh water input into Lake Clifton, and the death of stands of Tuart Trees along the eastern Boundary of the Lake System. This may therefore be the result of not properly assessing the environmental impact of Groundwater pumping.Possible remedial action is under consideration.

Burne R.V. (1991-92): Lilliput's Castles: Stromatolites of Hamelin Pool. *Landscope* V.**7** No.2 Summer ed. p. 34-40

Burne, R.V., Moore, L.S. (1987) Zircons from Syros, - Microbialites: Organosedimentary deposits of benthic microbial communities. *Palaios*, **2**:241 – 254

Moore, L.S., Burne, R.V. (1994):-The modern thrombolites of Lake Clifton, Western Australia. in Phanerozoic Stromatolites II .(Bertrand Sarfati, J., & Monty C. L., Editors), Kluwer Academic, Pages 3 - 29.

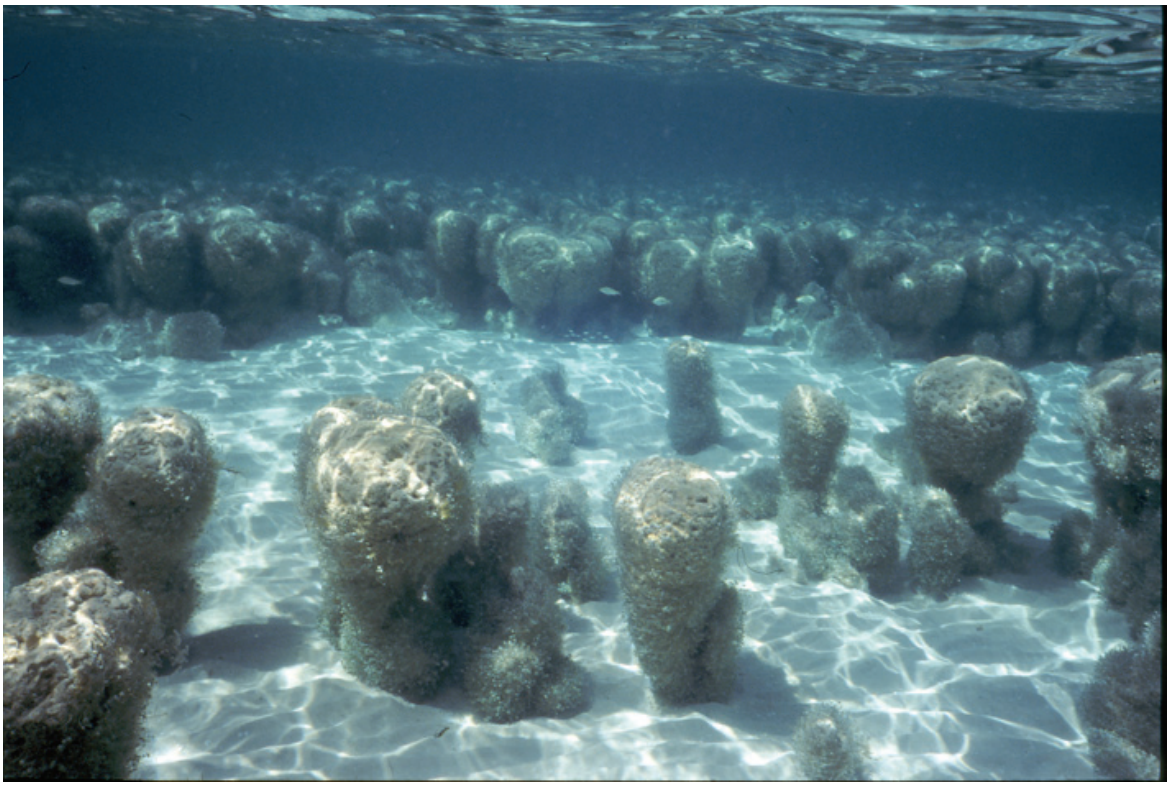

Figure 1. Subtidal Stromatolites, Hamelin Pool

The significance of the Gogo Fauna

Ken Campbell[1]

[1] *Research School of Earth Sciences, The Australian National University, Canberra, ACT 0200, Australia*

This fauna is of Early Devonian age. It as deposited as a fore-reef carbonate deposit in embayments in the reef system along the Canning Basin edge of the Kimberley Precambrian Massive. Because of the quiet conditions in these embayments, the enclosing sediments frequently covered the bottom dwelling fauna. Many of these organisms were vertebrates, and because some of them after burial wee not disturbed by preditors, they are preserved in almost three dimensions and their histological structure is preserved in the finest detail. For this reason a large number of organisms have been described. In most other areas the specimens are squashed flat, and the finer details are lost because of alteration. Gogo specimens can be freed from the limestone sediment by etching with acetic acid and such features as the neural system, the vascular systems and the growth patterns of the bones can be displayed. What is more, the techniques developed by Professor Tim Senden and A.J. Lemay in the School of Applied Mathematics , IAS, have enabled us to see details that were not revealed even by etching. This includes internal structures of the braincase and the genital systems.

As examples of the quality of the preservation we refer to four recent discoveries that have hit the headlines.

Andrews, S.M., long, J.A. Ahlberg, P. Barwick, R.E. & Campbell, K.S.W. 2006 . The structure of the sarcopterygian Onychodus jamdemarrai n.sp from Gogo, Western Australia : with a functional interpretation of the skeleton. Transactions of the Royal Society of Edinburgh; Earth Sciences : Vol 96: 197-307 Figs 1-75.

Campbell, K.S.W. & Barwick, R.E. 2006 Morphological innovation through gene regulation from Onychodontiform fish. International Journal of Developmental Biology, Vol 50: 371-375.

Long, J.A. Trinajstic , K., Young,G.C. & Senden T, 2008. Live birth in the Devonian Period. Nature : Vol 453: 650-652

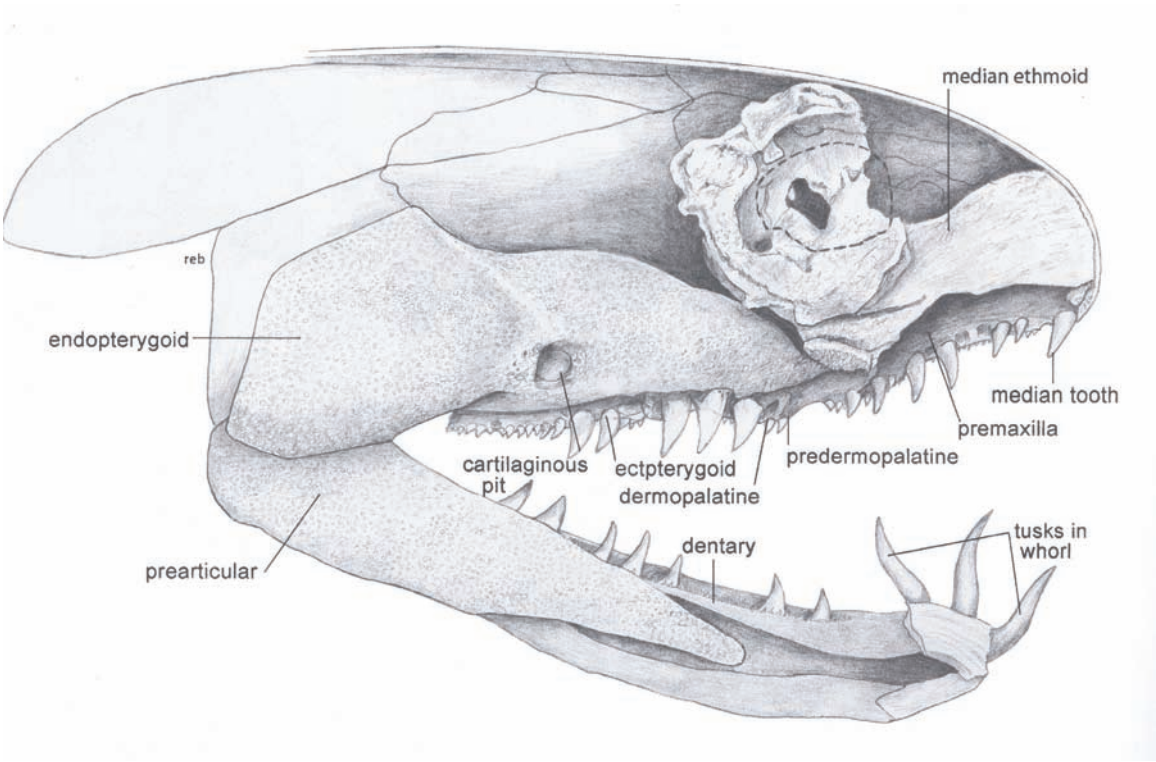

Stoichiometry and kinetics of jarosite dissolution in acid sulfate soils

Andrew G. Christy[1,2], Susan A. Welch[1,2,3,4], Dirk Kirste[2,3,5], Fern R. Beavis[1,2,3],

Sara G. Beavis[1,2,3,6]

[1] *Research School of Earth Sciences, Australian National University, Canberra, ACT 0200, Australia*
[2] *Department of Earth and Marine Sciences, Australian National University, Canberra, ACT 0200, Australia*
[3] *Cooperative Centre for Landscape Environments and Mineral Exploration (CRC LEME) , Australian National University, Canberra, ACT 0200, Australia*
[4] *The Ohio State University, Columbus, Ohio, USA*
[5] *Simon Fraser University, Burnaby, British Columbia, Canada*
[6] *Fenner School of Environment and Society, Australian National University, Canberra, ACT 0200, Australia*

Jarosite, ideally $KFe^{3+}_3(SO_4)_2(OH)_6$, is stable under acid oxidising conditions and is an important mineral in acid sulfate soils. It accommodates a wide range of trace cations in solid solution, which can be remobilised if it dissolves. We have found jarosite dissolution to be strongly incongruent: large cations such as K^+ can be lost or exchanged even when the iron sulfate framework remains largely intact. Rare earth cations display extreme fractionation of LREE into jarosite and exclusion of HREE from it, with the result that dissolution of jarosite produces characteristic MREE enrichment in the associated water. Long-duration kinetic studies show that the dissolution stoichiometry in a closed system evolves in a complex fashion through time, from fast release of sulfate to slower release of Fe to constant in Fe as the system becomes buffered by saturation of Fe-oxyhydroxide phases.

Welch SA, Kirste D, Christy AG, Beavis SG, Beavis F (2007) Jarosite dissolution I - trace cation flux in acid sulfate soils. *Chem. Geol.* **245**: 183-197.

Welch SA, Kirste D, Christy AG, Beavis FR, Beavis SG (2008) Jarosite dissolution II - reaction kinetics, stoichiometry and acid flux. *Chem. Geol.* **254**: 73-84.

Welch SA, Kirste D, Christy AG, Beavis F, Beavis SG (2008) Jarosite reactivity and trace metal geochemistry in acid sulfate soils. Goldschmidt 2008 Geochemistry Conference, Vancouver, Canada, 13 -18 July, 2008. *Geochim. Cosmochim. Acta* **72**: A1013 Suppl. (Refereed conference abstract).

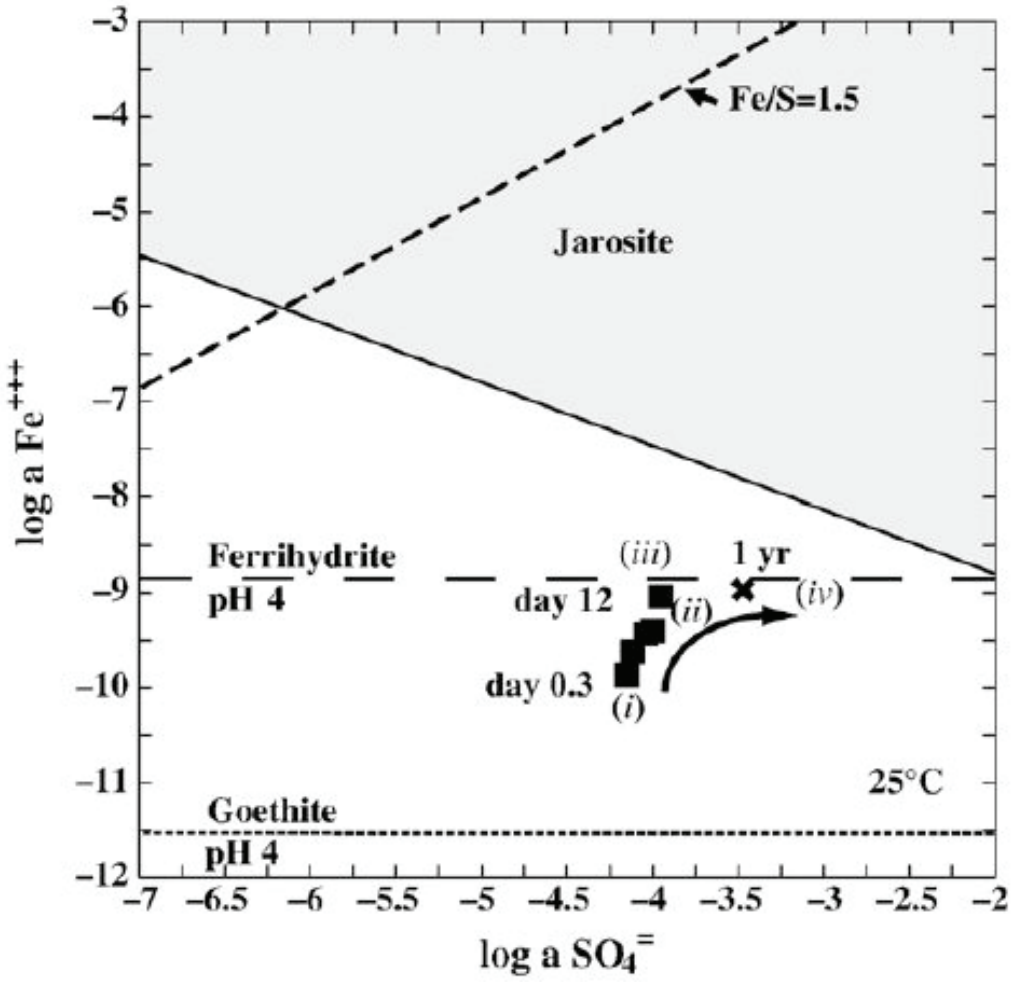

Figure 1. Time evolution of ferric iron and sulfate concentrations in water associated with dissolving jarosite. Stoichiometric dissolution indicated by Fe/S = 1.5 dashed line. Earliest measurements show substantial release of sulfate, followed by slower release of Fe (steep part of curve) until ferrihydrite becomes saturated (flat part of curve). Jarosite saturation ultimately achieved at far right of activity-activity diagram.

Enhanced detection capability at infrasound stations in the global CTBT verification network

Douglas R. Christie

Research School of Earth Sciences, Australian National University, Canberra, ACT 0200, Australia

A 60-station global infrasound monitoring network is being constructed as part of the verification regime for the Comprehensive Nuclear-Test-Ban Treaty (CTBT). Nearly 70% of this network has been established and it is anticipated that the network will be completed in the next few years. The network, which is far larger and much more sensitive than any previous infrasound monitoring network, consists of state-of-the-art infrasonic array stations distributed as uniformly as possible over the face of the globe. Current studies indicate that the final global network will reliably detect signals from a 1-kiliton atmospheric nuclear explosion at two or more monitoring stations.

Research at the ANU during the past few years has focused on the development of techniques that can lower detection thresholds, improve location capability and enhance the overall reliability of the network. This has resulted in the development of an optimal infrasonic array design that eliminates problems with spatial aliasing of high frequency signals and problems with signal coherence between array elements. Substantial work has also been carried out on the development of a new and effective technique for reducing wind-generated background noise.

Wind-generated background noise is still the most significant problem at many stations in the global infrasound monitoring network. Wind-generated noise may seriously limit detection capability at stations located in high wind environments with little shelter from the ambient winds. A wind-noise-reducing pipe array is currently used at all infrasound stations in the CTBTO verification network. While these devices provide significant noise reduction, the level of background noise at some stations remains unacceptably high, especially during the daytime. It is generally recognized that further improvements in pipe array design will not resolve this problem. Work at the ANU on infrasound background noise reduction has therefore been concerned with a new approach to the wind-noise problem that appears to have the potential to effectively eliminate wind noise at most monitoring stations.

This technique is based on the use of a turbulence-reducing enclosure constructed from a series of screens positioned around the sensor inlet ports. A large variety of enclosures have been constructed and tested near one of the standard International Monitoring System (IMS) array elements at IS07, Warramunga. A larger than usual 20-m diameter enclosure (version 6) with three concentric porous walls was tested during the year in an attempt to improve the longer period performance of the device. Rather surprising, the performance of this large diameter device was found to be almost identical to a smaller 14-m diameter enclosure (version 5B) with two concentric walls. Both of these enclosures suppress wind-generated noise by up to four orders of magnitude at higher frequencies, even when the sensor is connected to only a single inlet port located at the center of the enclosure.

We conclude that version 5B shown in Figure 1 is the most effective practical design for a turbulence-reducing enclosure.

The performance of version 5B has also been compared directly with the performance of a standard IMS 96-port 18-m diameter pipe array at site H1 at IS07 Warramunga. This comparison shows that the degree of noise reduction provided by the turbulence reducing enclosure with only a single inlet port is more than two orders of magnitude better than the standard 96-port pipe array at higher frequencies. The performance of the pipe array is, however, slightly better at low frequencies.

This suggests that the performance of existing pipe arrays at IMS infrasound stations can be improved very substantially by enclosing the pipe array inside a turbulence-reducing enclosure similar to version 5B. It is recommended that all new IMS stations should be constructed with wind-noise-reducing pipe arrays located inside a turbulence-reducing enclosure.

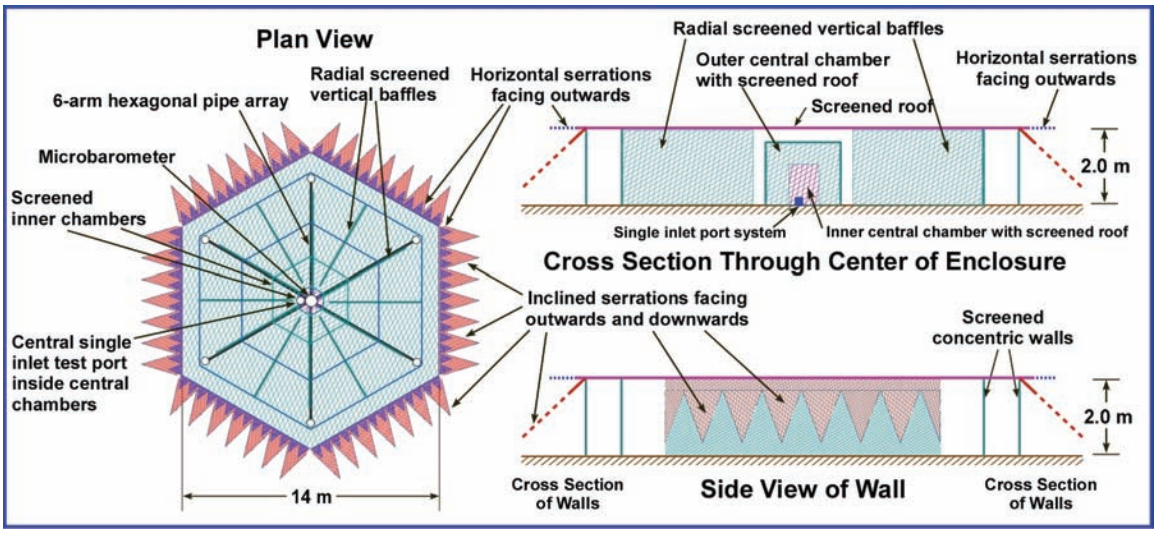

Figure 1. Version 5B of the infrasonic wind-noise-reducing enclosure.

Effects of Archaean to early Proterozoic asteroid impact clusters on crustal evolution

Andrew Glikson[1]

[1]*School of Research School of Earth Science and School of Archaeology and Anthropology*
The Australian National University, Canberra, ACT 0200, Australia
(joint with, and logistically assisted by, the Pilbara project of the Geological Survey of Western Australia).

The role of asteroid and comet impacts as triggers of mantle-crust processes poses one of the fundamental questions in Earth science. Evidence has been documented for close association between impact ejecta/fallout units with major unconformities and lithostratigraphic boundaries in early Precambrian terrains, including abrupt changes in the nature of volcanic and sedimentary environments across stratigraphic impact boundaries, with implications for the composition of provenance. In the Barberton Greenstone Belt, eastern Kaapvaal Craton, South Africa, 3.26-3.24 Ga asteroid mega-impact units are juxtaposed with abrupt break between mafic-ultramafic volcanic crust and an overlying association of turbidites, banded iron formations, felsic tuff and conglomerates.

Contemporaneous stratigraphic relationships are identified in the Pilbara Craton, Western Australia. Evidence for enrichment of seawater in ferrous iron in the wake of major asteroid impacts reflects emergence of new source terrains, likely dominated by mafic compositions, attributed to impact triggered oceanic volcanic activity. Relationships between Impact and volcanic activity are supported by the onset of major mafic dyke systems associated with ~2.48 Ga and possibly the 2.56 Ga mega-impact events. Abrupt breaks at 3.26-3.24 Ga between ~12 km-thick mafic-ultramafic volcanic sequences of Archaean greenstone belts and overlying felsic volcanic-turbidite-banded iron formation assemblages in the Transvaal and the Pilbara cratons are accompanied by 4 asteroid ejecta units. Mass balance calculations based on Ni/Cr, PGE and $^{52/53}$Cr isotope data indicate mafic-ultramafic target crust and parent asteroid on a scale of 20 – 50 km diameter. Kinematic models of impact by such asteroids on thin geothermally active Archaean crust and lithosphere suggest consequent reorganization of mantle convection cell systems, accounting for contemporaneous peak igneous activity.

The onset of ferruginous sedimentation immediately following the impacts, indicated by occurrence of BIF above ejecta units, indicates increased supply rates of soluble ferrous iron to the oceans under the low Eh conditions of the Archaean hydrosphere, indirectly suggesting the erosion of mafic volcanics possibly triggered by the impacts. A new impact crater discovered by Dr A.H. Hickman and documented by the author is reported in the current issue to the Australian Journal of Earth Science (see Figure 1). The results of this study are reported in 16 papers in international and national scientific journals and in books during 2004 – 2008.

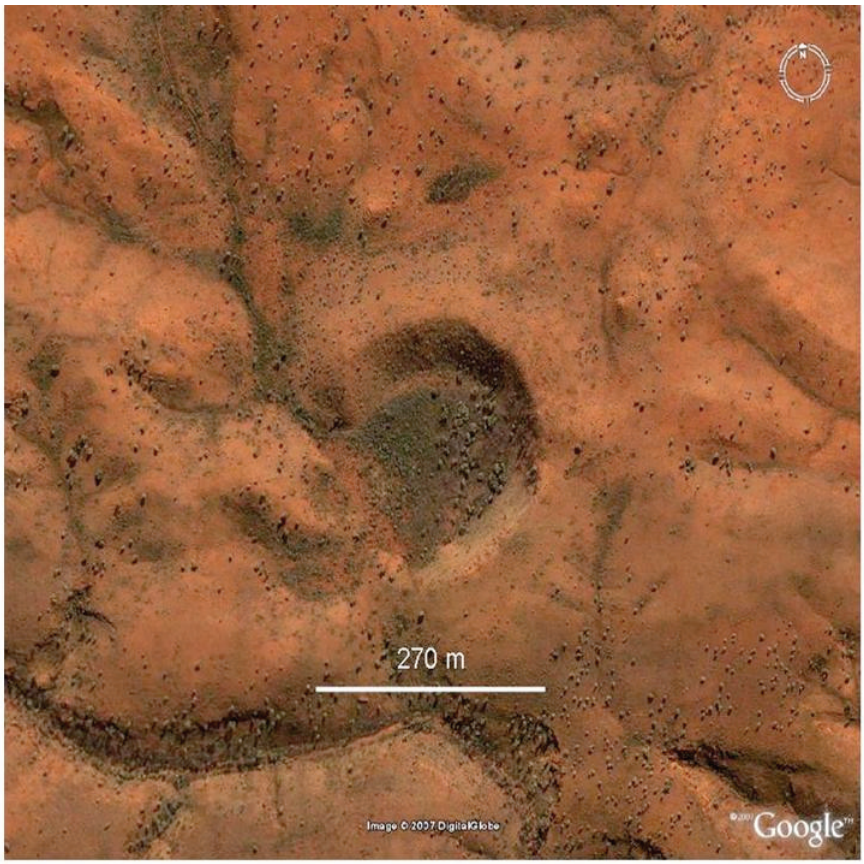

Figure. 1. The newly found Hickman Crater, Ophthalmia Range, Western Australia, reported in Glikson et al., Australian Journal of Earth Science, December, 2008.

Clarification of the Influence of Water on Mantle Wedge Melting

David H Green, William O Hibberson. Anna Rosenthal and Istvan Kovacs

Research School of Earth Sciences, Australian National University, Canberra, ACT 0200, Australia

Water is a significant component in primitive island arc magmas and its ubiquitous presence is attributed to release of water from dehydration reactions in subducted oceanic crust and lithosphere. Water released from the subducted slab is inferred to be transferred as aqueous vapour or water-rich melt into the overlying peridotite of the mantle wedge. Because of the inverted temperature gradient inferred for the mantle wedge immediately above the subducted slab, access of aqueous vapour or water-rich melt will initiate melting close to the water-saturated peridotite solidus. The location of a region of water-saturated mantle melting, if it exists, can be predicted if we know the P,T dependence of the water-saturated peridotite solidus and can model the temperature distribution in a particular subduction setting. We have confirmed the results of a number of experimental studies in the 1970's which defined the P,T conditions for the water-saturated solidus of lherzolite up to 3GPa..

We conducted 60 experiments from 1.5 GPa to 6 GPa using different water contents and several bulk compositions. Electron microprobe analyses of 4-7 phases in each experiment document systematic compositional changes in co-existing phases. In addition Fourier Transform Infra-Red (FTIR) spectroscopy was used to measure the water contents of nominally anhydrous minerals (commonly abbreviated NAMS) in 25 of the experiments. The solidus decreases rapidly from ~1100˚C at atmospheric pressure to 0.5 GPa, 1000˚C, and continues to decrease slightly to a minimum of 970˚C at 1.5 to 2 GPa. We demonstrate that for hydrous silicate melt, the fluid-saturated solidus of lherzolite model mantle composition with small (0.2-2%) water contents and very small carbon content, is ~1010˚C at 2.5 GPa, ~1210˚C at 4GPa. and at least 1375°C at 6GPa.. The melt composition at the water-saturated solidus at 2.5GPa is a very silica-undersaturated olivine nephelinite and is extremely silica-undersaturated at higher pressure.

We also used olivine single crystal discs and either olivine aggregates or carbon sphere aggregates as melt and fluid traps forming interstitial films or inclusions within olivine. For several experiments with high water contents, the capsule was pierced under high vacuum at room temperature and the vapour released was analysed by gas chromatography. We have conducted layered experiments for the purpose of measuring the water content of nominally anhydrous minerals under conditions where we were simultaneously observing melting, water-rich vapour, pargasite or phlogopite in fertile lherzolite. We obtained data using the layered capsules with 'sensor' layers of olivine, low-Al and high-Al orthopyroxene and clinopyroxene, at pressures of 1.5, 2.5, 4, and 6 GPa..

Allowing for the uncertainty in calibrations in the quantification of IR spectra, our results show that if water contents in fertile mantle lherzolite (i.e. HZ1 Lherzolite, MORB Pyrolite, MM3 lherzolite) are as low as 100-250 ppm H_2O, then pargasite is stable at 2.5 GPa and melting begins at the 'fluid-absent lherzolite+ H_2O dehydration solidus' which is close to 1100°C for these compositions. With increasing water content the proportion of pargasite at the solidus increases to ~10-15% (i.e. with 1500-2000 ppm H_2O in the lherzolite) but the water content of NAMS remains unchanged. At higher water contents a water-rich vapour is present and melting begins at the vapour-saturated solidus with pargasite stable at and slightly above the solidus. Our data on the water content in olivine in the sequence from the first appearance of a water-rich vapour (e.g. between 0.073% and 0.145% H_2O at 2.5Gpa, 1000°C) to 'leached' experiments with 14.5% H_2O show little change with increasing

bulk water content, suggesting that water activity is effectively buffered by the pargasite-bearing assemblage.

At >3GPa, pargasite is unstable and with water contents of 100-250 ppm or more, melting begins at the vapour-saturated solidus which for a water-rich vapour and fertile lherzolite composition is at ~1225 °C at 4Gpa and ~1375°C at 6GPa. The data also show that if a melt is formed at the vapour-saturated solidus at >3GPa ('incipient melting regime') and migrates out of the vicinity, then the water content retained in the residual but still fertile lherzolite (in nominally anhydrous minerals) is 100-250ppm H_2O. Decompression melting of such residual lherzolite at temperatures in the 'major melting regime' i.e. slightly above the anhydrous solidus, will produce magmas at ~10% or ~20% melting containing 0.1-0.25% or 0.05-0.13% H_2O respectively, i.e. controlled by the residual water contents retained in NAMS. Such magmas would have incompatible element contents reflecting the history of their source including the loss of very small melt fraction(s) in the garnet lherzolite stability field. These characteristics match those of N-MORB or D-MORB, whereas E-MORB characteristics reflect source lherzolite to which a migrating incipient melt has been added.

The preservation of microbial lipids in saline and acid-saline environments

Claudia Jones[1,2], Jill Banfield[1] and Jochen Brocks[2]

[1] *Department of Earth & Planetary Science, University of California, Berkeley, USA*
[2] *Research School of Earth Sciences, Australian National University, Canberra, ACT 0200, Australia*

We are currently working on a pair of separate, but related, lipid biomarker analyses on samples from Lake Tyrrell, VIC, Australia, in order to ascertain the timescales and extent of biomarker preservation within a hypersaline lacustrine system. In the context of the primary project, we have obtained a ~13m drill core (see Fig. 1) from the northern end of the lake during field work in July 2008; from this core we are extracting lipids to construct a temporal sequence. Prof S. George and his PhD student, Mr. P.S. Bray, both from Macquarie University, will perform compound specific radiocarbon dating on archaeol extracted from the core and optically stimulated luminescence dating (in collaboration with Dr Kathryn Fitzsimmons, RSES) on quartz lenses within the core to ascertain the timescales over which environmental change occurred. To determine the magnitude and nature of this change, we are examining suites of lipids from each sub-sampled depth to reconstruct the microbial community that was present in the lake at the time the compounds were deposited. The objectives of this work are to 1. Determine the potential for Australian salt lakes to be used as data sources for paleo-environmental reconstruction; 2. Refine estimates of past aridity for the Tyrrell Basin; and 3. Investigate the extent of community re-structuring by micro-organisms in response to salinity changes.

The secondary project examines biomarker preservation at pH 4 acidic seeps found at the southern end of Lake Tyrrell. Anoxic, iron-rich ground waters flowing from these seeps oxidize near the surface and result in ferricrete deposition. The ferricretes are composed of quartz-rich lake sediments cemented into meter-scale rocks by iron oxides (magnetite) and oxyhydroxides (goethite). These ferricretes are underlain by typical acid-saline depositional facies, very similar to that encountered at Meridiani Planum on Mars by the rover Opportunity. To determine whether molecular markers for life can coexist with oxidized mineral deposits, we extracted samples of ferricrete and underlying sediments to establish the presence and provenance of free and bound lipid biomarkers.

In order to assess the effects of oxic lithification on redox sensitive lipids, we monitored the concentration of phytanol and its oxidation product, phytanic acid, in ferricretes and surrounding sediment samples. Results indicate that the jarosite-rich ($KFe_3+3[(OH)_3SO_4]_2$) sediment directly underlying the concretion is a poor matrix for lipid preservation: only small concentrations of phytanol were evident, and phytanic acid was below detection limits. By contrast, both the goethite-rich layer of the concretion and the reduced sulfide-rich sediments surrounding it showed greater concentrations of each compound (20x and 250x, respectively). Interestingly, the ratio of phytanol to phytanic acid is approximately equal within the oxic concretion and the reduced sediment, indicating that abiotic oxidation is not likely to be a relevant diagenetic pathway for phytanol in this setting.

Differences in compound concentrations between samples demonstrate the differential preservation of lipids within the ferricrete and the underlying sediment. While the concentrations of lipids are ~10 times lower in ferricrete than in sediment, their presence indicates that biomarker molecules may survive the oxidizing conditions of ferricrete formation broadly analogous to those that existed on the Martian surface.

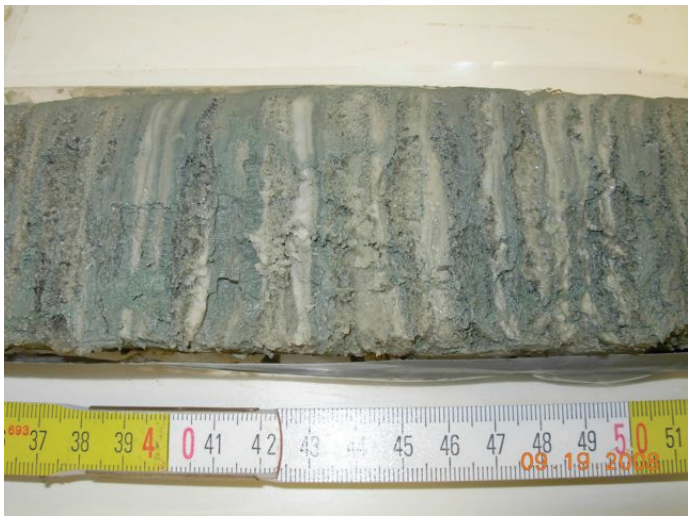

Figure 1. Section of drill core from Site 12 at Lake Tyrrell, ~5m depth

Oxygen isotope values from Permian high latitudes: clues for palaeolatitudinal sea-surface temperature gradients and Late Palaeozoic deglaciation.

Korte, C.[1], Jones, P.J.[2], Brand, U.[3], Mertmann, D.[4] & Veizer, J.[1,5]

[1] *Institut für Geologie, Mineralogie und Geophysik, Ruhr Universität 44801 Bochum, Germany*
[2] *Research School of Earth Sciences, Australian National University, Canberra, ACT 0200, Australia*
[3] *Department of Earth Sciences, Brock University, St Catharines, Ontario, Canada L2S 3A1*
[4] *Institut für Geowissenschaften, FU Berlin, Malteserstrasse 74-100, 12249 Berlin, Germany*
[5] *Ottawa-Carleton Geoscience Centre, University of Ottawa, Ottawa, Ontario, Canada K1N 6N5*

Institut für Geologie, Mineralogie Korte, C., Jones, P.J., Brand, U., Mertmann, D. & Veizer, J. (2008) Oxygen isotope values from Permian high latitudes: clues for palaeolatitudinal sea-surface temperature gradients and Late Palaeozoic deglaciation. *Palaeogeography, Palaeoclimatatology, Palaeoecology 269, 1-16*.

The Permian was a period of waning large-scale continental glaciations in the southern Hemisphere. The waning of these ice sheets during the Early Permian led to discharge of ^{18}O-depleted ice-melt water into the oceans. This, coupled with rising seawater temperatures, resulted in a concomitant decline of about 2.5 ‰ in the $\delta^{18}O$ of seawater, as recorded by brachiopod shells from low-latitude (< 30°) habitats. The transition from ice- to greenhouse conditions is reflected also in the oxygen isotope data of unaltered brachiopods and bivalves from high latitudes. Moreover, the high-latitude specimens have consistently more positive $\delta^{18}O$, by about 2.5‰, than their coeval low-latitude counterparts, suggesting a Permian sea- surface temperature (SST) gradient of about 9 to 12°C between tropical-subtropical (<30°) and high southern (55 ±10°) latitude localities, apparently irrespective of whether in a greenhouse or an icehouse mode. This Permian SST gradient is comparable to the SST gradient of about 14°C. The $\delta^{18}O$ seawater records suggest that the global warming that resulted in the waning of the Permo-Carboniferous ice sheets during the Sakmarian was followed by another cooling during the late Kungurian and by renewed warming during the Mid- and Late Permian.

Australia-Laurasia convergence, Alice Springs Orogeny and tectonic extrusion of the Thomson Orogen

Chris Klootwijk

Research School of Earth Sciences, Australian National University, Canberra, ACT 0200, Australia

Most of the year has been spent on fine-tuning the concept by expressing it into figures and finalizing literature searches. The hypothesis has been presented at the Australian Earth Science Convention in Perth. Work is now geared towards publication. Current status of the concept summarizes as follows:

Palaeomagnetic results from the ignimbrite-rich Carboniferous succession of the Tamworth Belt, Southern New England Orogen (SNEO), show a northward excursion over more than 30° of latitude with an apex in middle-late Visean (Figure 1A). The excursion is identifiable also in limited palaeomagnetic data from the Australian craton and the Tasman Orogenic System (TOS) and may have started in the Early Devonian. By middle-late Visean, the promontory of the Australian craton in New Guinea, as part of Gondwanaland, reached 30°-40°N, well within the latitudinal range of the Central Asian Orogenic Belt (CAOB).

Devonian-Carboniferous convergence/collision of northeastern Gondwana (Australia) and southern Laurasia (CAOB) is thought the cause of contemporaneous, Variscan, tectonism in the CAOB and in Australia (Alice Springs Orogeny [ASO], Quilpie and Kanimblan Orogenies). Compressional deformation in Australia was largely confined behind the New Guinean promontory, between the Bintuni, Bonaparte and Ord Basins, Halls Creek Fault Zone and the Lasseter Shear Zone in the west and the Aure Trough, Queensland Basin and Bowen-Gunnedah-Sydney Fault Zone in the east.

Convergence-driven N-S compression, hot crust in the Larapintine Graben and a free oceanic boundary, constituted Variscan Australia-Asia conditions that were comparable to the Cenozoic India-Asia indentation/extrusion. Tectonic extrusion of ductile lower crust (and melt?) from the central Larapintine Graben caused eastward displacement of the Thomson Orogen and the Northern New England Orogen (NNEO) along the Diamantina River Lineament-Clarke River Fault Zone in the north and along the Darling River/Cobar-Inglewood Lineaments and Cato Fracture Zone in the south (Figure 1B). The buttress of the NNEO caused telescoping of an unpinned SNEO during Stephanian reversal of Gondwana's rotation.

Different tectonic grains (ASO, Quilpie, Kanimblan, kinkbanding) represent the integrated effects from convergence/collision on the brittle upper crust (direct N-S compression) and on the ductile, partially molten?, lower crust (hydraulic transmission, fanning out from N-S compression toward alignment with an E-W pressure gradient). A single N-S compressional event can thus lead to contemporaneous deformations with widely different tectonic grains, varying from N-S to E-W.

Seismic tomography shows continental-like velocities in the lower crust/upper mantle of the more internal TOS and E-W fanning of SV azimuthal anisotropy in support of the extrusion model. Large-scale negative magnetic anomalies in the Larapintine Graben and the TOS are likely to represent hematite-residing Kiaman reverse remanence in the lower and upper crust and may trace lower crustal flow throughout the TOS.

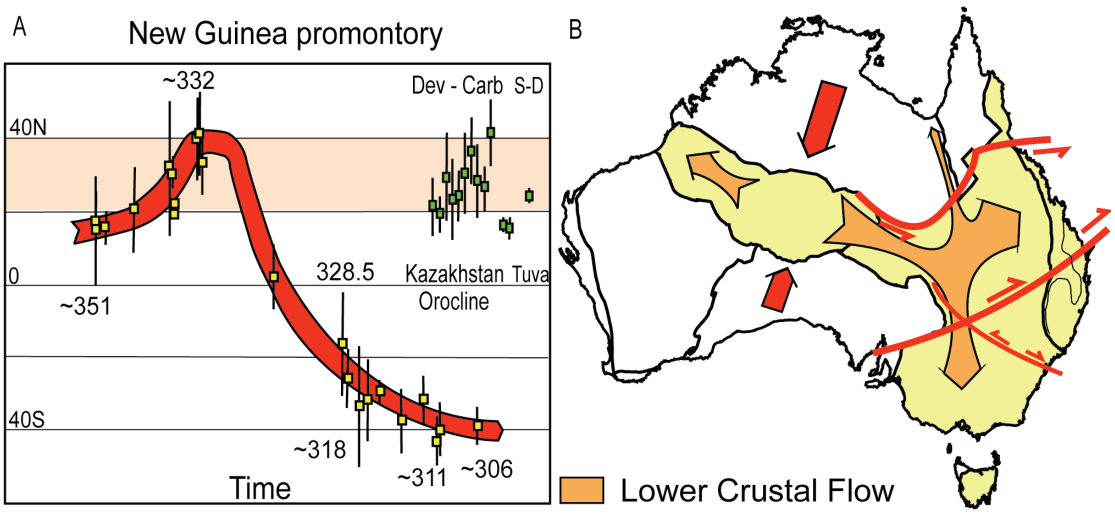

Figure 1 A) Red band shows Carboniferous palaeolatitudes for the New Guinean promontory of the Australian craton according to SNEO results (yellow squares, Klootwijk 2002, 2003, in prep.). Green squares show Devonian-Carboniferous palaeolatitudes for the Kazakhstan Orocline and Tuva terrane of the Central Asian Orogenic Belt. B) Red arrows indicate compression from Australia-Laurasia convergence during the Devonian-Carboniferous. Orange arrows indicate ductile flow of lower crust from the Larapintine Graben into mainly the Thomson and Lachlan Orogens. Major ENE-WSW fault zones guided up to 200 km upper crustal eastward displacement of the Thomson Orogen and the NNEO. The yellow compartments indicate at large the weaker, heated, crust of the Larapintine Graben and the weaker, originally oceanic, crust of the Tasman Orogenic System.

Chronological control of Plio-Pleistocene strata in the Omo-Turkana Basin, Ethiopia and Kenya

Ian McDougall[1] and Frank Brown[2]

[1]*Research School of Earth Sciences, Australian National University, Canberra, ACT 0200, Australia*
[2]*Department of Geology and Geophysics, University of Utah, Salt Lake City, Utah 8412, USA*

The Omo–Turkana Basin of northern Kenya and southern Ethiopia developed in the northern Kenya Rift about 4.3 Ma ago in the Early Pliocene, with deposition occurring over an area as much as 400 km (N-S) by 70 km (E-W), centred on Lake Turkana. Nearly 800 m of sediments, mainly sands, silts and clays deposited in fluvial, deltaic and lacustrine environments, comprise the Omo Group. Numerous rhyolitic tuffs in the sequence not only have facilitated secure correlations between the formations of the Omo Group but also have provided material for precise $^{40}Ar/^{39}Ar$ age measurements on single crystals of alkali feldspar separated from pumice clasts within the tuffs.

Ages are now available on over 30 stratigraphic levels, all of which are consistent with their relative stratigraphic order (McDougall & Brown, 2006, 2008). The new ages, which have a precision of the order of 1% (standard deviation of the population), based on pooling of many single crystal ages, are all consistent with the stratigraphic order, providing confidence that they accurately record the timing of the volcanic eruptions, with deposition of the tuffs and pumices occurring shortly thereafter. Thus we now have a robust numerical time framework for the depositional history of the Omo-Turkana Basin.

The majority of the ages lie between 4.2 and 0.75 Ma and have been measured on samples from the three main formations mapped in this large area, with correlations made between sequences on the basis of the distinctive geochemistry of the individual tuffs. The sequence is famous for the very large number of hominin and other vertebrate fossils that have been recovered from it, providing an important record of evolution. It is through the geochronological measurements that we are able to date individual fossils, often to significantly better than 0.1 Ma, through stratigraphic correlations of their position relative to known tuffaceous beds.

This has provided an accurate time scale that is independent of assumptions as to the direction and rate of vertebrate evolution. In some cases we are able to correlate the depositional history in the region with paleoclimatic indicators in deep sea cores, related to Milankovitch cycles and the astronomical time scale. This has been successfully accomplished in relation to the younger Kibish Formation, where correlations have been made with sapropel deposition in the Mediterranean Sea some 3000 km to the northwest (McDougall et al., 2008). With increased precision of the ages, potentially possible using the new generation of multiple collector mass spectrometers for argon isotopic analysis, controls on deposition in the Omo-Turkana Basin related to paleoclimatic factors will become correlateable with the more detailed records in the deep sea cores.

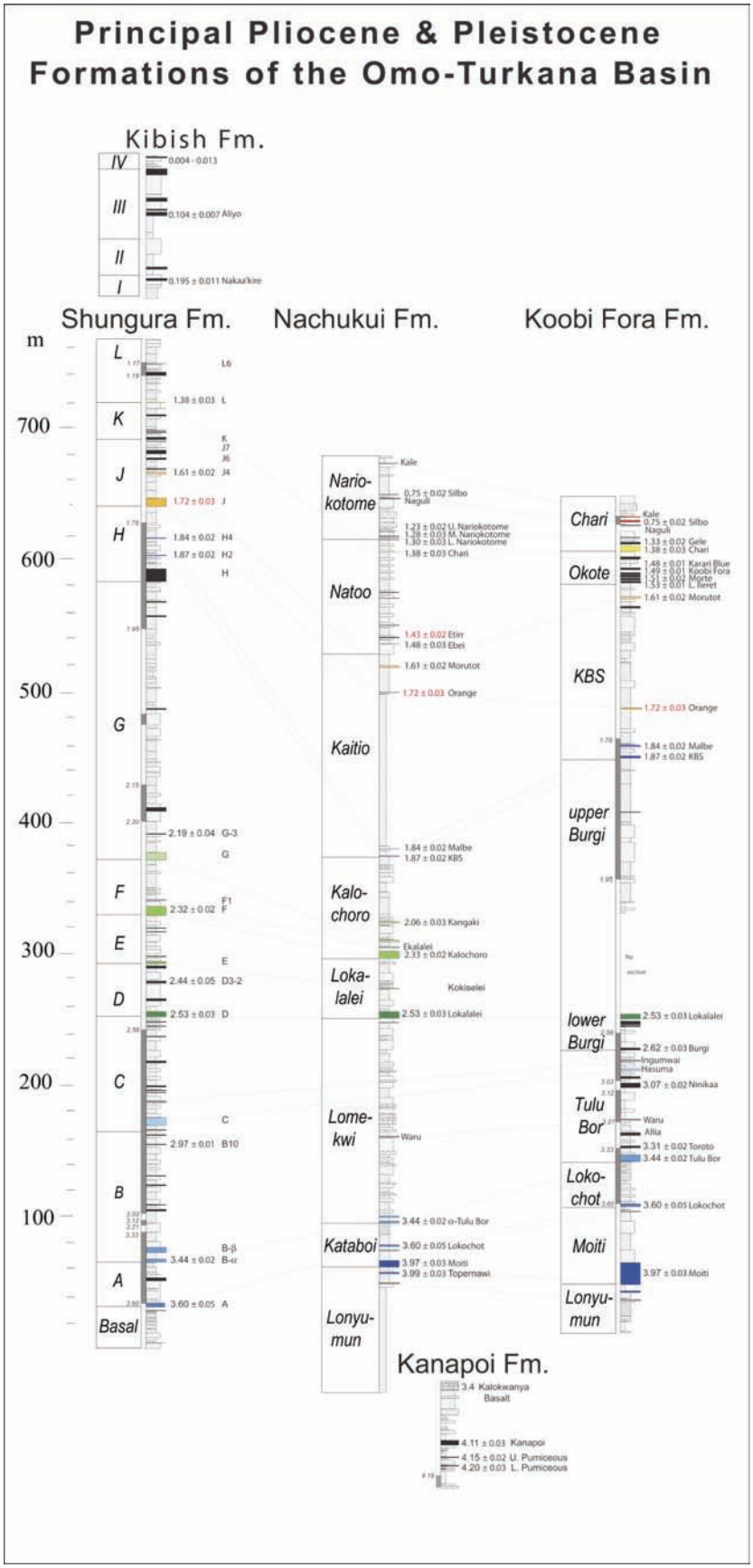

Figure 1: Principal Pliocene and Pleistocene formations of the Omo-Turkana Basin showing the $^{40}Ar/^{39}Ar$ ages determined on alkali feldspars from pumice clasts within the tuffs, and correlations between the formations based upon the distinctive chemistry of the tuffaceous beds.

McDougall I, Brown FH (2006) Precise $^{40}Ar/^{39}Ar$ geochronology for the upper Koobi Fora Formation, Turkana Basin, northern Kenya. *Journal of the Geological Society, London* **163**: 205-220

McDougall I, Brown FH (2008) Geochronology of the pre-KBS Tuff sequence, Omo Group, Turkana Basin. *Journal of the Geological Society, London* **165**: 549-562

McDougall I, Brown FH, Fleagle JG (2008) Sapropels and the age of hominins Omo I and II, Kibish, Ethiopia. *Journal of Human Evolution* **55**: 409-420

Early geological investigations of the Pleistocene Tamala Limestone, Western Australia

Wolf Mayer

Research School of Earth Sciences, Australian National University, Canberra ACT 0200, Australia

Abstract: The first geological studies of the Quaternary deposits, which crop out extensively along the coast of Western Australia, were carried out by members of English and French expeditions of discovery, between 1791 and 1836. The exploring parties included scholars with a background in geology, zoology and botany, as well as knowledgeable surgeons and sea captains with a strong interest in the natural sciences. Their collective work established the continuity, over vast distances, of a sequence of sedimentary rocks composed of quartz grains and shell debris, which today form the major part of the Tamala Limestone sequence. Their observations of the internal features of these rocks led some among them to develop views on the nature and origin of the cementing substance that bonds sand grains and shell debris in sedimentary layers and in concretions. There was disagreement among successive parties of visitors on the nature and origin of rhizoliths and other petrified woody matter in calcareous rocks. The finding of well-preserved sea shells in rocks now above sea level provided convincing evidence to investigators that the ocean had, in recent times, retreated from the land. The discovery of species of mollusc, known to be extinct in Europe, raised questions about an assumed world-wide extent of sedimentary sequences.

Evolution of the Svecofennian orogenic province

R.W. Roye Rutland[1], Ian. S. Williams[1] and Jukka Kousa[2]

[1] Research School of Earth Sciences, Australian National University, Canberra, ACT 0200, Australia
[2] Geological Survey of Finland, Regional Office for mid-Finland, P.O. Box 1237 , FIN-70211 Kuopio, Finland

In several areas of the Svecofennian Province, a major discontinuity has been recognized between Svionian complexes, strongly deformed and metamorphosed at ~1.92 Ga, and overlying post-1.92 Ga Bothnian volcano-sedimentary sequences (Annual reports, 2005, 2006, Skiöld and Rutland, 2008). In Ostrobothnia, Finland (Williams et al., 2008), a similar discontinuity has now been identified within the mostly metasedimentary Western Pohjanmaa Belt and separates two distinct stratigraphic groups. The western Lappfors group, interpreted as a Svionian basement complex, has strong W-trending folding and aeromagnetic signatures that contrast with the unconformably overlying eastern Evijärvi group, interpreted as lower Bothnian, which has more open N-trending folding and magnetic patterns. Several lines of evidence date the unconformity at ~1.92 Ga. Detrital zircons from two samples of Lappfors group metasediment, and a sample of the basal Nivala gneisses in the Eastern Pohjanmaa Belt, have 1.92–1.91 Ga post-depositional low-Th/U metamorphic overgrowths.

The maximum deposition age of the Lappfors sedimentary protoliths, based on detrital zircon ages, is between ~1.97 and ~1.94 Ga. Three samples of Bothnian sediments lack pervasive ~1.91 Ga overgrowths, instead having a variety of detrital zircons as young as ~1.95–1.91 Ga, reflecting recycling of the underlying basement complex. The maximum deposition age of the lower Bothnian sedimentary protoliths is inferred to be ~1.91 Ga. The Niska granite, which intrudes the Evijärvi group and is deformed only by the younger tectonic episode affecting that sequence, has a zircon age of 1896 ± 6 Ma. That episode, which established the present relationships between basement and cover, is dated by ~1.88 Ga metamorphic zircon overgrowths in both the Svionian and Bothnian samples, and by 1878 ± 4 Ma metamorphic monazite from a metasediment from the Savo Belt, east of the Nivala district.

Part of the FIRE 3A reflection seismic profile (Kukkonen et al., 2006; Sorjonen-Ward, 2006) ran NW from the western part of the Central Finland Granitoid Complex (CFGC) across the boundary with the Evijärvi group and into the Lappfors group. Our preliminary interpretation of this section (Kousa et al., 2008) suggests that the Svionian Lappfors group is the surface expression of a middle crustal unit that displays a widespread system of E- to SE-dipping reflectors with listric-type geometry, identified by Kukkonen et al. (2006, pp.29-30). This crustal unit may therefore correspond to the accreted Svionian marginal basin, buried to the east beneath the younger, Bothnian, volcano-plutonic complex. As a corollary, the widespread vertical change in reflectivity between upper and middle crust, (op. cit. p.21), and which is present beneath the western CFGC, may be closely related to the change from the overlying Bothnian complexes to underlying Svionian metamorphic complexes.

We now interpret the observed stratigraphic and structural relationships in Ostrobothnia in terms of an extended orogenic evolution, viz.

(1) Deposition of the Lappfors group, with local maximum deposition ages between ~1.97 and ~1.94 Ga as part of an extensive Svionian marginal basin.
(2) Early Svecofennian (D_1) closure of the Svionan Basin at ~1.92 Ga involving possible subduction zones.

(3) An extensional episode during which the Svionian complex was eroded and the lower Bothnian Evijärvi group with its submarine mafic volcanism was deposited at ~1.91-1.90 Ga in a successor marginal basin.
(4) Transition from marine to terrestrial deposition at ~1.90-1.89 Ga as bimodal calc-alkaline volcanism developed, the upper Bothnian sequence was deposited, and early plutonism occurred.
(5) Continued plutonism and Middle Svecofennian (D_2) deformation at ~1.88 Ga, during which D_2 folds, faults and shear zones were superimposed on the earlier W-trending penetrative D_1 structures in the Lappfors group (Fig. 1). These D_2 structures are largely responsible for the present relationship between the Svionian basement and the Bothnian cover.

Kousa, J., Rutland, R.W.R., Sorjonen-Ward, P., Williams, I.S., 2008. Geological significance of the regional change in reflectivity between the upper and middle crust in the Svecofennian Province. SEISMIX 2008, Saariselka, Finland. *Abstracts*.

Kukkonen, I.T., Heikkinen, P., Ekdahl, E., Hjelt, S,-E., Yliniemi, J., Jalkanen, E., and FIRE Working Group, 2006. Acquisition and geophysical characteristics of reflection seismic data on FIRE transects, Fennoscandian Shield. *Geological Survey of Finland Special Paper* **43**;13–43Skiold, T., Rutland, R.W.R., 2008. "Successive ~1.94 Ga plutonism and ~1.92 Ga deformation and metamorphism south of the Skellefte district": a Reply to H&L. *Precambrian Research (in press).*Sorjonen-Ward, P., 2006. Geological and structural framework and preliminary interpretation of the FIRE 3 and FIRE 3A reflection seismic profiles, central Finland. *Geological Survey of Geological Survey of Finland Special Paper* **43**;105-159.
Williams, I.S., Rutland, R.W.R., Kousa, J., 2008. A regional 1.92 Ga tectonothermal episode in Ostrobothnia, Finland: Implications for models of Svecofennian accretion. *Precambrian Research* **165**;15-36

Figure 1. Tight ~1.92 Ga pre-Bothnian folds in the Lappfors group overprinted by open minor folds, crenulations and veins (left to right) of the post-Bothnian ~1.88 Ga episode. Note the glacial striae from top left to bottom right.

Silurian brachiopod faunas, Yass Syncline – taxonomy and biostratigraphy

Desmond L. Strusz[1]

[1] *Department of Earth and Marine Sciences, Research School of Earth Sciences, Australian National University, Canberra, ACT 0200, Australia*

A paper on the rhynchonellide species in the Yass fauna, previously undescribed, has been accepted for publication in the Proceedings of the Linnean Society of NSW, with an expected publication date of February 2009. Work is well advanced on revising, and adding to, the species of spiriferide brachiopods from the same succession. This will also involve revision of some species known from the slightly older succession in Canberra. The only remaining aspect of the study will be a compilation of all the biostratigraphic data, for presentation at the next Brachiopod Congress in Melbourne in February 2010.

Sections on Silurian stratigraphy and palaeontology were provided for the recent publication on the geology of the Canberra region compiled by D. Finlayson and published by the ACT Division of the Geological Society of Australia, and I was one of the few involved in reviewing and editing the whole volume. I was also involved in editing a generalized geological map of the ACT prepared by R.S. Abell and D. McCue also under the auspices of the Geological Society of Australia.

As a result of recent excavations in the heritage area on Woolshed Creek, Pialligo, large collections have been made which will be used to revise the species present, particularly the dominant one (*Atrypa duntroonensis*). It was this species which was recognized by Rev. W.B. Clarke as being, for the first time, an indicator of the presence in Australia of Silurian rocks. This study will follow completion of the Yass study, and will be the start of further work on the brachiopod faunas of the Canberra region.

I was consulted by the contractors and Heritage ACT on the possible impact of the work on the Woolshed Creek heritage site, and as a result of that early involvement the workers have been extremely cooperative and interested in preserving as much as possible – the original outcrops are untouched.